Loughborough University

SYNTHESIS GAS PRODUCTION FROM BIOGAS USING Ni-BASED CATALYST

by

RHODA HABOR GUMUS

A Doctoral Thesis

submitted in partial fulfillment of the requirement for the award of the degree of Doctor of Philosophy of Louoghborough University

Product Engineering Group
Department of Chemical Engineering
7th July 2005

PREFACE

The work presented in this dissertation was carried out in the Department of Chemical Engineering, Loughborough University between October 2001 and July 2005. I hereby declare that this work is, to the best of my knowledge and belief, original and my own work except as stated in the text The material of this dissertation has not been submitted, either in whole or in part, for a degree at this or any other University This research was funded by Bayelsa State Government, Nigeria

Rhoda Habor Gumus
7th July 2005
Department of Chemical Engineering
Loughborough University

ACKNOWLEDGEMENTS

First and foremost, I would like to express my heartfelt thanks to the Almighty God for His daily care, strength and faithfulness

I would like to thank Dr Klaus Hellgardt for his constant supervision and guidance over the past three years His pursuit of excellence, enthusiasm and total commitment as an educator have made this work possible. Special recognition is also paid to his incredible patience, his many fruitful discussion and excellent idea, throughout the research. In addition, thanks to him for his proof reading of this dissertation, for meaningful corrections. I would like to express my appreciation to Dr Gilbert Shama for patience and proof reading of the dissertation. My utmost appreciation goes to Bayelsa State Government, for the full study fellowship given, making this research possible.

Thanks also indebted to Dr Iian Cumming for his constructive advice during my first and second year viva I would like to thank Dr Paul Russel and Dr Davidson for their constant help during the period of my experimental work. I would also like to thank all the staff in the workshop, and the laboratory, especially Mr Andy Milne, Mr Dave, Mr Terry Neale, and graham moody, who were always available to help during the of my experiments. I also appreciate Mr Paul Izzard for the computer assistance given mostly at critical moments Furthermore, I am grateful to all the friends that I have made during my stay here and friends back home in Nigeria. I want to particularly thank Pastor and Mrs Gerewei, Mrs Ibiba Harry, Mrs Dorathy Atteng, Mrs Ebidei Kumokou and Dr Kueng Low, Mr Odiri Dafinone, Mr Tolumoye Tuaweri, Mr Richard Mutabazi, Mr Promise Mebine and Mr Emmauel Adigio, for their support and encouragement, both physically, emotionally and unceaseless prayers that has sustained me during my research

Last but not the least, I would like to express my sincere gratitude to my husband Chief Timi Gumus and three sons, Preye Gumus, Tari Gumus and Seigha Gumus whose continued love, patience and support, have always inspired me in my endeavours. I would also thank my only brother and sister, Tengi Allison and Martha Allison for their support especially for the children during this long period.

ABSTRACT

As a result of global climate changes brought about by human activity, more sustainable sources of energy are being sought as alternatives to fossil fuels. Biomass is of particular interest as a sustainable source of energy since it does not contribute to net CO_2 emissions. Reforming of methane derived from biomass with CO_2 may form the basis of an efficient means to produce synthesis gas which has many applications in the petrochemical and allied industries.

The objective of this study was the investigation of CO_2 reforming of methane (simulating biogas) over effective supported nickel catalysts capable of long term operation without significant loss of activity and stability. Two sets of catalysts were designed for this purpose (1) modification of the standard support material alumina (γ-Al_2O_3) with oxides such as ZrO_2, MgO and La_2O_3, by the incipient wetness impregnation method using the nitrates as Ni precursor and oxides. The catalysts prepared included the following: a reference catalyst (Ni/γ-Al_2O_3), Ni/Pr_2O_3, Ni/ZrO_2//γ-Al_2O_3, Ni/MgO/γ-Al_2O_3 and Ni/La_2O_3/γ-Al_2O_3). The loadings of both nickel and support promoters were 15 wt% and 5 wt% respectively. (2) Promotion of the active phase (nickel) using palladium and copper: Ni-Pd/γ-Al_2O_3 and Ni-Cu/γ-Al_2O_3 with promoter loadings of 0 25 wt%, 0.5 wt% and 1 wt% After preparation the catalysts were characterised using different techniques: BET surface area, dispersion of active phase (CO chemisorption), and crystalline structure (X-ray Diffraction). The characterisations also include the morphology of catalyst surface (Scanning Electron Microscope) and catalyst reduction (Temperature-Programmed Reduction)

The activity and stability of the catalysts were investigated during continuous operation for period of 6 hours using a tubular reactor 1 m long of diameter 7.6 x 10^{-3} m and having a volume of 4 5 x 10^{-4} m^3 at temperatures ranging from 923K-1073K. The effect of space velocity was also investigated. Carbon deposition on the catalyst surface was determined by the burn-off method The influence of the support on catalyst activity and stability and carbon deposition was markedly different in each case Although the unpromoted catalyst (Ni/γ-Al_2O_3) deactivated significantly with 6 hours on stream at 1073K, zirconia-containing catalysts exhibited much higher stability showing activation during reforming. The zirconia promoted catalysts showed the highest CO yield at almost all temperatures A high CO rate constant ($k_3 = 101 * 10^{-5}\ s^{-1}$) was obtained for the Ni/ZrO_2/γ-Al_2O_3 catalyst compared to that of the unpromoted catalysts ($k_3 = 60*10^{-5}\ s^{-1}$) The activation energies of CH_4, CO_2 and CO were 29 8 kJ/mol, 26 0 kJ/mol and 89.0 kJ/mol for Ni/ZrO_2/γ-Al_2O_3 catalyst whilst values of 32.9 kJ/mol, 29.8 kJ/mol and 40 0 kJ/mol were obtained for the unpromoted catalyst. The catalytic activity decreased following the order Ni/ZrO_2/γ-Al_2O_3 > Ni/La_2O_3/γ-Al_2O_3 > Ni/MgO/γ-Al_2O_3 > Ni/γ-Al_2O_3. Comparable activity was observed for Ni/Pr_2O_3 catalyst, except at temperatures of 923K and 973K where no significant activity was shown.

The influence of palladium and copper on the activity and stability of catalysts was also studied over the same temperature range and space velocities for 6 hours.

A significant difference was observed in both activity and stability compared to the unpromoted catalyst. High initial activity was achieved for the palladium promoted catalyst especially at a low loading level of 0 25 wt% and this was sustained without deactivation.

In the case of copper promoted catalysts there was loss of initial activity but activity remained stable thereafter compared to the unpromoted catalysts that showed deactivation at higher temperatures. The CO yield was lower for both palladium and copper promoted catalyst compared to the unpromoted catalyst. The difference was possibly related to the high rate constant of the unpromoted catalyst compared to both palladium and copper promoted catalyst ($k_3 = 19*10^{-5}s^{-1}$ and $k_3 = 11*10^{-5}s^{-1}$). The activation energies for CH_4, CO_2 and CO for the palladium catalyst were 11.0 kJ/mol, 6 6 kJ/mol, 27.2 kJ/mol whlst 10 9 kJ/mol, 14 2 kJ/mol, and 64 9 kJ/mol were obtained for the copper promoted catalysts. The effect of space velocity on activity was also investigated The catalyst activity follows the order: Ni-Pd/γ-Al_2O_3 > Ni-Cu/γ-Al_2O_3 > Ni/γ-Al_2O_3. Coke deposition for Pd promoted catalyst increased with increasing Pd loading, whilst a decrease in coke formation was observed for the Cu promoted catalyst. The decrease in coke formation for the Cu promoted catalyst may have been due to high reduction in H_2 atmosphere, which can contribute to rapid gasification of coke formed during reforming.

A mathematical model was proposed based on the mechanism of CO_2 reforming of methane with the three occurring reactions. The model equations obtained were solved using a finite difference programme to yield the three key rate constant. The experimental data obtained was used to validate the proposed model.

Finally, the effects of NH_3, normally present in biogas, on the performance of unpromoted catalyst, Ni/ZrO_2/γ-Al_2O_3, Ni-Pd/γ-Al_2O_3 (0.25 wt%) and Ni-Cu/γ-Al_2O_3 (0 25 wt%) catalysts was studied It was found that the activity increased in the case of the unpromoted catalyst, while a decrease in activity was observed in the case of the other catalysts The difference in activity may be due to surface rearrangement caused by nitrogen diffusion into the unpromoted catalyst surface.

Keywords· CO_2 reforming, methane, support promotion, alumina, nickel promotion, palladium, copper, catalyst poisoning, ammonia

TABLE OF CONTENT

Chapter 4 Experimental Results and Discussion-Effect of support on Activity and Stability over Ni-based catalyst

Chapter 5 Effect of palladium and copper on activity and stability over Ni-based catalyst

LIST OF FIGURES

LIST OF TABLES

NOMENCLATURE

		Units
Å	micro pore diameter	angstrom
A	pre exponential factor	
a, b	stoichiometric constants	
C_A	concentration of reactant of water	mol m^{-3}
CAo	initial concentration of reactant of methane	mol m^{-3}
C_B	concentration of reactant carbon monoxide	mol m^{-3}
C_c	concentration of reactant of carbon dioxide	mol m^{-3}
C_D	concentration of reactant of Hydrogen	mol m^{-3}
C_E	concentration of reactant of Hydrogen	mol m^{-3}
c_α	active carbon species	-
c_β	inactive carbon species	-
c_γ	inactive carbon species	-
dC_A/dt	rate of change of water	moles.s^-
dC_B/dt	rate of change of carbon monoxide	moles.s^-
dCc/dt	rate of change of carbon dioxide	moles s^-
dC_D/dt	rate of change of Hydrogen	moles s^-
dC_E/dt	rate of change of methane	moles s^-
F_{Ao}	Feed flow rate	m^3 s^{-1}
K_1	equilibrium constant	-
K_2	equilibrium constant	-
K_3	equilibrium constant	-
k_1	forward reaction rate constant	mol $m^{-3}s^{-1}$
k_2	backward reaction rate constant	mol m^{-3} s^{-1}
k_3	forward reaction rate constant	mol $m^{-3}.s^{-1}$
k_4	backward reaction rate constant	mol m^{-3} s^{-1}
k_5	forward reaction rate constant	mol m^{-3} s^{-1}
k_6	backward reaction rate constant	mol m^{-3} s^{-1}
M	molar concentration	mol m^{-3}
P_{CH4}	partial pressure of methane	pascal
P_{CO}	partial pressure of carbon monoxide	pascal
P_{H2O}	partial pressure of water	pascal
P_{H2}	partial pressure of Hydrogen	pascal
P_{CO2}	partial pressure of carbon dioxide	m^2
R	gas constant	-
R_{CH4}	rate of reaction	mol.$m^{-3}.s^{-1}$
R_{CO2}	rate of reaction	mol m^{-3} s^{-1}
R_{CO}	rate of reaction	mol m^{-3} s^{-1}
R_{H2}	rate of reaction	mol m^{-3} s^{-1}
S	surface area	m^2 g^{-1}
T_1	initial temperature	K
T_2	final temperature	K
TPR_n	temperature programmed reduction reaction	-

T_m	melting temperature	K
V	volume of reactor	m^3
X_1	extent of reaction	-
X_2	extent of reaction	-
X_3	extent of reaction	-
Y_{CH4}	equilibrium mole fraction of methane	-
Y_{CO2}	equilbrium mole fraction of carbon dioxide	-
Y_{CO2}	equilbrium mole fraction of carbon dioxide	-
Y_{CO}	equilibrium mole fraction of carbon monoxide	-
YH_2	equilibrium mole fraction of Hydrogen	-
YH_2O	equilibrium mole fraction of water	-

Acronym

ASAP	accelerated surface Area and porosimetry system	
Ag	silver	
BET	Braunuer-Emment-Teller (Technique)	-
CaO	calcium oxide	-
CeO_2	cerium oxide	-
CH_x	carboneous species	-
Co	cobalt	-
Cu	copper	-
Cr	chromium	-
C	carbon	-
Fe	iron	-
GHSV	Gas hourly space velocity	-
Ir	iridium	-
K	potassium	-
La_2O_3	lanthanum oxide	-
K_2O	potassium oxide	-
MgO	magnesium oxide	-
ME	micro emulsion	-
Mn	manganese	-
Mo	molybedenum	-
Ni	nickel	-
NiO	nickel oxide	-
Pd	palladium	-
Pt	platinium	-
PVA	poly vinyl acrylonite	-
Rh	rhodium	-
Ru	ruthenium	-
RuO_2	ruthenuim oxide	-
RWGS	reverse water gas shift	-
Sn	tin	-
S_iO_2	silica oxide	-
Ti	titanium	-
TiO_2	titanium oxide	-
WGS	water gas shift	-
WHSV	weight hourly space velocity	-
WO_3	tungsten oxide	

WO_3	tungsten oxide	-
YSZ	yttıra stablısed zeolıte	-
Y_2O_3	yttırıum oxide	-
ZrO_2	zırconıa	-

Greek symbols

γ-Al_2O_3	Gamma alumına	
τ	space tıme	s
θ_{carbon}	amount of carbon accumulated	Kg
λ	Lamda	
β_m	half width length of dıffractıon peak (sample)	
β_s	half wıdth length of dıffraction peak(standard)	
ΔE_{act}	actıvatıon energy	$kJ.mol^{-1}$
ΔH_r	heat of reactıon	$kJ\ mol^{-1}$
ΔH	enthalpy of vaporısatıon	$kJ\ mol^{-1}$
ΔG	gıbbs free energy	$kJ\ mol^{-1}$

CHAPTER 1

INTRODUCTION

1.1 Background and Applications

Synthesis gas constitutes a very important feed in the petrochemical industry. It is a mixture of CO and H_2, an intermediate product for synthesis of oxo-alcohol, acetic acid, dimethyl ether, hydroformylation, and polycarbonates and in the Fisher-Tropsch synthesis to higher liquid hydrocarbons. Also, it finds use in ammonia synthesis and hydro-desulphurisation. Synthesis gas is a major raw material for many chemical industries and is conventionally produced from methane mostly by steam reforming (Kirk and Othmer *et al.*, 1980; Qin and Lapszewicz 1994; 1996, Souza *et al.*, 2001; Ruckenstein and Wang., 2001; Chen *et al.*, 2002).

There has been recently a revival of interest in carbon dioxide reforming of the methane reaction, a process that was originally studied by Fisher and Tropsch in 1928 (Sethuraman *et al*, 2001; Blom *et al*, 1994) The reason for this growing interest is for both environmental and commercial considerations (Blom *et al.*, 1994, Souza *et al.*, 2001). Carbon dioxide and methane are green house gases and also abundant carbon containing resources, and are thus consumed in a useful manner (Xu *et al.*, 2001; Crisafulli *et al.*, 2002) This process offers important advantages compared to steam reforming of methane:

(a) it yields lower H_2/CO product ratios, which are preferable feeds for Fisher – Tropsch plants (Tsipouriari *et al.*, 1994), and oxo-alcohol (methanol) (Seshan *et al.*, 1994; Crisafulli *et al.*, 2002)

(b) it reduces CO_2 and CH_4 emissions, which are both greenhouse gases; (Guerrro-Ruiz *et al.*, 1994; Roh *et al*, 2001) and it is well suited for chemical energy transmission systems (Richardson and Paripatyadar 1990; Blom *et al*, 1994).

There is also a considerable increase in the demand for light olefins such as ethylene, propylene and isobutylene (Sethuraman *et al.*, 2001). The growing interest in their application for the manufacture of highly desirable products such as polyethylene, polypropylene, methyl tertiary butyl ether (MTBE) and ethyl tertiary butyl ether (ETBE)

are highly important in the petrochemical industry. The latter two, being polymeric materials, are produced from isobutylene. These are in turn used as oxygenate additives in reformulated gasoline, a fuel likely to meet the stringent requirement of US clean air act of 1990 (Bridgwater 1994; Ajay *et al.*, 2001)

The need for C_4 hydrocarbons (Fisher-Trospsch): namely isobutene, n-butane, isobutylene and 1, 2- butanes cannot be over emphasised (Sethuraman *et al.*, 2001; Ajay *et al.*, 2001). These intermediate products, in turn, are raw materials for the alkylation processes to produce branched C_8 hydrocarbons (such as isooctane and tri-methyl pentane (TMP)– constituents responsible for the high octane rating of alkylate gasoline (used as high performance gasoline fuel). The C_4 hydrocarbon is also widely used in the production of acetic acid, maleic anhydride and butanediol, and these are important feedstocks for the manufacture of resins, chemicals and tetrahydrofuran (THF). The latter is useful in the manufacture of solvents, specialty chemicals and 1, 4 butane, which is further used to produce plastics and plasticisers. Traditionally, C_4 hydrocarbons are obtained from petroleum sources: natural gas, steam cracking of naphtha and gas oil. According to Rostrup-Nielson (1993), it appears the conventional source of these hydrocarbons by (Fisher- Trospsch synthesis) production is not economically viable, due to the associated high production cost. Therefore, the need to obtain synthesis gas from biomass, which has a large positive environmental impact and the better economics that would be achieved, is likely to make hydrocarbon production by Fisher-Trospsch synthesis an attractive process.
The reforming reaction of methane with carbon dioxide, studied by Fisher and Tropsch was based on nickel and cobalt catalysts (Tsipouriari *et al.*, 1994, Zhang *et al.*, 1996). The growing interest of many researchers towards this process is also generated by the potential for synthesis gas production from biomass (a renewable material) in which gases from a variety of wastes (agriculture, wood waste, crop residue, pulp mill waste, waste oils, municipal sludges (Sethuraman *et al.*, 2001) and animal manures (Nwanchukwu *et al.*, 2000) waste water treatment facilities and flue gas from power plant are used as sources for methane and carbon dioxide (see Figure 1.1). These waste materials can be subjected to conditions such as gasification or an anaerobic digestion under which they decompose to produce biogas. Gasification of solid waste and sewage is a recent innovation (Demirbas 2001). This process can be performed at high temperature in order to optimise gas production. The resulting gas is a mixture of carbon monoxide, hydrogen and methane, together with carbon dioxide and nitrogen.

Source	Component/composition	reference
Municipal sewage sludge	CH_4 = 20-80 vol. %, CO_2 = 15-60 vol. %, H_2O = 2-3 vol % N_2 = 0.5-1 vol. %, H_2S = 1 vol. %	Boyles (1984)
Wood waste	H_2 = 20%, CO = 25%, CO2 = 10%, C_xH_4 = 3%, Higher hydrocarbons = 1% N_2 = 40%, Other = 1%	White and Plaskett (1981)
Pig manure	CH_4 = 65%, CO_2 = 35%	White and Plaskett (1981
Cattle manure	CH_4 = 80%	Slessers and Lewis (1981)
Paper waste sludge	CH_4 = 60%	Slessers and Lewis (1981

Table 1 1 Biogas composition

Whilst, an anaerobic digestion is the decomposition of biomass through bacterial action in the absence of oxygen. Products from both gasification and anaerobic processes also include H_2O (1%) and trace amount of H_2S (1000-3000 ppm), and NH_3 (80-100 ppm) (Effendi *et al.*, 2002).

Conventionally, synthesis gas is produced by steam reforming of natural gas (methane). Until recently, partial oxidation (POX) (Ashcroft *et al*, 1990) and CO_2 reforming (Rostrup-Nielsen 1993) of natural gas to syngas have attracted much academic and industrial interest because of the potential to reduce the cost of synthesis gas and its potential application in energy storage technology. The overall stoichiometries for the three reactions are presented as follows:

$$CH_4 + H_2O \leftrightarrow CO + 3H_2 \qquad (\Delta H_{298} = +206 \text{ kJ/mol}) \qquad (1.1)$$

$$CH_4 + 1/2O_2 \leftrightarrow CO + 2H_2 \qquad (\Delta H_{298} = 38 \text{ KJ/mol}) \qquad (1.2)$$

$$CH_4 + CO_2 \leftrightarrow 2CO + 2H_2 \qquad (\Delta H_{298} = + 247 \text{ KJ/mol}) \qquad (1.3)$$

However, there are some drawbacks in reforming that employs all three routes. These are high product ratio, (steam reforming) carbon deposition and catalyst deactivation (CO_2 reforming). The latter is a major problem that has drawn attention of several researchers. Unfortunately, there is no established industrial technology for carbon dioxide reforming of methane, in spite of the potentially attractive incentives for a large number of applications The principal reason is the carbon-forming reaction

$$CH_4 \leftrightarrow C + 2H_2 \qquad (1\ 4)$$

which quickly deactivates conventional reforming catalysts if used without steam A similar problem occurs, if there is CO disproportionation as shown in equation (1.5).

$$2CO \leftrightarrow C + CO_2 \qquad (1.5)$$

1.2 Justification for CO_2/CH_4 reforming

Dry CO_2 reforming yields synthesis gas with a high CO concentration In the CALCOR process, dry reforming is used to produce pure CO (Wang *et al.*, 1996). CO_2 reforming is economically advantageous over the other synthesis gas producing processes, depending on the required H_2/CO ratio. CO_2 reforming is preferred over partial oxidation of natural gas when a H_2/CO ratio of lower range is needed. Moreover, an economic evaluation of the production of 100,000 tonnes of acetic acid also revealed that the use of CO_2 reforming provides synthesis gas resulted in lower operating costs compared to steam reforming, or partial oxidation. As was mentioned earlier, the major draw-back of dry CO_2 reforming is the high thermodynamic driving force to produce coke The CALCOR and the SPARG process (sulphur passivated reforming) (Udengaard *et al.*, 1992) have overcome the coking problem during reforming

1.2.1 CALCOR Process

The CALCOR process aiming at production of high purity CO from natural gas (Wang *et al.*, 1996) was developed to overcome problems involved in transportation of the toxic CO and the need for high product quality. These factors favour the CO production on-site.

This process operates under dry reforming conditions in an excess of CO_2 The prevention of carbon formation is achieved by using catalysts with different activities and shape and by their specific arrangement throughout the reformer tubes. The CO produced contains less than 0 1% of methane.

1.2.2 SPARG Process

The SPARG process was first commercialised at Sterling Chemical Inc. Texas, USA in 1987 in order to reduce the syngas H_2/CO ratio from 2.7 (obtained from steam reforming) to 1.8 without changing the steam reforming facilities (Udengaard *et al.*, 1992).

Introducing a partially sulphur-poisoned nickel catalyst minimized the increased probability of carbon formation and the associated catalyst deactivation. The process operates at 1188K–1218K that decreases the methane slip-unreacted methane in the product stream (one of the major problems in CO production. The impurities in the CO (mainly H_2 and CH_4) can cause inferior mechanical properties of polycarbonates made from CO. Therefore, low methane slip in the reforming step is required.

Although the problems related to catalyst deactivation are minimized, the SPARG process operates in the presence of sulphur. Thus, traces of sulphur might be present in the synthesis gas produced. When a pure synthesis gas is required an additional cleaning step will be necessary which involves an additional investment. Therefore, a catalyst that operates carbon-free without the addition of sulphur is preferred.

1.2.3 Chemical energy transmission

Highly endothermic reactions such as steam reforming and CO_2 reforming are candidates for chemical transmission systems (Richardson and Paripatyadar 1990, Wang *et al* , 1996). An example of an energy transmission system is the ADAM-EVA process (Figure 1.1).
In the EVA plant, steam reforming is carried out using a nuclear power source to supply the required energy. The resulting synthesis gas is transported to the ADAM plant where methanation of the synthesis gas is performed to release energy. When CO_2/CH_4 reforming is used for the energy storage (CO/H_2) there are two possibilities to regain the energy that exist. In the closed loop thermo chemical heat pipe, the CO/H_2 mixture is converted back to CO_2/CH_4 and the process can start again.

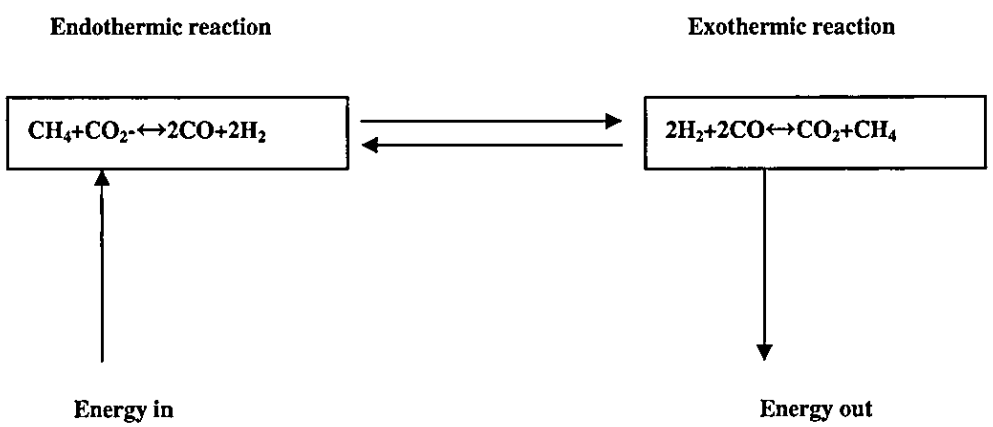

Figure 1.1 A chemical energy transmission system (Wang *et al.*, 1996)

While with the open loop system, the resulting CO/H_2 mixture is combusted to CO_2 and H_2O when energy is needed.

Despite the numerous and promising applications for CO_2 reforming of methane for synthesis gas production, it has not gone beyond laboratory research due to the coking of catalysts.
It has been established (Erdohelyi *et al.*, 1993; Zhang *et al* , 1996; Rostrup-Nielsen and Bak Hansen 1993) that though the noble metals (Rh, Ru, Pt) do not suffer carbon deposition, they are very expensive and of limited availability, making the process economically nonviable.

While the non noble metals Co, Ni and also Fe are very sensitive to deactivation by coking, they are cheap and readily available. Therefore, it would seem to be worthwhile to develop improved and effective catalysts that could be operated without carbon deposition to achieve the goal, commercialising CO_2 reforming of methane

1.3 Objectives

The advantages of conducting CO_2 reforming of methane have been discussed above. The major draw back of CO_2/CH_4 reforming of methane is catalyst deactivation due to carbon formation As discussed above, adding steam or O_2 to the reactants can enhance the stability of reforming of catalysts. A more effective way to overcome the coking problem is the development of a catalyst on which coke formation is kinetically suppressed.

Attempts to eliminate carbon deposition are known to lead to poisoning of the catalyst. Poisoning may also be caused by the presence of impurities in the feed gases (biogas) e.g. NH_3 etc. Added to the development of an effective catalyst capable of operation without significant carbon deposition is a desire to elucidate the mechanism leading to catalyst poisoning. The latter have not been addressed in the literature of CO_2 reforming of methane.

Therefore, the objectives are.

(1) To investigate CO_2 reforming of methane over effective supported nickel catalysts capable of long term operation without significant carbon deposition. Modification of active components (promotion and support materials).

(2) To investigate catalyst poisoning arising as a result of combating carbon deposition and/or inherent compounds in biogas that may cause catalyst poisoning

1.4 Structure of the thesis

Chapter 2 contains a review of the published literature, relevant to carbon dioxide reforming of methane, carbon deposition and the kinetics of reforming of methane.

A summary is presented at the end of each sub-section to draw together the common findings by various authors. A discussion of catalyst poisoning is also included.

Chapter 3 describes the experimental apparatus and the methods employed which include the reforming of methane, preparation and characterisation of catalysts. The techniques used for catalyst characterisation include surface area and pore size distribution, carbon monoxide chemisorption, atomic absorption spectrophotometry, scanning electron microscopy, X-ray diffraction and temperature–programmed reduction. Also included are reactor temperature profile determination, gas chromatograph optimisation, and calibrations, activity, stability and catalysts poisoning test. A kinetic model formulation is also included.

Chapter 4 discusses the experimental results obtained over nickel-based catalysts. This includes catalyst characterisation, the effects of support on activity, stability and space velocity on conversion of CH_4 and CO_2 as well as CO yield at different temperatures. The various catalysts studied are $Ni/\gamma\text{-}Al_2O_3$, $Ni/MgO/\gamma\text{-}Al_2O_3$, $Ni/La_2O_3/\gamma\text{-}Al_2O_3$, $Ni/ZrO_2/\gamma\text{-}Al_2O_3$ and Ni/Pr_2O_3.

Chapter 5 discusses the results obtained over palladium and copper promoted Ni catalyst. Catalyst characterisation and catalyst performance in terms of activity and stability are discussed. Also included is the effect of space velocity on CH_4 and CO_2 conversion and CO yield. The effects of metal loading (palladium and copper) are also included. The catalysts studied are 15 wt% $Ni\text{-}Cu/\gamma\text{-}Al_2O_3$ and 15 wt% $Ni\text{-}Pd/\gamma\text{-}Al_2O_3$

Chapter 6 discusses the effect of NH_3 and H_2O (catalyst poisoning) on catalyst activity and stability obtained using the following catalysts; $Ni/\gamma\text{-}Al_2O_3$ (reference catalyst) $Ni/ZrO_2/\gamma\text{-}Al_2O_3$, $Ni\text{-}Pd/\gamma\text{-}Al_2O_3$ (0.25 wt%) and $Ni\text{-}Cu/\gamma\text{-}Al_2O_3$ (0.25 wt%) catalyst Also included is the effect of space velocity on conversion of CH_4, CO_2 and CO yield.

Chapter 7 discusses a set of conclusions and recommendations for further work.

CHAPTER 2

LITERATURE REVIEW

2.1 Introduction

Catalytic reforming of methane with carbon dioxide (CO_2) to produce synthesis gas has attracted growing interest in the last few decades. Particularly with respect to the chemical utilisation of methane and CO_2 intimately related to the environment and energy resources (Tomishige *et al.*, 1998) Several investigations have been carried out on the production of synthesis gas from gas fields, and biomass, by the reforming process, employing steam reforming as the conventional method, is well documented in the literature (Choudhary *et al.*, 2001; 2002) However, a number of practical limitations such as coke formation, high product H_2/CO ratio which is not suitable for the Fisher-Trospsch synthesis of liquid hydrocarbons, high energy requirements, poor selectivity for carbon monoxide and high capital and operating cost making the process uneconomical.

2.2 Biogas production and economics

Increasing fuel prices during the last decade have focused interest on the utilization of biomass as an additional source for the production of gaseous and liquid fuels (Cheremisinoff *et al.*, 1980; Bridgwater 1990). Biomass, one of the most attractive renewable energy sources available, can be converted to biogas by anaerobic or aerobic digestion (Effendi *et al.*, 2003) Raw materials used in commercial methane generation have been traditionally classified as waste materials, which include crop residues, animal waste, domestic waste and various urban wastes.

The amount and quality of gas produced depends on the biomass used. About 50–70% methane and 30–50% carbon dioxide can be produced (Cheremisinoff *et al.*, 1980, Effendi *et al.*, 2003), including trace amount of ammonia, hydrogen sulphide and moisture

Methane was first recognised as having practical and commercial value in the 1890's in England, where a specially designed septic tank was used to generate the gas for the purpose of lighting streets (Cheremisinoff *et al.*, 1980).

Methane was produced to fuel automobiles in Europe, during World War 11. The generation of the gas have also been successfully applied to meeting energy needs in rural areas.

In India, methane generating units and plants using cow manure has been in operation for years (Cheremisinoff *et al.*, 1980). More than 7500 methane generating devices utilising pig manure has been constructed and Korea 24,000 units (from 1969–1973). In the united state, there has been considerable interest in process of anaerobic digestion as an approach to generating a safe, clean fuel, as well as a source of fertilizer (Cheremisinoff *et al.*, 1980).

2.3 Reforming Medium

The conventional method of methane reforming is to employ steam as the reforming medium. However, the reforming process can be conducted by other method. They are the oxy-steam (oxygen and steam), partial reforming (using oxygen) and carbon dioxide reforming (dry reforming). Steam reforming and carbon dioxide reforming are endothermic whilst partial reforming is exothermic. Partial oxidation reforming, an exothermic process has several advantages over steam reforming, notably, a greater selectivity and because of the more favourable H_2/CO product ratio obtained. The corresponding carbon dioxide reforming of methane has been extensively studied and is widely used in the secondary process to reduce the H_2/CO ratio obtained by steam reforming (Ashcroft *et al.*, 1991).

2.3.1 Steam Reforming of Methane

Steam reforming has been extensively studied particularly on nickel (Ni) catalysts (Qin *et al.*, 1996) and it has two distinct drawbacks. The reaction is industrially operated at temperature of 1000-1130K, total pressure between 2-4 MPa and a partial pressure of H_2O/CH_4 varying from 2-6 pascal. The use of excess H_2O in the reactant gas is to inhibit the carbon deposition The reaction, is strongly endothermic, to provide the required thermal energy for the methane–steam reforming reaction. Hence heavy demands are made on the thermo-stability of both the materials of the reactor tubes and the catalyst (Qin *et al.*, 1996).

Operation under these conditions has led to the higher H_2/CO ratio than is required for subsequent industrial processes (Qin *et al.*, 1996, Tomishge *et al.*, 1998). This is as a result of the presence of excess H_2O, which favours the successive water gas shift reaction, that is suitable for hydrogen production but not for the production of liquid hydrocarbons and methanol. Therefore, the major commercial interest in the catalytic reforming of CH_4 with CO_2 originates from this need to obtain a product having a low H_2/CO ratio. On the other hand, there are some natural gas fields containing considerable amounts of CO_2 which could be conveniently reformed at the gas fields and also, it is a possible means to process biogas from biomass.

2.3.2 Partial Oxidation Reforming of Methane

Partial oxidation reforming produces synthesis gas in a mildly exothermic reaction with lower H_2/CO ratio, compared to steam reforming. It has been suggested that partial oxidation proceeds via a two step mechanism. In spite of the fact that, the partial oxidation of methane to synthesis gas is mildly exothermic, (ΔH = -5.4 kcal/mol), the process is highly hazardous and difficult to operate. It is difficult to avoid local establishment of explosive gas mixtures during mixing of methane and oxygen.

Moreover, pure oxygen instead of air must be used despite the fact that the production of pure oxygen is expensive (Qin *et al.*, 1996). In order to overcome, these limitations, efforts have been made to carry out an exothermic oxidative conversion simultaneously with endothermic steam reforming Ashcrof *et al.*, 1991 (Choudhary *et al.*, 2001) Alternately, both the exothermic and endothermic reactions could be coupled making the process not only highly energy efficient but also safe to operate.

2.3.3 CO_2 Reforming of Methane (Dry Reforming)

In recent years, considerable attention has been paid to global warming due to the greenhouse effect. The reduction and utilisation of greenhouse gases such as carbon dioxide is, therefore becoming of ever-greater importance (Hayashi *et al.*, 2001).

The catalytic reforming of methane with carbon dioxide to synthesis gas has been proposed as one of the most promising technologies for the utilisation of carbon dioxide as carbon–containing materials. The synthesis gas produced by this reaction has a high CO content, which is favourable for the synthesis of valuable oxygenated chemicals. The synthesis gas thus generated, has a low H_2/CO ratio (≤ 1) and is therefore suitable for the Fisher–Trospsh synthesis of liquid hydrocarbons and for the oxo–synthesis or synthesis of oxygenates (Souza *et al*, 2001; 2002; 2004). CO_2 reforming of methane has been comprehensively studied over the past few years (Erdohelyi *et al.*, 1993; Zhang *et al.*, 1996; Mark *et al.*, 1996).

However, the major disadvantages of CH_4-CO_2 reforming, is the high potential for coke formation (Souza *et al.*, 2001). This process is more prone to coke deposition than steam reforming because of the low H/C ratio in the reactant gas.

In addition, carbon deposition seems to be unavoidable even under higher CO_2/CH_4 ratios (Tomishige *et al.*, 1998). Thermodynamically, the limitation of carbon deposition can be estimated by the H/C and O/C atomic ratios in the reactant gas (Rostrup-Nielsen *et* 1994; Ruckenstein and Hu 1996)

The amount of carbon deposition decreases as the atomic ratio of H/C and O/C increase. It has also been suggested that carbon deposition can be suppressed when the metal is supported on a metal oxide with a strong Lewis basicity (Zhang and Verykios 1994). The increase in Lewis basicity of the support increases the ability of the catalyst to chemisorb CO_2 in the reforming of methane, and H_2O in steam reforming forming adsorbed species. These species react with carbon to form CO, resulting in a reduction in coke formation

Carbon dioxide reforming is estimated to have economic advantages over other synthesis gas production routes (Bitter *et al.*, 1997). Basically, supported Ni or noble metals are reported as potential catalysts for the reforming reaction (Richardson and Paripatyadar 1990; Ascroft *et al.*, 1991; Udengaard *et al.*, 1992; Rostrup–Nielsen and Hansen 1993; and Erdohelyi *et al.*, 1993). However, catalyst deactivation is a serious challenge, particularly for the non noble metals and must be overcome by development of effective catalysts.

Two potential causes of catalyst deactivation exist;

(i) Carbon deposition (Ashcroft *et al*, 1991; Richardson and Paripatyadar 1990)
(ii) Sintering of the metal particles (Ruckenstein and Hu 1996)

However, most authors suggested, however, that coke formation is the main cause of deactivation (Nagaoka *et al*, 2001).

2.4 Deactivation of Catalysts during the Carbon Dioxide Reforming of Methane

There is no established industrial technology for the carbon dioxide (CO_2) reforming of methane, in spite of the fact that the economical and environmental benefits constitute an attractive incentive. The major problem lies in catalyst deactivation caused by carbon deposition and/ or sintering and plugging of reactors or breakdown of the catalysts (Rostrup-Nielsen 1994). Although Ni and Co based catalysts are easily available, they deactivate rapidly when the conventional supports, such as Al_2O_3 and SiO_2 are employed. The exception to this is MgO when it is used as alkaline promoters (Chang *et al.*, 2000).

Sintering accelerates carbon deposition since large metal ensembles stimulate coke formation. Due to the coexistence of both reductive (CH_4, H_2 and CO) and oxidative (CO_2 and H_2O) species in CO_2/CH_4 reforming, the atmosphere in the reactor is both reductive and oxidative During the reaction, a fraction of the catalyst being oxidised is reduced again to its former state by carbon species, thereby generating a dynamic redox process. The reductive atmosphere stimulates the generation of metallic catalysts and the dissociative adsorption of CH_4, while the oxidative atmosphere favours the oxidation of the metallic catalysts. When the former dominates, an excess of carbon is deposited; with the later dominating, the number of metallic sites decreases due to their oxidation state and subsequent restructuring of catalysts occurs and this may lead to severe catalytic deactivation.

Tsipouriari *et al.*, (1994) suggested that the rate of deactivation is lower at higher conversions and decreases with an increase in temperature

Ruckenstein and Wang (2002) investigated CO_2 reforming of methane over Co/γ-Al_2O_3 catalysts, at different calcination temperatures (T_C = 773K and 1273K), with different catalysts loading (2 wt%-20 wt%) in order to correlate carbon deposition and catalytic deactivation. According to their report, the stability of Co/γ-Al_2O_3 catalysts was strongly dependent on the Co loading and calcination temperature.

They observed stable activities with Co loadings of 6 wt%, $T_{calcination}$ = 773K and 9 wt%, $T_{calcination}$ = 1273K. With high Co loading (> 12 wt%) , notable amounts of carbon were accumulated and deactivation also observed. Severe deactivation over 2 wt% with carbon deposition was noted at $T_{calcination}$ = 773K or $T_{calcination}$ = 1273K. They suggested that the deactivation of the latter may be due to the oxidation of the metallic sites. They also observed a colour change during calcination with 2 wt% and 6 wt% Co/γ-Al_2O_3, and in the reforming reaction, probably as result of spinel ($Co_2Al_2O_4$ and $CoAl_2O_4$) formation (Wang and Ruckenstein 2001). The colour change is an indication that a large number of metallic Co sites were oxidised and restructuring of catalysts took place to form $CO_2Al_2O_4$ and $CoAl_2O_4$ during the reforming reaction over Co/γ-Al_2O_3 (1273K), with Co loading below 9 wt%.

Ruckenstein and Wang (2002) also observed that carbon deposition with 2 wt% loading was much lower than that with 20 wt%, although the deactivation was higher over the former than the latter. They also noted that the carbon deposited over 2 wt%/Co/γ-Al_2O_3 catalyst was more difficult to remove with CO_2 than that deposited over 6 wt%/γ-Al_2O_3 12 wt%/γ-Al_2O_3 and 20 wt%/γ-Al_2O_3 catalysts. The difficulty in the removal of the carbon deposited on the 2 wt%/γ-Al_2O_3 catalyst with CO_2 may be due to fewer accessible metallic Co sites being available

In summary, carbon deposition probably may not be the only cause for catalysts deactivation. The oxidation of the metallic sites leads to a decrease of the total number of metallic sites, which also causes catalytic deactivation.

2.5 Carbon Deposition with Carbon Dioxide Reforming of Methane

Due to the inherent inertness of methane, a high temperature (typically, 1073K–1173K) is needed to achieve a meaningful yield during reforming. Under such severe conditions, excess carbon deposition occurs on the surface of the catalyst. This constitutes a major drawback in carbon dioxide reforming of methane (Ruckenstein and Wang 2002). Although the noble metal -based catalysts (such as Rh, Ru, Pd and Pt) can provide high activity and selectivity with little or no carbon deposition, they are unsuitable for large-scale commercial use because of their limited availability and cost (Ascroft *et al*, 1991; and Rostrup-Nielsen 1993).

Numerous mechanistic studies have suggested that during CH_4/CO_2 reforming, CH_4 is decomposed on the metallic sites to a number of reactive carbon species. The carbon species are being oxidised to CO by the oxygen–containing species that originate from CO_2 that chemisorbed on the support (Rostrup–Nielsen 1993 and Qin *et al*, 1996). The rate of carbon accumulation on the catalyst surface is determined by the relative rates of the generation of carbon species and their oxidative removal When the rate of generation is faster than the oxidative removal, excess carbon deposition will occur (Ruckenstein and Wang 2002).

Nagaoka *et al*, (2001) described the reaction model and the coking scheme over Pt/Al_2O_3 at high reaction temperatures (≥ 1070K) presented in Figure 2 1. In this model, CH_4 is decomposed both on Pt and on the acid sites of the support to form CH_x (coke) species. In their investigation, they observed that only the species on Pt (active phase) are reactive towards CO_2 On the other hand, CO_2 is also activated both on Pt particles and on the support. The two existing reaction pathways presented in the model (see Figure 2.1) indicate that the carbon (on the Pt particles) is oxidised by CO_2 to CO, i.e. (r_1) and on the boundary of Pt and the support (r_2) According to their report, the removal of coke from the vicinity of the perimeter(r_2) is assumed to be faster than that of r_1 thereby keeping some activity for long time on stream while the CH_4 decomposition rate on $Pt\text{-}Al_2O_3$ (r_2) is faster than r_1 (resulting to the deactivation due to coking.

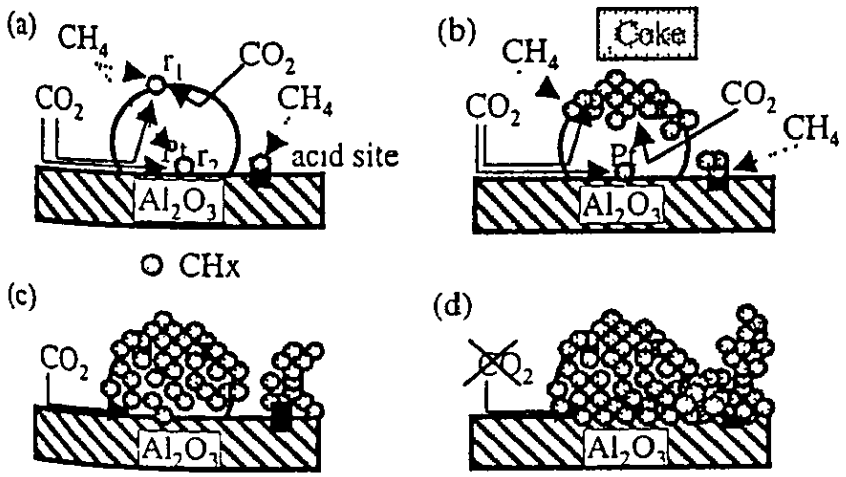

Figure 2.1 Model of Reaction and Coking scheme over Pt/Al_2O_3 at High Reaction Temperatures (Nagaoka *et al.*, 2001).

It is suggested that the perimeter is still available for reaction, even when most of the platinum (Pt) was covered by monolayer of coke. Nagaoka *et al.*, (2001) also noted that coke on the support was difficult to remove at the temperature employed that led to the build up of coke resulting in the blocking of the CO_2 activation sites on the perimeter, which eventually led to complete deactivation. They also observed that the initial CH_4 decomposition rate of Pt/ZrO_2 was slower compared to those achieved with Pt/Al_2O_3. They investigated the type of coke formed on the catalyst by Temperature-programmed reaction (TPRn) with CO_2. After exposure to CH_4/He stream for a period of 5 minutes, two types of coke were formed, and increased drastically after a period of 10 minutes.

Tsipouriari *et al.* (1994) have also studied the reforming of methane with CO_2 over rhodium supported on SiO_2, TiO_2, γ-Al_2O_3, MgO, CeO_2 and YSZ (ZrO_2, Y_2O_3) catalysts in the temperature range 923K–1023K. They noted very small amount of carbon accumulated on the catalysts and this was independent of reaction time ($\theta_{carbon} < 0.03$).

On the other hand, the amount of carbon accumulated on Rh/Al_2O_3 catalyst, after 10 minutes on stream decreased with an increase in reaction temperature ($\theta_{carbon} = 0.6$ at 923K against $\theta_{carbon} = 0.35$ at 1023K).

According to Tomishige *et al.*, (1998), deposited carbon is formed via different routes, each influencing the morphology of the carbon The most common types are whisker-like carbon, encapsulating carbon and pyroytic carbon.

In conclusion, coke formation may depend both on the support and temperature employed. The two catalysts Pt/ZrO_2 and Pt/Al_2O_3 under study revealed that the former showed stable activity at 1070K temperatures while Pt/Al_2O_3 catalysts deactivation occurred only partly at high temperatures ($\geq$ 1070K) and completely lost their activity at lower temperatures (< 875K). This difference may probably be due to hydrogen desorption via metallic Pt which facilitates coking and the formation of Lewis acid sites which also catalyse the decomposition of methane. The Lewis acid site catalyse in a formation of carbon was concluded to have been dominant at higher temperature ($\geq$ 1070K), leading to an enhanced coke accumulation on the support. In the case of Pt/ZrO_2, the absence of appreciable amounts of acid sites on zirconia resulted in Pt being the dominant site for coke formation and hence, at both high and low temperatures more coke was formed on Pt/ZrO_2 compared to ZrO_2. However, this is not in agreement with the work by (Bitter *et al*, 1999), who observed less coke formed on Al_2O_3 compared to Pt/Al_2O_3, at lower temperature.

2 5.1 *Sintering of Catalyst during Reforming of Methane*

Sintering is caused by growth or agglomeration of small crystals which make up a catalyst or support. In supported metal catalysts, sintering may occur when the catalysts are used for long periods at high temperature. The structural rearrangement observed during sintering may lead to a decrease in the surface area of the catalyst, and consequently an irreversible reduction in catalytic sites. Supported metals are often stable at low temperatures in highly dispersed forms and may work for years in a commercial catalyst, but their stabilities are limited and the dispersions subject to change (Gates, 1991) Two mechanisms, believed to occur simultaneously which are used to explain sintering (Teixeira and Giudici 2001).

(1) Atomic migration as a result of variations in the interfacial energy is the driving force for particle growth. This involves the detachment of species from the metal crystallites (Flynn and Wanke, 1974). These species diffuse on the support or through the gas phase, and they are subsequently captured by collision with either stationery or mobile particles. These particles can also nucleate new particles or redistribute themselves to minimize the overall interfacial energy resulting in the growth of larger particles at the expense of smaller ones.

(2) A random migration of the whole particles over the support surface followed by collision and coalescence.

Teixeira and Giudici (2001) identified the problem of sintering in steam reforming at temperature ranges (773K–1223 K) and high steam partial pressures over Ni/Al_2O_3 catalysts Sintering occurs if the temperature of the catalyst exceeds approximately (1/3) of its melting temperature (applies if steam is present, because steam facilitates the reorganisation of many metals) to (1/2) of its melting temperatures (dry condition) (Missen *et al.*, 1999). Table 2 lists common metals catalysts and temperatures at which the onset of sintering can be expected to occur. The effect of sintering includes·

(i) Loss of activity
(ii) Changes in selectivity of reactions

These two effects have implications for reactor life and safety (Rostrup–Nielsen 1994)
To prevent sintering, catalysts can be doped with stabilisers that may have a high melting point and /or prevent agglomeration of small crystals (e g. magnesia) Missen *et al.*, 1999).

Metal	Sintering temperature (K)[(1/3) T_m]
Cu	633
Fe	773
Ni	773
Pt	843
Pd	773

T_m melting temperature

Table 2. Sintering temperatures for common metals (Missen *et al* , 1999)

Flynn and Wanke (1974) reported changes in metal surface area on supported catalysts during use or treatment at high temperatures. They found that loss of catalytic activity was associated with an increase in the particle size of the metal.

Similarly, Ermakova *et al.*, (1999) found that nickel catalysts prepared by calcining NiO at 573K contained very fine particles of NiO (3 nm). Hence the metal particles were found to be protected against sintering in the course of reduction, after impregnation with hard-to-reduce oxides (HRO) SiO_2, Al_2O_3, ZrO_2, TiO_2 and MgO. They found that intermediate efficiency was observed with MgO and ZrO_2 but Al_2O_3 and TiO_2 offered only low protection against sintering

2.5.2 *The Origin of Coke Formation and its effect on catalyst deactivation during reforming of Methane with CO_2*

Several groups have proposed that coke-causing deactivation originates from CH_4 decomposition (Rostrup-Nielsen and Hansen 1993; and Staag *et al* , 1998).

Kevlen *et al.*, (1997) performed thermogravimetric tests on Pt/Al_2O_3 and Pt/ZrO_2. They observed that for supported Pt catalyst carbon was not formed via CO disproportionation, but CH_4 decomposition occurred despite the fact that the Bouduoard reaction ($2CO \rightarrow CO_2 + C$) is thermodynamically feasible under reaction conditions.

This is in good agreement with the conclusion reached by Nagaoka *et al.*, (2001), using temperature–programmed oxidation (TPO) over Pt/Al_2O_3 and Pt/ZrO_2 at 1070K.

According to Tomishige *et al.*, (1998), the main carbon deposition routes are methane decomposition and CO disproportionation. However, it is not a generally accepted opinion, because many research groups are still investigating the true origin of coke formation.

Similarly, Swaan *et al.*, (1994) have also reported that reactive surface carbon originates from methane and that the less active carbon accumulation leads to catalyst deactivation, using 13 C labelling studies. This is in contrast to an earlier report in literature, claiming that accumulated carbon species originate from CO_2

2.5.3 *Effect of Active Site (Lewis Acid Site) on Coke Formation*

Lewis acid sites are solid surfaces that can accept a pair of electrons. Metal oxides such as AL_2O_3 can be treated with compounds of high Lewis acid strength to attain high activity during reforming but it attracts carbon deposition. Bitter *et al*, (1999) noted that high concentration of Lewis acid sites on supports also enhances carbon deposition. As already mentioned in section 1.2.3, reduction of carbon formation in catalysts can also be achieved by increasing the Lewis basicity on the support (Zhang and Verykios 1994).

2.6 The Effect of Support on catalyst stability during CO_2 reforming of Methane

Although the development of catalysts based on non noble metals (e.g. Fe, Co and Ni), is of interest from the industrial point of view, numerous studies have demonstrated that noble metal catalysts exhibit better activity and suffer less carbon deposition (Erdohelyi *et al.*, 1993; Rostrup-Nielsen *et* and Hansen 1993; and Zhang *et al.*, 1996). There is good evidence that the support utilised may have a significant effect on the overall catalytic behaviour (Souza *et al.*, 2001).

Shimizu *et al.*, (2001) reported high selectivities (76–85%) for CH_4 reforming over ZrO_2 supported WO_3 as an oxidant whilst being heated by direct irradiation with solar –simulated light to 1080K-1156K. The H_2/CO ratio of the produced synthesis gas was about 2.4, which is more favourable for methanol production than the synthesis gas produced by conventional steam reforming of methane. The solid product being WO_2 phase was re-oxidised into WO_3 to generate H_2 below 1173K. Under the solar–simulated reforming over WO_3, the formation of reactive oxygen species such as O^- is considered to accelerate the oxidation of CH_4 to synthesis gas.

Ikenga and co-workers (2000) examined CO_2 reforming of methane over Ru-loaded La_2O_3, Y_2O_3, Al_2O_3, TiO_2, SiO_2 and MgO catalysts. They found that Ru/La_2O_3 and Ru/Y_2O_3 catalysts showed a high methane conversion without carbon deposition The catalytic activity increased gradually in the course of the reaction. They also noted that pre-treatment of the catalyst, under various atmospheres (CH_4, H_2, CO_2) revealed that the CO_2 pre-treatment markedly enhanced catalytic activity. Also, the product H_2/CO ratio increased from 0 83 to 0.93 after CO_2 pre-treatment The CO_2 pre-treatment reduced part of the Ru species to Ru metal. They attributed the high activity to the metallic Ru coexisting with RuO_2.

Nagaoka *et al* , (2001) carried out a comparison between Pt/Al_2O_3 and Pt/ZrO_2 catalysts and noted a variation in stability as a function of temperature. They studied the mechanistic details of coking and its relation to catalyst performance at temperatures (< 1070K) (TPO), They noted that Pt/ZrO_2 catalysts maintained stable activity for 500 hours at all temperatures, while Pt/Al_2O_3 catalysts deactivate almost completely at low temperature (875K) but only partly at high temperature (< 1070K) using Temperature programmed desorption and TPR_n. They speculated that Pt/ZrO_2 catalysts were stable due to the high reactivity of CO_2 at the metal–support boundary, which is in good agreement with the conclusion reached by Michael *et al.*, (1998). Three factors were suggested to have caused the high catalytic stability of Pt/ZrO_2 in CO_2/CH_4 reforming.

(i) Coke on Pt (supported on ZrO_2) is more reactive toward CO_2 than coke on Pt (supported on Al_2O_3) under reforming conditions).

(ii) Methane decomposition is slower on Pt/ZrO_2 than on Pt/Al_2O_3 and;

(iii) Coke is hardly formed on the ZrO_2 support because it lacks a significant concentration of strong Lewis acid sites.

Souza *et al*, (2001) reported the effect of different supports on catalyst activity and carbon deposition resistivity by studying the reforming reactions over Pt on Al_2O_3, ZrO_2 and various mixtures of ZrO_2 and Al_2O_3 ranging from (1 to 20%). Although the Pt/Al_2O_3 catalyst deactivated significantly in 20 hours on stream at 1073K, they observed that zirconia-containing catalyst exhibited much higher stability even after 60 hours on stream. This is in good agreement with the findings by (Nagaoka *et al.*, 2001).

Similarly, Solymosi *et al.*, (1994) reported the effect of support on the decomposition of methane over supported Ir catalysts with Al_2O_3, TiO_2, SiO_2 and MgO as supports. They noted that the most effective among the supports was MgO.

Richardson and Paripatyadar (1990) compared the catalytic performance of 0.5 wt% (Rh/γ-Al_2O_3) and 0 5 wt% (Ru/γ-Al_2O_3) catalysts for the reforming of CH_4 with CO_2, in the range of 873K-1073K. They found that the two catalysts have comparable activities, but the Ru/γ-Al_2O_3 catalyst exhibits better stability than the Rh/γ-Al_2O_3

Erdohelyi *et al.*, (1993) studied the influence of the catalyst support on the catalytic performance of CO_2 reforming over Rh and Pd crystallites supported on TiO_2, Al_2O_3, SiO_2 and MgO at temperatures ranging from (673K–1073K), $CH_4/CO_2 = 1$. In their study, they observed that Pd/TiO_2 catalysts appeared to be the best both in terms of specific activity and low coke deposition compared to the other supports Al_2O_3, SiO_2 and MgO studied.

Tsipouriari *et al.*, (1994) studied the effect of supports on the reforming of methane with carbon dioxide over Rh supported on SiO_2, TiO_2, γ–Al_2O_3, MgO, CeO_2 and YSZ (ZrO_2 and Y_2O_3) catalyst in the temperature range of 923K–1023K and pressure of 1 bar.

The activity of the catalysts decreased in the following order, Rh/YSZ > Al_2O_3 > TiO_2 > SiO_2 >> MgO, which is in good agreement with the report by (Basini and Sanfilippo, 1995) whose report also indicated the decreasing order Rh/Al_2O_3 > Rh/TiO_2 > Rh/SiO_2.

Claridge *et al.*, (1993) have shown that cerium oxide is able to convert methane and carbon dioxide to synthesis gas at 873K-1073K. They found that the catalyst has intrinsically low activity and high tendency towards carbon formation.

Bradford and Vannice (1999) noted the order of turnover frequencies of Ru catalyst supported on different supports (TiO_2 > Al_2O_3 >> C) with CO_2 reforming of CH_4 in the absence of heat and mass transfer effects. However, the most popular support for platinum catalysts is ZrO_2. Bradford and Vannice (1999); and Bitter *et al.* (1998; 1999) have shown that there is less coke formation on Pt/ZrO_2 A very limited number of cobalt catalysts have been studied with carbon, SiO_2 and Al_2O_3 supports (Inui 2001). However, it was found that the coke deposition is markedly reduced in the presence of MgO. According to Bradford and Vannice (1998), the higher stability and coking resistively of Pt/ZrO_2 may be associated with strong Pt–Zr interactions, resulting in the formation of ZrOx species on the Pt surface. Moreover, ZrO_2 seems to have significant influence on the reaction mechanism of CH_4–CO_2 reforming (Staag *et al* , 1998 and Bitter *et al.*, 1997; 1998)

In summary, the catalyst support can play a significant role in the dry reforming reaction by promoting the dissociation of CO_2. This dissociation aids the removal of carbon deposits from the metal. ZrO_2 supports, which has the ability to promote CO_2 dissociation exhibits higher activities and stability, compared to other supports reported in literature. The role of the support has received significant attention, because it is involved in the participation of two independent reaction paths. According to the mechanism proposed, CH_4 decomposition takes place on the metal, resulting in the production of H_2 and formation of carbonaceous deposit. The role of the support would be to adsorb CO_2 and facilitate dissociation at the metal-support interface (Nagaoka *et al.*, 2001). CO_2 dissociation would result in the formation of CO and O. Adsorbed O could then react with carbon deposited on the metal to produce additional CO.

2.7 Comparison of the Intrinsic Activity of Nickel and Noble Metals

The comparison of the activity between the group VIII metals such as platinum, iridium, rhodium, palladium and ruthenium, and non noble group metals, such as nickel, cobalt and iron for CO_2 reforming has been studied by various research groups (Rostrup-Nielsen 1993; Basini and Sanfilippo 1995; and Qin *et al.*, 1996).

Rostrup–Nielsen (1993) compared the catalytic activity of nickel, ruthenium, rhodium, palladium, iridium and platinum supported on MgO. They showed that replacing steam with CO_2 had no significant impact on the reforming mechanism According to their report, the order of activity for these metals was similar but they were nevertheless able to identify the order as follows: Ru, Rh >> Ir> Ni, Pt, Pd for steam reforming and Ru, Rh, Ni >> Ir > Pt > Pd for CO_2 reforming. The order of coke formation is Ni, Rh > Ir = Rh > Pt, Pd at 773 K and Ni > Pd = Rh >> Pt >> Ru at 873 K. They noted that rhodium and ruthenium showed high selectivity for carbon free operation.

Qin and Lapszwicz (1994) observed that Rh, Ru, and Ir catalysts supported on MgO had only little carbon deposition, during steam, CO_2 and mixed reforming. They observed that after 8 hours on stream, there was no deactivation, though carbon deposition was noted. They observed carbon black on the test tubes containing Pt and Pd catalysts. This is an indication, that, the removal of surface carbon is very efficient for Ru, Rh and Ir catalyst, by the Boudouard reaction and steam-carbon reaction.

$$CO \leftrightarrow C + CO_2 \qquad (-\Delta H_{298}{}^{o}=172 \text{ kJ/mol}) \qquad (2.1)$$

$$CH_4 \leftrightarrow C + 2\,H_2 \qquad (-\Delta H_{298}{}^{o}= -75 \text{ kJ/mol}) \qquad (2.2)$$

$$C + H_2O \leftrightarrow CO + H_2 \qquad (-\Delta H_{298}{}^{o}=-131 \text{ kJ/mol}) \qquad (2.3)$$

They also observed that the difference between metals was distinct. Supported on MgO, Ru, Rh, and Ir were better than Pt and Pd under the same experimental conditions. However nickel catalyst exhibited a strong tendency for coking.

Rostrup–Nielsen and Bak Hansen (1993) also reported a similar activity order for steam reforming and CO_2 reforming on noble metals supported on alumina–stabilised MgO at 823 K. Rostrup-Nielsen (1994) also reported carbon deposition sequence for various metals as Ni > Pt, > Ru.

Ashcroft *et al.* (1990) demonstrated that over nickel-supported catalysts, for a CO_2/CH_4 molar ratio, carbon deposition could not be avoided. Ashcroft *et al.* (1991) however suppressed carbon deposition in CO_2 reforming by replacing Ni with the platinum group catalysts; Ru 69 % and Ir 89% for CO yield

2.8.Effect of Support with Carbon Dioxide Reforming of Methane over Nickel based-Catalysts

Ruckenstein and Hu (1996) carried out investigation on the dynamic changes in activity and selectivity for the CO_2 reforming of methane over un-supported and supported Ni catalyst. At reaction conditions carried out under atmospheric pressure, 790K, and with a molar ratio of CO_2:CH_4 = 1:1, and gas hourly space velocity (GHSV = 6000 ml/g hr) they found that Ni supported catalysts are profoundly affected by the nature of support. The catalysts investigated were: NiO–Al_2O_3, 1 wt% Ni/SiO_2, 1 wt% Ni/Al_2O_3, 13 6 wt% Ni/Al_2O_3, 13.6 wt % Ni/SiO_2 and 13 6 wt% Ni/TiO_2. The initial CO yield over 13.6 wt% Ni varied with the different supports in the order Ni/Al_2O_3 > Ni/SiO_2 > Ni/TiO_2, but decreased with time. The activity and selectivity of the reduced NiO mixed mechanically with Al_2O_3 increased rapidly with time at the beginning of the reaction but only moderately later.

They observed that carbon deposition occurred over the entire catalyst surface, and the sequence of carbon deposition was 13 6 wt% Ni/Al_2O_3 > 13.6 wt% Ni/SiO_2 > the reduced mixture of NiO and Al_2O_3 (13 6 wt% Ni), 1 wt% Ni/TiO_2 > 1 wt% Ni/Al_2O_3 > 1 wt% Ni/SiO_2. Both the 1 wt% Ni/Al_2O_3 and SiO_2 catalysts exhibit low carbon depositions. For 13.6 wt% Ni-based catalysts, the sequence of carbon deposition was Ni/Al_2O_3 > Ni/SiO_2 > Ni/TiO_2.

Takehira *et al.* (2000) tested Ni supported catalysts on perovskite–type oxides: $CaTiO_3$, $BaTiO_3$ and $SrTiO_3$, prepared by solid phase crystallisation method, for CO_2 reforming of methane. They observed that the $Ni/SrTiO_3$ catalyst showed the highest activity as well as the highest resistance against coke formation. The next most active catalyst was $Ni/BaTiO_3$ followed by $Ni/CaTiO_3$. The high and stable activity was attributed to highly dispersed and stable Ni metal particles (diameter 1 nm) on the perovskite, where the nickel species thermally evolved from the cations homogeneously distributed in an inert perovskite matrix as the precursors during the reaction

Similarly, Wei *et al.*, (2000) used an ultra-fine ZrO_2 support over nickel catalyst prepared by sol–gel precipitation followed by supercritical drying for CO_2 reforming of CH_4. They found that the U-ZrO_2 itself is active in the reaction and the reaction exhibited an oscillatory nature which accounted for the high activity and stability. The catalytic reaction was performed at atmospheric pressure, 1030K with a feed of 1:1 (CH_4/CO_2). The fact that U-ZrO_2 itself possesses some activity in CH_4 reforming with CO_2 implies that despite being a support, it can activate both CH_4 and CO_2. This property of the ultra-fine ZrO_2 support seems to appreciably increase the number of the active sites. In addition, surface oxygen formed as a result of the dissociation of CO_2 on U-ZrO_2 surface might migrate onto Ni particles and aid in eliminating carbon. The oscillation was attributed to the alternate generation and elimination of carbon.

Effendi *et al.*, (2000) reported coke reduction over NiO supported on SiO_2/MgO catalysts at 973K, 1 atmosphere with CO_2/CH_4 ratio = 1, with a diluted catalyst bed using α-alumina, both micro-fixed and fluidised reactor. They found that the synthesis gas produced using a fluidised bed led to higher selectivity of H_2/CO and higher CH_4 and CO_2 conversions, due to reduced mass transfer limitations.

In summary, coke deposition can be reduced to a minimum, using nickel catalyst, depending on the support employed, the reactor type and the mode of catalyst design.

2.9 Effect of Ni Content on the Activity of Ni Supported Catalyst with CO_2 Reforming of Methane

Ruckenstein and Hu (1996) observed the effect of Ni content on the activity of supported Ni catalyst. They compared the activity over 1 wt% Ni/Al_2O_3 and 13.6 wt% Ni/Al_2O_3 and found that the initial conversion of CH_4 and CO_2 and CO yield over 1 wt% Ni/Al_2O_3 was high but that it decreased with time. The relatively small amount of carbon deposited during reaction was attributed as probable cause for the slow decrease in activity with time. Carbon deposition in the reduced 13 6 wt% Ni/Al_2O_3 catalyst occurred rapidly and even caused plugging of the reactor They observed a high decomposition of CO to CO_2 over the reduced 13 6 wt% Ni/Al_2O_3 than 1 wt% Ni/Al_2O_3 as revealed by Temperature–programmed desorption spectrum.

In summary, carbon deposition on nickel catalyst depends on the support employed. Also, it can be deduced that lower loading of Ni in the catalyst favours low carbon deposition

2.10 Effect of Precursor on Nickel Catalyst

Wang and Lu (1998) have confirmed that the precursor for nickel catalyst has some effect on the activity of the catalyst. They compared Ni/Al_2O_3 catalyst, prepared from different precursors such as $Ni(NO_3)_2$, $Ni(Cl_2)$ and nickel acetalcetonate $[Ni(C_5H_7O_2)_2]$. They found that the catalyst from the two latter precursors showed considerably lower activity than that prepared from $Ni(NO_3)_2$ A report made by Ermakova *et al*, (1999) also indicated that the texture of catalyst is affected by variation in precursors in catalyst development. They found that alumina prepared by the decomposition of isopropoxide showed that no chemical compound appeared to interact with the oxide of nickel. This possibility could not be excluded as occurring during the impregnation of nickel oxide with an aqueous solution of aluminium nitrate.

2.11 Effect of Combining Alkaline – Earth or Rare Earth Oxides with Nickel Catalysts

The addition of alkaline–earth oxides or rare earth oxides to supported nickel catalyst to prevent coke formation and consequence enhancement in methane reforming to synthesis gas is widely recognised technique (Inui, 2001; Theron *et al.*, 1984).

According to Kroll *et al*, (1996) some supported nickel catalysts have shown promising activity and long life without obvious deactivation.

Ruckenstein *et al*, (1995) reported that the addition of MgO inhibits the disproportionation reaction $2CO \rightarrow C + CO_2$ over nickel catalyst, which is in good agreement to the results reported by Guerrro-Ruiz *et al*, (1994), who carried out a similar investigation on Co/C-MgO. This may be due to the formation of a NiO–MgO solution as a result of the similar crystalline structure of NiO and MgO. Ruckenstein *et al.*, (1995) noted a striking contrast in stability between Ni/MgO and other catalysts. They reported constant conversion with the Ni/MgO catalyst for periods up to 12 hours, even though the catalyst lost subsequently its activity abruptly.

Tomishige *et al*, (1998) also compared the activity of nickel catalysts at 773–1123K with the addition of alkaline earth metal oxides such as $Ni_{0.03}Mg_{0.79}O$, Ni/MgO and NiO-Al_2O_3. They found that $Ni_{0.03}Mg_{0.79}O$ solid solution showed very high resistance to carbon deposition (Rostrup-Nielsen, 1994) during CO_2 reforming of methane. The inhibition of carbon deposition is in the order of $Ni_{0.03}Mg_{0.79}O$ < Ni/MgO < NiO–Al_2O_3. This is an indication that basic oxide supports for nickel-based catalysts play an important role in inhibiting carbon deposition. Ashcroft *et al.*, (1990) also noted that CO_2 dissociated more easily on the reduced $Ni_{0.03}Mg_{0.79}O$ catalyst than that on Ni/MgO. Therefore, they suggested the inhibition mechanism have been caused by the activation of CO_2 at the metal–support interface (Michael *et al.*, 1998), (see Figure 2.2).

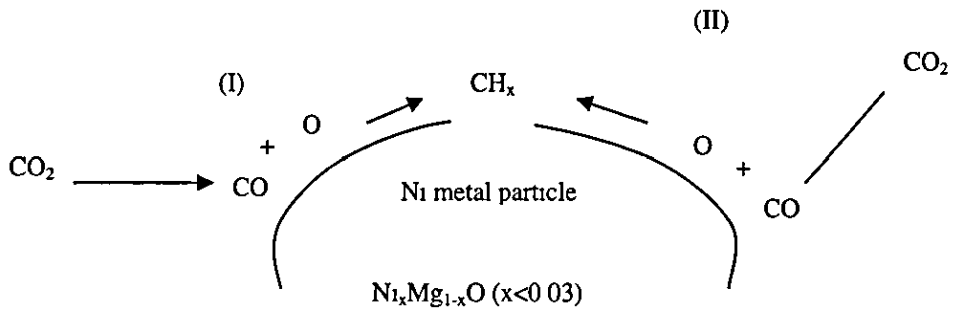

Figure 2.2 Model of the reaction scheme of CH_x adsorbed on nickel metal surface with CO_2 reforming of methane (Tomishige *et al.*, 1998)

Figure 2.2 shows the inhibition mechanisms of carbon deposition on $Ni_{0.03}Mg_{0.97}O$. There are two pathways for the reaction of carbon species on Ni with CO_2. (1) CO_2 is adsorbed on Ni and the other, CO_2 being adsorbed on the surface of the support. It is known that CO_2 can adsorb on a Ni metal surface from the gas phase and dissociates to oxygen and CO. Similarly, CO_2 can be activated easily at the interface between reduced Ni and the solid solution surface.

Reduced $Ni_{0.03}Mg_{0.79}O$ is basic on its surface and interacts strongly with CO_2 similarly to MgO. Therefore, CO_2 can be activated easily at the interface, between reduced Ni and the solid solution surface similar to MgO. It is considered that, in the case of $Ni_{0.03}Mg_{0.79}O$, the active species (CHx) formed on the nickel metal surface is via the activation of CH_4 and this is easily removed before it can be converted to whisker carbon.

In contrast, the formation of CHx on the other catalysts and transformation to whisker carbon may become faster than the removal by H_2 or CO_2. As a consequence, the concentration of CHx species may be higher and the possibility of being converted to a carbon precursor, or surface carbide before reacting with CO_2 is high.

Zhang and Verykios (1994) have also noted that a 17 wt% Ni/γ-Al_2O_3 and Ni/CaO/γ-Al_2O_3 of approximately the same metal dispersion showed differences in consumption of H_2 as revealed in a temperature programmed reduction study.

They found that the reduction of Ni/CaO/γ-Al_2O_3 catalyst initiated at lower temperatures consumed high amounts of hydrogen as compared to that of Ni/γ-Al_2O_3 catalysts. This observation is an indication that the fraction of nickel present as free Ni on the CaO/Al_2O_3 support is larger than that on the Al_2O_3 support, despite the fact that the number of the exposed metallic Ni atoms on both supports is approximately the same. Apparently nickel reacts easily with the acidic Al_2O_3 carrier to form the stable nickel aluminate compound, whilst basic CaO promoter retards the reaction between nickel and Al_2O_3

Goula *et al.*, (1996) also reported that the reactivity of carbonaceous species towards oxidation and hydrogenation strongly depends on the support composition (molar ratio of CaO to Al_2O_3) a good agreement with the report by (Zhang and Verykios 1994).

Chang *et al* , (2000) also investigated carbon dioxide reforming of methane, using KNiCa catalyst loaded on a highly siliceous NAZSM-5 zeolite support at 1073K which was promoted with alumina. They compared the catalytic behaviour of supported KNiCa catalysts to that of Ni supported catalyst (Ni/ZSI). The report showed excellent catalyst stability over KNiCa catalysts in a period of 140 hours due to the promotional effect of surface carbonate species leading to surface enrichment of carbon dioxide.

This is in good agreement with work by Juan-Juan *et al.*, (2004), who reported a coke formation decrease by the addition of potassium to nickel metal. The supported Ni catalyst showed catalyst deactivation due to extensive coke deposition, after less than 40 hours on stream. The KNiCa/ZSI catalyst exhibited high activity in terms of CO_2 conversion, almost attaining near equilibrium (96%) to produce CO without catalyst deactivation.

Chang *et al.*, (2000) found that the composite support, which was composed of a highly siliceous NaZSM-5 zeolite and alumina binder offered high catalyst stability, compared to NaZSM–5 zeolite They proposed that, besides the role of alkaline promoters, high catalyst stability for KNiCa/ZSI, is partially originated from a synergistic effect due to the contribution of each component.

The assumption being that a zeolite component in ZSI supported Ni catalyst plays a role in minimizing the formation of $NiAl_2O_4$ spinel due to the presence of microporous zeolite, which is considered to be a factor of catalyst ageing.

It was also pointed out that ZSM-5 type catalyst is the most thermally stable among the many zeolite molecular sieves, and a favourable adsorbent for carbon dioxide. On the other hand, the role of the alumina component in the KNiCa/ZSI catalyst was considered to form a $CaAl_2O_4$ phase through solid–state reaction with calcium oxide that suppresses the coke formation as well as the formation of $CaAl_2O_4$ spinel. They recommended that the composition of potassium in the catalyst should be between 0 6 and 1 wt%, as above this amount may result to the poisoning of the catalyst.

In conclusion, the addition of alkaline-earth oxides plays a vital role in CO_2 reforming of methane over nickel catalyst. It is possible to have a carbon free process with CO_2 reforming of methane with the addition of these oxides. Alkaline promoters do not only increase the active area but also retard the reaction between nickel and Al_2O_3 and improve the catalyst stability and also increases the reaction rate.

2.12 Surface Species Formed on Nickel Catalyst with CO_2 Reforming

Zhang and Verykios (1994) studied the surface species formed on $Ni/CaO/\gamma\text{-}Al_2O_3$ and Ni/Al_2O_3. They observed adsorbed formate species and bicarbonates species formed on both catalysts, at lower temperatures (< 373K) and suggested that this occurred probably on the carrier. They suggested that the Ni surface is essentially covered with different carbonaceous species. Their investigation with oxygen and temperature-programmed surface reaction (O_2–TPSR) showed that three types of carbonaceous species could exist on the Ni/Al_2O_3 catalysts, designated as C_α at 425K–473K, C_β at 803K–873K and C_γ at 923K. Large amounts of C_β and C_γ, were revealed on the promoted catalyst compared to the unprompted one, but the quantity of C_α was approximately the same.

A population of C_β species on the catalysts, at lower temperatures (773K–873K), corresponds to several monolayers of equivalent carbon on Ni crystallites, and small amounts of C_α species. The C_γ species were negligible below < 10 min but compete favourably with C_β at longer times. Therefore they suggested that the active C_α species (Solymosi and Cserenyi 1994) at higher temperatures may be responsible for the formation of synthesis gas while the most inactive C_γ species may be responsible for catalyst deactivation. The C_β species may be a surface poison or inactive at low reaction temperature (< 803K), but may participate in CO formation at high temperatures (873K). The increased amounts of C_β and C_γ species on the promoted catalyst could be attributed to the larger Ni crystallite on the promoted catalyst. This favourably contains more carbon in the form of Ni carbide and/or graphitic carbon compared to the increased amounts of the formate species strongly bound on the promoted catalyst.

In summary, the addition of CaO to nickel catalysts improved the stability of the catalyst. Therefore it suggests that the improved stability with alkaline promoted (CaO) catalysts may be related to relatively enhanced reactivity of the C_β and C_γ species at high reaction temperatures (> 873K) This favours the removal of a small fraction of the inactive C_β and C_γ species and secures the surface Ni sites required for the formation of the active C_α The removal of the C_β and C_γ species at high reaction temperatures, presumably by CO_2 or oxygen adatoms originating from CO_2, appears to be the reason that the deactivation rate was significantly reduced with increasing reaction temperature.

2.13 Deactivation of Supported Nickel Catalyst with CO_2 Reforming of Methane

Gadalla and Bower (1988) reported that only nickel supported on alpha alumina is stable while other supports tend either to decompose or react with nickel. They noted that sintering of nickel particles occurred at 873K and that coke formation is enhanced at lower temperatures.

Swaan *et al.* (1994) investigated the deactivation process on nickel based catalysts, using various supports and a promoter known to inhibit coke formation. The catalysts studied are: Ni/SiO_2, Ni/La_2O_3, Ni/MgO, Ni/TiO_2, Ni/Al_2O_3–SiO_2, Ni-K/SiO_2 and Ni-Cu/SiO_2.

They found that the catalyst with higher degree of reduction showed smaller nickel dispersion. This correlation probably arises from several factors:

(i) Size of the precursor
(ii) Support basicity, and;
(iii) Chemical interaction which may develop between nickel ions and the support e.g. the insertion of Ni^{2+} ions in the MgO matrix during calcinations and this may hinder reduction.

For Ni/SiO_2 catalyst, the formation of either nickel silicate with support or Si–Ni alloy during reduction may have caused the low degree of reduction CH_4 conversion (50%) varied as a function of support: Ni/SiO_2, Ni/ZrO_2, Ni/-Cu/SiO_2 and Ni/La_2O_3 showed a similar activity while a conversion of only 5% was achieved at 823K for Ni/MgO. Ni/Al_2O_3–SiO_2 also showed relatively low activity, while Ni/TiO_2 lost activity with 1 hour on stream although it showed some conversion at 673K.

Swaan *et al.* (1994) also observed moderate deactivation on Ni/ZrO_2, Ni/La_2O_3, Ni/SiO_2 and Ni-K/SiO_2 In contrast, the rate of deactivation of Ni/Al_2O_3–SiO_2 and Ni-Cu/SiO_2 was found to be much higher. They noted slight sintering on the nickel phase during the reforming reaction while the degree of reduction was found to increase significantly (42–64%) in the case of Ni/SiO_2. This implies that the active phase of the catalyst has increased during time on stream. Accordingly, catalyst aging is related to factors such as coke formation rather than sintering effects on Ni/TiO_2 and Ni-K. They found that /SiO_2 showed support–metal surface interaction effect by the support on the active phase. Therefore, they argued that:

(i) The activity of nickel–based catalyst appears to depend essentially on the nickel phase and not on the nature of the support
(ii) A catalyst of low dispersion of nickel but a high degree of reduction (Ni/ZrO_2) is initially as active as a partially reduced catalyst with high nickel dispersion (Ni/SiO_2)
(iii) Less dispersed catalyst is more easily deactivated than a highly dispersed one

Seshan *et al.*, (1994) examined Ni and Pt catalysts on various supports: Ni/Al_2O_3, Pt/γ-$Al_2O_3$and Pt/ZrO_2. They noted that Pt/ZrO_2 catalyst has a good activity for the CO_2 reforming of methane and that there was little or no deposition of carbon under the reaction conditions. The Pt/ZrO_2 had excellent stability with CO_2/CH_4 ratios of 3.9 and 1, which is in sharp contrast to other catalysts. They observed a large amount of carbon formation on Ni/γ-Al_2O_3 although it was more active at 723K than that of (Ni/Al_2O_3).

They suggested an investigation of the interaction of CO_2 on the physical mixture of Pt/ZrO_2 catalyst and coke in order to gain a better understanding of the system.

Also, the noxious form of carbon was observed which had the ability to encapsulate nickel particles and this could hinder the access of the reacting gases to the active surface. This work is in good agreement with earlier studies of carbon deposit in steam reforming of methane by (Bartholomew, 1984). In the case of porous supports such as Ni/Al_2O_3-SiO_2, the deactivation rate accelerated by the effect of pore blocking. They tentatively suggested that carbon in question arises from the Boudouard reaction.

2.14. Effect of Temperature on CH_4–CO_2 Reforming on Ni Catalyst

The effect of temperature on both, the activity, stability and conversions with CO_2 reforming of methane on nickel catalyst have been reported by many research groups Zhang and Verykios (1994). Seshan *et al.*, (1994) noted Ni/γ-Al_2O_3 to be very active at 723K but deactivated completely at about 748K The same applied to 10 wt% Ni/ZrO_2 at 823K, which showed stability at 723K.

2.15. Effect of CH_4/CO_2 ratios on the Conversion of CO_2 and CH_4 over Ni–based catalysts

Hong *et al.*, (2001) observed the effect of the molar ratio of CH_4/CO_2 conversion by DC pulse corona discharge on the nickel catalyst. They obtained the highest conversion at CH_4:CO_2 molar ratio of 1 0 but conversion of CH_4 decreased with an increase in molar ratio from 1 0 to 5 0 The conversion of CO_2 indicated a minimum value at the CH_4/CO_2 molar ratio of 2.0 but this increased slightly with an increasing molar ratio.

The linear decrease in CH_4 conversion may have been be due to the relative increase in the amounts of CH_4 whilst keeping the total flow rate of reactants constant. They believed that the decomposed mole number of CH_4 in reactants actually increased as the CH_4/CO_2 molar ratio increased.

2.16 Product Distribution

Often products are formed in addition to those that are desired, and a catalyst has an activity for each particular reaction. A ratio of the catalytic activity is referred to as selectivity, which is a measure of the catalysts ability to direct the conversion to the desired product.

The product distribution for several catalysts at different conversions, along with the theoretical relationship determined from the water gas shift (WGS) equilibrium varied from 1/1 at complete conversion to ½ at low conversion following strictly the WGS equilibrium. This feature strongly suggests that the conversion of H_2 depends on the water gas shift (WGS) equilibrium at low conversions of CH_4 with relatively large amount of H_2 by water gas shift (WGS) equilibrium that leads to high H_2/CO ratios. The reverse is the case when conversion of CH_4 is high, with low amounts of H_2 converted by water gas shift (WGS), leading to low H_2/CO ratios. Mark and Maier (1996) found that increasing the CO_2 in the feed, led to a decreasing H_2/CO ratio in the product. This is an indication of a decreasing contribution of the reverse water–gas shift (RWGS) reaction to the overall process.

In summary, these observations indicate that CH_4 reforming selectivity is thermodynamically determined in the case of all the tested nickel catalysts, irrespective of the supports and promoters.

2.17 Promoters

Promoters are added in relatively small quantities (1-5%) to enhance and/or maintain texture or catalyst surface area, or chemically increase catalytic activity.

2.17.1 Textural promoters

Textural promoters are generally used to facilitate (1) The preparation of well dispersed catalytic phase (2) Maintain their well- dispersed state during reaction conditions. Textural promoters include supports as well as additives such as alumina, silica or other relatively inert, high surface oxides that can serve the above two purposes.

2.17.2 Chemical promoters

These are additives that tend to enhance the activity, stability and/or selectivity of the catalytic phase (e.g. alkali and alkaline earth metals or metal oxides. CaO, K_2O, MgO).

2.18. Modified supported nickel catalyst for reforming of methane

As been already been extensively discussed, the major drawback of CO_2/CH_4 reforming is catalyst deactivation due to coke formation. Adding steam or O_2 to the reactants can enhance the stability of reforming catalyst. A more elegant way to overcome the coking problem is the development of catalysts on which coke formation is kinetically suppressed (Bitter *et al.*, 1999). Among the several ways of improving the performance of such catalysts are; the addition of metal additives, basic oxides or rare earth oxides into nickel based catalysts. These constitute relatively simple and effective method to increase coking resistance.

Blom *et al.*, (1994) compared modified supported Ni/La_2O_3-Al_2O_3 with unmodified alumina using a fluidised–bed reactor at 973K and 1073K. They observed that the lanthanum increased the strength of the support They noted lower reducibility and thus lower activity for the reforming reaction as compared to nickel on unmodified alumina However, the unmodified catalyst deactivated rapidly under the chosen test conditions. They also observed that a modified catalyst was stable over several hours.

Xu *et al.*, (2001) employed the sol-gel method of catalyst preparation (ultra fine Ni-La_2O_3-Al_2O_3) and compared this conventional impregnated catalyst. According to their report, the catalyst exhibited unusual physical and chemical properties.

The catalyst also showed very large specific surface area, well defined pore size distribution and good textural stability with high activity and low carbon deposition. The excellent catalytic performance is attributed to the homogeneously distributed $NiAl_2O_4$ spinel in aerogel catalyst at low heat treatment temperature and its higher capacity to adsorb CO_2. Shishido *et al.*, (2001) also confirmed the report of Xu *et al.*, (2001) who used solid phase crystallisation method from Mg-Al hydrotalcite–like precursors for the catalyst preparation. They also claimed that catalyst (Ni/Mg-Al oxide) prepared by the above method showed higher activity than those prepared by the conventional impregnation method. It is believed that Ni^{+2} can well replace the Mg^{+2} site in the hydrotalcite, resulting in the formation of highly dispersed Ni metal particle.

Roh *et al.*, (2002) examined $Ni/Ce\text{-}ZrO_2/\theta\text{-}Al_2O_3$ in the CO_2 reforming of methane. Their results indicated CH_4 conversion of more than 97% at 1073K with a maintained activity for period of more than 40 hours. They claimed that the high stability of the catalysts is mainly ascribed to the beneficial precoating of $Ce\text{-}ZrO_2$ resulting in the existence of stable NiO_x species, a strong Ni-support interaction and the abundance of mobile oxygen species in the support They suggested that NiO_x formation is more favourable than NiO or $NiAl_2O_4$ formation, resulting in the strong Ni-support interaction.

Choi *et al.*, (1998) modified Ni/Al_2O_3 catalysts with different metals such as Co, Cu, Zr, Mn, Mo, Ti, Ag and Sn. Relative to the unmodified Ni/Al_2O_3, catalyst modified with Co, Cu and Zr showed slightly improved activity while other promoters reduced the activity of the catalysts.

Their study revealed that Mn–promoted catalyst showed a remarkable reduction in coke deposition, while entailing only a small reduction in catalytic activity compared to unmodified catalysts.

Seok *et al.*, (2001) also claimed that, addition of manganese to Ni/AL_2O_3 improved the stability of the catalyst in CO_2 reforming of methane. They found that nickel is partly covered (decorated) by patches of MnO_x. They observed that addition of manganese also promotes the adsorption of CO_2 by forming a reactive carbonate species

These effects appear to be responsible for the suppression of carbon deposition over $Ni/MnO-Al_2O_3$. Lemonidou *et al.*, (2002).

Lemonidou *et al.*, (2002), reported high activity and good stability over 5 wt% $Ni/CaO-Al_2O_3$ catalyst in CO_2 reforming of methane at 873K–1093K. They tested the addition of steam in the reacting mixture and proved beneficial for the conversion of methane and drastic decrease in carbon deposition.

Chen and Wang (2000) studied CO_2 reforming of methane over $Ni/MgO-Al_2O_3-AlPO_4$ catalysts. These were compared to the conventional Ni/Al_2O_3 and $Ni/MgO-Al_2O_3$ catalysts. They found that $Ni/MgO-Al_2O_3-AlPO_4$ catalyst showed a higher activity than the other two catalysts especially at high temperatures This was attributed to the large pore size diameter and uniform pore size distribution of $Ni/MgO-Al_2O_3-AlPO_4$ catalyst, enabling pore diffusion effects under high temperature reaction condition to be overcome.

Hayashi *et al.*, (2000) studied the catalytic activity and durability with CO_2 reforming of methane over Ni/Al_2O_4 prepared using a water–in-oil (W/O) micro emulsion (ME) using the following reaction conditions: atmospheric pressure, space velocity = 6000 hr, 973K and with the varying molar ratios ranging from (1-2). They found that the initial activity of the prepared Ni/Al_2O_3 catalysts was higher than that of the impregnated one. The impregnated catalyst deactivated with time on stream, due to severe coking. In contrast, the catalysts prepared using W/O kept its activity for 50 hours but caused little coking with increased CO_2/CH_4 molar ratios above1.4.

They also noted that the carbon species deposited on the ME catalyst showed less crystallised structure than that on the impregnated one. The reactivity of carbon species is well known to increase with decreasing degree of crystallisation.

The carbon species formed on ME catalysts is considered to be easily gasified by CO_2 compared to that on impregnated catalyst during reaction which led to the superior resistance of the catalyst to carbon deposition They therefore suggested that the superior resistance of the later, may probably be caused by the generation of easily oxidised carbon species to that found on impregnated catalysts during reaction

Tomisghige *et al*, (2001) in their study, with ($N_{0.15}$ $M_{0.85}$ O) catalyst, observed high conversions of methane with CO_2 and O_2 under pressured conditions and temperature at 1023K using a fluidised bed reactor. They also noted inhibited carbon deposition, due to circulation of the catalyst, which is a serious problem in CO_2 reforming. At a lower space velocity (56,000 ml/g h), they observed that methane conversion in both fixed and fluidised bed was almost the same, with particle size (150-250 microns). This suggests that catalysts particle s were not fluidised under this flow condition. On the other hand, large difference was observed in methane conversion at higher space velocity (75,000 ml/g h)

Wang *et al.*, (2001) compared Ni/Al_2O_3 and Ni supported on Ceria and yttira doped catalyst and found that Ni/Al_2O_3 catalyst displayed rapid deactivation with time on stream but both Ceria and YDC–supported catalyst exhibited exceptional enhancement of activity and coking resistivity. They suggested that formation of interfacial centres and the existence of metal-support interaction may have been occurring decreased with increased yttria doping. They explained that the ability of CeO_2 to lose its lattice oxygen to form Ce^{3+} (Roh *et al*, 2002) was inhibited with yttria. According to their report, the lattice oxygen of ceria is inferred to have played some positive role in the activation of both CH_4 and CO_2. Thus promotion is attributed in part to the availability of Ce^{3+} species at the metal-support interface. A similar behaviour was observed by (Wang *et al.*, 2003a).

Work by Olsbye *et al.*, (2002) showed that there was a reduction of coke formation over La-promoted Ni/Al_2O_3 compared to the unpromoted. They suggested that it may be partly due to differences in cluster size. Carbon whisker formation rate on supported Ni catalysts can be determined by diffusion rate of carbon through the Ni cluster, which is proportional to the radius of each Ni cluster. Xu *et al*, (2001) observed similar high activity and very low carbon deposition over ultrafine $NiO-La_2O_3-Al_2O_3$ aerogel catalyst.

Olsbye *et al.*, (2002) further explained that the catalyst can easily form homogeneously distributed $NiAl_2O_4$ spinels at low temperature treatment which have much capacity to adsorb CO_2. This is in accordance with the observation reported Liu and Au, (2003). Their result also indicated that there was a decline in coke formation due to the formation of stable $NiAl_2O_4$ spinel temperature = 1073K.

In the investigation carried out by Dias and Assaf (2003), the addition of CaO to Ni/Al_2O_3 resulted in changes in its structure and catalytic performance in the methane reforming reaction with CO_2 The explanation is that at the structural level, it interacts with support and lowers its resistance to sintering. In the interaction it competes with nickel and favours the formation of reducible species of Ni at lower temperatures mainly when the nickel is added after the calcium. The review of nickel-supported catalysts modification has revealed the continuous research in catalyst development to alleviate coke formation in CO_2 reforming of methane. The results reported in literature are very promising.

2.18 Promoted Nickel-based catalyst with CO_2 reforming of methane.

Choi *et al.*, (1998) promoted Ni/Al_2O_3 catalysts with different metals such as Co, Cu, Zr, Mn, Mo, Ti, Ag and Sn. Relative to the unmodified Ni/Al_2O_3, catalyst modified with Co, Cu and Zr showed slightly improved activity while other promoters reduced the activity of the catalysts. Their study revealed that Mn–promoted catalyst showed a remarkable reduction in coke deposition, while entailing only a small reduction in catalytic activity compared to unmodified catalysts. Wang *et al.*, (2003b) used a bimetallic Ni-Cr/YD catalyst and found that there was an increase in conversion and stability. With the maximum loading of Cr, the activity decreased.

Wang *et al.*, (2003a) also reported that Co doped catalyst can enhance the catalytic properties with respect to resistance to metal sintering and carbon deposition Valentini *et al.*, (2003) studied the role of vanadium in Ni/Al_2O_3 and found that low content vanadium suppressed the $NiAl_2O_4$ formation. On the other hand, the sample with high vanadium presented the highest carbon deposition, which according to them was attributed to the CH_4 decomposition increase promoted by the vanadium

Frusteri *et al.*, (2001) also observed that addition of potassium to Ni-based catalyst depresses the reactivity of the catalyst strongly improving its resistance to both coking and sintering processes. Crissafulli *et al.*, (2000) also observed an improvement in the activity and stability on silica supported Ni-Ru. They explained that promoting Ni with Ru increased the dispersion of Ni, probably due to the formation of Ni-Ru clusters with the surface mainly covered by Ni.

In summary, metal promoted Ni catalyst can improve both the activity and stability in terms of coke resistance and sintering, depending on the amount of metal doping.

2.19 Design, preparation and characterization of a Ni based catalyst for CO_2/CH_4 reforming.

Methane reforming with carbon dioxide is thought to consist of similar elementary reaction steps as in steam reforming (Rostrup-Nielsen 1993) but the absence of water and the high C/H ratio in the reactant feed favours coke formation during CO_2/CH_4 reforming (Udengaard *et al.*, 1992). The effect of coke formation varies with the metal catalyst used. For Ni catalysts coke is formed as whiskers with Ni particles depositing on these whiskers. As a result, the contact between the metal and support is lost which makes it difficult to regenerate the catalyst. Also, it is believed that whisker formation causes a significant expansion of the catalyst bed resulting in severe operational problems.

As early as 1928, Fisher and Tropsch showed that group VIII metals are active for CO_2/CH_4 reforming (Sethuraman *et al.*, 2001). Many authors have investigated metals such as Ni, Ru, Rh, Pt, Ir and Pd (Rostrup-Nielsen and Hansen 1993).

However, Ni catalysts are commercially more interesting compared to noble metals but the main drawback is the high rate of coke formation, (Richardson and Paripatyadar 1990). From an economic point of view (relatively low price and good availability) Ni based catalyst had drawn the attention of many research groups.

2.20 Choice of support material

The catalytic active materials are often expensive, and their activity depends on the factors such as surface area, porosity, geometry of the surface and resistance to deactivation. It is therefore, a common practice to disperse the active ingredient of many catalysts on the surface of "inactive" solids referred to as supports or carriers, for optimised operation. The most stable supports include solids such as alumina, magnesia, silicon carbide and alumino-silicates ($3Al_2O_3$ $2SiO_2$).

Even refractory materials are susceptible to attack by alternate high and low temperature cycles or chemical reactions For example, in steam reforming materials such as silica, can volatise in the presences steam at high temperature to be considered are as follows. The most commonly used support for CO_2/CH_4 reforming is Al_2O_3 (Qin and Lapszewicz 1994). Modification of supports by the addition of oxides such as MgO, MnO and CaO has been shown by many authors to enhance the catalyst activity and stability (Cheng *et al*, 2001, Seok *et al.*, 2001; Lemonidou *et al.*, 2002 and Roh *et al.*, 2001).

This underlines the importance of the chemical nature of supports to achieve a stable catalyst. Suitable supports have to be resistant to the high temperatures employed during CO_2/CH_4 reforming and also, to maintain the metal dispersion of the catalyst during operation.

2.21 Catalyst poisoning

Catalyst poisoning may be classified as (1) reversible and (2) irreversible The reversible case occurs when materials presents in the reactor (reactant or products, or intermediates) are deposited upon the surface of the catalyst, blocking active sites. The most common form is by carbonaceous species (coking).

The form of coke depends upon that catalyst, as very little coke forms on silica or carbon supports, acidic supports or catalysts that are prone to coking However, the irreversible poisoning may be caused by chemisorption of compounds in the process stream; that can block or modify the active phase on the catalyst (Missen *et al.*, 1999). An inhibitor slows down a catalytic reaction but a competitive inhibitor slows down the reaction by competing with the reactants in bonding to the catalysts.

A very strong inhibitor is such one that bonds so strong that, it virtually excludes the reactant from bonding with changes in the surface morphology of the catalyst;

(i) Surface reconstruction or relaxation

(ii) Bond modification between the metal catalyst and the support

2.23 Kinetic study of carbon dioxide reforming of Methane

2.23.1 Reaction mechanism

In heterogenous catalysis, both the knowledge of chemical reactions, the way in which the rates of reactions depend upon process condition forms the basis for the design and optimisation of both catalyst and chemical reactors. The mechanistic study of carbon dioxide reforming of methane has been the interest of many researchers, both in terms of the noble metals and non metals. Although, CO_2 reforming of methane has been studied extensively but elementary steps which comprise the reaction mechanisms remain unclear and there currently exists no general reaction mechanism in the literature. However, many research groups have attempted to provide reaction mechanism derived from their developed rate expression.

Rostrup-Nielsen and Bak Hansen (1993) proposed that the reaction mechanism of CO_2 reforming has little or no significant difference form that of steam reforming. They based their argument on the fact that steam is also present in the CO_2 reforming process by the RWGS reaction

Erdohelyi *et al* , (1993) also suggested that on noble metals, carbon dioxide react directly form the gas phase with carbon adspecies, arising from methane decomposition as follows;

$$CH_4 + * = C^* + 2H_2 \qquad (2.4)$$

$$C^* + CO_2 = 2CO + * \qquad \text{(Erdohelyi } et\ al.\text{, 1993)} \qquad (2.5)$$

Kroll *et al.*, (1996; 1997) noted that the exact nature of the reacting intermediates arising from the two possible sources of carbon (CO_2 reforming of methane) and their fate within the mechanistic scheme remains an open fundamental question.

In their investigation they found that dehydrogenation carbon adspecies are derived from initial adsorption of methane and carbon dioxide using both steady and non steady state isotopic transient kinetic analysis combined with DRIFT spectroscopy.

Their findings were in contrast to the observations reported by Kevlen *et al.*, (1996). However, they also observed large amount of CO release from the surface under CO_2 atmosphere which is in agreement with observations made by (Erdohelyi *et al*, 1993) and H_2 produced under methane atmosphere. They also noted that the kinetic behaviour of water is close to that of CO_2 which suggests that water interacts reversibly with the catalytic surface via an adsorption/desorption equilibrium in a similar as CO_2. Therefore, they proposed the following reaction mechanism;

$$CH_4 + S_1 \rightarrow C_{ads} + 2H_2 \quad (2.6)$$

$$CO_2 + C_{ads} \rightarrow 2CO + S_1 \quad (2.7)$$

$$CO_2 + S_1 \rightarrow CO + O_{ads} \quad (2.8)$$

$$C_{ads} + O_{ads} \rightarrow CO + S_1 + S_2 \quad (2.9)$$

$$H_2O + S_2 \rightarrow O_{ads} + H_2 \quad (2.10)$$

Despite the uncertainties of evaluating the fraction of surface corresponding to methane adsorption, carbon dioxide and water activation, they noted that large difference between surface occupancy could reflect some structural effect on these reactions.

However, the competitive adsorption of methane and carbon dioxide on the same site remains a plausible alternative that they did not include in their investigation.

Chang *et al.*, (2000) also proposed a reaction mechanism over KNiCa catalyst, that dissociation adsorption of carbon dioxide occurs mainly on different Ni sites, leading to surface oxygen and gaseous CO. The surface reaction of these species produces gaseous CO and simultaneously rejuvenated nickel. They proposed that these reactions proceed by the Langmuir Hinshelwood mechanism where CO_2 either directly in the gas or as surface carbonates can also react with surface carbon species from methane dissociation.

They also proposed the RWGS reaction where part of the H_2 produced form methane decomposition would be consumed through the reaction with CO_2 to yield CO and water. From their findings, they also proposed the following reaction mechanism;

$$CH_4\,(g) + Ni\,(s) \leftrightarrow Ni\text{-}C + H_2\,(g) \tag{2.11}$$

$$CO_2\,(g) + Ni\,(s) \leftrightarrow Ni\text{-}O + CO\,(g) \tag{2.12}$$

$$Ni\_C\,(s) + Ni\text{-}O\,(s) \leftrightarrow CO\,(g) + 2Ni\,(s) \tag{2.13}$$

$$CO_2\,(g) + Ni\,(s) \leftrightarrow 2CO\,(g) + Ni\,(s) \tag{2.14}$$

$$CO_2\,(g) + Ni\text{-}H\,(s) \leftrightarrow Ni\text{-}OH\,(s) + CO\,(g) \tag{2.15}$$

$$Ni\text{-}OH\,(s) + Ni\text{-}H\,(s) \leftrightarrow 2Ni + H_2O\,(s) \leftrightarrow H_2O \tag{2.16}$$

Richardson and Paripatyadar (1990) provided a model derived from Langmuir-Hinshelwood approach involving redox mechanism which fit their experimental data well. The model provided the proper temperature dependencies of the rate and adsorption constants. However, they did not present the reaction mechanism from which they derived their model.

This discrepancy is because the adsorption entropies were too small, thus suggesting an inconsistency in their model.

$$R = \frac{K_r K_{CO_2} K_{CH_4} P_{CO_2} P_{CH_4}}{(1 + K_{CO_2} P_{CO_2} + K_{CH_4} P_{CH_4})^2} \tag{2.17}$$

Zhang and Verykios (1994) have also provided rate expression, derived from a Langmuir model assuming that methane dissociation was the rate determining step.

Although the model supposedly fit the experimental data reasonably well, they did not provide the values for the adsorption and kinetic parameters in their report.

Although the model supposedly fit the experimental data reasonably well, they did not provide the values for the adsorption and kinetic parameters in their report.

Similarly, Souza *et al.*, 2001) after analysing available data in literature and combining with their result, also proposed a bifunctional mechanism as follows;

$$CH_4 + P \xleftrightarrow{k_{CH_4}} H_{4x-p} + \left(\frac{4-x}{2}\right)H_2 \tag{2.18}$$

$$CO_2 + Z \xleftrightarrow{k_{CO_2}} CO_2 - Z \tag{2.19}$$

$$H_2 + 2P \longleftrightarrow 2H - P \tag{2.20}$$

$$CO_2 - Z + 2H - P \longleftrightarrow CO + H_2O \tag{2.21}$$

$$CO_2 - Z + CH_{x-p} \longleftrightarrow 2CO + \left(\frac{x}{2}\right)H_2 + Z + P \tag{2.22}$$

where p is platinium site and z is a support site

Michael *et al* (1996) also proposed the generalised reaction sequence for CH_4-CO_2 reforming. With available literature data combined with their experimental data, they suggested the following model

$$CH_4 + * \xleftrightarrow{k_1} CH_x + \left(\frac{4-x}{2}\right)H_2 \tag{2 23}$$

$$2\left[CO_2 + * \xleftrightarrow{k_2} CO_2 *\right] \tag{2.24}$$

$$H_2 + 2* \xleftrightarrow{k_3} 2H* \tag{2.25}$$

$$2\left\{CO_2 * + H * \xleftrightarrow{k_4} CO * + OH *\right\} \tag{2.26}$$

$$OH^* + H^* \xleftrightarrow{k_5} H_2O + 2^* \tag{2.27}$$

$$CH_x^* + OH^* \xleftrightarrow{k_6} CH_xO^* + H^* \tag{2.28}$$

$$CH_xO^* \xleftrightarrow{k_7} CO^* + \left(\frac{x}{2}\right)H_2 \tag{2.29}$$

$$3\left(CO^* \xleftrightarrow[k_8]{1} CO + *\right) \tag{2 30}$$

Aparico (1996) argued that his model is unique, although, similar models could have been developed with complete water dissociation to O^* or dissociation of CO_2 to CO and O^*. He pointed out that though surface formation species are justified by low temperature, their presence o at higher temperatures is not guaranteed The absence of O^* and the presence of *COOH in their model reflect simplicity and not actually specify if these species are involved in the actual mechanism. He further noted that the rate expressions for steam reforming have been found to be applicable only in limited range of conditions.

$$R = \frac{kP_{CH_4}}{\left(1 + a\left(\frac{P_{H_2O}}{P_{H_2}}\right) + bP_{CO}\right)} \quad \text{(Aparrico 1996)} \tag{2.31}$$

$$R = \frac{kP_{CH_4}P_{H_2O}\left(1 - \left(P_{CO}\left(P_{H_2}\right)^3 / K_{eq}P_{CH_4}P_{H_2O}\right)\right)}{f\left(P_{H_2O}P_{H_2}\right)\left(1 + \left(K_{H_2O}P_{H_2O} / P_{H_2}\right)\right)} \quad \text{Aparico 1996)} \tag{2.32}$$

where K_{eq} is the equilibrium constant for the overall reaction and $f(P_{H2O}\,P_{H2})$ is a polynomial.

and

$$R = \frac{kP_{CH_4}P_{H_2O} / P^{2.5}\left(1 - \left(P_{CO}\left(P_{H_2}\right)^3 / K_{eq}P_{CH_4}P_{H_2O}\right)\right)}{1 + K_{CO}P_{CO} + K_{H_2} + K_{CH_4}P_{CH_4} + \left(K_{H_2O} / P_{H_2}\right)} \tag{2.33}$$

Aparico argued that these expressions although described the experiment rates for steam reforming, could not predict the decrease in rate when replaced with carbon dioxide.

Similarly, Keulen *et al.*, (1996) also studied the mechanism of the CO_2 reforming of methane for 1 wt % Pt/ZrO_2 catalyst and found out that CH_4 and CO_2 molecules react independently, thus confirming the idea that CO arises from dissociation of CO_2 and also CO, CO_2, H_2 and H_2O from the dissociation of CH_4. Therefore, they suggested that there is an oxygen pool on the surface of the catalyst, with CO_2 contributing and CH_4 extracting. That the existence of an oxygen pool explained the fact that oxygen balance was never complete Although, they could not identify the exact nature of the oxygen pool, they suggested that the oxygen could be present as adsorbed oxygen species, hydroxyl or carbonates since the nature of O^* could not also be identified.

Basini and Sanfilippo (1995) also reported the CO_2 dissociation, although the mechanism is not clear. In contrast to the report by Basini and Sanfilippo (1995), Tol *et al.*, (1993) argued that CO_2 does not dissociate on platinum, even though it occurs on rhodium.

According to Rostrup-Nielsen (1993) the chemisorption of methane on nickel involves the direct breaking of a C-H bond with no adsorbed molecule as precursors. That the adsorbed CH_3^* species is converted into an adsorbed carbon atom through step-wise dehydrogenation as follows;

$$CH_4 = CH_3^* \rightarrow CH_2^* \rightarrow CH^* = C^*$$

In summary, although, many research groups have studied the mechanism of CO_2 reforming of methane, there is no accepted route of CO_2 dissociation.

Therefore, there is need to study the mechanism of CO_2 reforming of methane. Most authors, (Rostrup-Nielsen and Bak Hansen 1993), and (Kroll *et al.*, 1996) have suggested CO_2 dissociation into adsorbed O and gaseous CO while CH_4 activates stepwise into H_2 and CHx adspecies. On the other hand, Erdohelyi *et al.*, 1993 argued that for noble metals the mechanism is different. They suggested that CO_2 reacts directly from the gas phase with carbon adspecies arising from the activation of methane

In contrast Kevlen *et al.*, (1996) noted that CO_2 dissociation occurs with platinum catalyst but they could not ascertain the nature of oxygen if it is in hydroxyl form or as a carbonate species

CHAPTER 3

EXPERIMENTAL APPARATUS AND METHODS

3.1 Introduction

This chapter discusses the experimental apparatus and methods and materials used to obtain results for the following;

(1) Catalyst design and characterisation

(2) Carbon dioxide reforming of methane and investigation of catalyst poisoning

(3) Thermodynamic equilibrium calculations and kinetic modelling

3.2 Reforming experimental apparatus

Experimental investigations were conducted in a reactor made of stainless (316) material capable of withstanding temperatures up to 1273K (1m length and diameter of 7.6 x 10^{-3}m) with a volume of 4.54 x 10^{-4} m^3 . Quartz chips of sizes ranging from 480-1500 microns were used as the packing both the top and bottom of the reactor. The catalyst sample was positioned between packing and it was supported by quartz wool at both ends. The reactor was sealed at both ends with ferrules and ¼" nuts to prevent leaks The upper part of the reactor is a mixer with an opening, which provided a pipeline network connected to main process line. A detail of the designed reactor is shown in Figure 3.1. The reactor was mounted into a furnace which was connected to a temperature–programmed controller for heat supply (Carbolite, SN 0788).

Figure 3.2 shows a schematic diagram of the experimental rig. Gas cylinders containing methane, carbon dioxide, nitrogen and hydrogen gases were connected to the reactor through the process line via pipe fittings. The hydrogen and nitrogen gas cylinders connected through a 3-way valve were to be switched on/off for the purpose of catalyst reduction and/or cooling the reactor to a desired temperature. Pressure indicators, regulators and mass flow controllers were installed to measure the pressure and flow of reactant into the reactor. The reactant stream enters into the main process line through a filter to prevent impurities entering into the reactor.

Also the pressure drop across the reactor was measured with the fitted pressure indicators at both top and down stream of the reactor.

A thermocouple was located in the furnace but not directly in contact with the catalyst to measure the catalyst bed temperature. A gas chromatograph was connected to the product outlet of the reactor via a 6-way valve with a sample loop through which product stream enters into the gas chromatograph column for separation. Helium gas cylinder was also connected directly to the gas chromatograph which served as a carrier gas. A data processor was connected to the gas chromatograph for data collection From the 6-wayvalve, a connection was made via a needle valve for purging accumulated reaction products and unconverted reactants at interval. Gas booster (butane) was also connected to the purge line for easy burning. The whole down-stream pipeline network was wrapped with a heating tape and covered with insulating materials to heat up the product stream.

For the purpose of studying catalyst poisoning, the following modifications were made in the experimental rig. A saturator was connected to the methane line in order to introduce saturated NH_3 into the reactor. A bypass line allowed for easy operation, in case of changing the ammonia solution in the saturator For safety purposes, the system was pressured at the beginning of each experimental run to test for leakage using soap solution. A photograph for both the experimental rig and Gas Chromatograph are shown in Figure 3 3 and 3.4.

3.2.1 Calibration

3.2.1.1 Mass flow controller

In order to measure accurate gas flows delivered into the reactor, and for easy calculations, the mass flow controller (model 5876 and 5850 TR Brooks Instrument B.V Holand), used in this study were calibrated. The mass flow controller was positioned at 10, 20 30, 40, 50, 60 70, 80, 90 and 100 and gas was allowed to pass through a burette of 25ml with a soap solution. The time taken for the gas to pass through the 25 ml burette was recorded. Average values were taken after every three runs. The average values divided by the time gave the volume of gas delivered.

A mole of gas was calculated using the data obtained. The calibration data and plots are presented in Appendix I (Table A1.1 and Figure A1 2, A1.3).

3.2.1.2 Gas Chromatography (GC) calibration

GC calibration was performed both on reactant and product for the purpose of conversion calculations. Measured volumes (0 5, 1.0, 1.5 and 2.0 ml) of methane, using gas shringe of size 10 ml were injected into the GC and response area was recorded. The response areas were plotted against moles of gas converted from the volume of gas injected. See calibration data in Table 1.2 and A1.3 and plots in Figures A1.4, A1.5, and A1.6.

3.2.1.3 NH_3 calibration

Ammonia calibrations were carried out so that known concentrations will be introduced into the reactor for poisoning test. Prepared solution of 3000 ppm, 1000 ppm, 500 ppm and 100 ppm were mixed with argon and the tracing was recorded.

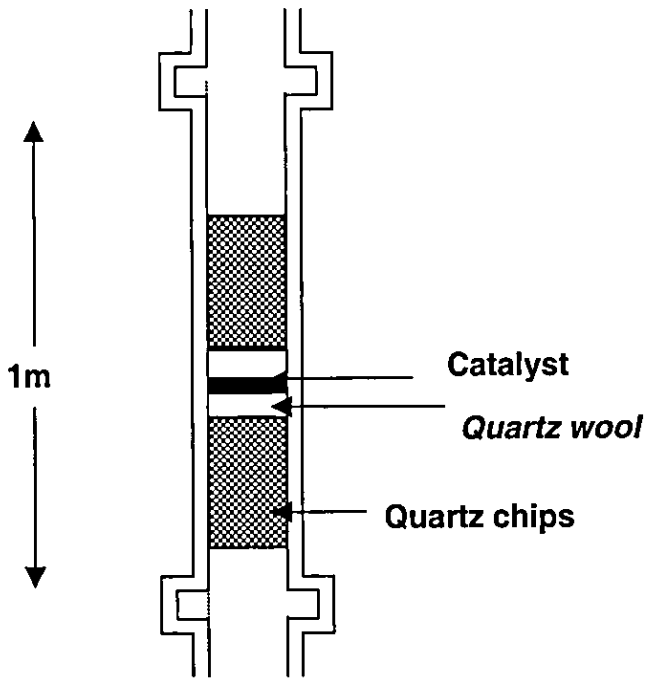

Figure 3 1 A cross section of Reactor

The response areas from the tracing were integrated and plotted against the measured values from the mass flow controller (see tracing and plots in Figure A1.9 and A1.20.

3.2.1.4 Reactor temperature profile calibration

The reactor temperature profile was calibrated so that the catalyst bed would be located at the highest temperature of the reactor. Temperatures at 773K, 873K, 973K, 1073K and 1173K were selected using the temperature-controller. At each temperature set point of the furnace, with 5 minutes dwelling time and ramping rate at 20 K/min the corresponding reactor temperatures were measured by a thermocouple when it has attained steady state. This was repeated at different position of the reactor, between 0.16-0.86 m. The catalyst bed was identified between 0.41-0.51 m, which gave a constant temperature range (1046-1048K) (see Table A1.4 and Figure A1.7).

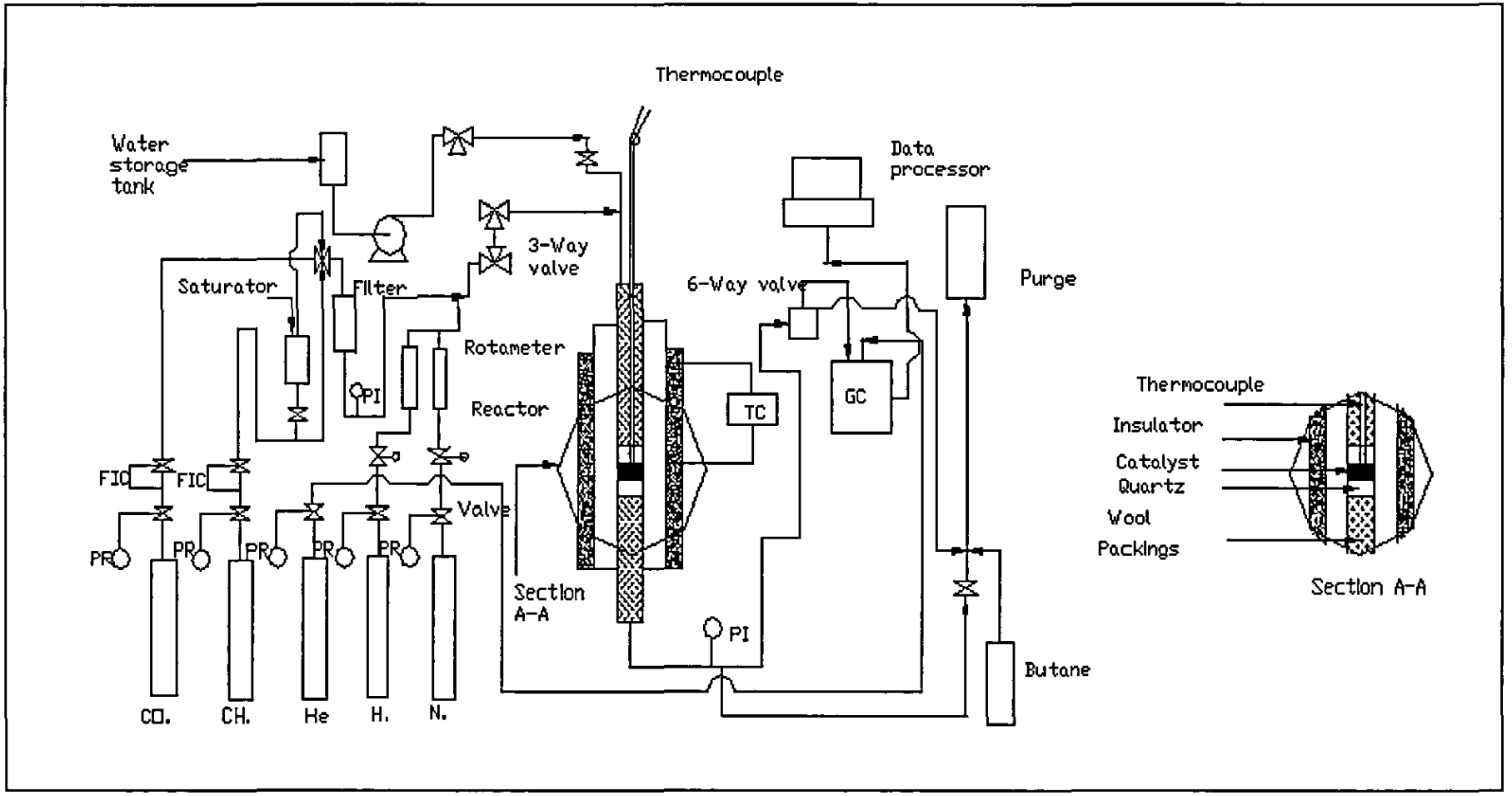

Figure 3.3 Experimental rig

Weight of catalysts (mg)	Length of reactor(m)	Diameter of reactor (m)	Volume of reactor (m^3)	Space velocity WHSV (ml/hr.g.cat)
50	1	$7.6x10^{-3}$	$4.54x10^{-4}$	19200

Table 3.1 Reactor design parameters

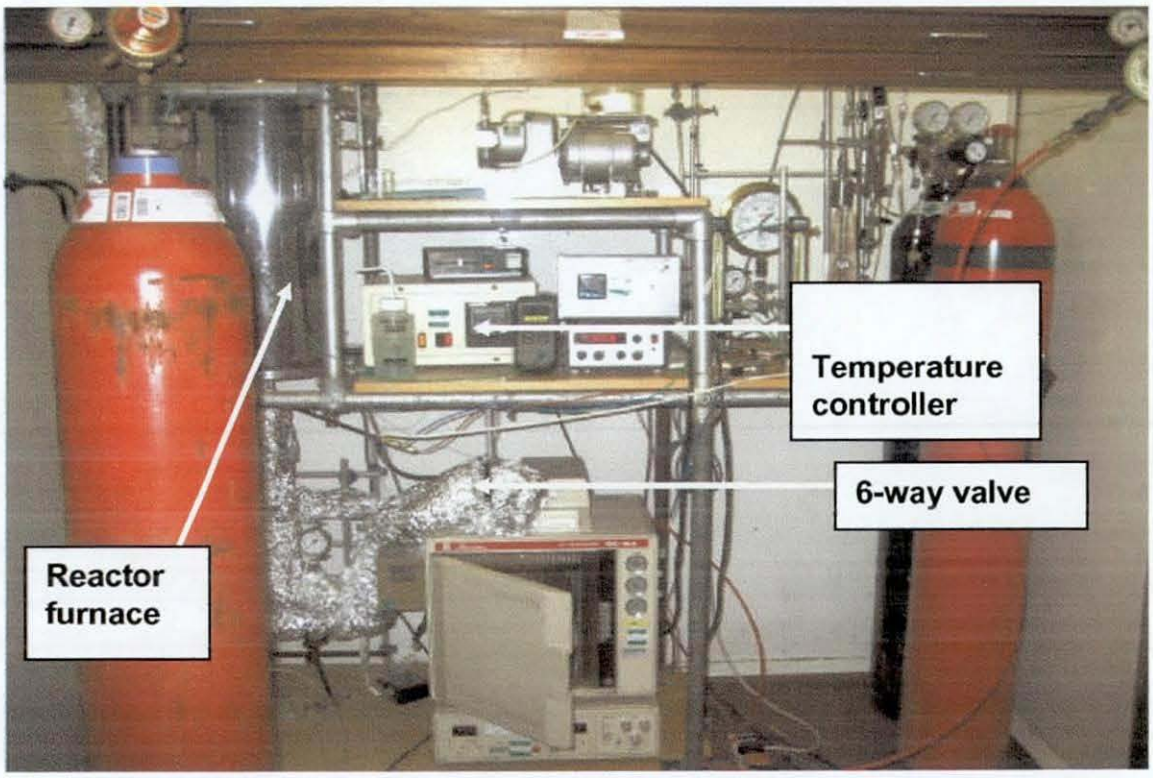

Figure 3.3 Photograph of experimental rig

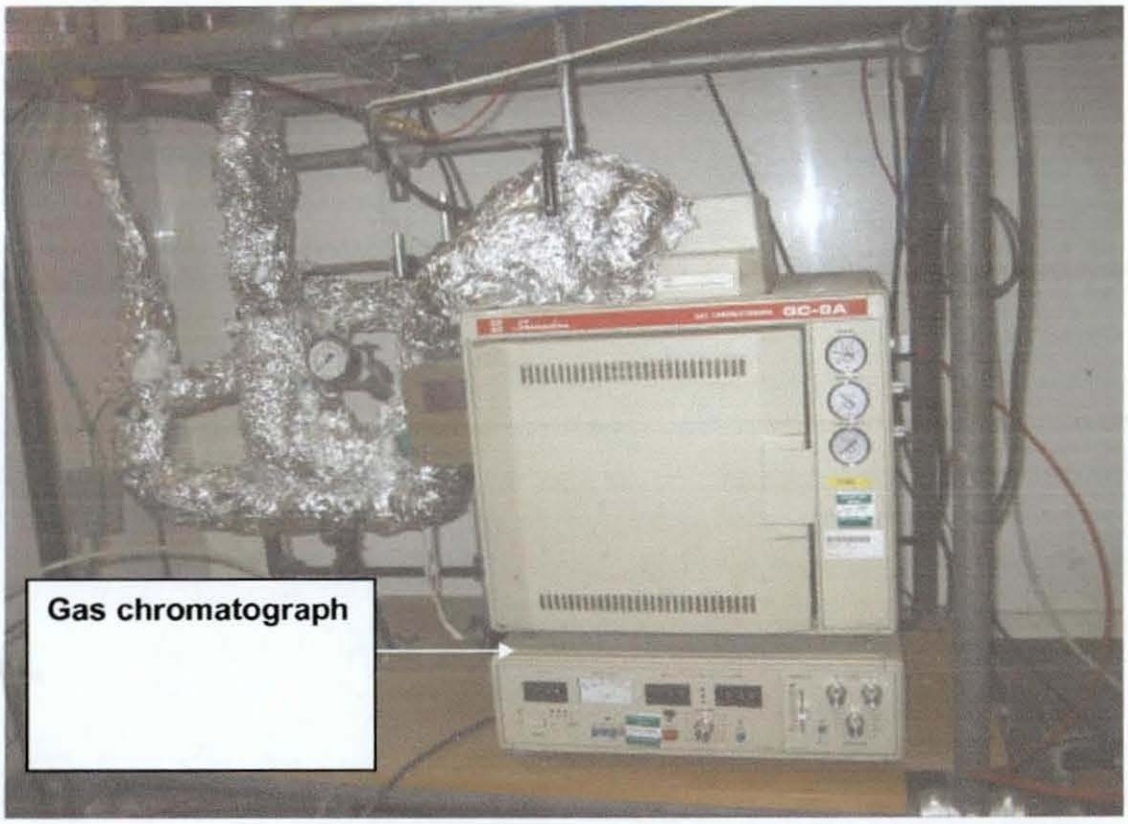

Figure 3.4 Photograph of Gas chromatography and down stream pipeline network

3.3 Experimental apparatus (Temperature–programmed reduction)

The temperature–programmed reduction experiment was carried out in a conventional apparatus as shown in Figure 3.5. A quartz glass was used as a reactor. The reactor was loaded with powdered catalyst samples (170 mg) and it was mounted into a furnace. The catalyst sample was held by quartz wool at both ends. A hydrogen generator and argon cylinder with fitted pressure indicators, regulators and mass flow controllers were connected to the reactor via pipe fittings to measure the mass flow of gases into the reactor. The reactor system was connected to a mass spectrophotometer to analyse the outlet gases as a result of reduction. The process line connected to the mass spectrophotometer was shield with heating tape to prevent produced water from entering into the mass spectrometer as a result of catalyst reduction. The hydrogen uptake was quantified by using data obtained from (peak fit software program) and calibration plot obtained using pure copper oxide.

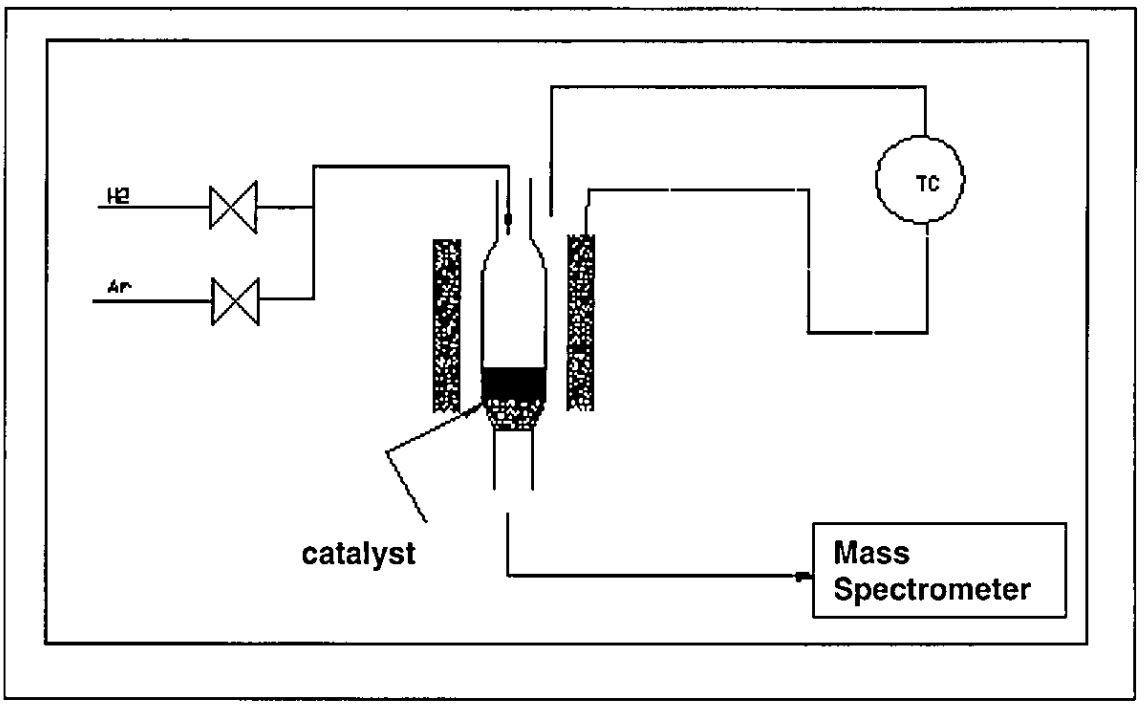

Figure 3.5 Temperature–programmed reduction rig

3 3.1 Calibration

To determine the hydrogen uptake during catalyst reduction, a known quantity of pure copper oxide (CuO 99 95%) was reduced in a conventional apparatus. Three reduction runs were conducted using varying amount of oxide (30 mg, 40 mg and 70 mg). The peak areas were integrated using (peak fit software program) and the values were used for calibration (see plots in Appendix I, Figure A1.24 and A1.25).

3.4 Catalyst design strategy

The major draw back preventing commercialisation of CO_2 reforming of methane lies in the poor activity and stability of conventional Ni-based catalyst due to deactivation by a high rate of carbon deposition (Rostrup-Neilsen and Hansen 1993) via methane dehydrogenation and the Bouduoard reaction ($2CO \Leftrightarrow C + CO_2$) (Choi *et al* , 1998). Due to the above reason, design strategies have been employed by many research groups to obtain an effective catalyst for the reforming of methane with minimal carbon deposition.

The application of both transition oxides for support modification and metal alloys as catalyst has opened up interesting possibilities, because of the properties modification on both the support and nickel active phase. Wang *et al.*, (2003) reported the strong influence on the catalytic performance of Ni/yttira-doped ceria catalyst towards CO_2 reforming of methane. Shishido *et al.*, (2001) have observed remarkable impact of Ni/Mg-Al catalyst prepared by solid phase crystallisation that recorded very high stable CO_2 and CH_4 conversion levels after 6 hours time on stream Frusteri *et al.*, (2000) also reported remarkable impact of potassium (K doping) over Ni/MgO catalyst which recorded a very slight decay in CO_2 and CH_4 conversion levels after 12 hours time on stream.

In this present study, different transition oxides such as (MgO, ZrO_2 and La_2O_3) and metals (Cu and Pd) have been used to modify both the support and the nickel active phase and the effects on activity and stability and also carbon deposition has been studied.

3.4.1 Materials and methods

3.3.1.1 Materials

For the purpose of studying the effect of support on activity and stability of catalyst, various supports were used to disperse the metal active phase. The supports used in this study were alumina (γ-Al_2O_3 Larpote Industries, Lanceshire) and Praseodymium oxide (Pr_2O_3, Fisher Scientific, UK) The Pr_2O_3 that was in a powdered form was isostatically pressed into pellets at 10 bars for 5 minutes. The pellets were then crushed and sieved to obtain size ranges of 250-355 microns. The alumina which was in granular form was also crushed and sieved to obtain the same particle size ranges. The physical properties were determined by BET surface area method (see data shown in Table 3.2).

Support	**Supplier**	**BET surface area(m^2/g)**	**Langmuir (m^2/g)**	**Pore volume (cm^3)**
γ-Al_2O_3	Laporte, Ltd	257	352	0.31
Pr_2O_3	Fisher Scientific	464	618	1 68

Table 3.2 Physical properties of supports

3.4.1.2 Ni-based catalyst preparation

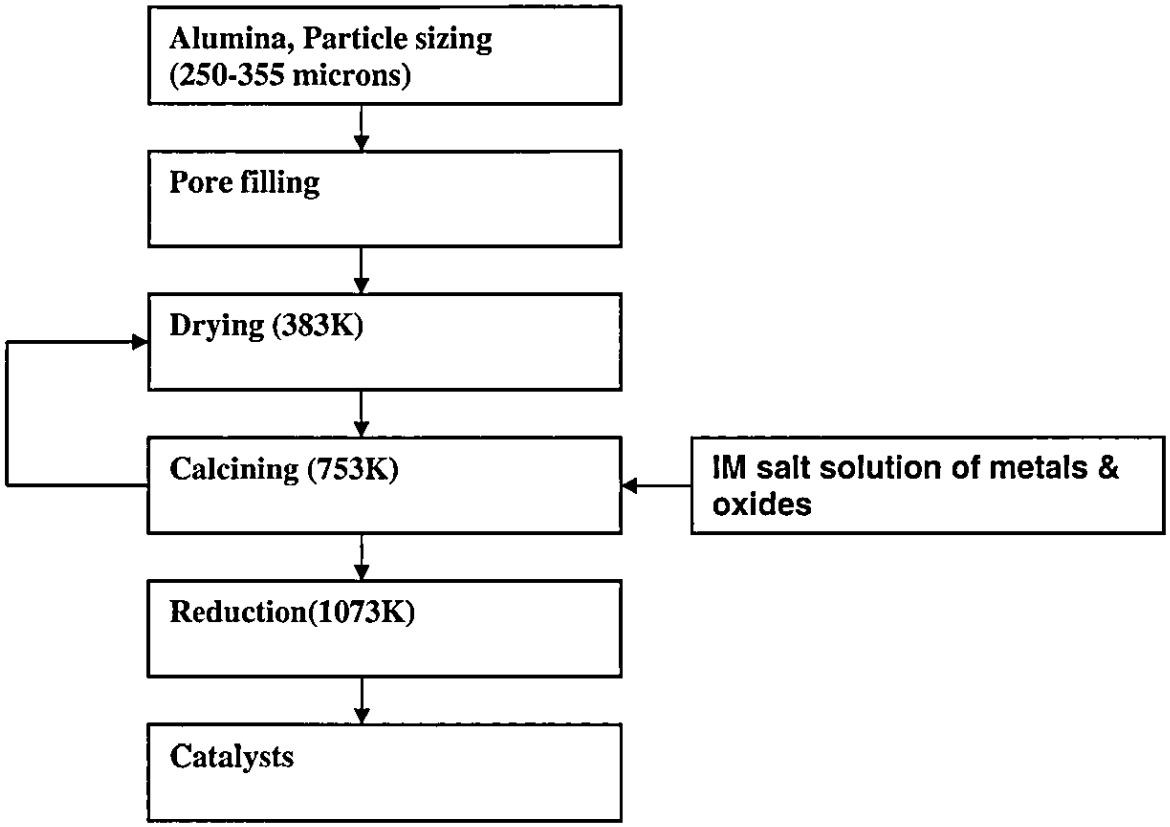

Figure 3.6 Procedures for catalyst preparation

The unpromoted $Ni/\gamma\text{-}Al_2O_3$ catalysts was prepared by incipient wetness impregnation technique of the support ($\gamma\text{-}Al_2O_3$) using aqueous solution of the precursor $Ni(NO_3)_2.6H_2O$ (Fisher Scientific UK) (see flow chart for procedure in Figure 3.6). The support (alumina) was supplied by (Laporte, Industries, Lanceshire) with a measured BET surface area of $257m^2/g$. The impregnated sample was dried overnight at 383K and calcined at 753K. The calcinning process was mainly to reduce the nitrates to oxides and it was then reduced at 1073K for 1 hour to stabilise nickel. The Ni/Pr_2O_3 catalyst was prepared with the same procedure described above. The morphology of the prepared unpromoted $Ni/\gamma\text{-}Al_2O_3$ and support are shown in Figure 3.7, which showed a marked difference in surface appearance.

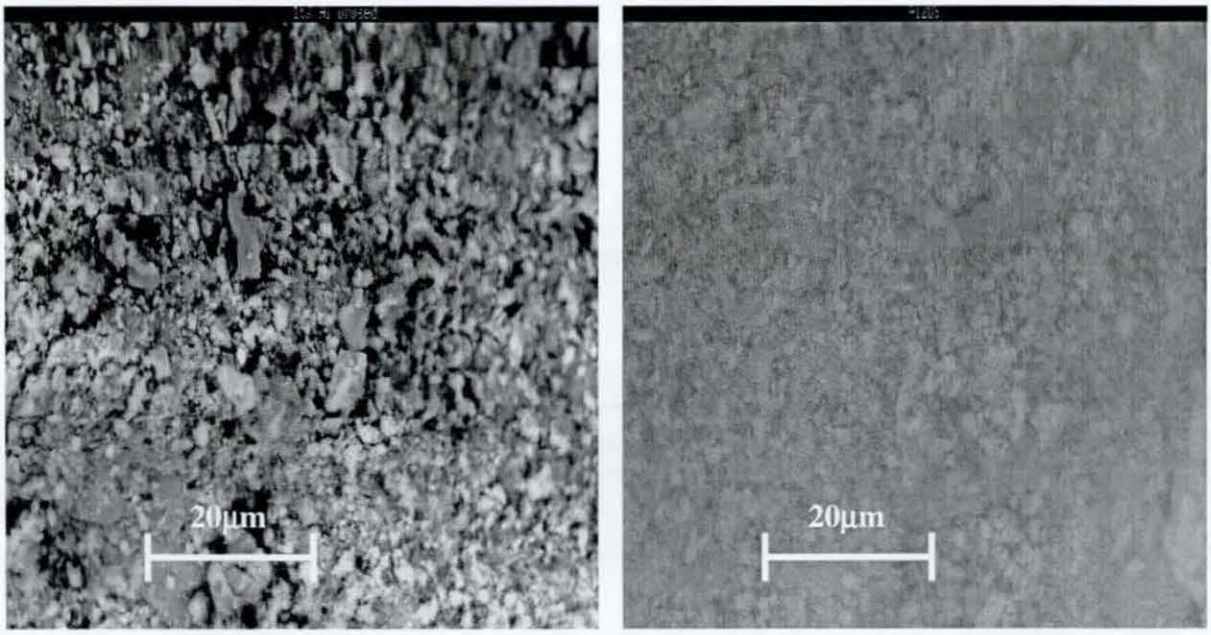

Figure 3.7 SEM images of (a) 15 wt% Ni/γ-Al_2O_3 (b) γ-Al_2O_3

3.4.1.3 Support modified Ni-based catalysts

The transition oxide promoted catalysts were obtained by first impregnation of the support with nitrate precursors of the various oxides ($Mg(NO_3)_2.3H_2O$, $La_2(NO_3)$ $6H_2O$ and $Zr(NO_3)_2$ $6H_2O$, Fisher Scientific, UK). After addition of promoters (5 wt%), the samples were dried over-night at 383K and then calcined at 753K for 6 hours. The calcined catalysts were further impregnated with 1M solution of nickel nitrate followed by the same thermal treatment as described above. A list of samples along with the Ni loadings determined by flame atomic absorption spectrophotometer, BET surface area, and the corresponding Ni dispersion data are shown in Chapter 4 Table 4.1.

3.4.1.4 Ni-promoted based catalysts

The palladium and copper promoted catalysts were also prepared. The procedure for catalyst preparation has been described in section 3.3.1.3. The aqueous solutions used were $Pd(NO_3)_2$ $3H_2O$ solution and $Cu(NO_3)_2$ $3H_2O$ (Fisher Scientific, UK) respectively. The loadings of both palladium and copper were 0.25 wt%, 0.5 wt% and 1 wt% respectively.

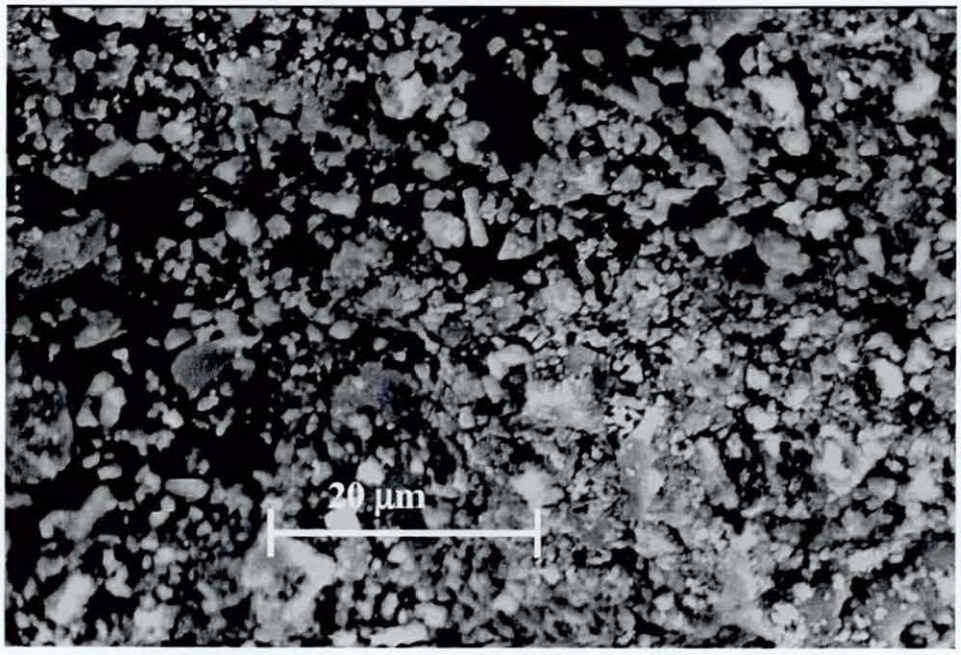

Figure 3.8 SEM image for Ni-Cu/γ-Al_2O_3 (0.25 wt%)

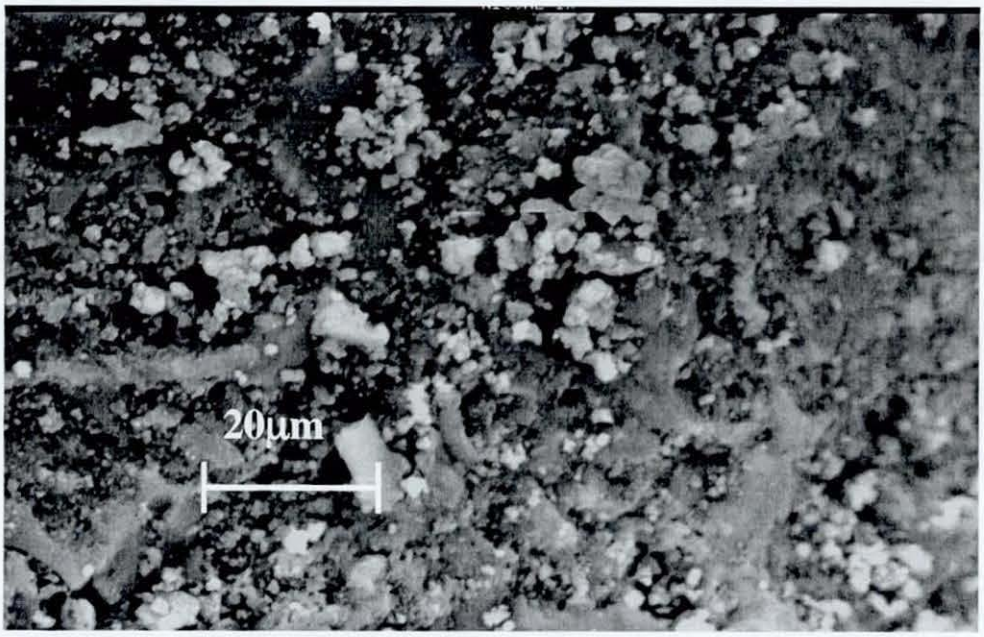

Figure 3.9 SEM image for Ni-Cu/γ-Al_2O_3 (1 wt%)

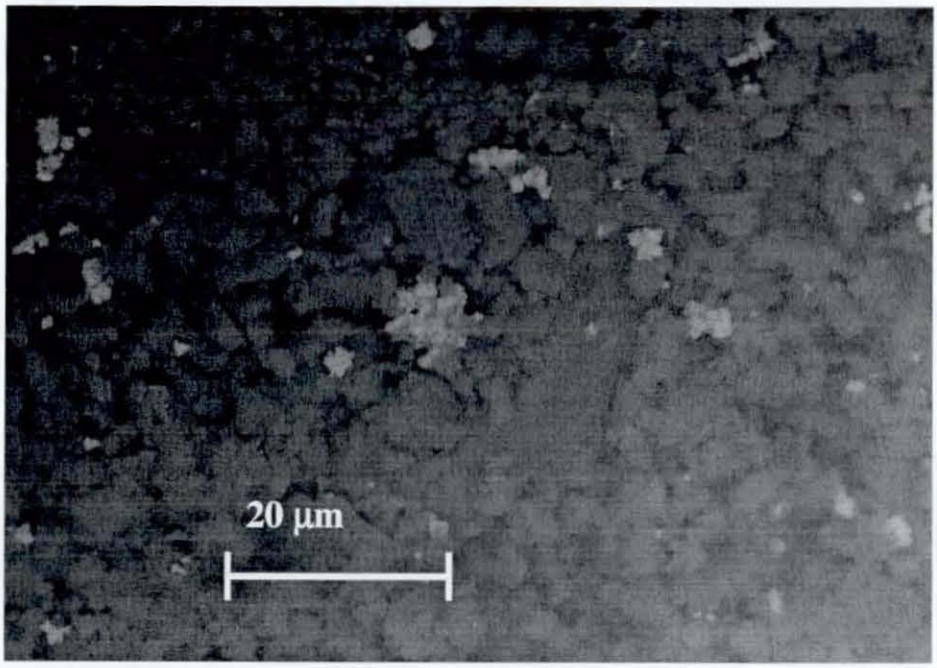

Figure 3.10 SEM images for Ni-Pd/γ-Al_2O_3 (0.25 wt%)

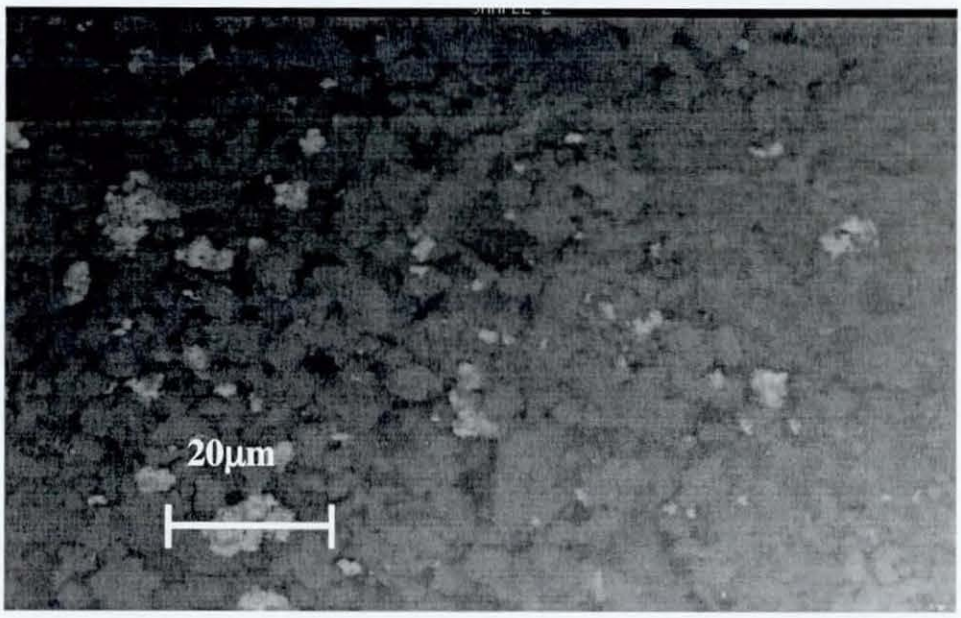

Figure 3.11 SEM images for Ni-Pd/γ-Al_2O_3 (1 wt%)

Examples of morphology for the Ni promoted catalysts are shown in Figures 3.8, 3.9, 3.10 and 3.11 respectively. There was no much difference shown in the surface appearance of the catalysts. A list of samples along with the Ni loadings as determined by flame atomic absorption spectrophotometer, BET surface area, and the corresponding Ni dispersion data are given in Chapter 5 Tables 5.1 and 5.2.

3.5 Catalysts characterisation

3 5.1 Surface area and pore size distribution

Textural properties of all catalysts were measured using a Micrometrics ASAP 2010 apparatus (Micrometrics Instrument Corporation, USA). All adsorption isotherms were generated by dosing 99 99% pure nitrogen at 77K. All catalysts were dried and out-gassed at 378.15K under a vacuum of < 10 mm Hg for a minimum period of 24 hours. The mass of the degassed sample was determined by subtracting the weight of the empty tube from the nitrogen back-filled sample containing tube. Barrentt Joyner Halenda (BJH) theory was used for the calculation of the pore size distribution of the catalyst.

The textural properties of the catalysts and pore size distribution plots are presented in Table 4.1, 4.2 and Figure 4.1 in Chapter 4 and Tables 5.1, 5 2 and Figure 5.1 and 5.2 in Chapter 5 Examples of the adsorption–desorption plots are also presented in Appendix I, Figures A1 21 and A1.22.

3.5.2 Carbon monoxide chemisorption (CO)

Nickel dispersion (active phase) of unpromoted and promoted catalysts were determined using the same Micrometric ASAP 2010 instrument. CO chemisorption measurement was carried out at room temperature. The sample was pre-treated using heat treatment for 4 hours After reduction at 623K under H_2 flow, the samples were evacuated for 30 minutes at the reduction temperature and cooled to room temperature. The irreversible CO uptakes were obtained from the total and reversible adsorption isotherms taken at a reducing pressure (see example plots in Appendix I, Figure A1.23).

3.5.3 Atomic absorption spectrophotometry (Ni active phase measurement)

The atomic absorption technique was used to determine more accurate nickel loading of the catalysts. The equipment consists of (1) a light source (2) an absorption cell (3) a monochromator (4) a detector and a display. A hallow cathode lamp acts as a light source which emits a light spectra specific to the element type.

The amount of light attenuation in the sample cell is converted into sample concentration. The solution for the atomic absorption experiment was prepared by digesting known weight of sample of the catalyst with 1M H_2SO_4 and 1M HNO_3 solutions. After digestion, the clear solution was diluted to desired concentration and measurements were taken using prepared standard calibrations. The data obtained in milligrams per litre (concentration) were used to calculate the actual nickel content of the catalyst. The data obtained are presented in Tables 4.2, in Chapter 4 and Tables 5.1 and 5.2 in Chapter 5 respectively.

3.5.4 Scanning electron microscope (morphology of catalysts)

The morphology of the catalyst sample was studied using a Cambridge Stereoscan 360 Scanning electron microscope at room temperature and at an accelerating voltage of 10kV. The preparation of the samples involved 4 hours drying in an oven at 373K and subsequent storage in a desiccating jar over silica gel prior to analysis. The samples were attached on to alumina platform using poly vinyl acroylnitrite (PVA) glue and sputter-coated with gold and the samples were placed in the scanning chamber. Nitrogen gas was introduced to flush out any impurity that was associated with the catalyst before the scanning. The SEM images of the fresh catalysts are presented in Chapter 3 and the used catalysts could be found in (Chapter 4, Chapter 5 and Chapter 6) respectively.

3.5.6 X- ray diffraction (crystalline structure of prepared catalyst)

The crystalline structure of the catalysts was also studied using X–ray diffraction technique A beam of X-rays, when impinges on a material, it is scattered in varying directions by the electron clouds of the atoms. Interference can occur, if the wavelength of the X-ray is comparable to the separation between the atoms. The data obtained was used to calculate the crystallite size, using the Scherrer formula.

$$t = \frac{0.9\lambda}{\sqrt{\beta_{m^2} - \beta_{s^2}}\,Cos\theta} \qquad \text{(Dann 2000) (3.1)}$$

where t = thickness of crystallite , 0.9 = constant, λ = 1 54 , β_m^2 and β_s^2 = half width length of diffraction peak for the sample and standard, which relates the crystallite size to the width of its diffraction peaks. The diffraction peaks are shown in Chapter 4, Figure 4 5, 4.6 and Chapter 5, Figure 5.3 respectively.

3.5.7 Temperature-programmed reduction (TPR)

Temperature-programmed reduction (TPR) of catalyst was conducted in a conventional apparatus. A reactor consisting of a quartz tube, with an inner diameter (size 4 mm). The catalyst was weighed (170 mg) and was loaded in the reactor using quartz wool to hold at both ends. The inherent water in the catalyst sample was removed first by increasing the temperature of the system from room temperature to 473K. At the end of 30 minutes a gaseous mixture of 10% H_2 /90% argon with a total flow rate of 50 ml/min was introduced in to the reactor as a reducing agent while the temperature was increased from 473K to 1073K. The ramping rate of the temperature was kept at 10 K/min. The maximal allowed temperature of the programmed reduction was 1073K.

The effluent gases, H_2 uptake and water produced from catalyst reduction was analysed by on-line mass spectrophotometry instrument. The hydrogen uptake was determined using pure copper oxide calibrations. The reduction trace plots are shown in Figures 4.4 and 5.2 and peakfit plots could be found in Appendix A1.24 and A1.25.

3.5 Catalyst activity and stability test

Catalytic activity test in the temperature range between 923K-1073K were performed using a packed bed reactor (i d. = 0.0076 m) and a catalyst sample of 50 mg diluted with (430 mg quartz chips) of 480-1500 microns and varying space velocities (WHSV) 4800-19200 ml/hr g cat. The experimental apparatus is shown in Figure 3.2. The reactor bed temperature was measured with a K-type thermometer (model KM 340) located inside the furnace, attached to the reactor but without direct contact to the catalyst.

At the start of each run, the catalyst (50 mg) charged into the reactor with 430 mg of quartz sand (480-1500 microns) to make up the catalyst bed, was reduced *in situ* at 1073K for 1 hour under flowing 5% H_2/N_2 (50 ml/min) and then cooled to reaction temperature under N_2 flow before switching to the CO_2/CH_4 1:1 reaction mixture.

An inherent, water in the catalysts was removed by heating up to 423K for 30 minutes in an inert atmosphere (N_2) before the start of the reduction process. The product stream was analysed by on-line gas chromatograph (Shimadzu 8APT, TCD Corporation, Japan) equipped with carboxen 1000 column and analytical system connected to a thermal conductivity detector. Methane and carbon dioxide used were high purity (99.999%) gases supplied by British Gas.

A stability test was also carried out for 300 minutes at different temperatures with the same process conditions employed. The effect of space velocity was also studied by varying the space velocities using different flow rates of the reactants. The amount of carbon deposited on the catalyst surface during reaction time for 6 hours was determined using burn off method in a furnace. The catalyst recovered after reforming was weighed and burnt in a furnace at 1173K for 1 hour in order to burn off all carbon deposit and was reweighed after the burn off exercise. The carbon deposited is expressed as the difference in weight obtained divided by the total catalyst used. Carbon balance was also carried out on reaction components and products for comparison. The conversion of CO_2, CH_4 and CO yield are expressed as the fraction of CO_2 or CH_4 converted divided by the initial concentration of reactant and CO formed divided by $(CO_{2\,in}+CH_{4in})x100$

3.7 Catalyst poisoning

A catalyst poisoning experiment was considered since biogas contains some traces of NH_3, H_2O and H_2S, etc. The aim was to investigate the effect of these gases on the catalyst during reforming of methane. In this study, the effect of NH_3 and H_2O were studied on the following: the unpromoted catalysts ($Ni/\gamma\text{-}Al_2O_3$), $NiZrO_2/\gamma\text{-}Al_2O_3$, $Ni\text{-}Pd/\gamma\text{-}Al_2O_3$ (0.25 wt%) and $Ni\text{-}Cu/\gamma\text{-}Al_2O_3$ (0.25 wt%).

The catalyst poisoning test was conducted by introducing 3000 ppm of NH_3 solution in to the reactor by a saturator through the methane line. The same process conditions were employed as earlier mentioned in the activity test.

The NH_3 concentration of 3000 ppm was chosen because it was the only concentration that gave a constant tracing during the calibration exercise. Other concentrations such as 1000 ppm, 500 ppm and 300 ppm showed decrease in concentration during the tracing experiment. Examples of the tracing plots for 3000 ppm and 1000 ppm could be found in Appendix I, Figure A1.8 Also the tracing plots for 3000 ppm for all the flow rates is presented in Appendix I, Figure A1.7.

3.8 Theoretical calculation of thermodynamics predicted values

3.8.1 Equilibrium calculations for carbon dioxide reforming of methane

With multicomponent systems, a number of reactions can potentially occur and this may lead to a collection of non-linear equations that makes it difficult for equilibrium calculations to be performed. The number of reactions that must be considered, and the number of simultaneous equations that must be solved can be reduced by taking into account the accuracy desired in the calculations (Sandler 1989).

The reactions that occur to only small extent and that produce products at concentrations below the level of interest are eliminated. These are recognised by very small equilibrium constants. Based on the above assumptions, the reactions that might occur in methane reforming with carbon dioxide were considered and using the Denbigh elimination method (Sandler 1989) the following equations were obtained.

(1) $C + 2H_2O \leftrightarrow CO_2 + 2H_2$ (3 2)

(2) $C + H_2O \leftrightarrow CO + H_2$ (3.3)

(3) $C + 2H_2 \leftrightarrow CH_4$ (3.4)

The three reactions are more mathematically favoured and are being considered for thermodynamic analysis. As these reactions are reversible they can never reach completion and are limited by the thermodynamic equilibrium. The equilibrium constant are defined as follows:

$$K_1 = \frac{P_{CO_2} P^2_{H_2}}{P^2_{H_2O}} = \exp\left(\frac{-\Delta G}{RT}\right) \tag{3.5}$$

$$K_2 = \frac{P_{CO} P_{H_2}}{P_{H_2O}} = \exp\left(\frac{-\Delta G}{RT}\right) \tag{3.6}$$

$$K_3 = \frac{P_{CH_4}}{P^2_{H_2}} = \exp\left(\frac{-\Delta G}{RT}\right) \tag{3.7}$$

where K_1, K_2, K_3 are the equilibrium constant for the equation (1), (2) and (3), P = partial pressure for reactant and product, ΔG = Gibbs free energy, R = gas constant and T = temperature.

Using the molar extent of reactions X_1, X_2 and X_3 for the three equations the mole balance table was obtained as follows: A mole balance based on 1 mole of carbon dioxide and 1 mole of methane over the system was constructed using the three equations, shown in Table 3.3 and the corresponding plots are also presented in Figure 3.12 and 3.13 respectively.

Species	**Number of moles in the gas phase**		**Equilibrium mole fraction**
	Initial	**Final**	
H_2O	0	$.2X_1-X_2$	$(-2X_1-X_2)/\Sigma$
CO	0	X_2	$(X_2/\Sigma$
H_2	0	$2X_1+X_2-2X_3$	$(2X_1+X_2-2X_3)/\Sigma$
CO_2	1	$1+X_1$	$(1+X_1)/\Sigma$
CH_4	1	$1+X_3$	$(1+X_3)/\Sigma$
Total	2	$\Sigma=2+X_1+X_2-X_3$	

Table 3.3 Mole balance

Using the above table the following three non-linear equations were obtained, relating the equilibrium constant to the component in the gaseous phase for the three equations.

$$K_{a1} = \frac{Y_{CO_2} Y_{H_2}}{Y^2{}_{H_2O}} = \frac{(1+X_1)(2X_1+X_2-2X_3)}{(2+X_1+X_2-X_3)} \tag{3.8}$$

$$K_{a2} = \frac{Y_{CO} Y_{H_2}}{Y_{H_2O}} = \frac{(X_2)(2X_1+X_2-2X_3)}{(2+X_1+X_2-X_3)(-2X_1-X_2)} \tag{3.9}$$

$$K_{a3} = \frac{Y_{CH4}}{Y^2{}_{H2}} = \frac{X_3(2+X_1+X_2-X_3)}{(2X_1+X_2-X_3)} \tag{3.10}$$

where Y = mole fraction, X_1, X_2, and X_3 are extent of reaction for equation 1, 2 and 3 respectively.

The thermodynamic equilibrium calculations under proposed experimental conditions were performed for the selection of reaction conditions and apparatus system For the CO_2 reforming of methane, $CH_4 + CO_2 \Leftrightarrow 2H_2 + 2CO$, there is an increment in the number of moles produced such that operation at high pressure does not favour the progress of the reaction (Aparicio *et al* 2002). Based on their report, which indicated a decrease in conversions from 26 to 15%, with an increase in pressure from (1 to 3 atm), pressure of 1 atmosphere and temperature range of 600-1600K were chosen for the calculations.

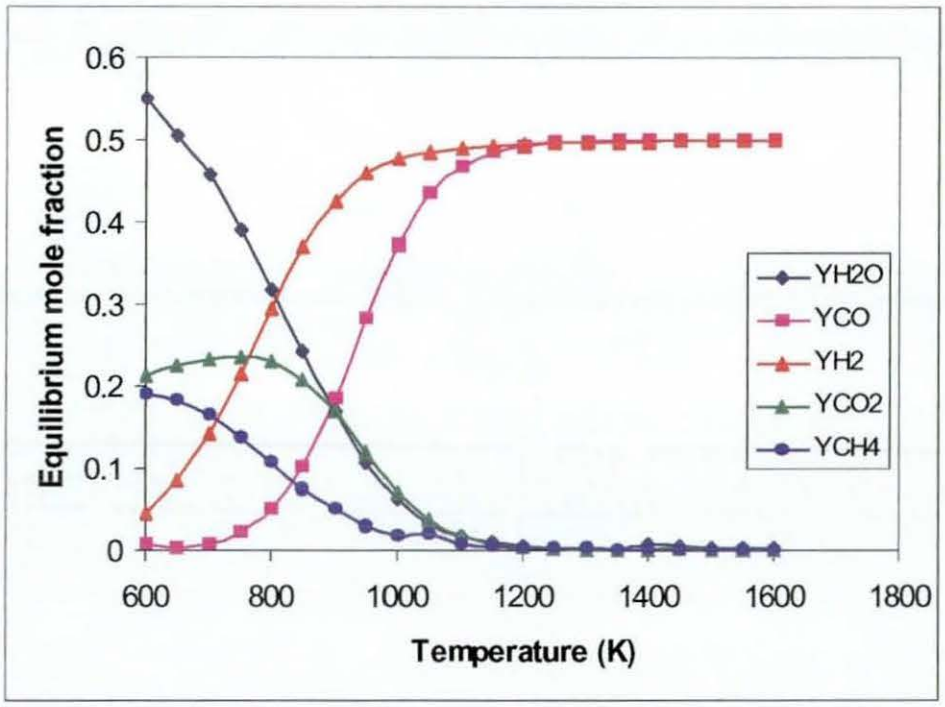

Figure 3.12 Equilibrium mole fractions

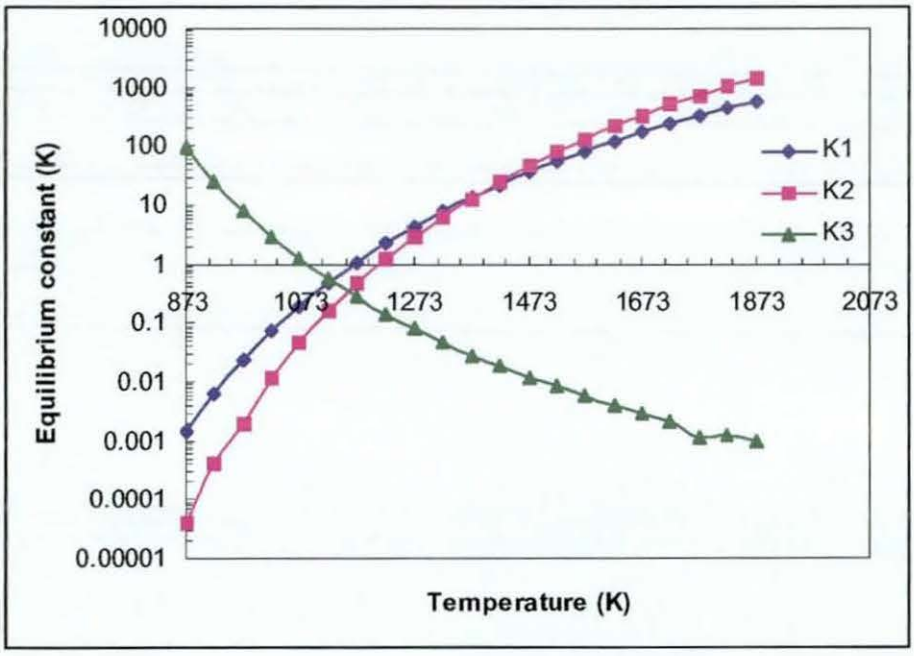

Figure 3.13 Equilibrium constant for the three independent reactions

These equations have been solved using a computer package, "Maple program" the data for thermodynamic conversions and the equilibrium constant were obtained for the given reaction conditions (see Tables A2.1 and A2 2 in Appendix II). Figures 3.12 and 3.13 show both the equilibrium quantity of each species and the equilibrium constant calculated.
Figure 3.12, indicates the equilibrium conversions for both carbon dioxide and methane which decreases with an increase in reaction temperature whilst reaction products increased, showing an endothermic reaction. The reaction temperature range was chosen between 923K–1023K, because product ratio of 0.6 to 1 could be attained. Further increase in temperature indicated no change in product ratio which is also reflected in the reactant conversion profile.

3.9 Kinetic modelling of CO_2 reforming system

A mathematical model could be used to obtain a better qualitative and quantitative understanding of the factors affecting the rate of a reaction process. In carbon dioxide reforming of methane processes with variation of feed concentration, temperature and pressure, there is generally a decline in reactant concentration with time, due to the disappearance of the reactants as a result of interaction between reactant molecules, depending on the variable, in order to produce desired products. For parallel reactions occurring in a system, more than one rate constant is expected and therefore becomes difficult to estimate with numerical analysis. CO_2 reforming of methane can be explained by many reactions, but three independent equations, the reforming reaction, the reverse water gas shift reaction and the Boudouard reaction respectively are usually used to describe the system. However, equation 3.1, 3.2 and 3.3 are mathematically favoured and therefore has been considered for the estimation of the rate constant, using a computer program (PDSolve) a finite difference programme for the three parallel reactions. The three parallel reaction equations considered for the CO_2 reforming of methane is given as:

$$C + 2H_2O \Leftrightarrow CO_2 + 2H_2 \qquad (3.1$$

$$C + H_2O \Leftrightarrow CO + H_2 \qquad (3.2)$$

$$C + 2H_2 \Leftrightarrow CH_4 \qquad (3.3)$$

where, $H_2O = A$, $CO = B$, $CO_2 = C$, $H_2 = D$, $CH_4 = E$

For reaction (3.1)

Forward reaction, $r_1 = k_1 C_A^{\ 2}$

Backward reaction, $-r_2 = k_2 C_C C_D$

Reaction (3.2)

Forward reaction, $r_3 = k_3 C_A$

Backward reaction, $-r_4 = k_4 C_B C_D$

Reaction (3.3)

Forward reaction, $r_5 = k_5 C^2{}_D$

Backward reaction, $-r_6 = k_6 C_E$

Rate of formation of CO at steady state approximation $r_3 = r_4$

$$\frac{dC_B}{dt} = 0 = k_3 C_A - k_4 C_B C_D, \text{where} \frac{k_4}{k_3} = K_2 \tag{3.14}$$

$$R_{CO} = k_3\left(C_A - \frac{C_B C_D}{K_2}\right) \tag{3.15}$$

Rate of reaction for CH_4

$$-\frac{dC_E}{dt} = 0 = r_5 = r_6 \tag{3.16}$$

$$k_5 C^2{}_D - k_6 C_E, K_3 = \frac{k_6}{k_5} \tag{3.17}$$

$$-R_{CH_4} = k_5\left(C^2{}_D - \frac{C_E}{K_3}\right) \tag{3.18}$$

Rate of reaction for CO_2

$$-\frac{dC_C}{dt} = 0 = r_1 = r_2 \tag{3.19}$$

$$k_1 C_A{}^2 - k_2 C_C C^2{}_D, K_1 = \frac{k_2}{k_1} \tag{3.20}$$

$$R_{CO_2} = k_1\left(C^2{}_A - \frac{C_C C^2{}_D}{K_1}\right) \tag{3.21}$$

Rate of reaction for H_2O

$$R_{H_2O} = -R_{CO} - 2R_{CO_2}$$

$$R_{H_2O} = -k_3\left(C_A - \frac{C_B C_D}{K_2}\right) - 2k_1\left(C^2{}_D - \frac{C_C C_D{}^2}{K_1}\right) \tag{3.22}$$

Rate of formation of H_2

$$R_{H_2} = 2R_{CO_2} + R_{CO} - R_{CH_4} \tag{3 23}$$

$$R_{H_2} = 2k_1\left(C^2{}_A - \frac{C_C C^2{}_D}{K_1}\right) + k_3\left(C_A - \frac{C_B C_D}{K_2}\right) - 2k_5\left(C^2{}_D - \frac{C_E}{K_3}\right) \tag{3.23}$$

3.9.1 Kinetic data

The kinetic data and the plots from both the experimental and model simulated results are shown in Table 3.4 and Figure 3.14 and 3.15 The reactor space time values in terms of mole fraction were compared to the model values The model data fitted very well with the experimental results, using different values at varying reaction temperatures.

As can be seen in Table 3.2 the largest rate constant for CO_2 reaction and CO formation was observed for $Ni/ZrO_2/\gamma\text{-}Al_2O_3$ catalysts compared to the unpromoted catalyst. Compared to the $Ni/\gamma\text{-}Al_2O_3$ catalysts, $Ni\text{-}Pd/\gamma\text{-}Al_2O_3$ (0 25 wt%) and $Ni\text{-}Cu/\gamma\text{-}Al_2O_3$ (0 25 wt%) catalyst exhibited lower rate constants (see Table A2.3, Appendix II). The rate constant for CO formation was very high compared to CH_4 formation. The rate constant for the CH_4 consumption rate is fairly constant for all the catalysts studied. Representative both model and experimental data of the concentration with time curves are shown in Figure 3.14 and 3.15 for the unpromoted catalyst and $Ni/ZrO_2/\gamma\text{-}Al_2O_3$ catalysts which fitted well with the experimental data. Figure 3.14 indicates that the exponential decay for the CO_2 concentration is slower compared to CH_4 for the unpromoted catalyst. A significant deviation was observed by adding $\pm$ 1 to the rate constants, k_1, k_3 and k_5 except for the CO formation curve which did not show any significant deviation. The CH_4 concentration also decreases exponentially with time. Similarly, the same concentration profile for CH_4 and CO_2 was observed for the ZrO_2 promoted catalyst.

The H_2 concentration increases exponentially and tends to approach equilibrium with time. The CO concentration increases rapidly to a maximum with time. It appears, the CO formation tend to approach equilibrium faster than that of H_2. However, the rate constant for CO_2 and CO were much higher for $Ni/ZrO_2/\gamma\text{-}Al_2O_3$ catalysts compared to the unpromoted catalyst. The plots for both $Ni\text{-}Pd/\gamma\text{-}Al_2O_3$ (0.25 wt%) and $Ni\text{-}Cu/\gamma Al_2O_3$ (0.25 wt%) could be found in Appendix II, Figure A2.1 and A2.2.

Catalysts	Component	Experiment (mole fraction)	Model (mole fraction)	Rate constant $k*10^5$ (s^{-1})
Ni/Al_2O_3	CO_2 CH_4 CO H_2	0 42 0.33 0.06 0 20	0.40 0.33 0.05 0.21	k1=80 k3=60 k5=3
$Ni/ZrO_2/Al_2O_3$	CO_2 CH_4 CO H_2	0 40 0.34 0.08 0 21	0.41 0.33 0.05 0.22	k1=201 k3=101 k5=3

Table 3.4 Kinetic data for experimental and modelling

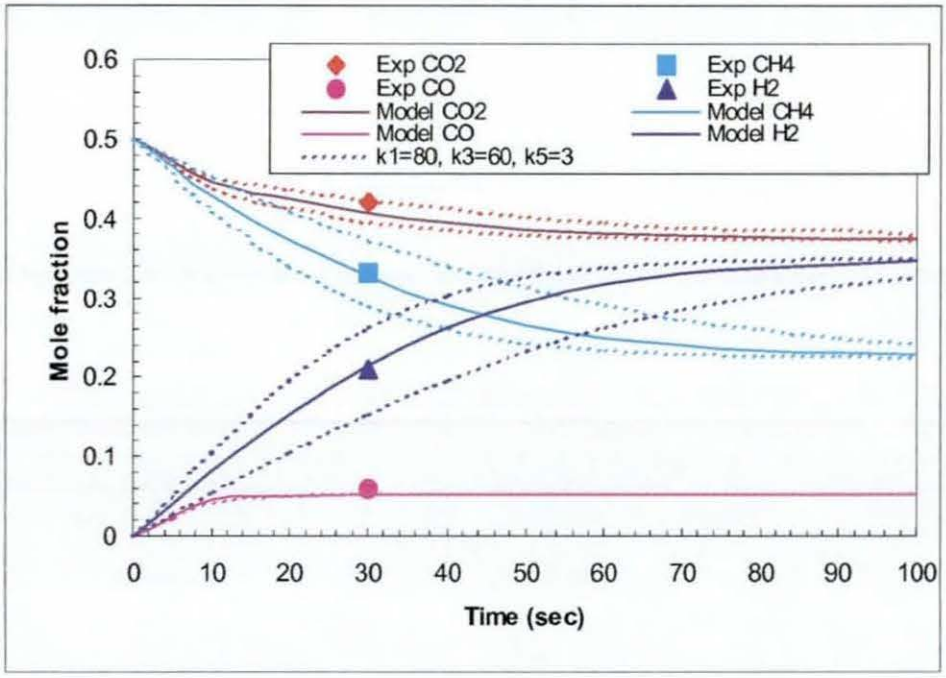

Figure 3.14 Kinetic plot of unpromoted Ni//γ-Al_2O_3, T=1073K

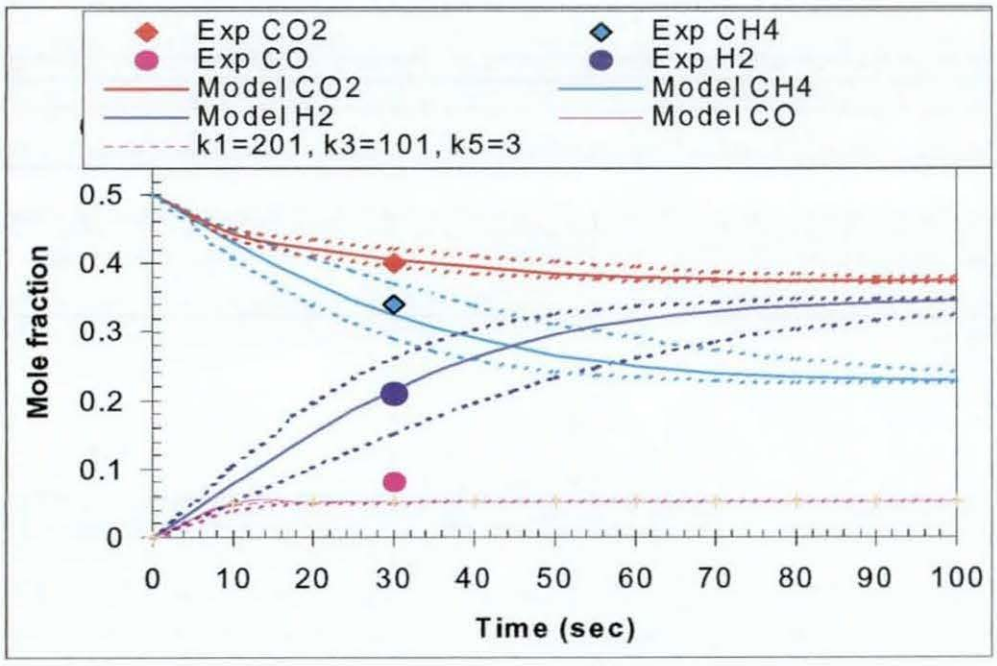

Figure 3.15 Kinetic plot of Ni/ZrO_2/γ-Al_2O_3 catalyst, T = 1073K

3.9.2 Activation energy

The Arrhenius plots of various reactants under plug reaction conditions are presented in Figure 3.16 for $Ni/ZrO_2/\gamma\text{-}Al_2O_3$ catalyst. The activation energies of CH_4, CO_2 and CO were 29.8 kJ/mol, 26. kJ/mol and 89 kJ/mol respectively, which indicate that the activation energy of CO is more sensitive to temperature, followed by CH_4. These activation energy values are comparable to values obtained in literature by other research groups, 40 kJ/mol and 26 kJ/mol for CH_4 and CO_2 (Guo *et al.*, 2004). The activation energies of CO_2, CH_4 and CO for the unpromoted catalyst $Ni/\gamma\text{-}Al_2O_3$ were 32.9 kJ/mol, 29 8 kJ/mol and 40.0 kJ/mol, respectively. The Arrhenius plot is shown in Figure 3.16

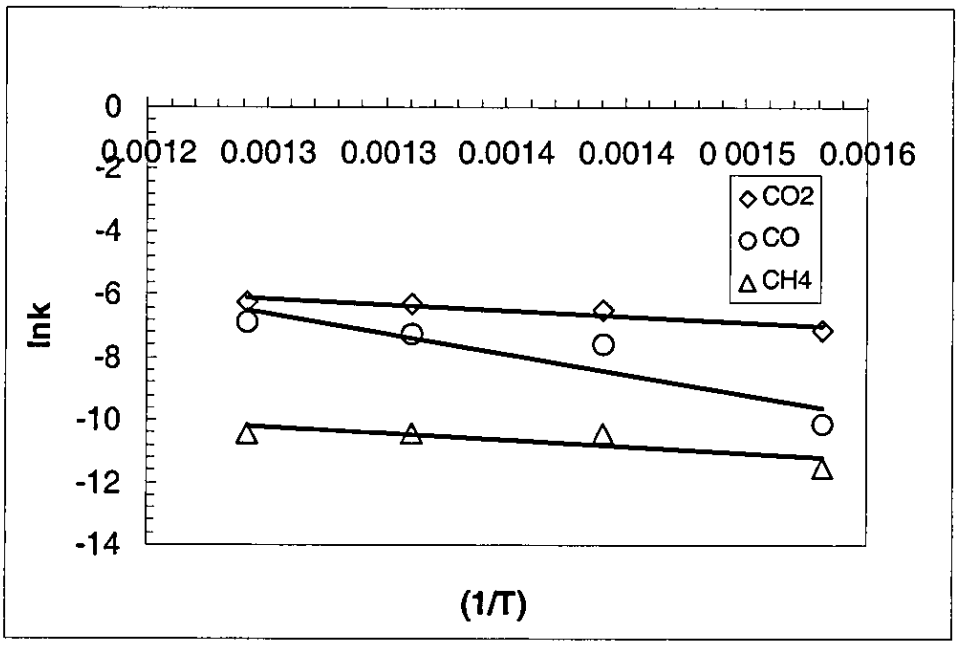

Figure 3.16 Arrhenius plot of $Ni/\gamma\text{-}Al_2O_3$ catalyst

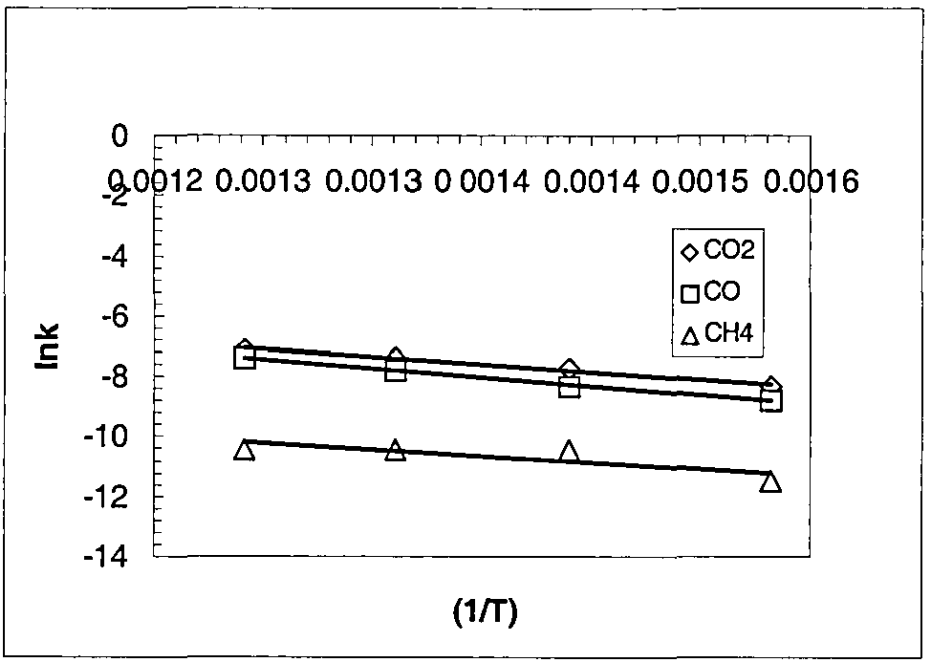

Figure 3.17 Arrhenius plot of $Ni/ZrO_2/\gamma\text{-}Al_2O_3$ catalyst

CHAPTER 4

EFFECT OF SUPPORT MODIFICATION ON ACTIVITY AND STABILITY OF Ni-BASED CATALYSTS

4.1 Introduction

This section reports and discusses results obtained for support modified Ni-based ($Ni/\gamma\text{-}Al_2O_3$, $Ni/La_2O_3//\gamma\text{-}Al_2O_3$, $Ni/MgO/\gamma\text{-}Al_2O_3$, and $Ni/ZrO_2/\gamma\text{-}Al_2O_3$) catalysts. A number of characterisation techniques were applied to be able to correlate subsequent activity measurements with characteristic data. An assessment is made of the effect of support modification on the activity and stability of catalysts during the CO_2 reforming of methane. The effect of space velocity on the conversions of methane and carbon dioxide as well as CO yield is investigated. Due to the usual activity performance for the ZrO_2-promoted catalyst, an example of kinetic data was evaluated on both $Ni/ZrO_2/Al_2O_3$ and unpromoted catalysts for comparison. The rate constants obtained were used to determine the activation energies for the two catalysts, using Arrhenius plot.

4.2 Catalyst characterisation

4 2.1 Surface area and pore size distribution

The surface areas and pore volumes for supported Ni-based catalysts are listed in Table 4 1 with the specific surface area of the supports, alumina ($\gamma\text{-}Al_2O_3$) and praseodymium (Pr_2O_3) for comparison purposes.

The surface area of $\gamma\text{-}Al_2O_3$ and Pr_2O_3 are 257 m^2/g and 464 m^2/g respectively and the corresponding average pore diameters about 46 nm and 134 nm with pore volumes of 0.31 cm^3/g and 1 68 cm^3/g The addition of the different oxides, MgO, ZrO_2 and La_2O_3 caused a significant reduction in BET surface area and pore volume of the promoted catalysts as shown in Figure 4 1. An increase in pore diameter was observed over catalysts modified with both MgO and ZrO_2, from 46 nm to 49 nm and 60 nm respectively while La_2O_3 modified catalysts showed a decrease from 46 nm to 42 nm. It is interesting to note that the bimodal pore size distribution of $\gamma\text{-}Al_2O_3$ support, shown in Figure 4 2 (~7Å and ~80Å) indicating the presence of micropores and mesopores did not change in the pore structure but a decrease in pore volume was observed after impregnation with nickel nitrate.

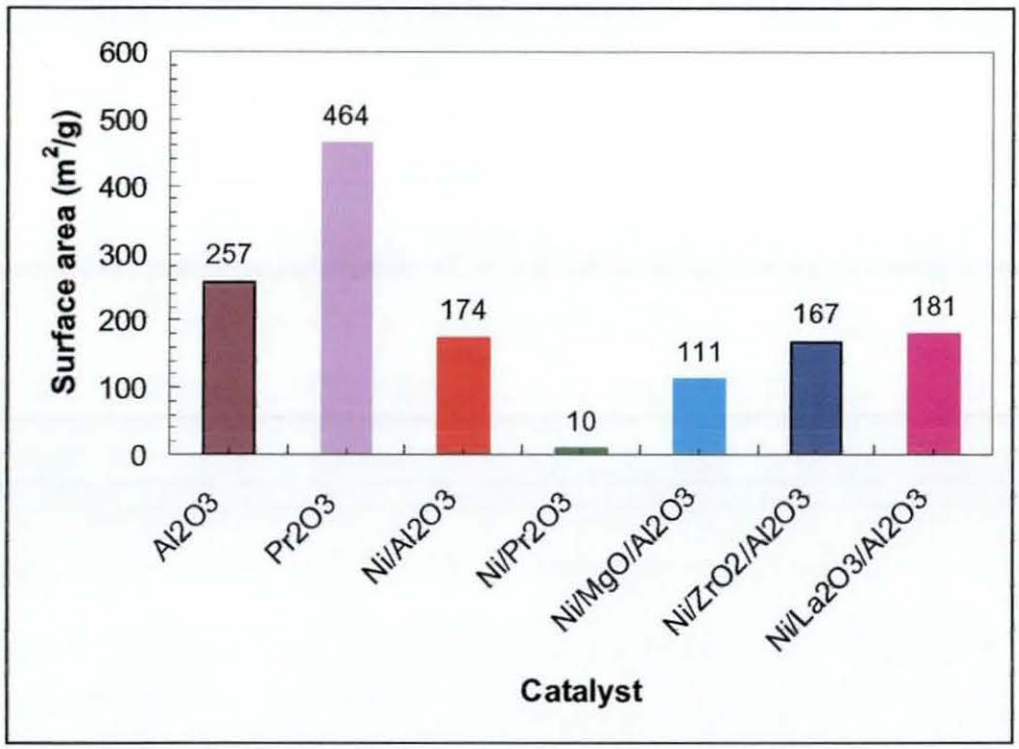

Figure 4.1 BET surface area of support and Ni-based catalysts.

Catalyst	BET Surface area (m^2/g)	Langmuir surface area (m^2/g)	Average Pore size (Angstrom)	Pore volume (m^3/g)
Al_2O_3 (support)	257	351	46	0.31
Pr_2O_3 (support)	464	618	135	1.68
NI/Pr_2O_3	10	13	210	0.07
$Ni/\gamma\text{-}Al_2O_3$	174	239	44	0.20
$Ni./La_2O_3/\gamma\text{-}Al_2O_3$	181	251	42	0.20
$Ni/MgO/\gamma\text{-}Al_2O_3$	111	154	60	0.18
$Ni/ZrO_2/\gamma\text{-}Al_2O_3$	167	230	49	0.21

Table 4.1 Surface area and pore structure of catalysts.

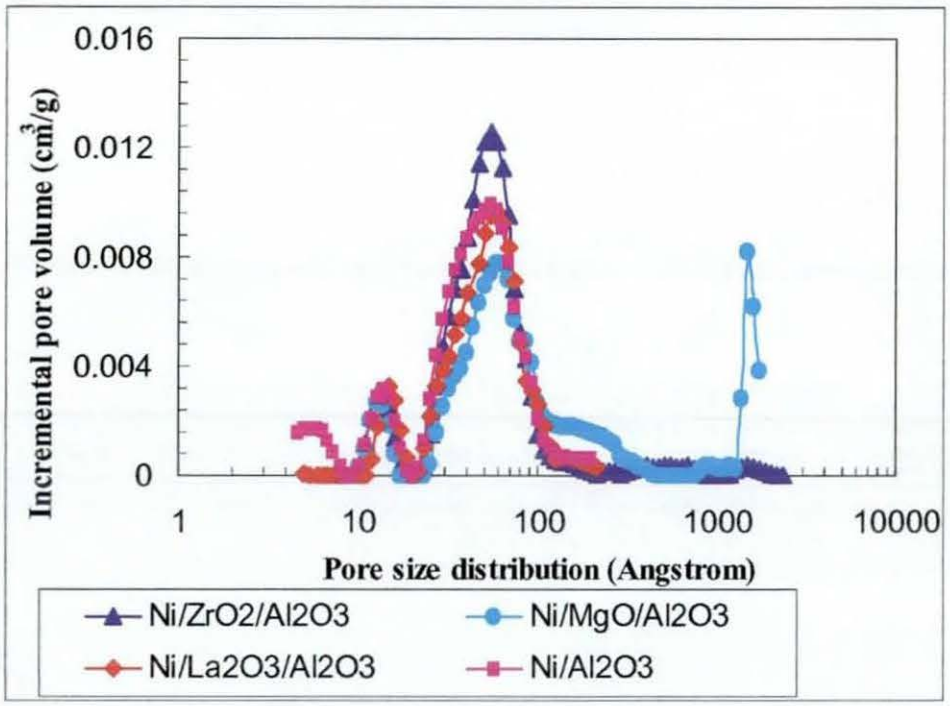

Figure 4.2 Pore size distribution of Ni-support modified catalysts

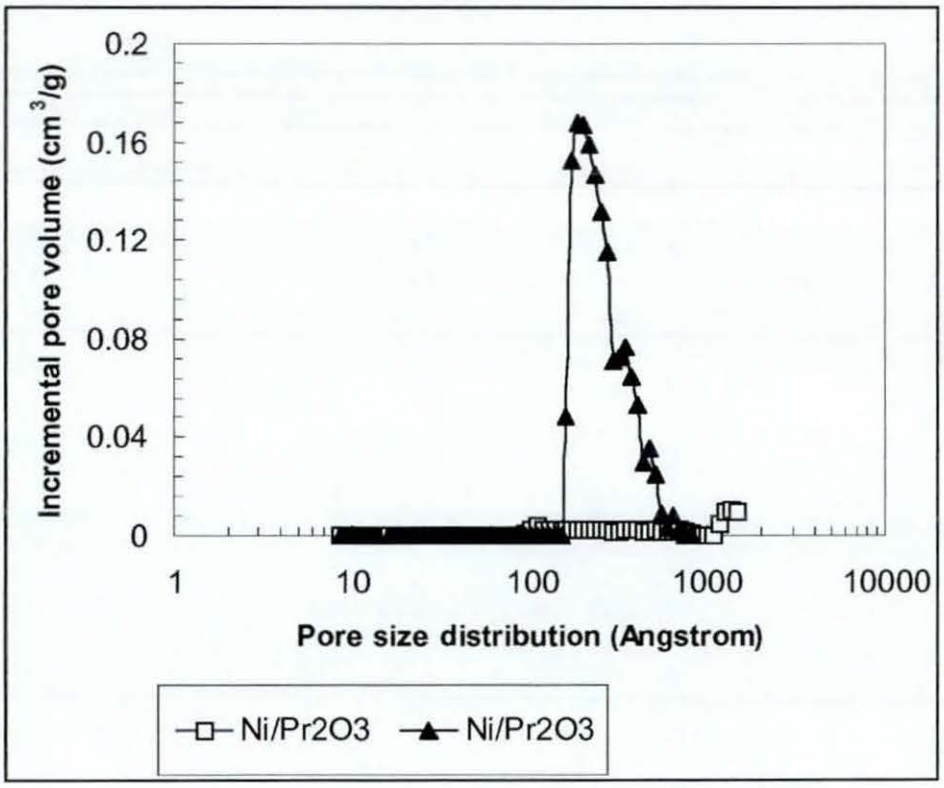

Figure 4.3 Pore size distribution of Praseodymium supported nickel catalysts

As can be seen in Table 4.1 pore volume was reduced for the unpromoted catalyst from 0.31 m^3/g to 0.2 m^3/g. A similar decrease in pore volume was observed for the $Ni/La_2O_3/\gamma\text{-}Al_2O_3$ catalyst.

Dias and Assaf (2003) have observed a similar decrease when CaO was used to modify $Ni/\gamma\text{-}Al_2O_3$ catalysts. They attributed the decrease to the covering and blocking of pores by calcium oxide. A significant decrease in surface area was also observed in the case of Ni/Pr_2O_3 catalysts, from 464m^2/g to 10 m^2/g, after impregnation with nickel nitrate, which was also reflected in the decrease in pore volume from 1.68 cm^3/g to 0.07 cm^3/g as shown in Table 4.1. This may be due to strong sintering processes that must have occurred during calcination of the catalyst (see Figure 4.3).

4.2.2 Temperature–programmed reduction of supported Ni-based catalysts

The reducibility of the supported Ni-based catalysts was studied using TPR technique under H_2 flow in the temperature range of 200K–800K. Figure 4.4 shows the TPR profile obtained for the oxide promoted samples prepared as described earlier in Chapter 3. The profile of the unpromoted $Ni/\gamma\text{-}Al_2O_3$ catalyst shows peaks at 593K and 799K, which can be assigned to the reduction of NiO and $NiAl_2O_4$ spinel structures (Lee *et al.,* 2004) which agrees with reports in literature. Previous studies during TPR have shown that temperatures above 800K are required to reduce stoichiometric $NiAl_2O_4$ spinel structures (Lee *et al.,* 2004). The Ni/Pr_2O_3 catalyst showed a similar profile to that of the unpromoted catalyst ($Ni/\gamma\text{-}Al_2O_3$).

Two peaks were also observed, for maximum hydrogen consumption, located at 580K and at 799K. For the $Ni/La_2O_3/\gamma\text{-}Al_2O_3$ catalysts a different profile was observed, with a sharp peak at 540K and a shoulder peak at 490K. In the lanthanum promoted catalyst, nickel is present in more than one species with different reduction temperatures (Lemonidou *et al.,* 2002; Liu *et al.,* 2003). The peak at 490K can be assigned to the reduction of bulk NiO while the peak found at 540K can be assigned to La_2NiO_4.

4.2.3 Temperature-programmed reduction

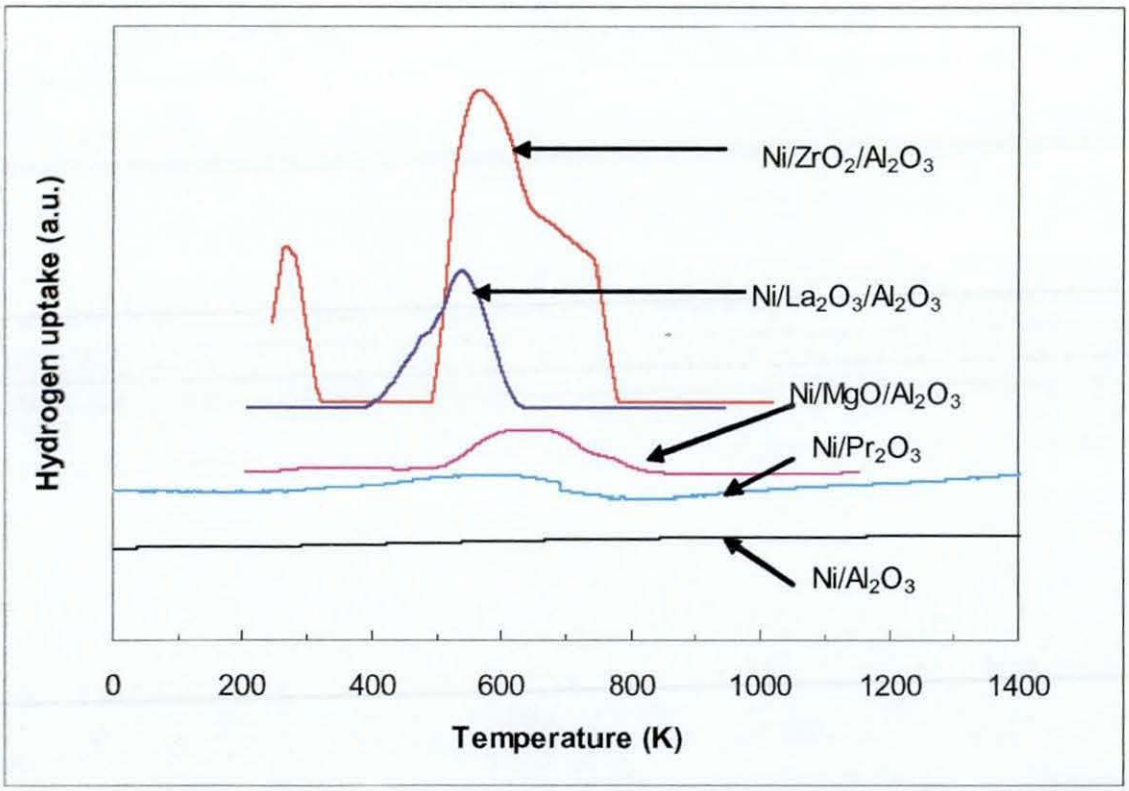

Figure 4.4 TPR profile for Ni-based catalysts, before reaction

In literature it is reported that deposited nickel on alumina, is basically present in two forms, due to different interaction with the support: nickel oxide and nickel aluminate. The NiO (segregated oxide) which requires little energy for reduction has a weak interaction with the support (Dias and Assaf (2003). The NiO is simply a deposit on the catalyst surface; therefore it is easily reducible at temperatures above 350K. On the other hand, the aluminate phase results from the strong interaction between nickel and the support and so the nickel is located in the support structure, since it is a surface compound (Dias and Assaf 2003). Thus the reduction temperature is always higher because it is more difficult to reduce. The TPR data clearly reveals that the activation treatment at 800K in H_2 flow during reduction was enhanced over alkaline earth oxide promoted catalyst compared to the unpromoted catalyst. The H_2 uptake for all catalysts studied followed the order: $Ni/ZrO_2/\gamma$-Al_2O_3 > $Ni/La_2O_3/\gamma$-Al_2O_3 > $Ni/MgO/\gamma$-Al_2O_3 > Ni/γ-Al_2O_3 > Ni/Pr_2O_3, with values; 18.8 mmole, 9.4 mmole, 3.4 mmole, 1.98 mmole and 0.9 mmole respectively.

The TPR data clearly reveals that the activation treatment at 800K in H_2 flow during reduction was enhanced over alkaline earth oxide promoted catalyst compared to the unpromoted catalyst. The H_2 uptake for all catalysts studied followed the order: $Ni/ZrO_2/\gamma$-Al_2O_3 > $Ni/La_2O_3/\gamma$-Al_2O_3 > $Ni/MgO/\gamma$-Al_2O_3 > Ni/γ-Al_2O_3 > Ni/Pr_2O_3, with values; 18.8 mmole, 9.4 mmole, 3.4 mmole, 1.98 mmole and 0.9 mmole respectively. Therefore twice the amount of Ni supported on ZrO_2 modified γ-Al_2O_3 can be reduced compared to La_2O_3 promoted material. The low H_2 uptake for Pr_2O_3 supported Ni catalyst may be due to low dispersion of Ni as a result of reduced surface area. The surface area of the calcined catalyst reduced drastically compared to the surface area of Pr_2O_3 support (see Figure 4.3) which may have been caused by sintering processes during calcination.

4.2.3 X-Ray diffraction (XRD) patterns of fresh supported Ni-based catalyst

The XRD patterns for the unreduced supported Ni-based catalysts after calcinations at 743K are shown in Figure 4.5. For the unpromoted Ni/γ-Al_2O_3 catalysts, a typical broadening of the diffraction peaks at $2\theta = 37^o$, 43.3^o, and 66.2^o, were observed. The broadening of peaks may have originated from evenly distributed micro-crystallites or random crystallites (Liu *et al.*, 2003) such as NiO, $NiAl_2O_4$ and γ-Al_2O_3. The peaks at 37.0^o and 43.3^o indicate the presence of the crystalline structure of NiO. This result agrees with the TPR observed for the unpromoted fresh catalysts that showed a reduction peak at 593K indicating the presence of NiO. The XRD pattern for Ni/Pr_2O_3 catalysts was different, double diffraction peaks at angles of $2\theta = 28.2^o$, 29.0^o, and 32.2^o, 33.0^o and 46.5^o, 47.0^o were observed. Also peaks appeared at higher diffraction angles, $2\theta = 54.5^o$ and 55.5^o. The diffraction peaks at 46.5^o, 47.0^o and 54.5^o, 55.5^o may be ascribed to Pr_2O_3. There was no indication of pronounced crystalline structure of NiO. One explanation may be due to submerged peaks (Xiao *et al.*, 2003) by the diffraction of praseodymium. Another possible reason may be due to occurrence of sintering processes and/or well dispersion. Similar observations were made in literature by (Wang and Lu 1998a), where they attributed the absence of nickel diffraction peaks in XRD pattern of Ni/CeO_2 catalyst to the reductive behavior of CeO_2 support and well dispersion of nickel.

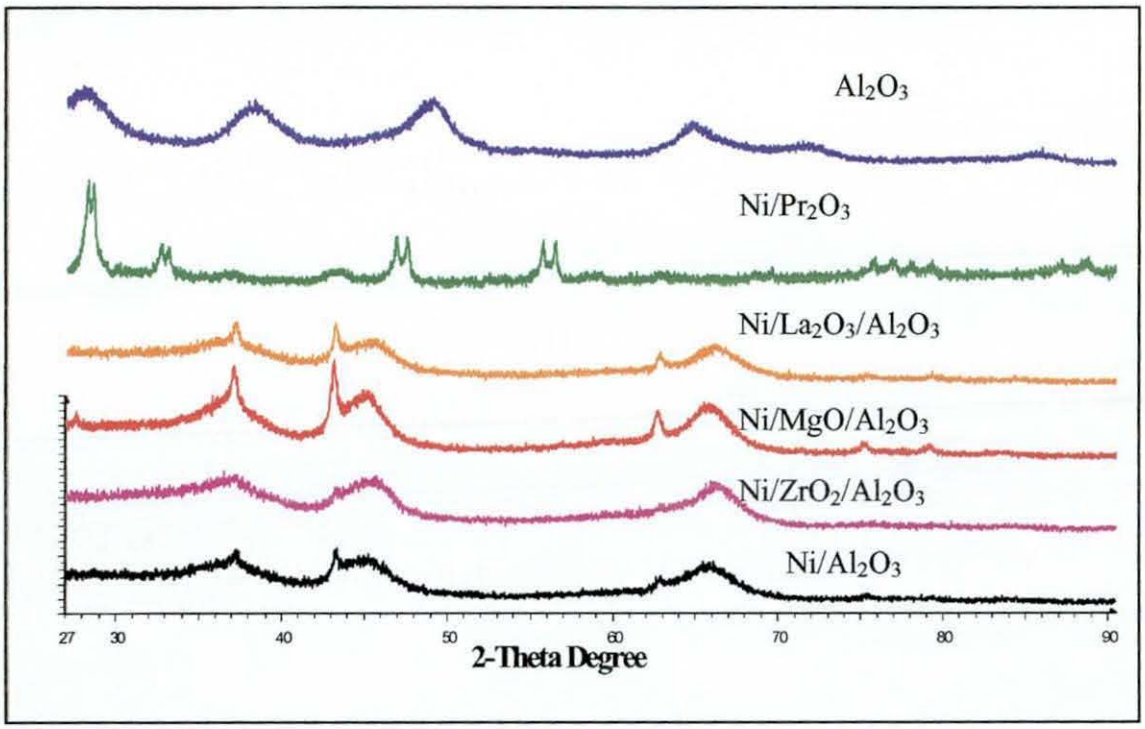

Figure 4.5 XRD spectrum for fresh Ni-based catalyst, calcination temperature = 743K.

The $Ni/La_2O_3/\gamma\text{-}Al_2O_3$ catalysts show a similar pattern to the unpromoted catalyst. However, the diffraction pattern is more pronounced at (2θ = 37.0°, 43° and 62.9° weak). Also reflections at 66.2° and 45.5° were observed indicating the presence of La_2NiO_4 and $NiAl_2O_4$. For the $Ni/MgO/\gamma\text{-}Al_2O_3$ catalysts, the position of reflection did not change but the intensity of the reflection increased compared to $Ni/La_2O_3/\gamma\text{-}Al_2O_3$ catalysts which indicates more crystalline structure. The XRD pattern of $Ni/ZrO_2/\gamma\text{-}Al_2O_3$ catalysts shows less pronounced reflections at 43.3°, 66.2°, 37.0° and 62.9°. This may have been caused by less crystalline structure and low dispersion (1.86%) obtained from CO chemisorption (see later in § 4.2.4).

4.2.5 X-Ray diffraction patterns of reduced supported Ni-based catalysts

The XRD patterns of the reduced Ni-based catalysts are shown in Figure 4.6. After reduction the reflections attributed to NiO (2θ =37°, 43.3° and 62.9° weak) crystallites almost disappeared, whereas those belonging to metallic Ni° phase (44.2°, 51.8° and 76.0°) became more pronounced.

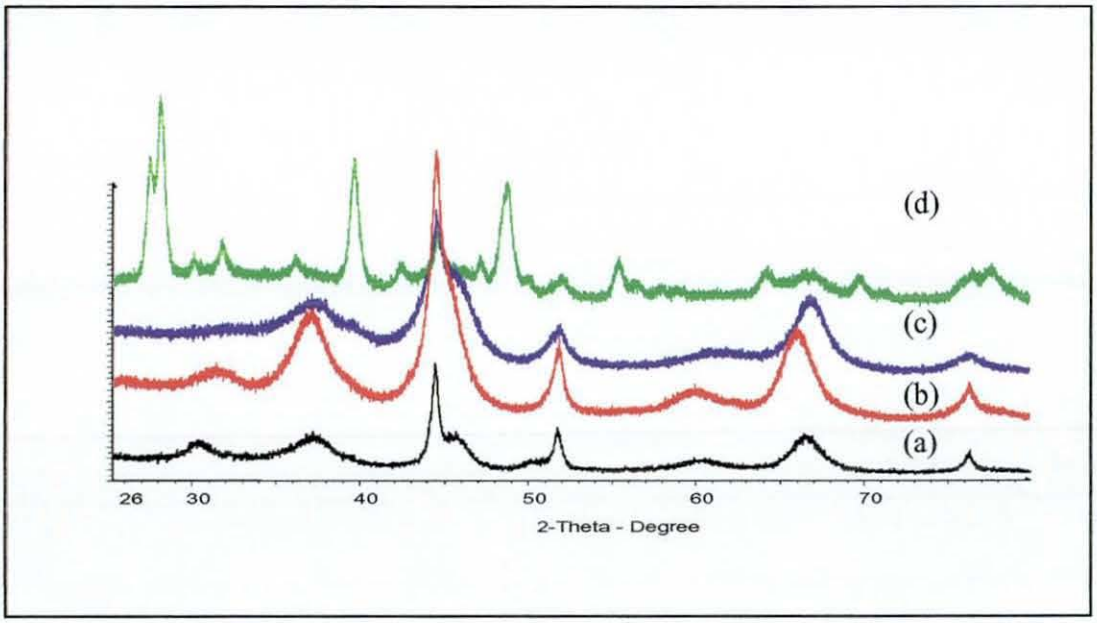

Figure 4.6 XRD spectrum of reduced Ni-based catalysts (a) $Ni/ZrO_2/\gamma\text{-}Al_2O_3$ (b) $Ni/MgO/\gamma\text{-}Al_2O_3$ (c) $Ni/\gamma\text{-}Al_2O_3$ (d) $Ni/La_2O_3/\gamma\text{-}Al_2O_3$, Reduction temperature = 1073K

The new reflections at 44.2° and 51.8° are ascribed to cubic nickel metal, this is in good agreement with the report by other research groups (Hao *et al.*, 2003) who also observed two reflection (2θ =44.52° and 51.9°) using Ni/Zr-Laponite catalysts. In the case of $Ni/MgO/\gamma\text{-}Al_2O_3$ catalyst broad reflection appear at 2θ =31.5° and 59.9°. The reflection observed especially at 31.5° may be due to the presence of MgO. Similar reflections were observed for $Ni/ZrO_2/\gamma\text{-}Al_2O_3$ catalysts but with reduced intensity, agreeing with the pattern of the fresh catalyst and a peak at 30°, which probably represents ZrO_2. This value is in good agreement with the value (30.6°) observed by Hao *et al.*, 2003.

The intensity of the reflection at 65.5° increased, although it was slightly shifted from the original position (66.0°) to the left. For the $Ni/La_2O_3/\gamma\text{-}Al_2O_3$ catalysts the pattern was different compared to the other catalysts. As can be seen in Figure 4.6 new reflection appeared between 27°-30°, 37.0°-44.2°, 51.8°-59.8°, 61.0-65.5° and 71°. The reflections that appeared between 27°-30° may be due to the presence of La_2O_3 crystallites as a result of $NiLa_2O_4$ conversion into Ni° and La_2O_3 during reduction (Ogawa *et al*, 2003)

4 2.5 CO chemisorption

The physico-chemical properties of the tested catalysts are summarised in Table 4.2 As can be seen from Table 4 2, the Ni dispersion increased with the La_2O_3 modified support ($Ni/La_2O_3/\gamma\text{-}Al_2O_3$), 9 81% compared to 5.9% for the unpromoted catalyst. According to a report by Ogawa *et al.*, 2003, lanthanum oxides are known to increase the dispersion of supported active components and also increase the thermal stability of alumina supports This agrees well with XRD results indicating the appearance of new reflection due to reduction of $NiLa_2O_4$ to form Ni^0 and La_2O_3.

Catalyst	Metal loading (AAS) wt %		Average dispersion (%)	Crystallite size of active phase (nm)		Surface area of active phase (m^2/g.metal)
$Ni/\gamma\text{-}Al_2O_3(0)$	15	8 4	5 9	26 4		35
$Ni/Pr_2O_3(0)$	15	n d	n d	n.d		n d
$Ni/ZrO_2/\gamma\text{-}Al_2O_3$(5 wt %)	15	13 5	1 86	38 8		12
$Ni/MgO/\gamma\text{-}Al_2O_3$(5 wt %)	15	13	3 51	24 4		23
$Ni/La_2O_3/\gamma\text{-}Al_2O_3$(5 wt %)	15	n d	9.81	35 0		64

n d not determined

Table 4.2 CO chemisorption result of supported Ni-based catalyst

The nickel dispersion for both MgO and ZrO_2 modified catalyst decreased from 5.9% to 3.51% and 1.86% respectively The crystallite size of both $Ni/ZrO_2/\gamma\text{-}Al_2O_3$ and $Ni/La_2O_3/\gamma\text{-}Al_2O_3$ catalysts increased from 26 4 nm to 38.8 nm and 35 nm respectively In the case of $Ni/MgO/\gamma\text{-}Al_2O_3$ catalyst, the crystallite size decreased from 26 4 nm to 24 4 nm.

For the $Ni/ZrO_2/\gamma\text{-}Al_2O_3$ catalyst, no Ni^0 peak was observed in the XRD result, which may be due to submerged Ni peaks by the support or low exposed active phase may have caused the low dispersion The decrease in dispersion is reflected in the corresponding surface areas of the active phase for the different catalysts as shown in Table 4 2.

The $Ni/La_2O_3/\gamma\text{-}Al_2O_3$ catalyst shows an increase in surface area from 35 m^2/g metal to 64 m^2/g metals, while the surface area of the active phase for $Ni/MgO/\gamma\text{-}Al_2O_3$ and $Ni/ZrO_2/\gamma\text{-}Al_2O_3$ catalyst show a decrease from 35 m^2/g-metal to 12 m^2/g metal and 23 m^2/g metal respectively

4.3 Effect of support on catalytic activity for CO_2 reforming of CH_4 over supported Ni-based catalysts

4 3.1 Effect of support on activity, WHSV =19200 ml/hr g cat

The CO_2 reforming reaction was conducted at atmospheric pressure and a space velocity of 19200 ml/hr gcat, and the catalytic performance of various supported Ni-based catalysts were evaluated in a quartz packed reactor in the temperature range of 923K-1073K. A high space velocity of 19200 ml/hr.gcat was chosen because a good comparison can be made among catalysts since conversions are away from equilibrium. The activity result of the various catalysts is shown in Figures 4.7-4 9 Figure 4 7 and 4.8 show the conversion of CH_4 and CO_2 with increasing temperatures. The conversion increased with an increase in the reaction temperature for all the catalysts studied, except the temperature > 1073K. At 1073K, all the catalysts showed a decrease in conversion except for $Ni/ZrO_2/\gamma\text{-}Al_2O_3$ catalyst that still maintained the trend of increase with increasing temperature. It has been reported that $Ni/\gamma\text{-}Al_2O_3$ (unpromoted) catalyst is unstable at high temperature (> 973K) because of the thermal deterioration of the $\gamma\text{-}Al_2O_3$ support as well as $\alpha\text{-}Al_2O_3$ and spinel formation ($NiAl_2O_4$) (Roh *et al*, 2002) The thermal deterioration is attributed to two reasons; (1) migration and coalescence of metal particles (sintering processes) that may lead to pore close up and reduction of surface area (Teixeira and Giudici 2001, Rasmussen *et al*, 2004) and carbon deposition (Hou *et al*, 2004). The CO_2 conversion followed a similar trend to CH_4 conversion for all the catalysts tested at this space velocity.

However, the CO_2 conversions were higher than that of CH_4, for the unpromoted catalyst at 1073K and 1023K which is ascribed to the occurrence of the reverse water gas shift (RWGS) reaction ($CO_2 + H_2 \leftrightarrow CO + H_2O$) simultaneously with CO_2 reforming ($CH_4 + CO_2 \leftrightarrow 2CO + 2H_2$) which is in agreement with literature (Dias and Assaf 2003). For promoted $Ni/MgO/\gamma\text{-}Al_2O_3$ catalysts higher CO_2 conversions are observed at temperatures < 1023K.

It then suggests that the modification of $Ni/\gamma\text{-}Al_2O_3$ with MgO has an effect on the reaction mechanism at higher temperatures because the RWGS reaction was observed at temperatures lower than 1023K.

On the other hand, there was no effect for $Ni/ZrO_2/\gamma\text{-}Al_2O_3$ catalyst, showing a similar RWGS mechanism at > 1023K. Also, Ni/Pr_2O_3 catalysts, promotes the RWGS reaction at temperatures > 1023K, because higher CO_2 conversion was observed at 1023K and 1073K, showing the same trend to the unpromoted $Ni/\gamma\text{-}Al_2O_3$. Dias and Assaf (2003) also reported higher CO_2 conversion compared to CH_4 conversion in dry reforming when they modified $Ni/\gamma\text{-}Al_2O_3$ catalyst with CaO due to the promotion of the reverse water gas shift reaction.

The catalytic performance (activity) followed the order $Ni/MgO/\gamma\text{-}Al_2O_3$ > $Ni/\gamma\text{-}Al_2O_3$> $Ni/ZrO_2/\gamma\text{-}Al_2O_3$ > $Ni/La_2O_3/\gamma\text{-}Al_2O_3$ > Ni/Pr_2O_3 except at > 1073K, where $NiZrO_2/\gamma\text{-}Al_2O_3$ exhibits higher activity However, as can be see in Figures 4 7, 4 8 and 4 9 the support modification with ZrO_2 oxide appears to improve activity at higher temperatures while other catalysts suffer activity loss.

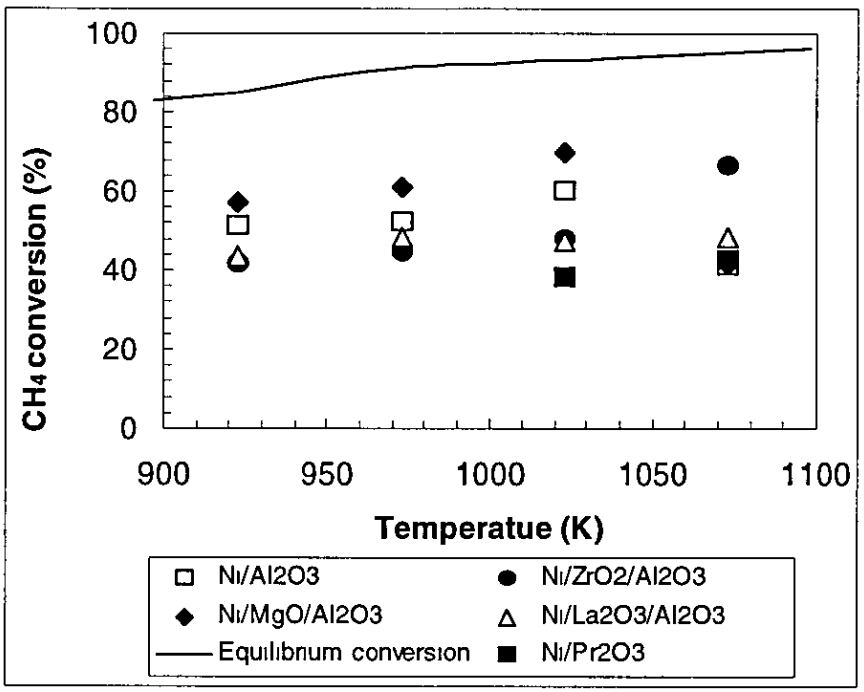

Figure 4 7 CH_4 conversion as a function of temperature, WHSV=19200 ml/hr g cat, CH_4/CO_2=1, catalyst weight=50 mg, P= 1 atm.

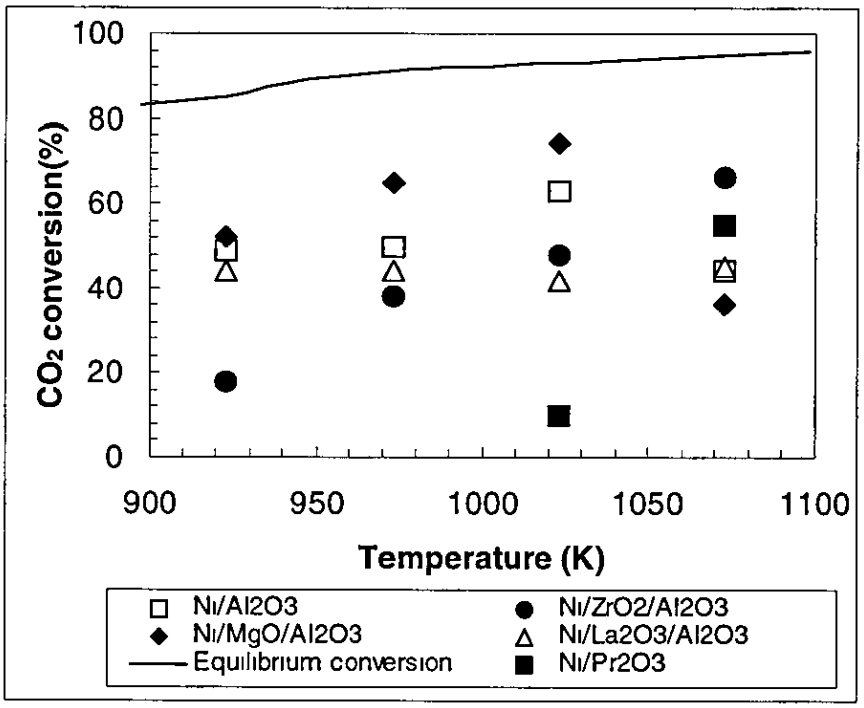

Figure 4.8 CO_2 conversion as a function of temperature, WHSV=19200 ml/hr g cat, CH_4/CO_2=1, catalyst weight=50 mg, P= 1 atm.

One possible reason for such loss in activity could be the loss of Ni^0 active area due to sintering of metal particles or blocking of the metal surface sites by carbonaceous deposits From the findings of carbon deposition (see section 4 8), the unpromoted catalyst and ZrO_2 promoted catalyst show the same amount of carbon deposits. The speculation of activity loss (due to carbon deposits) at > 1073K, is not completely ruled out, because deactivation may be caused by the type of carbon formed on the catalyst Although, further investigations were not carried out to verify on the catalysts surface area after reforming, the activity loss can also be attributed to sintering processes It was also noted that the conversion of CH_4 for $Ni/ZrO_2/\gamma$-Al_2O_3 catalysts, was higher than that of CO_2 at 923K and 973K, 41.7%, 44 6% (CH_4) and 17.8%, 38 1% (CO_2) respectively. It then suggests that at lower temperatures the $Ni/ZrO_2/\gamma$-Al_2O_3 catalyst did not favour the reverse water gas shift reaction ($CO_2 + H_2 \leftrightarrow CO + H_2O$).

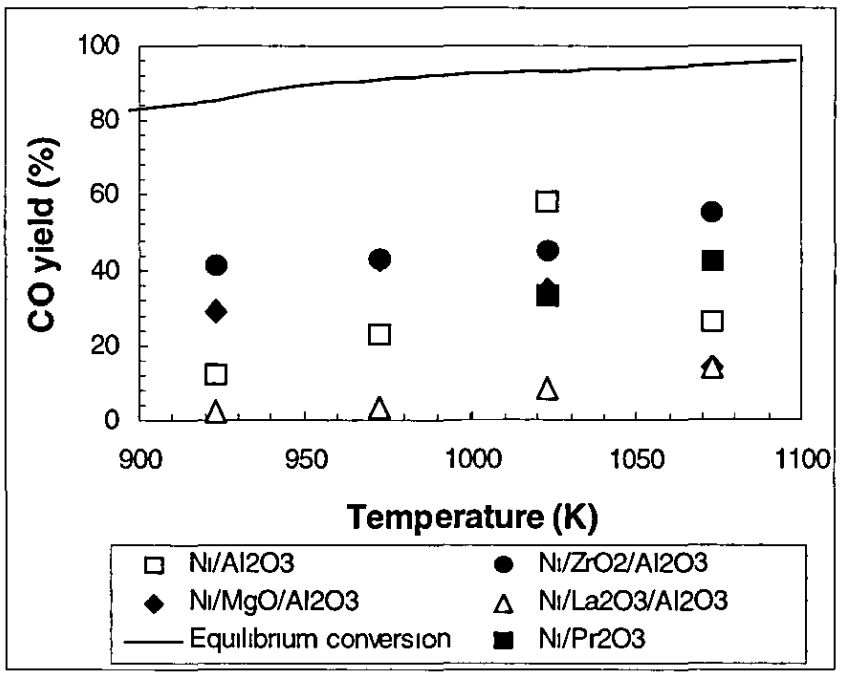

Figure 4 9 CO yield versus temperature, WHSV = 19200 ml/hr g cat, $CH_4/CO_2 = 1$, catalyst weight = 50 mg, P = 1 atm.

Although the ZrO_2 promoted catalyst has shown excellent performance compared to other catalysts, various research groups have different opinion on the activity of ZrO_2 supported Ni catalyst

Roh *et al*, (2002) reported that Ni/Ce-ZrO_2 catalysts increased activities as well as stability in steam reforming of methane, while the report by Bitter *et al.*, 1997, indicated that with high Ni loading, Pt/ZrO_2 catalysts exhibited better performance compared to Ni/ZrO_2

It suggests that the type of active phase deposited on the support may have effect on the activity because of strong metal–support Pt-Zr interactions (Souza *et al*, 2001). They found out that the latter suffered serious deactivation that eventually plugged the reactor during dry reforming. The activity of a catalyst is related to the metal surface area (i e. the number of active sites) This implies that, generally, the catalytic activity benefits from the high dispersion of the metal particles As can be seen in Table 4.2 Ni/ZrO_2/γ-Al_2O_3 catalyst shows the lowest Ni dispersion (1 86%). The excellent performance of Ni/ZrO_2/γ-Al_2O_3 catalyst has been ascribed to the acidic/basicity properties of ZrO_2 (Souza *et al*, 2001).

The $Ni/MgO/\gamma-Al_2O_3$ catalysts showed significant difference in conversion at 973K and 1023K 61.0%, 69 0% (CH_4) and 64 7%, 74.0% (CO_2) For the unpromoted catalyst ($Ni/\gamma-Al_2O_3$) and $Ni/La_2O_3/\gamma-Al_2O_3$ catalyst, there was no significant difference in conversion of CH_4 and CO_2 except at 1023K where 59.9% CH_4 and 62 9% CO_2 were observed. $NiPr_2O_3$ catalyst shows no significant activity at 923K and 973K but it attained a similar CO yield at both 1023K and 1073K This poor activity may be due to the decrease in surface area observed after heat treatment, (464 m^2/g to 10 m^2/g) which resulted to low Ni dispersion (see Table 4 2). For all the catalysts tested, the trend of CO yield was similar to that of the conversion of CH_4 and CO_2. The activity of all catalysts at space velocity of 13900 ml/hr gcat is similar to the space velocity of 19200 ml/hr g cat All plots are presented in Appendix III, Figure A3 1.

The kinetic data agreed with the experimental results because rate constant of CO formation obtained for $Ni/ZrO_2/\gamma-Al_2O_3$ catalyst ($k_3 = 101*10^{-5}\ s^{-1}$) was higher than that of the unpromoted catalyst ($k_3 = 60*10^{-5}\ s^{-1}$)

The order of catalyst conversion was not different at space velocity of 9820 ml/hr gcat with conversion increase with increasing temperature. All the catalysts show an increase in CH_4 conversion except at 1073K, where a decline of conversion was observed for $Ni/MgO/\gamma-Al_2O_3$ catalyst (see Appendix III, Figure A3.2). The unpromoted catalyst $Ni/\gamma-Al_2O_3$ and $Ni/MgO/\gamma-Al_2O_3$ catalysts show values of 57.4% and 59 0%, for CH_4 conversion at 923K while a significant difference in conversion was observed at higher temperatures 80 3% and 75.7% (see Appendix III, Figure A3 2) The CO yield followed a similar trend of 46 2% and 42.4% especially temperature > 1023K. A similar trend was observed for $Ni/La_2O_3/\gamma-Al_2O_3$ and $Ni/ZrO_2/\gamma-Al_2O_3$ catalysts. At this space velocity, low CH_4 conversions were observed for $Ni/ZrO_2/\gamma-Al_2O_3$ catalyst at lower temperatures, but high conversion (90 6%) was restored at temperatures (>1073K), almost approaching equilibrium value (95 6%).

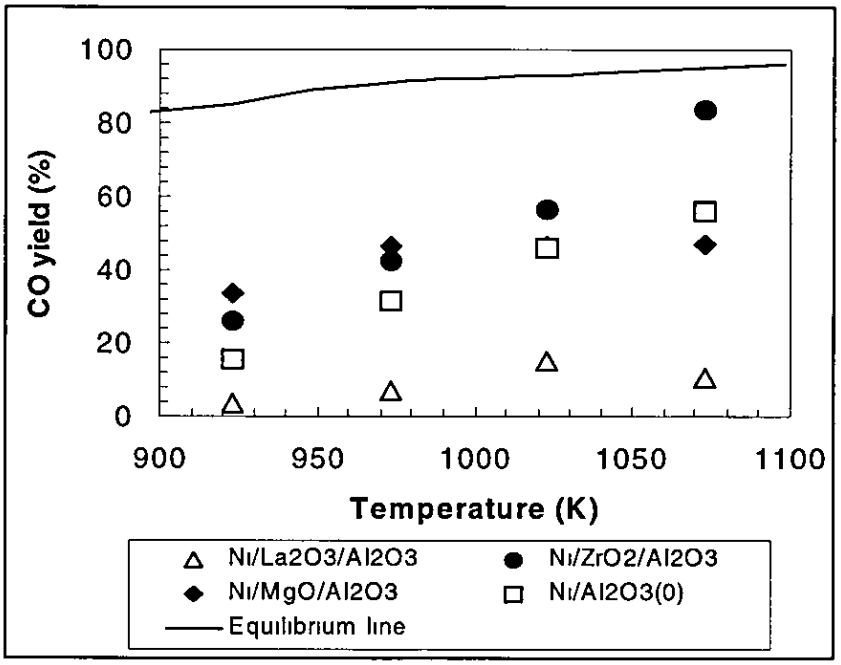

Figure 4.10 CO yield versus temperature, WHSV = 9820 ml/hr g cat, $CH_4/CO_2 = 1$, catalyst weight = 50 mg, P = 1atm

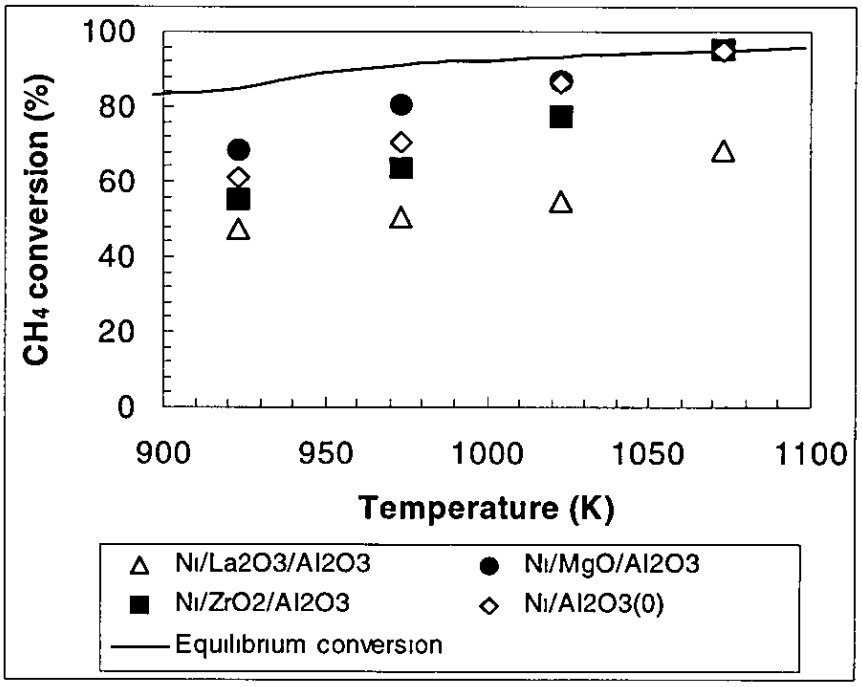

Figure 4.11 CH_4 conversion versus temperature, WHSV = 4800 ml/hr g cat, $CH_4/CO_2 = 1$, catalyst weight = 50 mg, P = 1atm

The CO_2 conversion was lower, 69%, indicating that WGS reaction was significant For the Ni/MgO/γ-Al_2O_3 catalysts higher CO_2 conversions were observed at lower temperatures, indicating that it promotes CO_2 adsorption even at lower temperatures. This suggests that the modification of alumina with MgO appears to have increased the basicity of the support The activities followed a similar trend to the space velocity of 19200 ml/hr g cat; Ni/MgO/γ-Al_2O_3 > Ni/γ-Al_2O_3 > Ni/ZrO_2/γ-Al_2O_3 > Ni/La_2O_3/γ-Al_2O_3 A good comparison could be made at lower space velocities with the $NiPr_2O_3$ because of limited amount of catalyst. The CO yield for all catalysts increased with increasing temperature except for Ni/MgO/γ-Al_2O_3 and Ni/La_2O_3/γ-Al_2O_3 catalysts that showed lower CO yield at 1073K The CO yield for Ni/ZrO_2/γ-Al_2O_3 catalyst was higher than that for the unpromoted catalyst (Ni/γ-Al_2O_3) at all temperatures At temperatures < 973K, the CO yield for Ni/MgO/γ-Al_2O_3 catalysts was higher 41.6% and 31.7% for the unpromoted catalyst (see Figure 4.10). As can be seen in Figures 4.11, the CH_4 conversion at 1073K for Ni/γ-Al_2O_3, Ni/MgO/γ-Al_2O_3 and Ni/ZrO_2/γ-Al_2O_3 catalysts showed values equal to the equilibrium values at space velocity of 4800 ml/hr g cat.

Similar CH_4 conversion was observed compared to the space velocity of 9820 ml/hr gcat for all catalysts It then suggests that at lower space velocities and specific temperatures, it is not possible to distinguish catalytic performance of the catalysts. The activities at space velocity of 7840 ml/hr g cat are also shown in Appendix III, Figure A3.3)

From the experimental findings, it is clear that catalyst performance depends on the operational conditions employed, especially with the variation of temperature and space velocity. The activities vary with varying support because of the changes in properties by oxide modification The activity of Ni/MgO/γ-Al_2O_3 catalyst was higher at all temperatures except at 1073K that showed a decrease in activity, which may be due to carbon deposition or sintering processes. However, with the addition of ZrO_2, high CO yield was achieved at higher temperatures. The unpromoted catalyst also show activity loss at higher temperatures >1073K. Again, the kinetic data agreed well with experimental results because there is consistency in high CO yield exhibited by the ZrO_2 promoted catalyst ($k_3 = 101*10^{-5}\ s^{-1}$) even at lower space velocities compared to the unpromoted catalyst ($60*10^{-5}\ s^{-1}$).

4.4 Effect of support on catalytic stability

4.4.1 Catalytic stability of supported Ni-based catalyst, WHSV = 19200 ml/hr g cat, T = 1073K

The catalytic behaviour of unpromoted and the transition oxide promoted catalysts in the CO_2 reforming of CH_4 at 1073K is compared in Figures 4.12, 4 13 and 4 14 in terms of CH_4, CO_2 conversions and CO yield as a function of time on stream The unpromoted $Ni/\gamma\text{-}Al_2O_3$ catalysts featured the highest activity with an initial CO_2 conversion of 80% but decreased to 42% after 340 minutes time on stream. The CH_4 conversion decreased from 59% to 42% following the same trend as that of CO_2 conversion indicating strong deactivation. The Ni/Pr_2O_3 catalyst exhibited low CH_4 conversion of 40% and increased to 45% but decreased again to stable activity of 40% This catalyst deactivated after 250 minutes, which eventually led to reactor blocked. The low activity and catalyst deactivation is due to carbon deposition. The decreasing surface area of Ni/Pr_2O_3 catalyst after the heat treatment (see Table 4.1) may have been the cause for low dispersion of nickel.

The carbon deposited on the catalyst must have covered up all active sites due to low dispersion However, it also depends on the type of coke deposited on the catalyst (filamentous or pyrolitic coke) since the filamentous carbon does not cause catalyst deactivation, but plugs pores and eventually led to catalyst cracking (Martinez *et al.*, 2004) The $Ni/La_2O_3/\gamma\text{-}Al_2O_3$ catalyst showed lower initial CH_4 conversion of 50% but stable activity was maintained during reforming reaction. Rare earth oxides, such as La_2O_3 are well known as weak Lewis basic compound (Ogawa *et al*, 2003) which can cause low CO_2 adsorption capacity that lead to low conversion. On alumina support pyrolitic coke is produced, depending on the acidity support (Martinez *et al*, 2004). The addition of La_2O_3 would favour a decrease in this pyrolitic coke formation as support acidity is lower due to the basic properties of La_2O_3 which subsequently improve the adsorption capacity of the support for CO_2. Wang and Lu (1998b) attributed the stable performance of Ni/La_2O_3 to synergetic sites which consists Ni and La elements. According to their report, a decorating phenomenon occurs where LaO_x species form decoration on the Ni crystallites in the form of $La_2O_3CO_3$

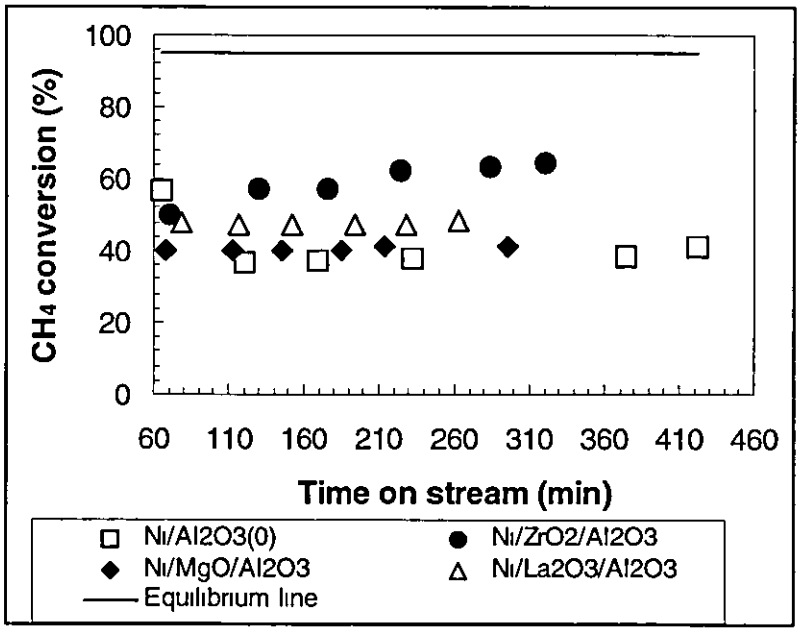

Figure 4 12 CH_4 conversion as a function of time, WHSV = 19200 ml/hr g cat, CH_4/CO_2 = 1, P = 1atm, T = 1073K

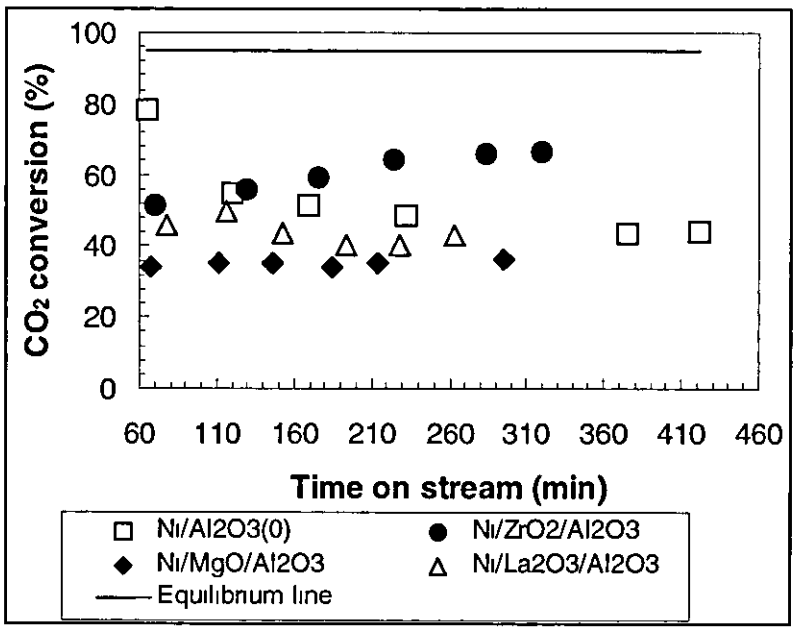

Figure 4 13 CO_2 conversion as a function of time, WHSV = 19200 ml/hr g cat, CH_4/CO_2 = 1, P = 1atm, T = 1073K

At higher temperatures the carbon species formed on the Ni sites are favourably removed by the oxygen species originated from $La_2O_3CO_3$, thus resulting in stable performance
For Ni/MgO/γ-Al_2O_3 catalysts the initial CH_4 conversion was almost the same as that of the unpromoted catalyst although slightly lower but stability was also maintained. The addition of MgO did not affect the initial activity. MgO is a strong basic oxide and its addition would lower the acidity of alumina to basic properties, enhancing CO_2 adsorption. Ruckenstein and Hu (1996) reported that MgO inhibits the Boudouard's CO disproportionation reaction (2CO ↔ C + CO_2) over nickel due to the formation of NiO-MgO solid solution as a result of the similar crystalline structure. The CO yield for NiMgO/γ-Al_2O_3 catalyst in this work (Figure 4 14) agrees with the report by Ruckentsein and Hu (1996), because despite the low conversion observed, the CO yield is higher than that of Ni/La_2O_3/γ-Al_2O_3 catalyst. The Ni/ZrO_2/γ-Al_2O_3 catalyst exhibited the highest initial CH_4 conversion among the promoted catalysts, although it was lower than that of the unpromoted catalyst. However the activity increased linearly from 55% to 66% with time on stream It is well known that ZrO_2 possesses the redox properties, that can act as oxygen supplier and its oxygen mobility is higher than that of alumina (Souza *et al.*, 2002) which is capable of oxidising deposited carbon The higher stability and coke resistivity of Ni/ZrO_2/γ-Al_2O_3 may be due to the strong Ni-Zr^+ interaction, (strong metal-support interaction) which result in the formation of ZrO_x species on the Ni surface. Thus the Ni-ZrO_x interface in the ZrO_2-Al_2O_3 system appears to be more active and stable for CO_2 reforming.

Further more, the thermal stability of ZrO_2 is higher at high temperatures and because it has both basic and acidic sites, ZrO_2 could be resistant to coke formation (Roh *et al*, 2001) Additionally, because of the oxygen conducting properties, ZrO_2 promoted support can actively participate in the catalytic reaction by oxidizing or reducing reaction intermediates. CH_4 conversions increase with increasing time on stream which may be due to activation of the catalyst during reaction time (see Figure 4 12) The CO_2 conversion and CO yield followed a similar trend to CH_4 conversion The CO yield for the unpromoted catalyst was different, with an initial CO yield of 22%, although increases to 33% it linearly decreases again to 24%. For Ni/MgO/γ-Al_2O_3 and Ni/La_2O_3/γ-Al_2O_3 catalysts, low CO yields were observed 11% and 9%, respectively but stable activity was maintained during reaction time on stream.

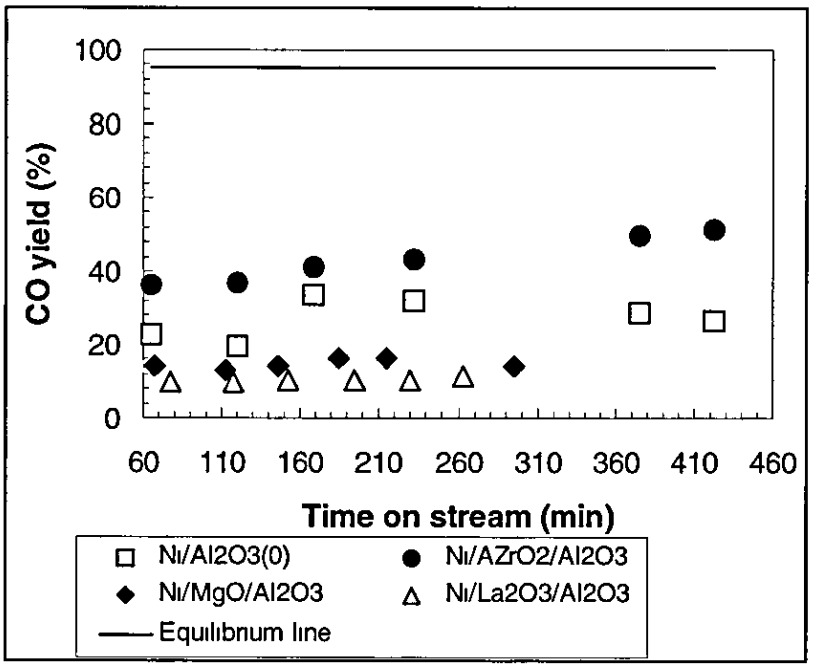

Figure 4.14 CO yield as a function of time, WHSV = 19200 ml/hr g cat, $CH_4/CO_2 = 1$, P = 1atm, T = 1073K

Carbon deposition on the nickel catalyst surface has been a well known reason for the deactivation of catalyst during CO_2 reforming CH_4 (Joo *et al*, 2002) Joo *et al*, (2002) found that a difference in calcinations temperature (723K and 1123K) can cause a significant difference in the amount of carbon deposition but a catalyst with high carbon deposition may still maintain high activity with time on stream. They identified two category of carbon formation whisker formation and amorphous carbon It then suggests that the deactivation of Ni supported catalyst probably is related to the type of carbon deposited rather than the amount of the carbon deposited

Kinetic calculations of rate constant for the various catalysts show that $Ni/ZrO_2/\gamma\text{-}Al_2O_3$ has high reaction rate constant for CO formation ($k_3 = 101 \times 10^{-5}\ s^{-1}$) compared to the unprompted catalyst ($k_3 = 60 \times 10^{-5}\ s^{-1}$) (see Table 3.4, chapter 3), confirming the high CO yield observed for the ZrO_2 promoted catalyst. The apparent activation energies for CH_4, CO_2 and CO have been presented in (Chapter 4, Table 3.5). It is noteworthy that the activation barrier for the consumption of CO_2 for the unprompted catalyst $Ni/\gamma\text{-}Al_2O_3$ was higher than that of $Ni/ZrO_2/\gamma\text{-}Al_2O_3$ catalyst.

Although the CO yield for $Ni/ZrO_2/\gamma\text{-}Al_2O_3$ was higher, the apparent activation energy for the CO production was greater for $Ni/ZrO_2/\gamma\text{-}Al_2O_3$ (89 kJ/mol) compared to the unpromoted catalyst (40 kJ/mol) which may be attributed to the occurrence of WGS at lower temperatures The activation energy values for CH_4 and CO_2 (26 kJ/mol and 40 kJ/mol) obtained agrees well to values in literature (Gou *et al*, 2004)

No significant difference was observed in both CH_4 and CO_2 conversions at 13900 ml/hr gcat, compared to the space velocity of 19200ml/hr g cat for all catalysts tested (results at space velocity of 13900 ml/hr g cat except for the improved stability on the unprompted catalyst (Figure not shown)

With the decrease in space velocity (9820 ml/hr gcat) a stable activity was observed even for the unpromoted catalyst (see Appendix III, Figure A3 2.1) The $Ni/ZrO_2/\gamma\text{-}Al_2O_3$ still exhibits the highest activity with initial CH_4 conversion of 91% with stable activity with time on stream There was no significant difference in CH_4 conversion between $Ni/MgO/\gamma\text{-}Al_2O_3$ and the unpromoted catalyst However similar CO_2 conversions to CH_4 were observed for all the catalyst tested (see Appendix III, Figure A3 2 1) Although the CO_2 conversion for $Ni/ZrO_2/\gamma\text{-}Al_2O_3$ was lower compared to other catalyst, it exhibits the highest CO yield of 93% which increases to equilibrium conversion, although it linearly stabilises at 89%.

Reducing the space velocity to 7840 ml/hr gcat and 4800 ml/hr gcat increases conversion but followed similar trend for most of the catalysts tested. Apart from $Ni/La_2O_3/\gamma\text{-}Al_2O_3$ catalysts, both, the unpromoted catalyst, $Ni/ZrO_2/\gamma\text{-}Al_2O_3$, and $Ni/MgO/\gamma\text{-}Al_2O_3$ catalysts exhibit almost the same activity and stability in terms of CH_4 conversion at 7840 ml/hr g cat. For the CO_2 conversion, a similar trend was observed for the unpromoted catalyst and the $Ni/La_2O_3/\gamma\text{-}Al_2O_3$ catalyst where all showed lower initial CO_2 conversions which increase to 92% and 61% with constant activity The order of CO yield followed the trend; $Ni/ZrO_2/\gamma\text{-}Al_2O_3 > Ni/\gamma\text{-}Al_2O_3 > Ni/MgO/\gamma\text{-}Al_2O_3 > Ni/La_2O_3/\gamma\text{-}Al_2O_3$. A similar trend of CH_4, CO_2 conversions and CO yield were observed for all catalysts at 4800 ml/hr g cat. (see Appendix III, Figure A3 2 3)

As can be seen in all space velocities, the kinetic data agreed with the experimental results because the rate constant of CO formation for Zr_2O_3 promoted catalyst (k_3 = 101*10^{-5} sec) was higher than that of the unpromoted catalyst (k_3 = 60*10^{-5} sec) However, CO activation energy for the ZrO_2 promoted catalyst and unpromoted catalyst were (89 kJ/mol) and 40 kJ/mol).

4.5 Effect of support on catalytic stability

4.5.1 Catalytic stability of supported Ni-based catalyst, WHSV=19200 ml/hr.g.cat, T=1023K

The unpromoted catalyst shows deactivation at 1023K similar to the trend observed at 1073K (see section 4 3.1, Figures 4 12 and 4.13). At this temperature (1023K) and space velocity of 19200 ml/hr g cat, $Ni/MgO/\gamma\text{-}Al_2O_3$ catalyst, exhibits the highest CH_4 conversion among the promoted catalysts although it decreases to 69.7%, while CO_2 conversion of 72 5% was observed which increases to 74 0% The CO_2 conversion was higher than that of CH_4, conversion which indicates occurrence of RWGS ($CO_2 + H_2 \leftrightarrow CO + H_2O$) reaction The CH_4 conversions for $Ni/La_2O_3/\gamma\text{-}Al_2O_3$ and $Ni/ZrO_2/\gamma\text{-}Al_2O_3$ catalysts were very close, i e 45 4% and 47 7% and they also exhibited stable behaviour The CO_2 conversion was higher than that of CH_4 conversion for $Ni/ZrO_2/\gamma\text{-}Al_2O_3$ catalyst suggesting that the $Ni/ZrO_2/\gamma\text{-}Al_2O_3$ catalyst promoted the RWGS ($CO_2 + H_2 \leftrightarrow CO + H_2O$) reaction at this temperature and space velocity.

Although the initial CO yield of the unpromoted catalyst (51%) was higher, the final CO yield (38 4%) was almost the same as that for $Ni/ZrO_2/\gamma\text{-}Al_2O_3$ and $Ni/MgO/\gamma\text{-}Al_2O_3$ catalysts 37.1% and 34 8%, respectively The lowest CO yield was observed for the $Ni/La_2O_3/\gamma\text{-}Al_2O_3$ catalyst with stable activity. The unpromoted catalyst suffered deactivation at this temperature and space velocity The conversion trend for lower space velocities were not different from the observation made at 1073K At 13900 ml/hr gcat, the initial CO yield for $Ni/MgO/\gamma\text{-}Al_2O_3$ catalysts was higher than for all the other catalysts, although it stabilised at 30%, almost the same level as that of the unpromoted catalyst and $Ni/ZrO_2/\gamma\text{-}Al_2O_3$ catalyst For the space velocity of 9820 ml/hr g cat, CO yield for the $Ni/ZrO_2/\gamma\text{-}Al_2O_3$ catalysts was higher compared to all other catalysts

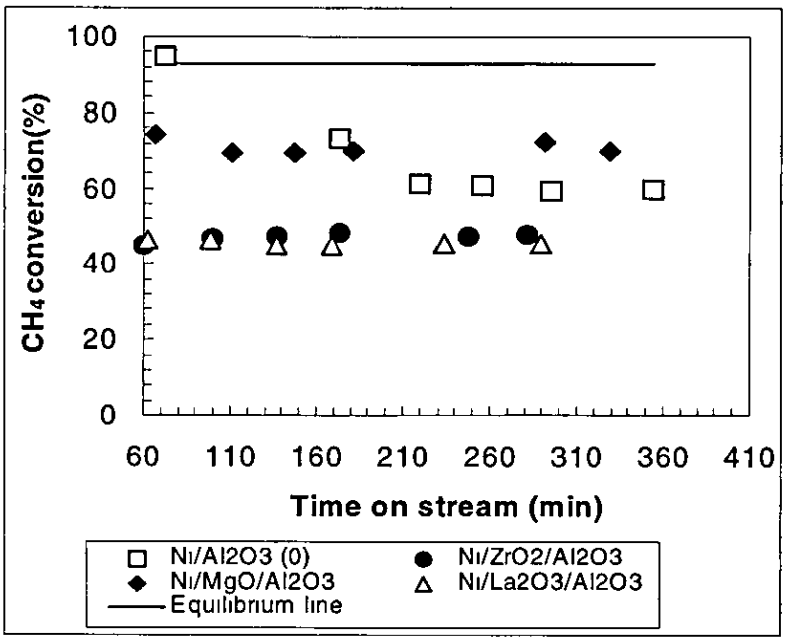

Figure 4 15 CH_4 conversion as a function of time, WHSV = 19200 ml/hr g cat, CH_4/CO_2 = 1, catalyst weight = 50 mg, P = 1 atm , T = 1023 K

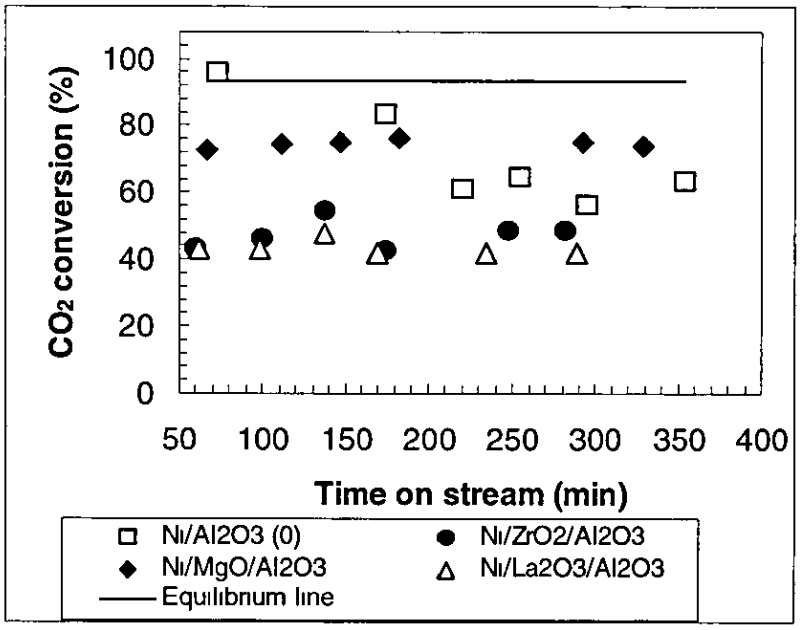

Figure 4 16 CO_2 conversion as a function of time, WHSV = 19200 ml/hr g cat, CH_4/CO_2 = 1, catalyst weight = 50 mg, P = 1 atm., T = 1023 K

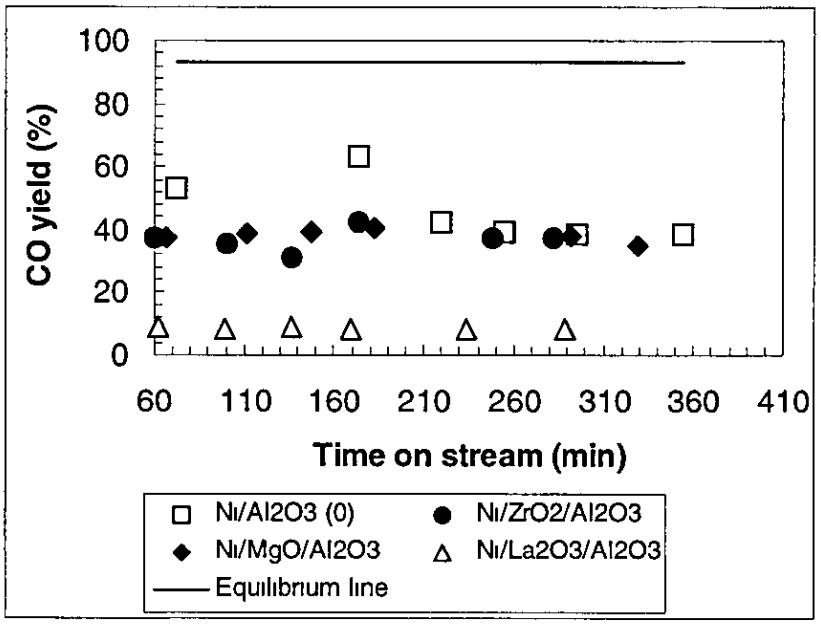

Figure 4.17 CO yield as a function of time, WHSV = 19200 ml/hr g cat, $CH_4/CO_2 = 1$, catalysts weight = 50 mg, P = 1 atm , T = 1023K

The CO trend was different at the space velocity of 4800 ml/hr gcat, almost the same initial CO yield was observed, although there was variation during reaction, they all stabilised at close final values (Figure not shown) The rate constant obtained at 1023K for CO formation for the $Ni/ZrO_2/\gamma\text{-}Al_2O_3$ catalyst was still higher ($k_3 = 70*10^{-5}\ s^{-1}$) compared to the unpromoted catalyst ($k = 40*10^{-5}\ s^{-1}$).

4.6 Effect of support on catalyst stability

4 6.1 Catalytic stability of supported Ni-based catalyst, WHSV = 19200 ml/hr g cat, T = 973K

At 973K and space velocity of 19200 ml/hr g cat, CH_4 conversion for the unpromoted catalyst did not show deactivation both in terms of CH_4 and CO_2 conversions The unpromoted catalyst and $Ni/ZrO_2/\gamma\text{-}Al_2O_3$ catalyst show similar activity in terms of CH_4 although with different initial activity of 44 1% and 36 2%.

The CO_2 conversion for unpromoted catalysts, $Ni/ZrO_2/\gamma\text{-}Al_2O_3$ and $Ni/La_2O_3/\gamma\text{-}Al_2O_3$ show almost the same activity though with different initial CO_2 conversions (see Figure 4.18)

The CO yield values for $Ni/ZrO_2/\gamma\text{-}Al_2O_3$ and $Ni/MgO/\gamma\text{-}Al_2O_3$ catalysts were almost the same, but the CO yield for $Ni/MgO/\gamma\text{-}Al_2O_3$ catalyst decreases from 40.8% to 34.5% and remained constant with time on stream, while the CO yield for $Ni/ZrO_2/\gamma\text{-}Al_2O_3$ did not show any deactivation. The unpromoted catalyst shows lower CO yield compared to $Ni/ZrO_2/\gamma\text{-}Al_2O_3$ and $Ni/MgO/\gamma\text{-}Al_2O_3$ catalysts As can be seen (Figure 4 19) the CO yield for $Ni/La_2O_3/\gamma\text{-}Al_2O_3$ catalyst showed the lowest CO yield among all the catalyst tested but it was also stable with time on stream. The activity of the unpromoted catalyst increased at 13900 ml/hr gcat, higher than that of $Ni/ZrO_2/\gamma\text{-}Al_2O_3$ and $Ni/La_2O_3/\gamma\text{-}Al_2O_3$ catalysts in terms of CH_4 and CO_2 conversions while $Ni/MgO/\gamma\text{-}Al_2O_3$ catalyst still maintained the highest activity. However, despite the low conversions observed for $Ni/ZrO_2/\gamma\text{-}Al_2O_3$ catalyst it still exhibits the highest CO yield showing a similar trend to the space velocity of 19200 ml/hr g cat The activity at space velocity of 9820 ml/hr gcat and 7840 ml/hr g cat did not show any significant differences in conversion trend (see Appendix III, Figure A3 4.3)

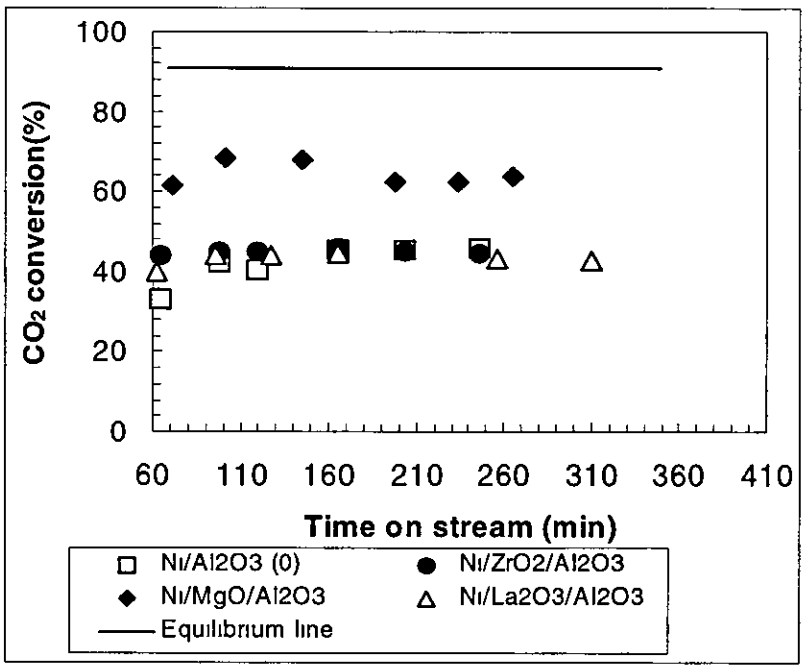

Figure 4 18 CO_2 conversion as a function of time, WHSV = 19200 ml/hr g cat, CH_4/CO_2 = 1, catalyst weight = 50 mg, P = 1 atm , T = 973K

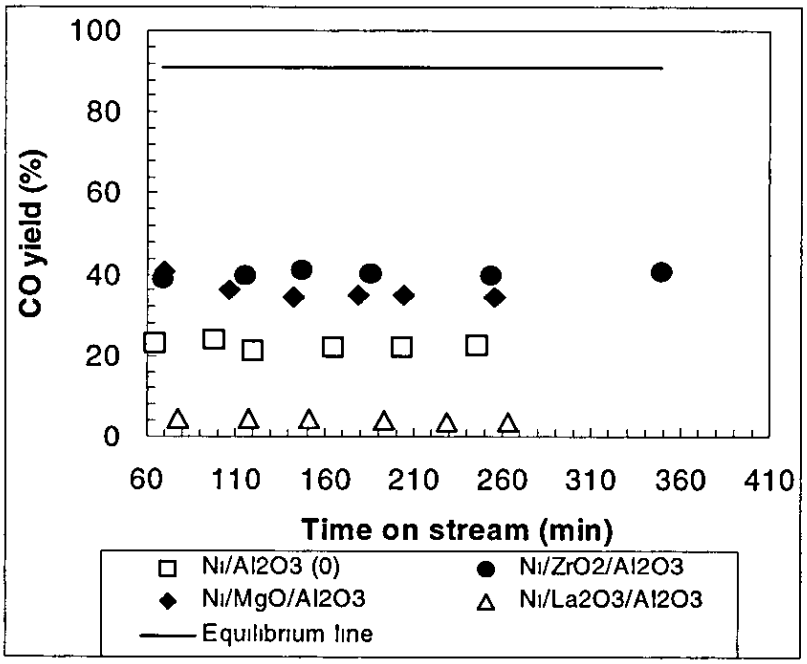

Figure 4.19 CO yield as a function of time, WHSV = 19200 ml/hr g cat, CH_4/CO_2 = 1, catalyst weight = 50 mg, P = 1 atm, T = 973K

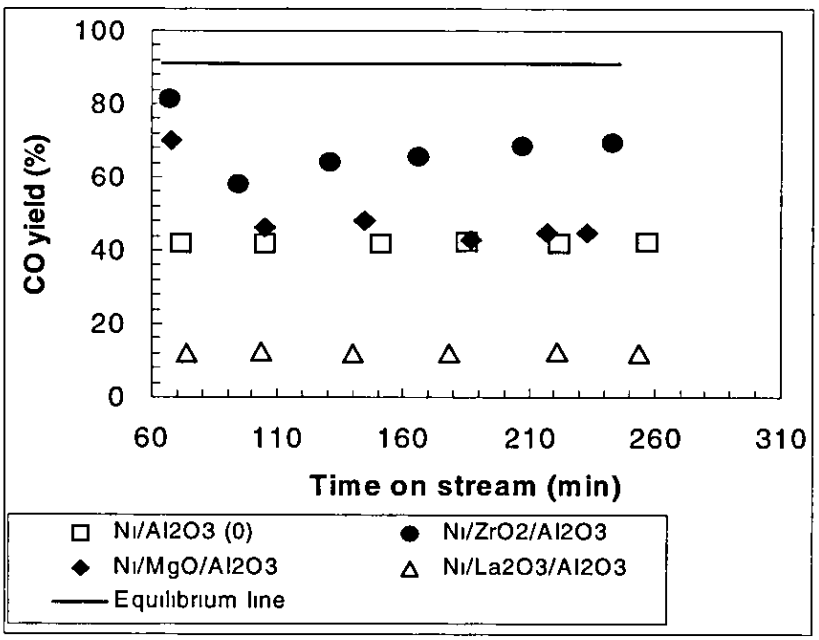

Figure 4.20 CO yield as a function of time, WHSV = 4800 ml/hr g cat, CH_4/CO_2 = 1, catalyst weight = 50 mg, P = 1 atm., T = 973K

The activity of all the catalysts at space velocity of 4800 ml/hr gcat was not different, apart from the significant difference observed between $Ni/ZrO_2/\gamma\text{-}Al_2O_3$ and $Ni/La_2O_3/\gamma\text{-}Al_2O_3$ catalysts, with activities of 60% and 50% respectively (see Appendix III, Figure A3.4.4) The CO yield for both $Ni/ZrO_2/\gamma\text{-}Al_2O_3$ and $Ni/MgO/\gamma\text{-}Al_2O_3$ catalysts show high values but decreases with time on stream (see Figure 4.20) The decrease in CO yield may be due to WGS reaction ($CO + H_2O \leftrightarrow CO_2 + H_2$) that is being favoured at low temperatures, especially for the $Ni/ZrO_2/\gamma\text{-}Al_2O_3$ catalyst. There was still consistency of the high rate constant of CO formation for the $ZrO_2/\gamma\text{-}Al_2O_3$ catalyst ($k_3 = 50*10^{-5}\ s^{-1}$) compared to unpromoted catalyst of $k_3 = 25*10^{-5}\ s^{-1}$) which agreed to the experimental results.

4.7 Effect of support on catalytic stability

4.7.1 Catalytic stability of supported Ni-based catalyst, WHSV=19200 ml/hr g cat, T = 923 K

The catalytic performance of the unpromoted catalyst, $Ni/MgO/\gamma\text{-}Al_2O_3$, $Ni/ZrO_2/\gamma\text{-}Al_2O_3$ and $Ni/La_2O_3/\gamma\text{-}Al_2O_3$ catalysts at temperature of 923K and space velocity of 19200 ml/hr gcat are shown in Figure 4 21 and 4 22. The activity is different from that observed at 973K, with close initial conversions of CH_4 for both the unpromoted catalyst, $Ni/La_2O_3/\gamma\text{-}Al_2O_3$ and $Ni/MgO/\gamma\text{-}Al_2O_3$ catalyst of (51%, 51.3% and 54 5%) respectively. A lower activity was observed for $Ni/ZrO_2/\gamma\text{-}Al_2O_3$ catalyst for CH_4 and CO_2 at this temperature and space velocity but it maintained the highest CO yield observed at higher temperatures (see section 4 4 and 4.6) for explanation. The reason for this unusual high CO yield is unclear because $Ni/ZrO_2/\gamma\text{-}Al_2O_3$ catalyst appears to favours WGS reaction at low temperatures. The rate constant for the $Ni/ZrO_2/\gamma\text{-}Al_2O_3$ catalyst ($k_3 = 4*10^{-5}\ s^{-1}$) was also lower compared to unpromoted catalyst ($k_3 = 15*10^{-5}\ s^{-1}$)

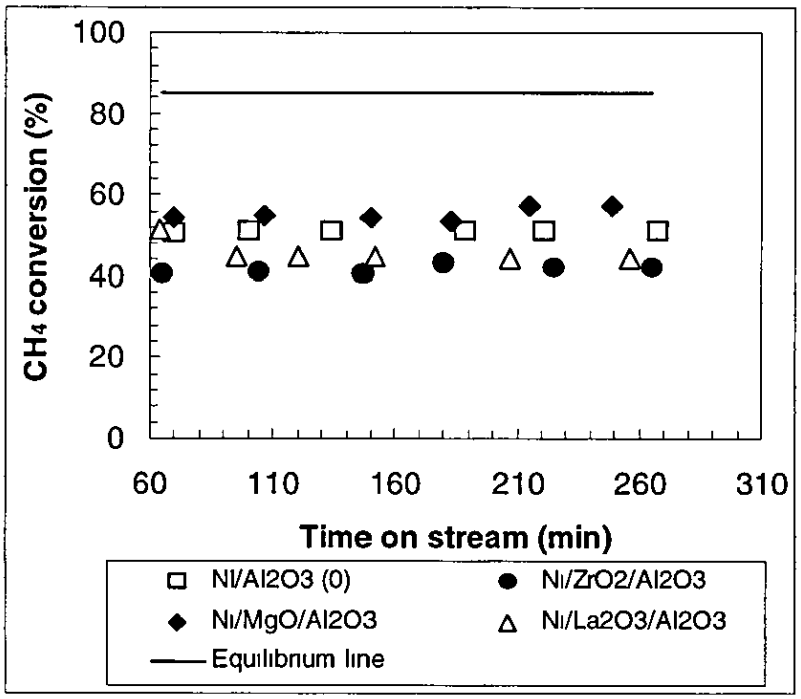

Figure 4.21 CH_4 conversion as a function of time, WHSV = 19200 ml/hr g cat, CH_4/CO_2 = 1, catalyst weight = 50 mg, P = 1 atm , T = 923K

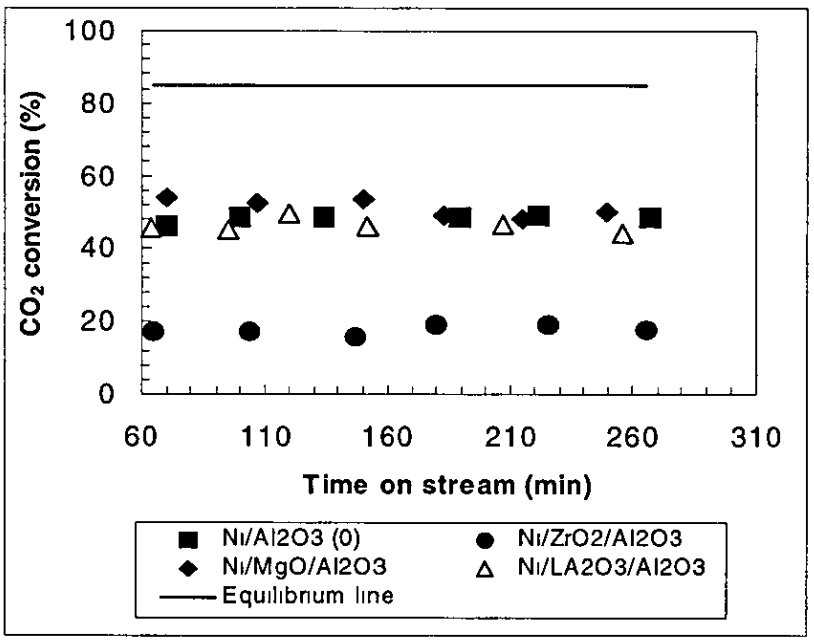

Figure 4 22 CO_2 conversion as a function of time, WHSV = 19200 ml/hr g cat, CH_4/CO_2 = 1, catalyst weight = 50 mg, P = 1 atm , T= 923K

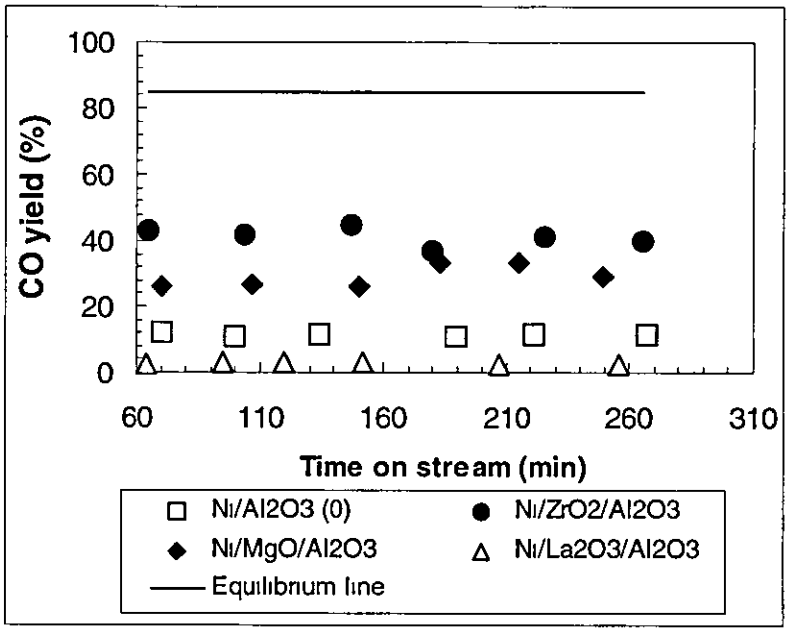

Figure 4 23 CO yield as a function of time WHSV = 19200 ml/hr g cat, $CH_4/CO_2 = 1$, catalyst weight = 50 mg, P = 1 atm , T = 923K

The only explanation may be due to hydroxyl groups which may have remained on the surface of the zirconia supported catalyst (Stagg *et al*, 1998) Stagg *et al*, (1998) reported that such functional groups may interact with CO_2, which can generate formate and bicarbonate intermediates at lower temperatures. These species may play a role under relevant conditions The performance of all catalysts at 13900 m/hr g cat shows similar trend to the space velocity of 19200 ml/hr g cat in terms of CH_4 (see Appendix III, Figure A3 5 1) The activity trend at lower space velocities of 9820 ml/hr gcat, 7840 ml/hr g cat and 4800 ml/hr g cat were similar compared to higher space velocities of 13900 ml/hr g cat and 19200 ml/hr g cat (see Appendix III, Figures A3 5 2, A3.5 3 and A3 5 4)

4 8 Effect of space velocity on catalytic activity, T = 1073K

The effect of space velocity on CH_4, CO_2 conversions and CO yield was conducted over the range of 4800-19200 ml/hr g cat at 1073K, 1023K and 973K.

The dependence of conversions of CH_4 and CO_2 on space velocity decreased with increasing space velocity (Figure not shown)

The CO yield at 1073K, 1023K and 973K are shown in Figure 4 24, 4 25 and 4 26 respectively. The CO yield decreases with increasing space velocity, because the contact time become shorter, which is in good agreement to the report published by (Tomishige *et al*, (2001). It is a clear fact that the $Ni/ZrO_2/\gamma\text{-}Al_2O_3$ catalyst exhibited the highest CO yield at 1073K for all the space velocities (explanation given in section 4.4 1) For all catalysts, the CO yield decreases with increasing space velocities. There was no significant difference between the unpromoted catalyst and that of $Ni/MgO/\gamma\text{-}Al_2O_3$ at lower space velocities, but the CO yield for the unpromoted catalyst was higher than that of $Ni/MgO/\gamma\text{-}Al_2O_3$ at 9820 ml/hr g cat The activity for $Ni/La_2O_3/\gamma\text{-}Al_2O_3$ catalysts was restored at higher space velocity of 19200 ml/hr gcat compared to the low activity at 13900 ml/hr g cat and 9820 ml/hr g cat. The effect of space velocity at 1023K was different compared to that of 19200 ml/hr gcat (see Figure 4 25) The $Ni/ZrO_2/\gamma\text{-}Al_2O_3$ catalyst still exhibits highest CO yield at only space velocities of 7840 and 9820 ml/hr g cat At higher space velocities >13900 ml/hr g cat the CO yield is the same for $Ni/ZrO_2/\gamma\text{-}Al_2O_3$, $Ni/MgO/\gamma\text{-}Al_2O_3$ and the unprompted catalyst.

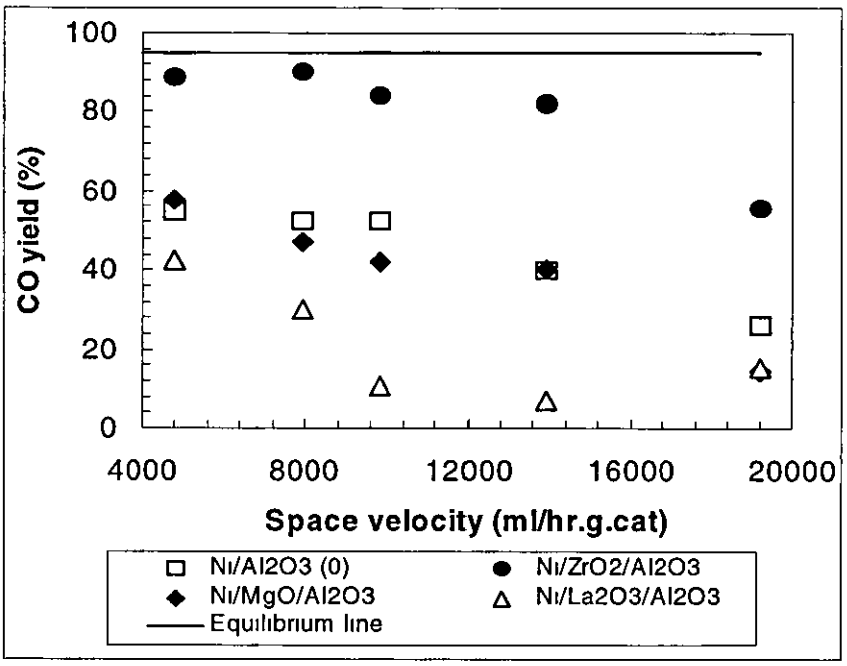

Figure 4.24 CO yield as a function of space velocity, $CH_4/CO_2 = 1$, catalyst weight = 50 mg, P = 1 atm., T = 1073K,

The Ni/MgO/γ-Al_2O_3 catalyst exhibits the highest CO yield at space velocity of 4800 ml/hr g cat. At 973K highest CO yield was observed for Ni/ZrO_2/γ-Al_2O_3 catalyst, apart from the CO yield at 9820 ml/hr g cat, where the highest CO yield was exhibited by Ni/MgO/γ-Al_2O_3 catalyst. Although activity decreases with increasing space velocity, the CO yield was restored at 19200 ml/hr gcat for Ni/ZrO_2/γ-Al_2O_3 catalyst (see Figure 4.26). Among the catalysts tested, Ni/ZrO_2/γ-Al_2O_3 catalyst shows the highest CO yield at 1073K and 973K except the space velocity at 9820 ml/hr g cat. The kinetic data agrees well with the experimental results obtained The rate constant for CO formation was higher for the Ni/ZrO_2/γ-Al_2O_3 catalysts compared to the unpromoted catalyst ($k_3 = 101*10^{-5}\ s^{-1}$) and ($k_3 = 60*10^{-5}\ s^{-1}$) respectively A similar trend of high CO formation was observed because the rate constant for ZrO_2 promoted catalyst is consistently higher at all temperatures except < 923K especially at higher space velocities > 19200 ml/hr g cat.

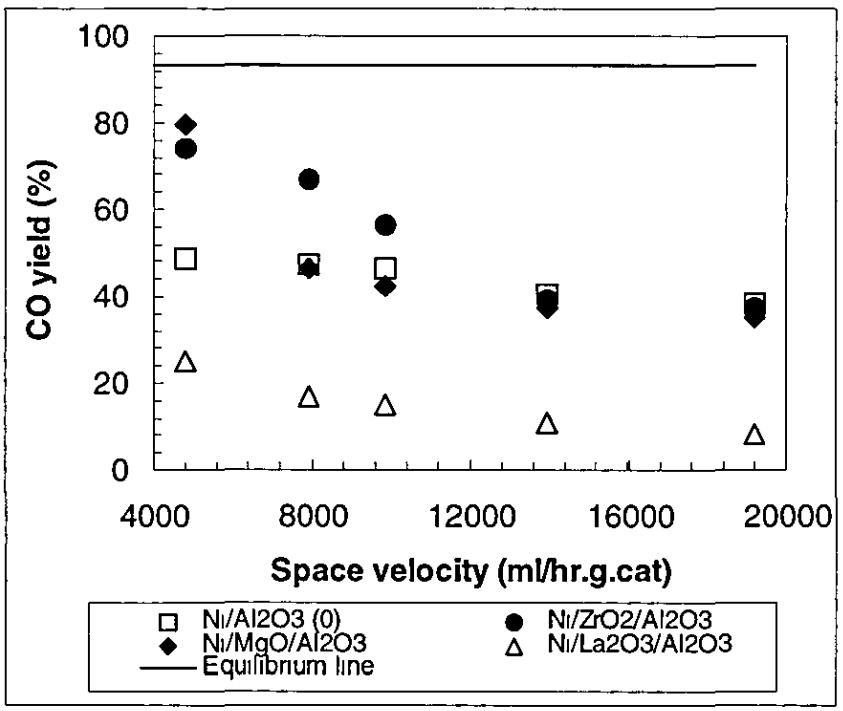

Figure 4 25 CO yield as a function of space velocity, $CH_4/CO_2 = 1$, catalyst weight = 50 mg, P = 1 atm, T = 1023K

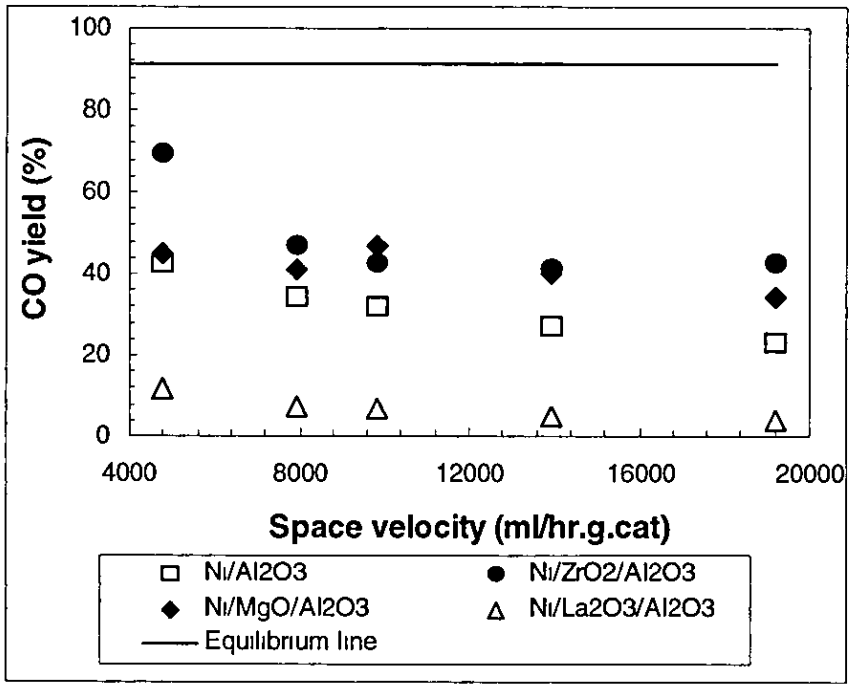

Figure 4.26 CO yield versus space velocity, $CH_4/CO_2 = 1$, catalyst weight = 50 mg, P = 1 atm, T = 973K

It is very apparent that ZrO_2-support modification has enhanced CO yield mostly at higher temperatures as can be seen in Figure 4 24, 4 25 and 4 26.

4.9 Carbon deposition, WHSV = 19200ml/hr g cat, T = 1073K

The SEM images of catalysts exposed to CO_2 reforming of CH_4 are shown in Figure 4.27 and 4 28 for comparison with the fresh catalysts. As can be seen in Figure 4.28 filamentous carbon was not visible on the $Ni/ZrO_2/\gamma\text{-}Al_2O_3$ catalyst but carbon deposition was quantified after burnt off Another observation is that, the ZrO_2–promoted catalyst shows smooth surface morphology which also indicate that there was surface modification For the unpromoted catalyst, cracks are observed on the catalyst with a rough surface after reaction. The carbon deposit followed the order $Ni/La_2O_3/\gamma\text{-}Al_2O_3$ > $Ni/MgO/\gamma\text{-}Al_2O_3$ > $Ni/\gamma\text{-}Al_2O_3$ > $Ni/ZrO_2/\gamma\text{-}Al_2O_3$, 0 36g/g cat, 0 23g/g cat and 0 14g/g

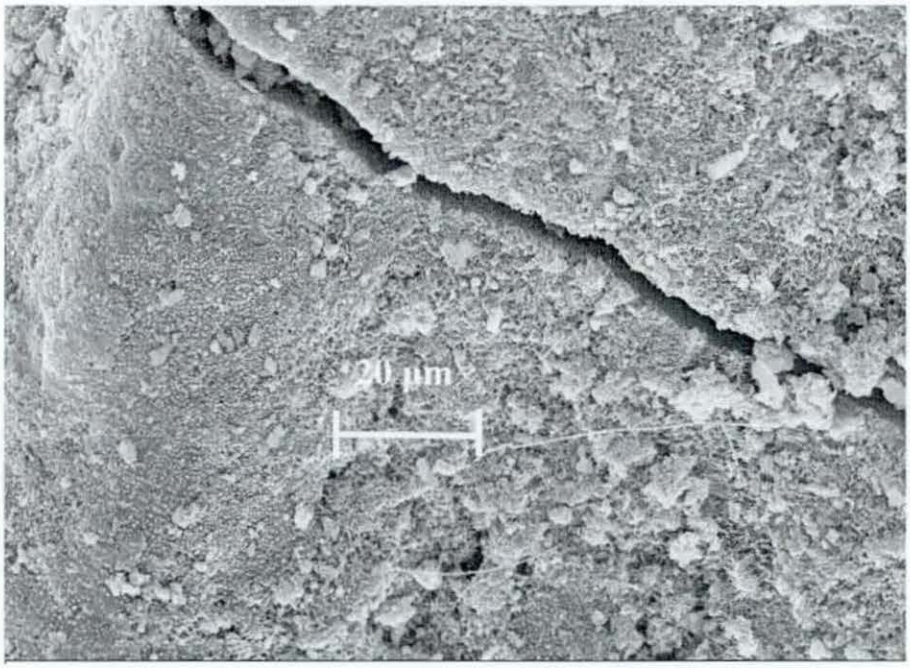

Figure 4.27 SEM images of Ni/γ-Al_2O_3 after reforming, WHSV = 19200 ml/hr g cat CH_4/CO_2 = 1, catalyst weight = 50 mg, P = 1 atm, T = 1073K

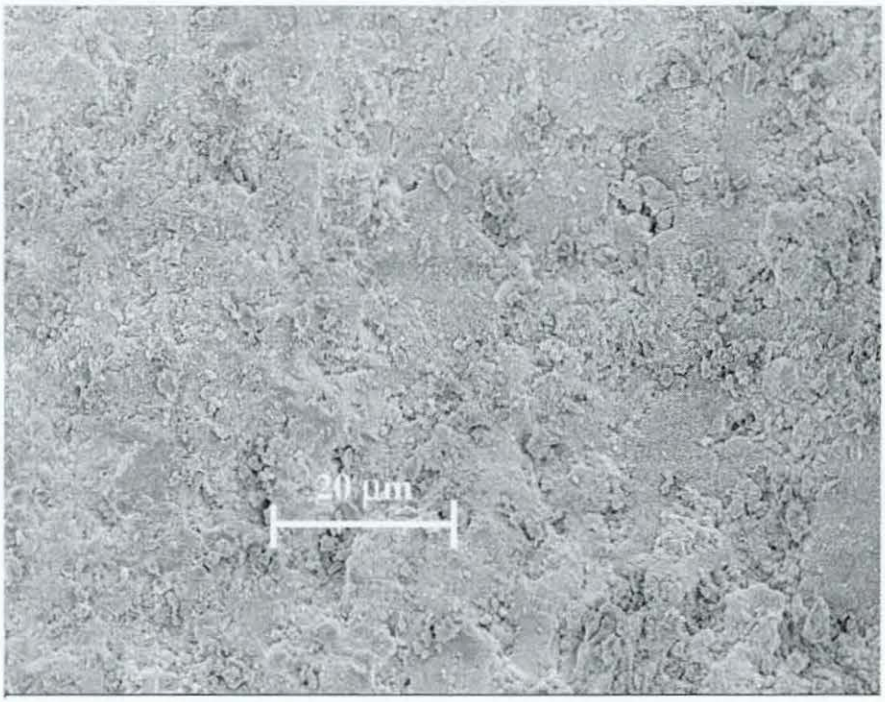

Figure 4.28 SEM images of Ni/ZrO_2/γ-Al_2O_3 after reforming, WHSV = 19200 ml/hr g cat CH_4/CO_2 = 1, catalyst weight = 50 mg, P = 1 atm, T = 1073K

The rate constant for CO formation was higher for the $Ni/ZrO_2/\gamma\text{-}Al_2O_3$ catalysts compared to the unpromoted catalyst ($k_3 = 101*10^{-5}\ s^{-1}$) and ($k_3 = 60*10^{-5}\ s^{-1}$) respectively The activation energy for the ZrO_2 promoted catalyst for CH_4 and CO_2 are 29.8 kJ/mol and 26 kJ/mol while 32.9 kJ/mol and 29.8 kJ/mol were obtained for the unpromoted catalyst However, the activation energies for CO were 89 kJ/mol and 40 kJ/mol respectively

4 10 Conclusions

The transition oxide-promoted catalysts exhibited stability compared to the unpromoted catalyst ($Ni/\gamma\text{-}Al_2O_3$) at temperatures > 973K and higher space velocities (1900 ml/hr gcat). The activity of $Ni/ZrO_2/\gamma\text{-}Al_2O_3$ and $Ni/La_2O_3/\gamma\text{-}Al_2O_3$ increases with increasing temperature but that of the unpromoted catalyst and $Ni/MgO/\gamma\text{-}Al_2O_3$ catalyst decreases at temperatures above 1073K at a space velocity of 19200 ml/hr g cat due to carbon deposition. This is confirmed with the observation made in the present study comparing the $Ni/ZrO_2/\gamma\text{-}Al_2O_3$ catalyst and the unpromoted catalyst.

The same amount of carbon deposit was observed but $Ni/ZrO_2/\gamma\text{-}Al_2O_3$ did not show deactivation during reaction while that of the unprompted catalyst showed loss in activity with time on stream The highest CO yield was observed for the ZrO_2–promoted catalyst, almost at all space velocities at 1073K This observation agrees well with the kinetic results because the highest rate constant for CO formation was obtained for the $Ni/ZrO_2/\gamma\text{-}Al_2O_3$ catalyst The $Ni/ZrO_2/\gamma\text{-}Al_2O_3$ catalyst shows a smooth surface morphology with no visible carbon deposition after reforming reaction for 6 hours. Catalytic activity order in terms of CO yield is $Ni/ZrO_2/\gamma\text{-}Al_2O_3$ > $Ni/\gamma\text{-}Al_2O_3$ > $Ni/MgO/\gamma\text{-}Al_2O_3$ > $Ni/La_2O_3/\gamma\text{-}Al_2O_3$. For the unpromoted catalyst, cracks are observed on the catalyst with a rough surface after reaction The carbon deposit followed the order $Ni/La_2O_3/\gamma\text{-}Al_2O_3$ > $Ni/MgO/\gamma\text{-}Al_2O_3$ > $Ni/\gamma\text{-}Al_2O_3$ > $Ni/ZrO_2/\gamma\text{-}Al_2O_3$ with 0 36g/g cat, 0.23g/g cat with 0 14g/g cat and 0 14g/g cat.

Rate constant values for CO formation, obtained for the ZrO_2 promoted catalyst was higher ($k_3 = 101*10^{-5}\ s^{-1}$) compared to that of the unpromoted catalyst ($k_3 = 60*10^{-5}\ s^{-1}$) Activation energies obtained for CH_4 were 29.8 kJ/mol, 26 kJ/mol and for CO_2 were 32 kJ/mol, 29 8 kJ/mol for the ZrO_2 promoted catalyst and unpromoted catalyst respectively.

CHAPTER 5

EFFECT OF PALLADIUM AND COPPER PROMOTION FOR Ni/γ-Al_2O_3 CATALYSTS ON THE CATALYTIC ACTIVITY

5.1 Introduction

Chapter 5 discusses all the experimental results obtained from the studies of CO_2 reforming of methane over Ni/γ-Al_2O_3 promoted catalysts. Palladium is among the noble metals reported to be active and fairly stable for CO_2 reforming of CH_4 (Asami *et al.*, (2003) but too expensive for practical purposes. On the other hand, Ni is not expensive but suffers deactivation at higher temperatures when used on common carriers such as alumina. Therefore, in this study palladium and copper were used as promoters for Ni/γ-Al_2O_3 catalyst. The characterisation results of catalysts promoted with palladium, their catalytic activity and stability are presented first, followed by the results obtained with copper promoted nickel catalyst The effects of palladium and copper on carbon deposition and space velocity are also discussed.

5.2 Catalyst characterisation-Effect of Palladium Promotion

5.2 1 Surface area and pore size distribution

As can be seen in Table 5.1, the BET surface area of the Ni/γ-Al_2O_3 catalyst decreases with the addition of palladium loading of (0.25-1 wt%) (174 m^2/g to 135 m^2/g and 117 m^2/g) for Ni-Pd/γ-Al_2O_3 (1 wt%) and Ni-Pd/γ-Al_2O_3 (0.5 wt%) while no significant increase was observed for Ni-Pd/γ-Al_2O_3 (0.25 wt%) 178 m^2/g. The surface area decrease may be due to increase in palladium loading and pore blocking. Figure 5.1 displays the pore size distribution of the unpromoted and palladium promoted catalysts which indicate a shift in the average pore size to 32Å, 33Å and 27Å for Ni-Pd/γ-Al_2O_3 (0.25 wt%), Ni-Pd/γ-Al_2O_3 (1 wt %) and Ni-Pd/γ-Al_2O_3 (0 5 wt%) catalysts Although the unpromoted catalyst, exhibits mainly mesopores with little traces of micropores, the addition of palladium and subsequent thermal treatment enhances the development of microspores.

Catalyst	Ni loading (wt%)		Crystallite Size (nm[b])	BET Surface area BET(m^2/g)	Dispersion[c] (%)	Pore volume (cm^3/g)
Ni/γ-Al_2O_3(0)	15	8.4[a]	26.9	174	5.9	0.20
Ni-Pd/γ-Al_2O_3(0.25 wt%)	15	14.4[a]	38	178	5.82	n.d
Ni-Pd/γ-Al_2O_3 (0.5 wt%)	15	13.3[a]	28.3	135	3.03	n.d
Ni-Pd/γ-Al_2O_3 (1 wt%)	15	-	44	117	2.09	0.13

Atomic adsorption spectrophotometry[a]
X-Ray diffraction[b]
CO chemisorption[c]
n.d not determined

Table 5.1 Physicochemical properties of prepared supported Ni-based catalysts

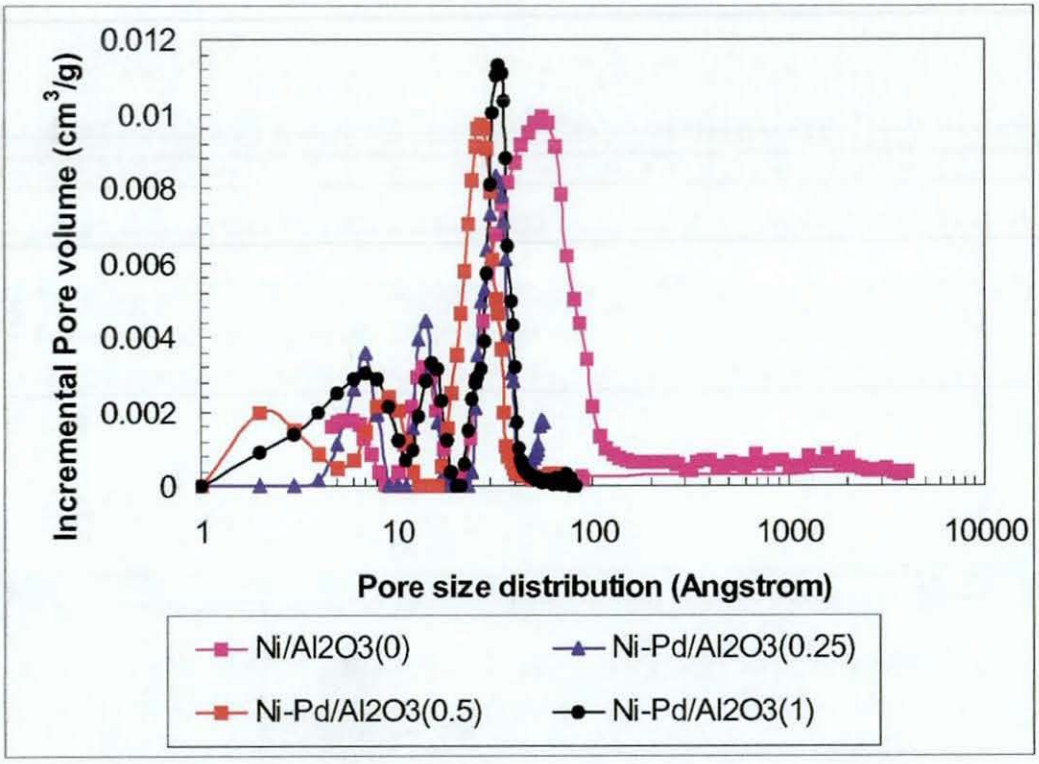

Figure 5.1 Pore size distribution of unpromoted and palladium promoted nickel catalysts

The surface area loss for both Ni-Pd/γ-Al_2O_3 (0.5 wt%) and Ni-Pd/γ-Al_2O_3 (1 wt%) catalysts may be due to loss of mesopores in the promoted catalysts (Hou and Yashima, 2004).

With the similar surface area observed for Ni-Pd/γ-Al_2O_3 (0.25 wt%), compared to the unpromoted catalyst, it is suggested that the maximum amount of palladium loading should be below 0.25 wt%. Similarly, the Ni dispersion decreases with increasing palladium loading, from initially 5.9% for the unpromoted catalyst to 2.09% for 1 wt% palladium promoted catalyst, while 5.8% was observed for the Ni-Pd/γ-Al_2O_3 (0.25 wt%) catalyst

The crystallites size for the unpromoted catalyst determined from XRD line broadening was 26.9 nm while 44 nm, 28.3 nm and 38 nm were obtained for 1 wt%, 0.5 wt% and 0.25 wt% of palladium respectively. Dispersion depends on the fraction of catalytic atoms exposed which increases with decreasing crystallite size. The decrease in dispersion of Ni observed may be due to increased crystallites size and the specific surface area loss of the promoted catalyst. The low Ni dispersion compared to the unpromoted catalyst may also be caused by coverage of Ni by Pd species or spinel formation $NiAl_2O_4$.

5.1.2 Temperature-programmed reduction pattern (TPR)

TPR traces for the promoted and 0 5 wt% palladium promoted catalyst were studied. The TPR plots are shown in Figure 5.2. For the unpromoted catalyst Ni/γ-Al_2O_3, the TPR shows a peak at 599K and 799K, which can be attributed to reduction of NiO and $NiAl_2O_4$ spinel structures (Lee *et al.*, 2004). The Ni-Pd/γ-Al_2O_3 (0.5 wt%) catalyst shows a different pattern given a maximum peak at 974K. The high reduction temperature suggests that addition of 0.5 wt% palladium has a negative effect on the reduction temperature. The H_2 uptake for the palladium promoted catalyst was 1.49 mmole compared to 1.98 mmole for the unpromoted catalyst. The low uptake of the 0 5 wt% Pd catalyst indicates that there was strong interaction between Ni and the support. The single reduction peak temperature 974K may be due the formation of spinel $NiAl_2O_4$ which is difficult to reduce.

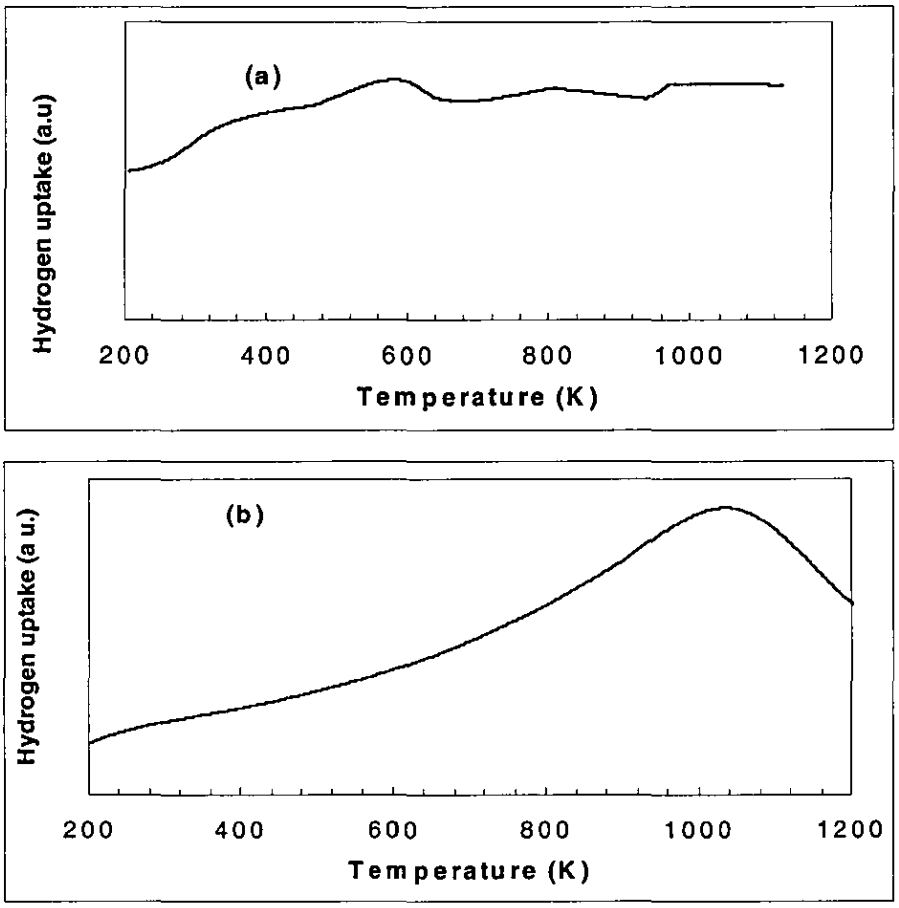

Figure 5.2 TPR profile of (a) $Ni/\gamma\text{-}Al_2O_3$ (b) $Ni\text{-}Pd/\gamma\text{-}Al_2O_3$ (0 5 wt%) catalysts

5.2.3 X-ray diffraction (XRD)

The X-ray diffraction patterns of the palladium promoted nickel catalysts were not significantly different from that of the unpromoted $Ni/\gamma\text{-}Al_2O_3$ catalyst (see Figures 5.3 Broad peaks at 37°, 43.3°, 63° and 66.2° indicate the presence of crystallite NiO, and Al_2O_3, for the unprompted catalyst. The broadening of diffraction peaks observed may have originated from evenly distributed micro-crystallites or random crystallites (Liu *et al.*, 2002) such as NiO, $NiAl_2O_4$ and Al_2O_3. This is in good agreement with the TPR results with reduction peaks at 593 K and 799 K, indicating the existence of two types of nickel oxide which may be due to metal-support interactions.

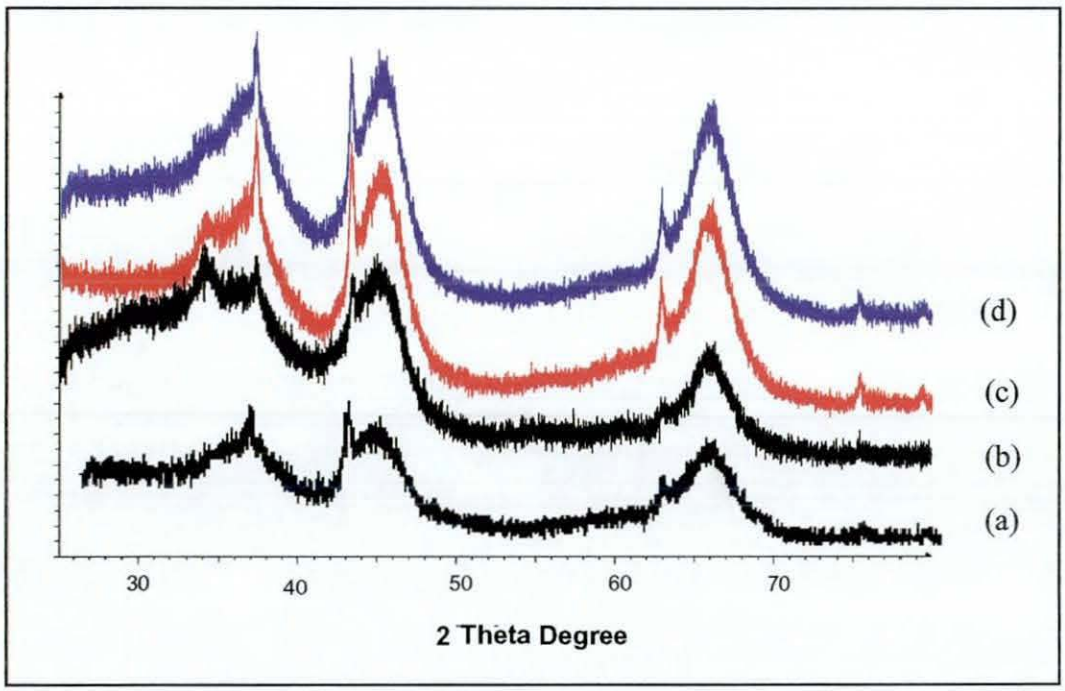

Figure 5.3 XRD pattern of Ni-promoted catalysts (a) Ni/γ-Al_2O_3(0) (b) Ni-Pd/γ-Al_2O_3 (0.25 wt%) (c) Ni-Pd/γ-Al_2O_3 (0.5 wt%) (d) Ni-Pd/γ-Al_2O_3 (1 wt%)

An increased intensity of peaks of the palladium promoted catalysts agrees well with the results obtained from CO chemisorption which indicates a decrease in dispersion with increasing content of palladium and surface area loss.

5.3 Effect of palladium promotion on catalytic activity

5.3.1 Effect of Palladium on catalytic activity, WHSV = 19200 ml/hr g cat, T = 1073K

Figures 5.4, 5.5 and 5.6 illustrate the CH_4/CO_2 conversion as well as the CO yield as a function of temperature obtained over Ni/γ-Al_2O_3, Ni-Pd/γ-Al_2O_3 (0.25 wt%), Ni-Pd/γ-Al_2O_3 (0.5 wt%), and Ni-Pd/γ-Al_2O_3 (1 wt%) catalysts. The CH_4 conversion increases with increasing temperature except at 1073K, where a decline of conversion was observed for both the unpromoted and the Ni-Pd/γ-Al_2O_3 (1wt%) catalyst.

As can be seen in Figure 5.4, there was no significant difference in CH_4 conversion at 923K for Ni/γ-Al_2O_3 and Ni-Pd/γ-Al_2O_3 (0.25 wt%) catalysts while a difference in CH_4 conversion was observed at temperatures (> 973K). Although, low CH_4 conversion over Ni-Pd/γ-Al_2O_3 (0.25 wt%) catalyst has been observed at lower temperatures, it can be restored at higher temperatures (> 1073K). The CH_4 conversion for both Ni-Pd/γ-Al_2O_3 (0.25 wt%) and Ni-Pd/γ-Al_2O_3 (0 5 wt%) show similar values at all temperatures except at 973K.

The activities of Ni-Pd/γ-Al_2O_3 (0.5 wt%) and Ni-Pd/γ-Al_2O_3 (1 wt%) were significantly higher in terms of CH_4 conversion at 923K–1023K but a decrease in conversion was observed at 1073K especially for Ni-Pd/γ-Al_2O_3 (1 wt%) and the unpromoted catalyst, which may be due to carbon deposition. Although the carbon accumulated on the unpromoted catalyst was lower compared to the palladium promoted catalyst, further investigation is needed to verify if the cause of deactivation is a result of carbon deposition or sintering processes since all the palladium promoted catalysts showed carbon accumulation.

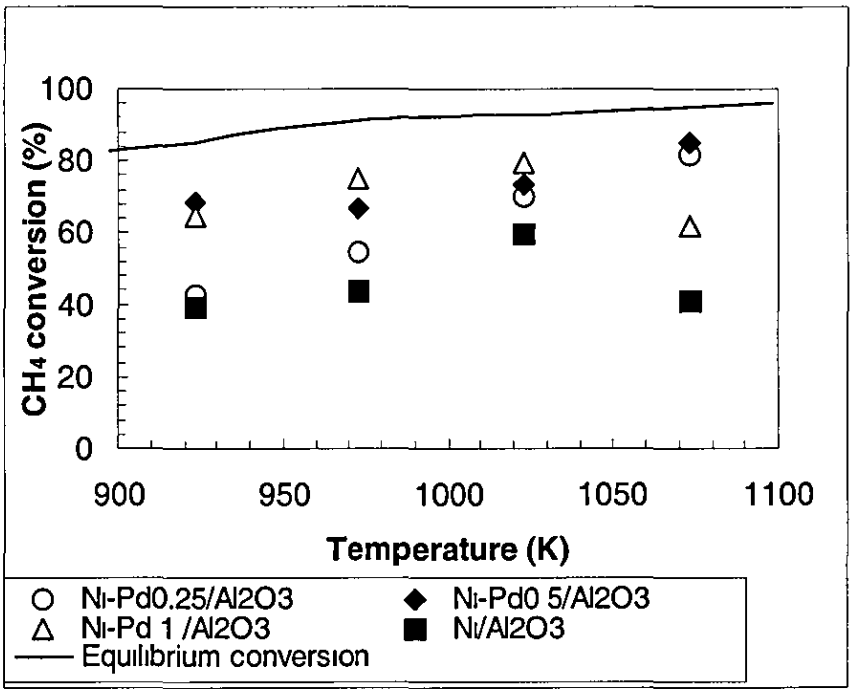

Figure 5.4 CH_4 conversion as a function of temperature, WHSV = 19200 ml/hr.g.cat, CH_4/CO_2 = 1, catalyst weight = 50 mg, P = 1atm.

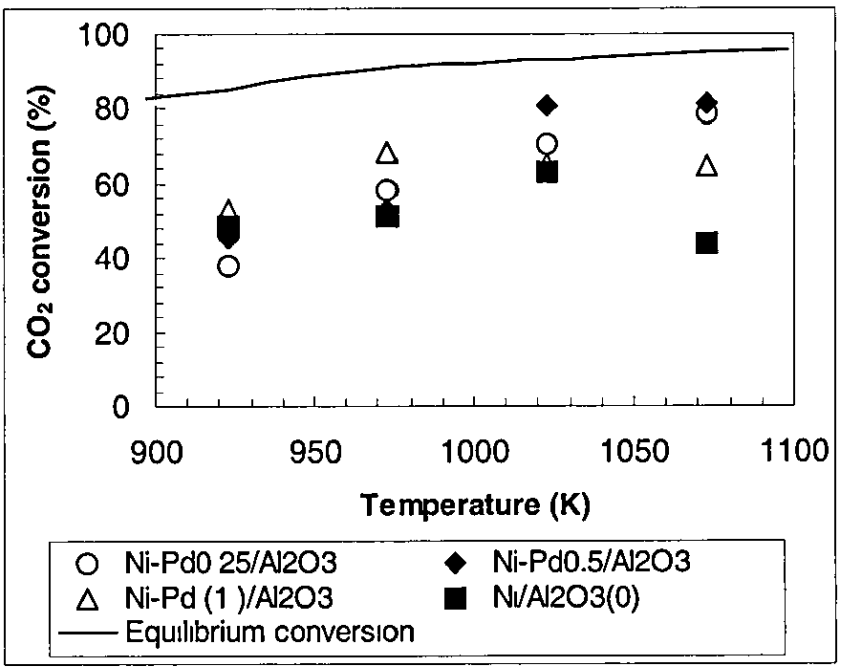

Figure 5 5 CO_2 conversion as a function of temperature, WHSV = 19200 ml/hr.g cat, $CH_4/CO_2 = 1$, catalyst weight = 50 mg, P = 1atm.

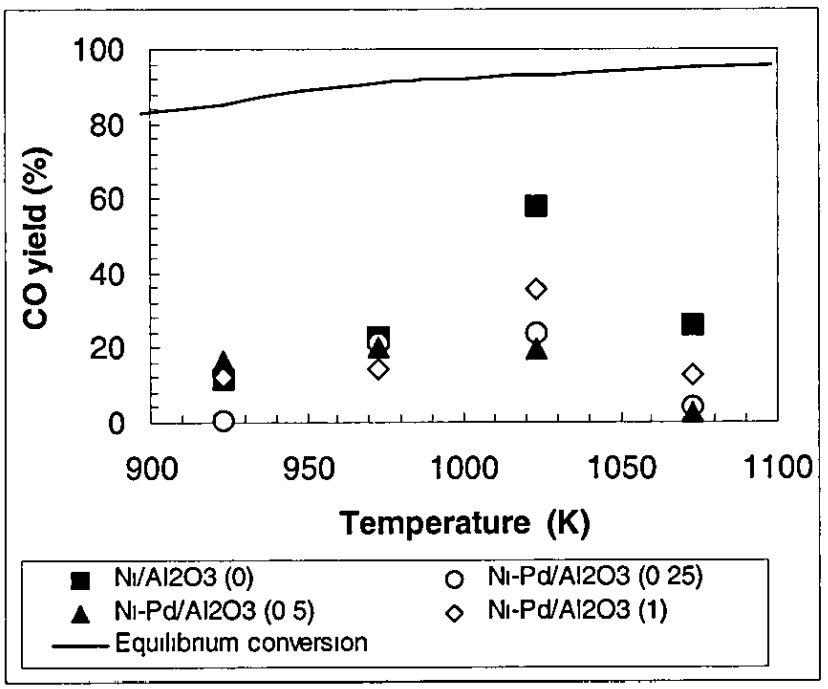

Figure 5.6 CO yield as a function of temperature, WHSV = 19200 ml/hr.g.cat, $CH_4/CO_2 = 1$, catalyst weight = 50 mg, P = 1atm.

As can be seen in Figures 5.4 and 5.5, the palladium with lower loadings did not show decrease in CH_4 and CO_2 conversion at temperatures > 1073K.

The CO_2 conversion increases, following thus a trend similar to that of the CH_4 conversion for all catalysts although the difference in conversion is not significant, especially at lower temperatures (923K-1023K). No significant difference was observed for CO yield at lower temperatures for 0.25 wt% Pd catalyst and the unpromoted catalyst. A remarkable difference was observed at 1023K and 1073K. The rate of reaction for both CH_4 and CO_2 increases with increasing temperature for Ni-Pd/γ-Al_2O_3 (0 25 wt%) and Ni-Pd/γ-Al_2O_3 (0 5 wt%) catalysts. The CO yield for the unpromoted catalyst (Ni/γ-Al_2O_3) was higher compared to all the palladium promoted catalysts especially at higher temperatures.

The high CO yield for the unpromoted catalyst at 1023K and 1073K may be due to the reverse water gas shift reaction (RWGS) $CO_2 + H_2 \leftrightarrow CO + H_2O$ being significant, which is confirmed by the CO_2 conversion, being slightly higher than that of the CH_4 conversion. The rate constant for CO formation of the unpromoted catalyst was higher ($k_3 = 60*10^{-5}\ s^{-1}$) compared to the Pd promoted catalyst ($k_3 = 19*10^{-5}\ s^{-1}$). However, the activation energies for CH_4 and CO_2 of the unpromoted catalyst were 32.9 kJ/mol and 29.8 kJ compared to the Pd promoted catalyst of 11 kJ/mol and 6.6 kJ/mol respectively. According to the experimental findings, the effect of palladium on the nickel catalytic activity for CO_2 reforming of methane strongly depends on the temperature and the reaction conditions employed. The presence of palladium increases the activity for CO_2 reforming at temperatures higher than 973K but no significant effect was observed at temperatures < 923K. At higher temperatures a good comparison can be made because there was a significant difference in conversion for the various catalysts, especially at higher space velocities since conversions are far away from equilibrium.

The catalytic activity at space velocity of 13900 ml/hr g cat showed not much difference compared to that at a space velocity of 19200 ml/hr g cat. All the catalysts show activity loss at temperatures > 1073K for both CH_4 and CO_2 conversions except for the Ni-Pd/γ-Al_2O_3 (1 wt%) catalyst which shows an increase with increasing temperature for the CO_2 conversion. However, the CO yield follows a similar trend to the CH_4 conversion (see Appendix IV, Figure A4.1.1).

Similar activities were achieved for both CH_4 and CO_2 conversions at a space velocity of 9820 ml/hr g cat. The CH_4 conversion reached an equilibrium value for the Ni-Pd/γ-Al_2O_3 (0 5 wt%) catalyst especially at 1023K.

The CO yield followed a similar trend to CO_2 conversion for all catalysts. At lower space velocities of 7840 ml/hr g cat and 4800 ml/hr g cat, equilibrium values were attained at > 1023K for CH_4 and CO_2 conversion for both Ni-Pd/γ-Al_2O_3 (0.5 wt%) and Ni-Pd/γ-Al_2O_3 (1 wt%) see Figure A4.1.2 in Appendix IV. Equilibrium values were attained at 973K when the space velocity was reduced further to 4800 ml/hr g cat. All the catalysts attained equilibrium at 1073K at the space velocity of 4800 ml/hr g cat.

5.3.2 Effect of Palladium on catalytic stability, WHSV=19200 ml/hr g cat, T=1073K

Figure 5.7 shows the stability plots for both unpromoted and the three palladium promoted catalysts; Ni-Pd/γ-Al_2O_3 (0.25 wt%), Ni-Pd/γ-Al_2O_3 (0.5 wt%) and Ni-Pd/γ-Al_2O_3 (1 wt%) at 1073K, for 6 hours and a space velocity of 19200 ml/hr g cat. Only little activity difference was observed between Ni-Pd/γ-Al_2O_3 (0.5 wt%) and Ni-Pd/γ-Al_2O_3 (0.25 wt%) catalysts with high and stable activity. The activity of Ni-Pd/γ-Al_2O_3 (1 wt%) catalyst was lower compared to Ni-Pd/γ-Al_2O_3 (0.25 wt%) and Ni-Pd/γ-Al_2O_3 (0.5 wt%) but also exhibits stable activity with time on stream. The unpromoted catalyst deactivated linearly from 58% to 40% in CH_4 conversion as discussed earlier in chapter 4. The initial CO_2 conversions for Ni-Pd/γ-Al_2O_3 (0.25 wt%), Ni-Pd/γ-Al_2O_3 (0.5 wt%) and Ni-Pd/γ-Al_2O_3 (1 wt%) were 82%, 78% and 61% with the final conversions of 80%, 80% and 61% respectively (see Figure 5.8).

The addition of palladium causes an increase in the activity of the Ni/γ-Al_2O_3 system, the extent of which is a function of the Pd loading. A 1 wt% Pd loading causes a negative impact on the initial activity of the Ni/γ-Al_2O_3 system as indicated by the initial CO_2 conversion value of 62% compared to 79% of the unpromoted catalyst. However, it is evident from Figures 5.7 and 5.8 that the most remarkable impact of the Pd doping lie in a strongly improved stability of the Ni/γ-Al_2O_3 system according to the stable conversion levels recorded on the promoted systems after 6h of time on stream.

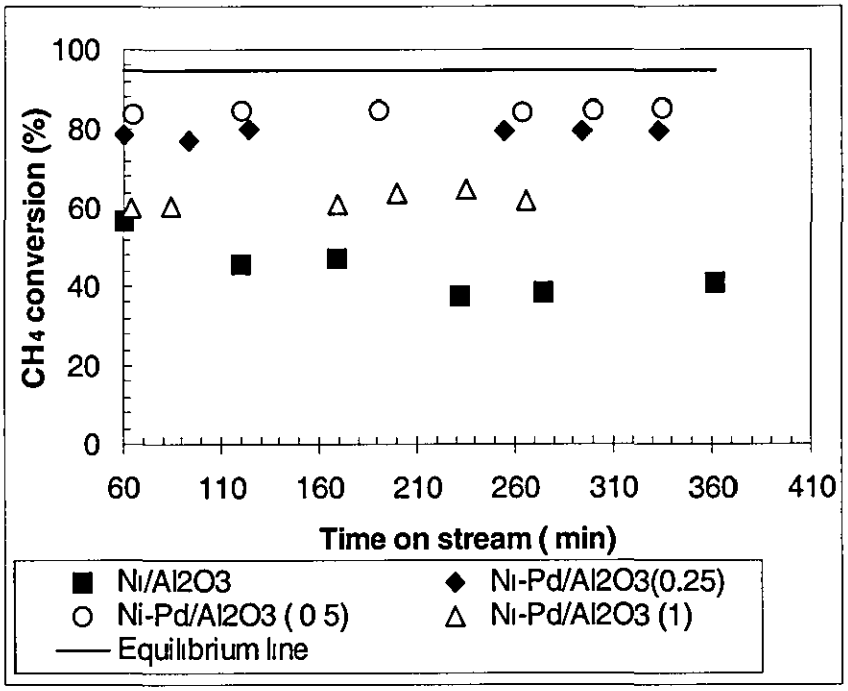

Figure 5.7 CH_4 conversion as a function of time, WHSV = 19200 ml/hr g cat, CH_4/CO_2 = 1, catalyst weight = 50 mg, P = 1atm.

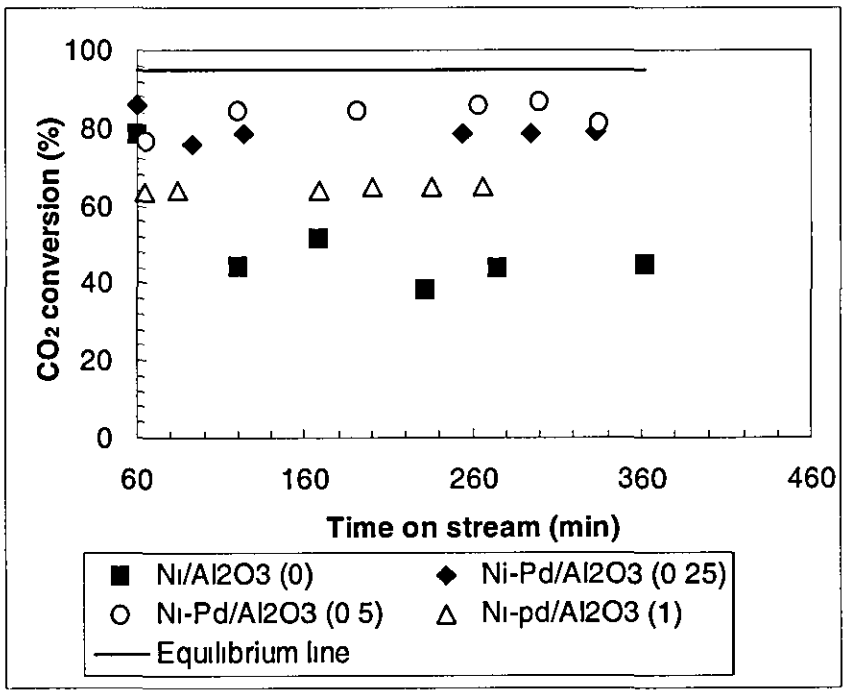

Figure 5.8 CO_2 conversion as a function of time, WHSV = 19200 ml/hr g cat, CH_4/CO_2 = 1, catalyst weight = 50 mg, P = 1atm. T = 1073K

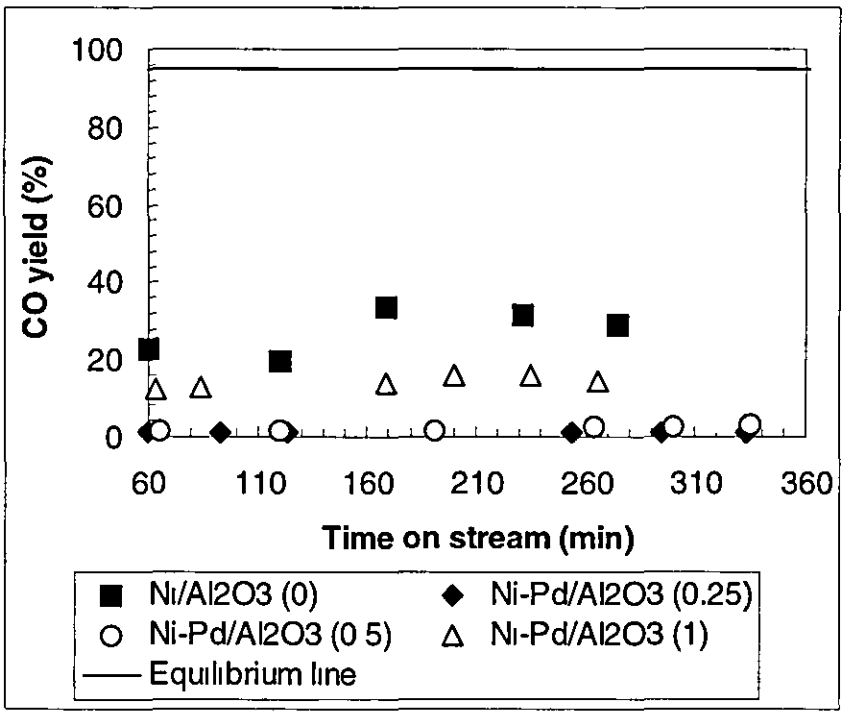

Figure 5.9 CO yield as a function of time on stream, WHSV = 19200 ml/hr g cat, $CH_4/CO_2 = 1$, catalyst weight = 50 mg, P = 1atm T=1073K

As can be seen in Figure 5.9, the CO yield for the palladium promoted catalysts was lower compared to the unpromoted catalyst. The CO yield for the unpromoted catalyst was higher (26%) than all the Pd promoted catalysts of 0.83%, 2 9% and 14.6% with the increasing palladium loadings. In fact, for the Ni-Pd/γ-Al_2O_3 (0.25 wt%) and Ni-Pd/γ-Al_2O_3 (0 5 wt%) catalysts, the CO yield was much lower, which is an indication of much higher WGS activity. The rate of CO formation for the unpromoted catalyst was higher ($k_3 = 60*10^{-5}\ s^{-1}$) compared to ($k_3 = 19*10^{-5}\ s^{-1}$) of the 0.25wt % Pd promoted catalyst with activation energies of 40 kJ/mol and 27 kJ/mol respectively

This is a clear indication that the unpromoted catalyst enhances the RWGS reaction with the CO_2 conversion being higher than the CH_4 conversion. These observations agreed with the kinetic results obtained from the model because the rate constant for the unpromoted catalyst was higher for CO yield compared to that of the palladium promoted catalyst

The activation energies of the unpromoted catalyst and 0.25 wt% Pd promoted catalyst are 40 kJ/mol and 27 kJ/mol respectively. No catalyst attained equilibrium values in terms of CH_4, CO_2 conversion and CO yield. However, the addition of palladium has increased the stability of Ni/γ-Al_2O_3 catalyst which agrees with the report by Crisafulli *et al*, (2002), although lower CO yields were observed.

It is unclear what the reason might be for the high activity result observed accompanied by the very low CO yield for the palladium promoted catalysts. The carbon deposits accumulated after burn off are relatively high compared to the unpromoted catalyst. One speculation may be that decomposition or dissociation of CH_4 occur earlier, i e. prior to the reforming reaction and does not take place simultaneously with CO_2.

Another speculation may be due to significant occurrence of the Bouduoard reaction (2CO $\leftrightarrow$ C + CO_2). Frusteri *et al*, (2001) indicate that potassium addition alters the electronic properties of the Ni active phase which resulted in a strong inhibition of the Bouduoard reaction Further studies should be conducted to verify this speculation at lower Pd loading.

At the space velocity of 13900 ml/hr g cat, the activity in terms of CH_4 conversion for the unpromoted catalyst did not show deactivation, instead a little catalyst activation was observed with time on stream (Appendix IV, Figure A4 4 1) The CH_4 conversion decreases for both Ni-Pd/γ-Al_2O_3 (0 5 wt%) and Ni-Pd/γ-Al_2O_3 (1 wt%) catalyst with time on stream but the rate of deactivation for Ni-Pd/γ-Al_2O_3(0.5 wt%) was faster than that of Ni-Pd/γ-Al_2O_3 (1 wt%) On the other hand, the CH_4 conversion for Ni-Pd/γ-Al_2O_3 (0.25 wt%) catalysts increases with increasing time on stream. Similar trend of CO_2 conversions were observed for both the unpromoted catalyst, Ni-Pd/γ-Al_2O_3 (0 25 wt%) and Ni-Pd/γ-Al_2O_3 (0.5 wt%) catalysts. In the case of Ni-Pd/γ-Al_2O_3 (1 wt%) catalyst a low initial CO_2 conversion was observed which increases and stabilises to 87.7% The CO yield for Ni-Pd/γ-Al_2O_3 (1 wt%), Ni-Pd/γ-Al_2O_3 (0 25 wt%) and the unpromoted catalysts follow a similar trend to CH_4 conversion.

The stability at space velocity of 9820 ml/hr g cat showed not much difference compared to that of 13900 ml/hr g cat In the case of 7840 ml/hr g cat all catalysts attained above 85% of initial CH_4 conversions and remained stable with time on stream

Although all catalysts show low initial CO_2 conversions, both the unpromoted and Ni-Pd/γ-Al_2O_3 (0.25 wt%) deactivated slightly which was restored with time (see Appendix IV, Figure A4 4 3) On the other hand, the NiPd/γ-Al_2O_3 (0.5 wt%) and Ni-Pd/γ-Al_2O_3 (1 wt%) catalysts show an increase in activity and remained stable A significant difference was observed for the CO yield at lower space velocities compared to 13900 ml/hr g cat. The CO yield for all the three palladium promoted catalysts showed again, lower CO yield compared to that of the unpromoted catalyst (Figure not shown).

The result shows that at high space velocity of 19200 ml/hr g cat, the CO yield trend is not different compared to very low space velocities of 4800 ml/hr cat, despite the differences in conversions

5 3.3 Effect of palladium on catalytic stability, WHSV=19200 ml/hr g cat, T = 1023K

The catalytic activity at 1023K and WHSV= 19200 ml/hr g cat in terms of CO_2 and CO yield are shown in Figures 5.10 and 5 11 Unlike the activity at 1073K, the unpromoted catalyst exhibits a higher conversion (95%) compared to the palladium promoted catalysts of 66%, 65% and 59% for Ni-Pd/γ-Al_2O_3 (0 25 wt%), Ni-Pd/γ-Al_2O_3 (0.5 wt%) and Ni-Pd/γ-Al_2O_3 (1 wt%) respectively. It is clear evidence that the initial conversion of the Pd promoted systems was lowered at lower temperatures Again 1 wt% Pd loading shows the lowest initial CO_2 conversion (see Figure 5.10). The same activity loss was recorded for the unpromoted catalyst at this temperature which may be due to carbon deposition. However, carbon burn off was not performed to verify this speculation. The addition of palladium reduced the initial activity of the promoted catalyst, which may be due to inactive carbon formed at the start of the reforming

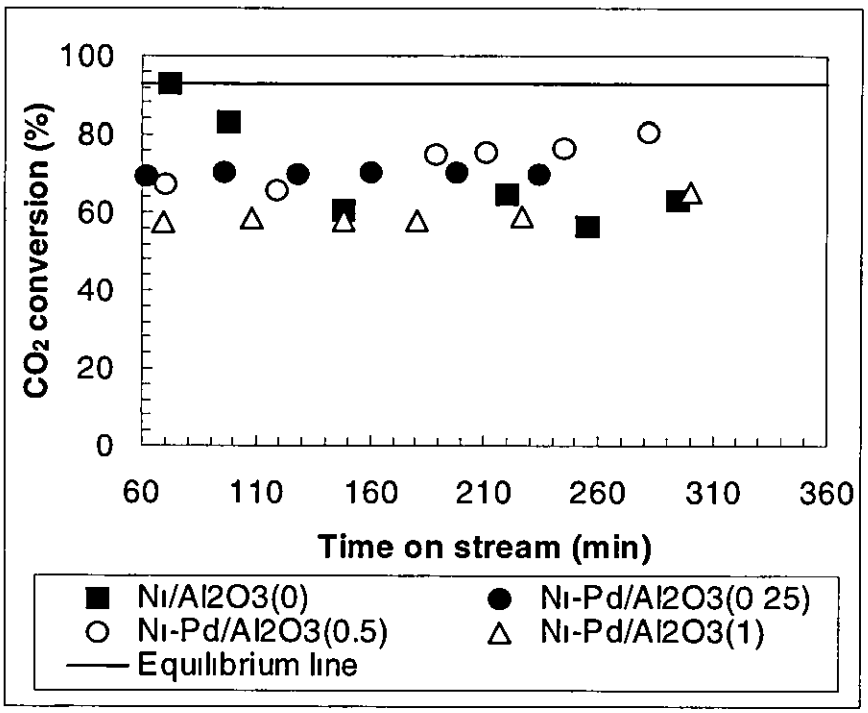

Figure 5 10 CO_2 conversion as a function of time on stream, WHSV = 19200 ml/hr g cat, CH_4/CO_2 = 1, catalyst weight = 50 mg, P = 1atm. T = 1023K

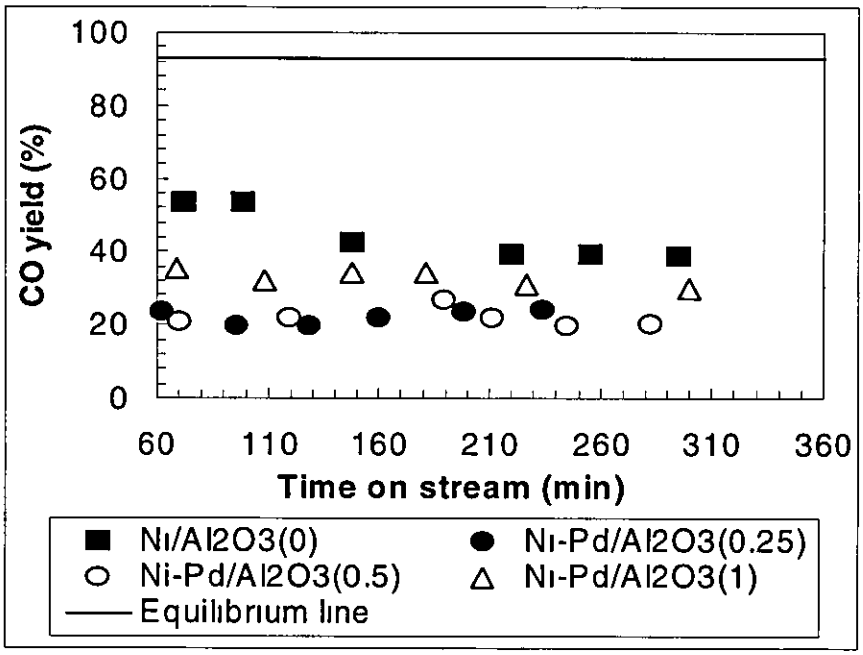

Figure 5.11 CO yield as a function of time on stream, WHSV = 19200 ml/hr g cat, CH_4/CO_2 = 1, catalyst weight = 50 mg, P = 1atm T = 1023K

However, stable activity was achieved during reaction with time. Again the Ni-Pd/γ-Al_2O_3 (0.5 wt%) catalyst exhibits the highest CO_2 conversion followed by Ni-Pd/γ-Al_2O_3 (0 25 wt%) catalysts with time on stream. On the other hand, the Ni-Pd/γ-Al_2O_3 (1 wt %) catalyst exhibits the highest CO yield among the three palladium promoted catalysts agreeing with the observation at higher temperatures. The CH_4 conversion follows a similar trend to CO_2 conversion for all catalysts, except for Ni-Pd/γ-Al_2O_3 (1 wt%) which was higher in terms of CH_4 conversion compared to others (Figure not shown). Again the CO yield for the unpromoted catalyst was higher compared to the palladium promoted catalysts The stability test at lower space velocities could be found in Appendix A IV, Figures A4.2.1, A4 2.2, A4.2.3 and A4.2 4.

Again the rate constant for CO formation of the unpromoted catalyst was higher (k_3 = $40*10^{-5}$ s^{-1}) compared to the 0 25 wt% Pd promoted catalyst of (k_3 = $10*10^{-5}$ s^{-1}). However the activation energies for CO were 40 kJ/mol and 27 kJ/mol for the unpromoted catalyst and Pd promoted catalyst respectively. Activation energies for CH_4 and CO_2 of the Pd promoted catalyst are lower (i e.11 kJ/mol and 6 6 kJ/mol) compared to the unpromoted catalyst of 33 kJ/mol and 29 8 kJ/mol.

5.3 4 Effect of palladium on catalytic stability, WHSV = 19200 ml/hr g cat, T = 973K

The catalytic behaviour in terms of stability at 973K was different for the unpromoted catalyst (see Figure 5.12). Compared to the palladium promoted catalysts, the unpromoted catalyst showed activation with time on stream in terms of CH_4 conversion This shows a significant effect of Pd loading (0 25 wt%-1 wt%) on CH_4 conversion at 973K and higher space velocity of 19200 ml/hr g cat (see Figure 5 12). CH_4 conversion increases with an increase of Pd loading with 54.8%, 66.7% and 74.9% for 0.25 wt%, 0.5 wt% and 1 wt% Pd respectively The CO_2 conversion followed a similar trend. It is interesting to note that the CO yield for the unpromoted catalyst was still higher compared to all the palladium promoted catalysts. It may be speculated that the catalyst was active at this temperature despite initial activity loss as conversion was lower than that of the promoted catalysts. It also indicates that the unpromoted catalyst promotes the RWGS reaction ($CO_2 + H_2 \leftrightarrow CO + H_2O$ at this temperature

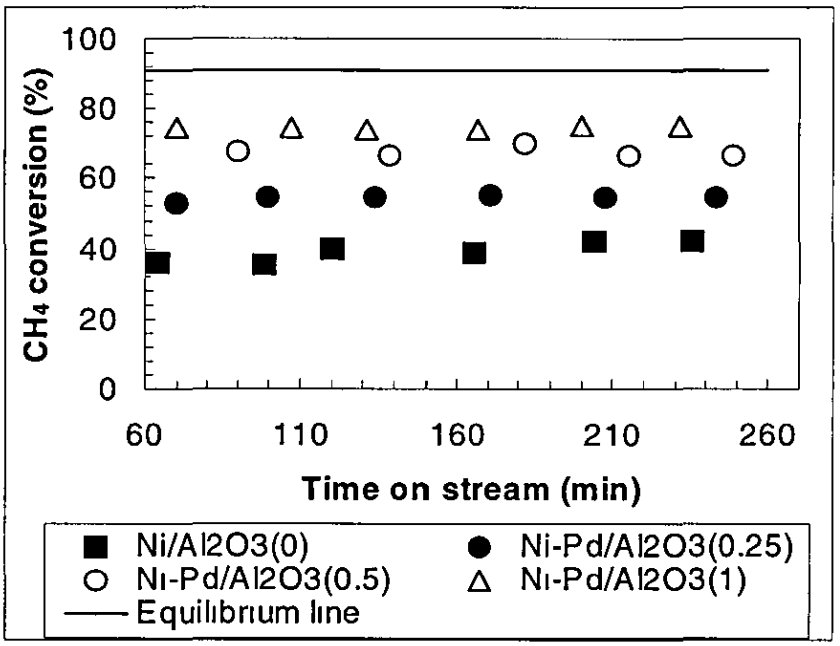

5 12 CH_4 conversion as a function time, WHSV = 19200 ml/hr g cat, CH_4/CO_2 = 1, catalyst weight = 50 mg, P = 1atm. T = 973K

The activity followed the order: Ni-Pd/γ-Al_2O_3 (1 wt%) > Ni-Pd/γ-Al_2O_3 (0.5 wt%) > Ni-Pd/γ-Al_2O_3 (0 25 wt%) > Ni/γ-Al_2O_3 (0) with CH_4 conversions of 74 9% > 66 7% > 54.8% > 42.3%.

The CO_2 conversion profile was similar with the same initial activity for Ni-Pd/γ-Al_2O_3 (1 wt%) and Ni-Pd/γ-Al_2O_3 (0 5 wt%) but a decrease in activity was observed for Ni-Pd/γ-Al_2O_3 (0 5 wt%) catalyst after 80 minutes on stream (Figure not shown) It appears that the Ni-Pd/γ-Al_2O_3 (1 wt%) catalyst must have accumulated much coke due to CO disproportionation reaction which readily occurs at lower temperatures (Effendi *et al*, 2002) because the CO yield was the lowest despite the higher conversions observed at this temperature (Figure not shown). Stability test on lower space velocities of 13900 ml/hr g cat, 9820 ml/hr g cat, 7840 ml/hr g cat and 4800 ml/hr g cat showed stable activities for both the unpromoted and palladium promoted catalysts Although activity was lower for the unpromoted catalyst, high CO yield was observed at all space velocities. The results could be found in Appendix A IV, Figures A4 3 1, A4 3 2, A4 3 3, and A4 3 4.

5.3.4 Effect of palladium on catalytic stability, WHSV = 19200 ml/hr g cat, T = 923K

At 923K, the activity of the unpromoted catalyst was higher than that of Ni-Pd/γ-Al_2O_3 (0 25 wt%) catalysts in terms of CH_4 conversion (see Figure 5 13). Again the CH_4 conversion for both 0 5 wt% and 1 wt% Pd promoted catalyst were higher compared to the unpromoted catalyst For CO_2 conversions, only 0 5 wt% Pd promoted catalyst showed higher conversion compared to the unpromoted catalyst. The CO_2 conversions for 0.25 wt % and 1 wt% Pd promoted catalyst were lower compared to the unpromoted catalyst (see Appendix IV) All catalysts show stable activity with time on stream The CO yield of Ni-Pd/γ-Al_2O_3 (0.5 wt%) was higher than all other catalysts at this temperature (see Figure 5.14). It exhibited initial CO yield of 18% although showed a slight deactivation with time. The Ni-Pd/γ-Al_2O_3 (1 wt%) and the unpromoted catalyst showed almost the same CO yield of 14% and 13% respectively. For Ni-Pd/γ-Al_2O_3 (0.25 wt%) catalyst, initial CO yield of 7% was observed, which decreases to 2% as time increases From the results obtained, it appears the WGS reaction was significant for all the catalysts tested under the condition employed, giving very low CO yield.

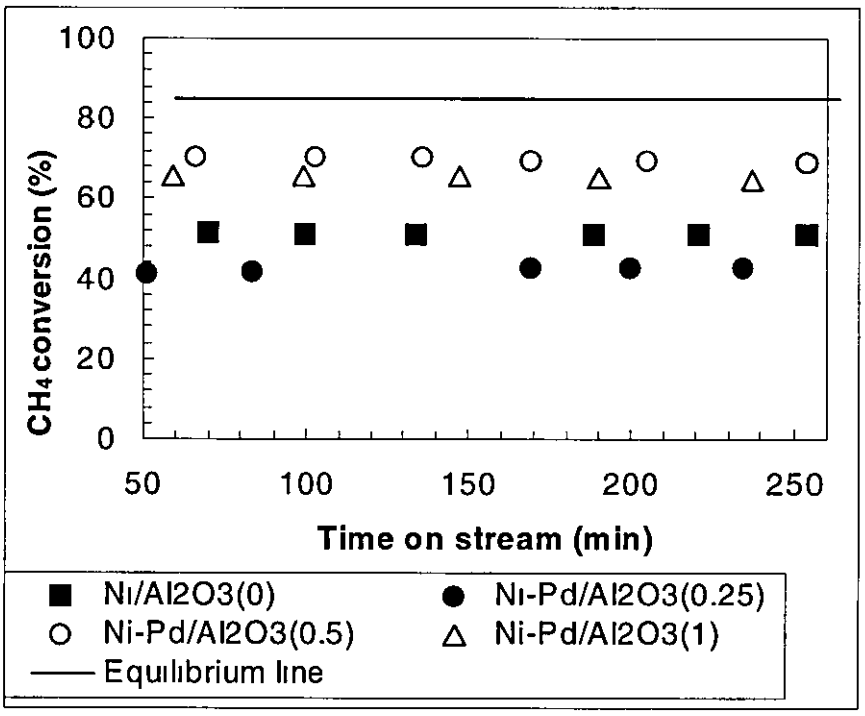

Figure 5 13 CH_4 conversion as a function of time, WHSV = 19200 ml/hr g cat, CH_4/CO_2 = 1, catalyst weight = 50 mg, P = 1atm T = 923K

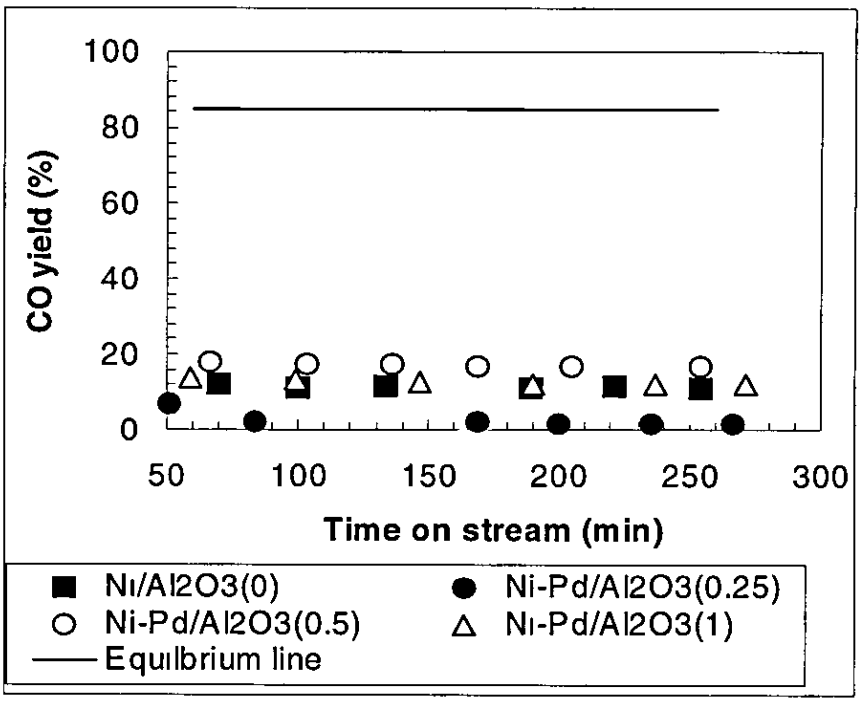

Figure 5 14 CO yield as a function time on stream, WHSV = 19200 ml/hr g cat, $CH_4/CO_2 = 1$, catalyst weight = 50 mg, P = 1atm T = 923K

5.4 Effect of space velocity on catalytic activity of palladium promoted nickel catalyst

The dependences of both, CO_2 and CO yield, on space velocities are shown in Figures 5.15, and 5 16. As can be seen, high CO_2 conversions were observed at lower space velocities < 7840 ml/hr g cat over all the catalysts, especially at 4800 ml/hr g cat. The CO_2 conversion decreases as the space velocities increases from 7840 ml/hr g cat to 19200 ml/hr g cat, except for Ni-Pd/γ-Al_2O_3 (0 5 wt%) catalysts that exhibited higher CO yield even at higher space velocities of 19200 ml/hr g cat compared to space velocity of 13900 ml/hr g cat. For CO yield the trend follow the decreasing yield with increasing space velocity for all catalysts The result agreed with report in literature (Tomishige *et al*, 2001). The unpromoted catalyst showed the highest CO yield at all space velocities

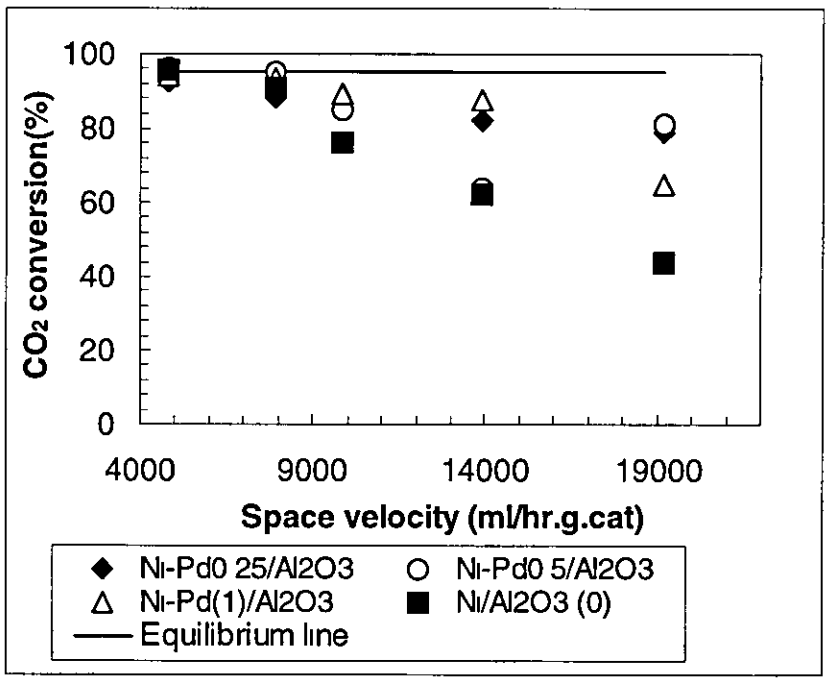

Figure 5 15 CO_2 conversion as a function of space velocity, CH_4/CO_2 = 1, catalyst weight = 50 mg, P = 1atm T = 1073K

The kinetic data (rate constant, $k_3 = 60*10^{-5}\ s^{-1}$) for the unpromoted catalyst agreed with the experimental results which was higher than that of the Pd promoted catalyst ($k_3 = 19*10^{-5}\ s^{-1}$) especially at higher space velocities of 19200 ml/hr g cat Conversions at space velocities < 7840 ml/hr g cat reached equilibrium values. Therefore lower space velocities are not useful for kinetic analysis.

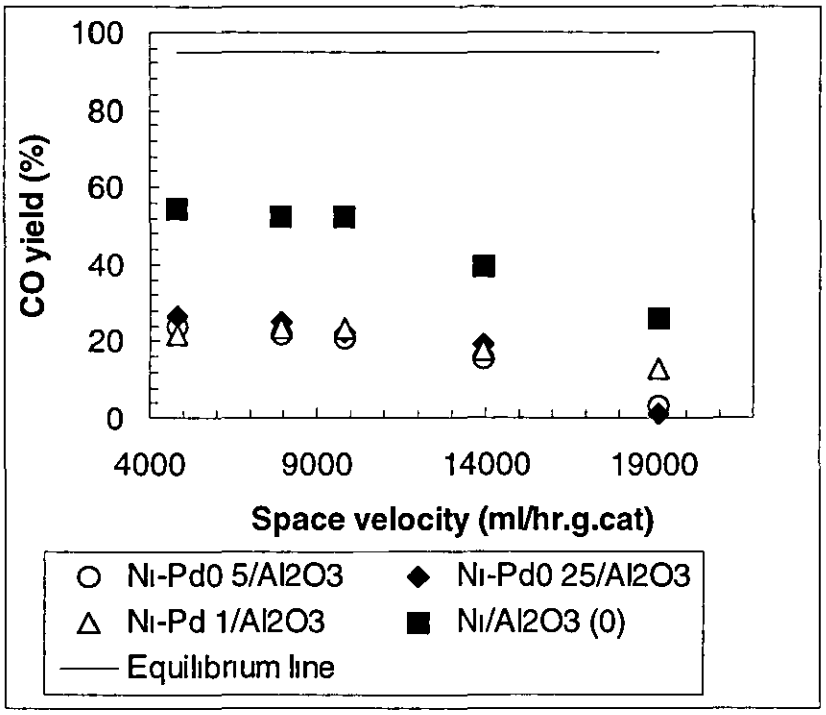

Figure 5.16 CO yield as a function of space velocity, $CH_4/CO_2 = 1$, catalyst weight = 50 mg, P = 1atm T = 1073K

5 5 Carbon deposition on palladium-promoted nickel catalyst, WHSV = 19200 ml/hr g cat, T = 1073K

Coke deposition was studied on the palladium promoted catalysts after 6 hours at 1073K and a space velocity of 19200 ml/hr g cat SEM analysis has been used to probe the morphology of the "used" catalyst The burn-off method was employed to obtain carbon accumulations on the "used" catalyst. The SEM images of the palladium promoted catalysts are shown in Figure 5 17 (see Figure 4 26 section 4.9 in Chapter 4) for the unpromoted catalyst) Although there was no visible filamentous carbon on the catalyst surface, the burn off excise revealed carbon deposition on the catalysts, which suggests that coke seems to have been formed during the CO_2 reforming of CH_4. The maximum carbon yield for the catalysts tested followed the order. Ni-Pd/γ-Al_2O_3 (1 wt%) > Ni-Pd/γ-Al_2O_3 (0 5 wt% > Ni-Pd/γ-Al_2O_3 (0.25 wt%) > Ni/γ-Al_2O_3 (0) with the values 0.81 g/g cat, 0.78 g/g cat and 0.56 g/g cat > 0.14 g/g cat. The coke deposition appears to decrease with decreasing amount of palladium loading Coke deposition increased greatly when the amount of palladium was higher than 0.25 wt%.

It is possible that higher loading of Pd 1wt% can cause Ni coverage by Pd, which is also reflected in the lower Ni dispersion result (2.09%) compared to 5.8% for 0.25 wt% Pd promoted catalyst.

The result suggests that the effect of palladium on the activity of Ni/γ-Al_2O_3 catalysts decreases with decreasing amount of palladium at 973K which agrees well with reports in literature (Hou *et al*, (2003). Hou *et al.*, (2003) observed a similar trend in their study with varying Ca/Ni ratios on Ni/α-Al_2O_3 catalyst.

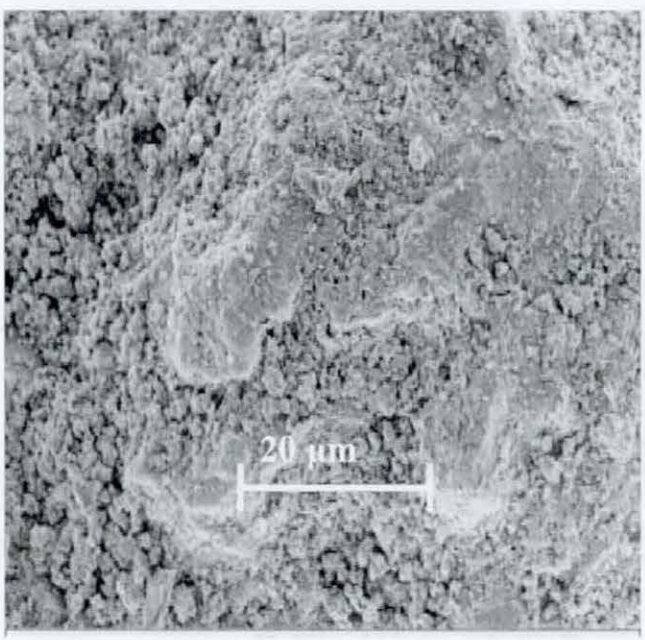

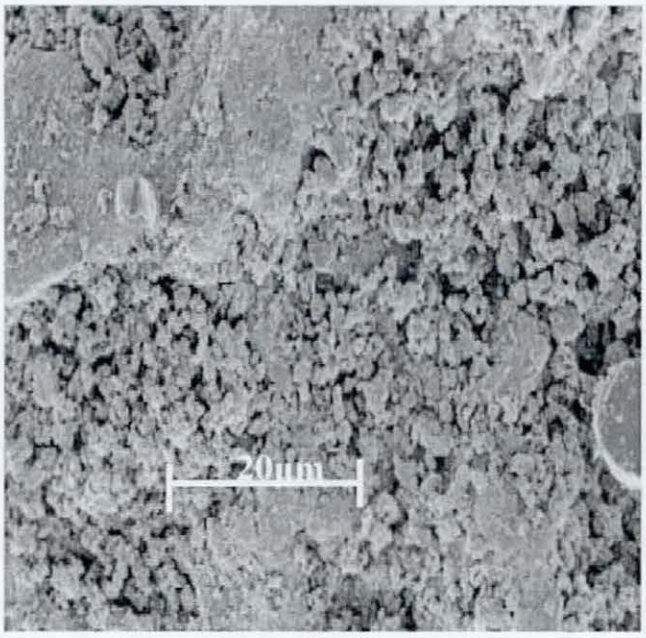

(a) **(b)**

Figure5.17 SEM images of (a) Ni-Pd/γ-Al_2O_3 (0.25 wt%) (b) Ni-Pd/γ-Al_2O_3 (1 wt%) after reforming, T = 1073K, WHSV = 19200 ml, hr g cat, CH_4/CO_2 =1, P = 1 atm

5.6 Conclusions

Palladium promoted catalyst exhibited high activity and stability, especially at higher temperatures, compared to the unpromoted catalyst. The activity decreases with increasing in palladium loading in terms of CO_2 and CH_4 conversion. This is in agreement with studies by Xiao *et al.*, (2003).

The catalyst with the loading of 0.25 wt% and 0 5 wt% palladium showed similar activities while lower activity was observed for Ni-Pd/γ-Al_2O_3 (1 wt%) catalyst as well as the unpromoted catalyst at higher temperatures. However, the highest CO yield was found in the unpromoted catalyst compared to the palladium promoted.

However, the highest CO yield was found in the unpromoted catalyst compared to the palladium promoted catalysts especially at higher temperatures Also, the 1 wt % palladium catalyst showed coke deposition of Ni-Pd/γ-Al_2O_3 (1 wt%) associated with the highest CO yield among the promoted catalysts is not very clear.

The addition of palladium appears to increase the coke formation compared to the unpromoted catalyst despite stability recorded with the promoted catalysts Coke deposition on the unpromoted catalyst was lower (0.14g/g cat) compared to the Pd promoted catalyst of 0.81 g/g cat, 0 78 g/g cat and 0 56 g/g cat for 0 25 wt %, 0 5 wt% and 1 wt% Pd respectively. One speculation may be the type of coke formed on the unpromoted catalysts since catalysts deactivation also depends on the type of coke formed. Filamentous carbon is non deactivating compared to carbidic carbon. Although the time duration (6hours) for the CO_2 reforming reaction in this study was not long enough for visible filamentous carbon to appear in the morphology of catalyst studied, the deactivation of the unpromoted catalyst may be due to the formation of carbidic carbon Further study is proposed to investigate the type of carbon formed on the catalysts so that better conclusion can be drawn. The BET surface area decreases with increasing palladium content, which subsequently led to decrease in dispersion This might as well have effect on the activity since accessibility of reactants to active site is high on meso-porous supports which maintain dispersion and hence increase in the adsorption of CO_2 for high reactivity.

5.7 Catalyst characterisation -Effect of copper promotion

5 7.1 BET surface area and pore size distribution

Figure 5 18 shows the pore size distribution for unpromoted catalyst and copper promoted Ni catalyst As can be seen in Figure 5 18 the bimodal pore size distribution is maintained The surface area decreases with the addition of copper; 174 m^2/g to 140 m^2/g, 164 m^2/g and 146 m^2/g for Ni-Cu/γ-Al_2O_3 (0 25 wt%), Ni-Cu/γ-Al_2O_3 (0 5 wt%) and Ni-Cu/γ-Al_2O_3 (1 wt%) respectively (see Table 5 2).

Catalyst type	Ni loading (wt%)		Crystallite size[b] (nm)	BET Surface area (m^2/g)	Dispersion[c] (%)	Pore volume (cm^3/g)
Ni/γ-Al_2O_3 (0)	15	8.4[a]	26 9	174	5 9	0 20
Ni-Cu/γ-Al_2O_3 (0.25 wt%)	15	9 4[a]	84	140	-	-
Ni-Cu/γ-Al_2O_3 (0.5 wt%)	15	8 5[a]	32	164	0 14	0 20
Ni-Cu/γ-Al_2O_3 (1 wt%)	15	11 3[a]	45	146	0 14	0.19

[a] Atomic adsorption spectophotometer
[b] X-Ray diffraction
[c] CO chemisorption

Table 5 2 Properties of copper promoted Ni-based catalysts

As can be seen in Figure 5 18, there is a shift of pore size to smaller pores sizes with the addition of copper compared to the unpromoted catalyst and also new micro pores were developed, especially with the 0 25 wt% and 1 wt% copper promoted catalysts. There was a drastic decrease in dispersion from 5.9 to 0 14, with increased crystallite sizes from 26.9 nm to 84 nm, 32 nm and 45 nm, determined from XRD pattern for 0.25 wt%, 0 5 wt% and 1 wt% copper promotion respectively. Dispersion depends on the fraction of catalytic atoms exposed which increases with decreasing crystallite size The decrease in dispersion observed may be due to increased crystallites size and the specific surface area loss of the promoted catalyst.

An optimum surface area of 164 m^2/g was obtained with the copper loading of 0 5 wt%, after which the surface area decreases to 146 m^2/g (see Table 5.2) which clearly indicated the influence of copper loading.

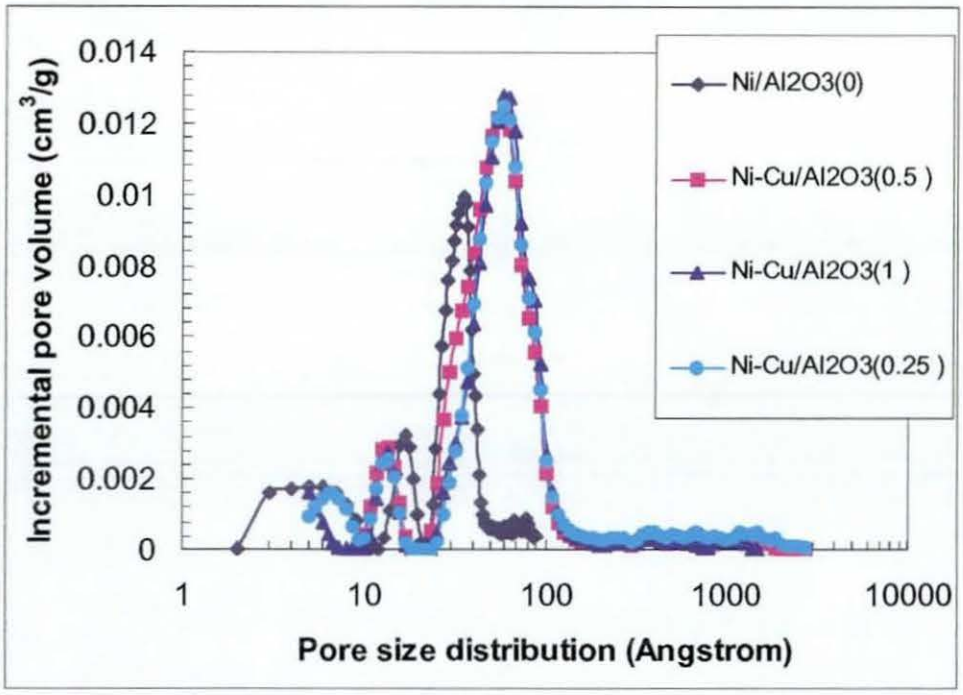

Figure 5.18 Pore size distribution for copper promoted nickel catalyst

*5.7.2 X-Ray diffraction of copper promoted Ni- based cat*alyst

Figure 5.19 shows the XRD patterns for the unpromoted and copper promoted Ni catalysts. The XRD reflection of the unpromoted catalyst (Ni/γ-Al_2O_3) shows the formation of Ni oxide is in different forms (Lee *et al.*, 2004). The XRD reflection at 45.5° and 66.2° can be assigned to a mixture of $NiAl_2O_4$ and Al_2O_3. The reflection of Ni/γ-Al_2O_3 agrees with the assignment of the peak at 1143K in TPR to the reduction of $NiAl_2O_4$. The XRD reflections of Ni-Cu/γ-Al_2O_3 (1 wt%), Ni-Cu/γ-Al_2O_3 (0.5 wt%) and Ni-Cu/γ-Al_2O_3 (0.25 wt%) are not different from those of the unpromoted catalyst Ni/γ-Al_2O_3. Peaks at 37.0°, 43.3°, 45.3°, 62.8° and 66.6 ° were observed except that the peak intensity increased at 37.0°, 43.3° and 75.8° especially for the Ni-Cu/γ-Al_2O_3 (0.25 wt%) catalysts.

The pronounced peak at 62.8° for Ni-Cu/γ-Al_2O_3 (0.25 wt%) catalyst can be assigned to the presence of different copper oxides such as Cu-Ni oxides, CuO and $CuAl_2O_4$.

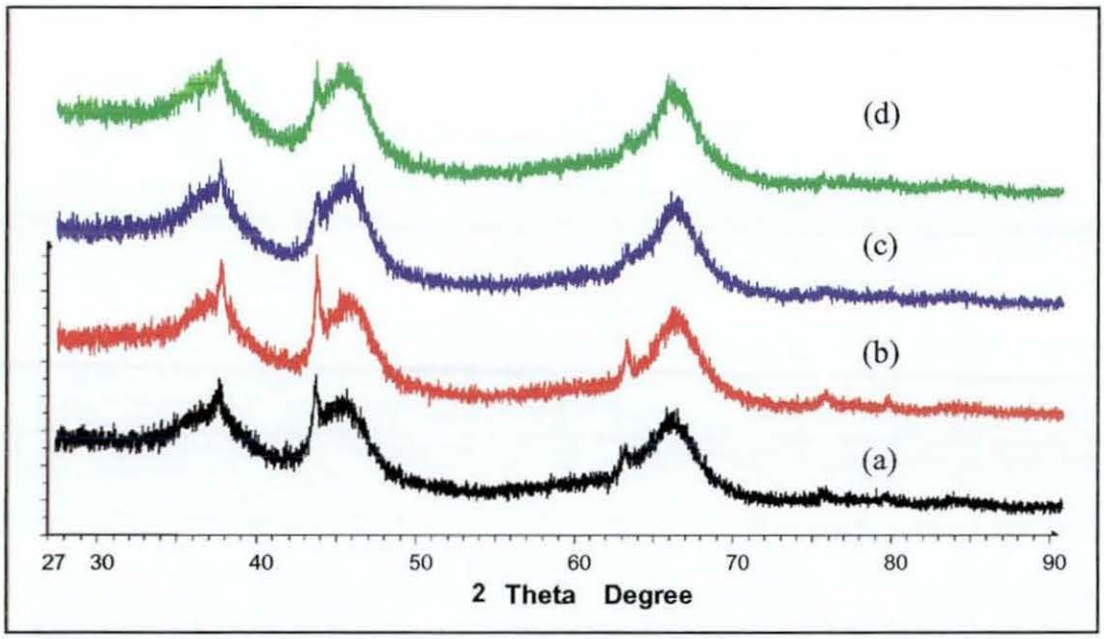

Figure 5.19 XRD spectra of fresh N-based catalysts, calcinations temperature = 743K, (a) Ni/γ-Al_2O_3. (b) Ni-Cu/γ-Al_2O_3 (0.25 wt%) (c) Ni-Cu/γ-Al_2O_3 (0.5 wt%) (d) Ni-Cu/γ-Al_2O_3 (1 wt%)

5.7.3 TPR profile for the unpromoted and copper promoted Ni- based catalyst

The TPR profile for the unpromoted and 0.5 wt% copper promoted catalyst was studied (see Figure 5.20). For the unpromoted catalyst Ni/Al_2O_3, the TPR shows peak at 599K and broad peak 799K which can be attributed to reduction of NiO and $NiAl_2O_4$ spinel structures. The TPR trace of the copper (0.5 wt%) promoted catalyst was different from that of the unpromoted catalysts showing peak at 540K indicating a shift of reduction to lower temperature, compared to 599K and 799K for the unpromoted catalyst. The result suggests that Cu and Ni have close interaction leading to the formation of bimetallic Ni-Cu particles. It is possible that Cu precursor which has a lower reduction temperature must have activated hydrogen, thus favouring the reduction of Ni precursor by a spill over effect (Inui., 2001).

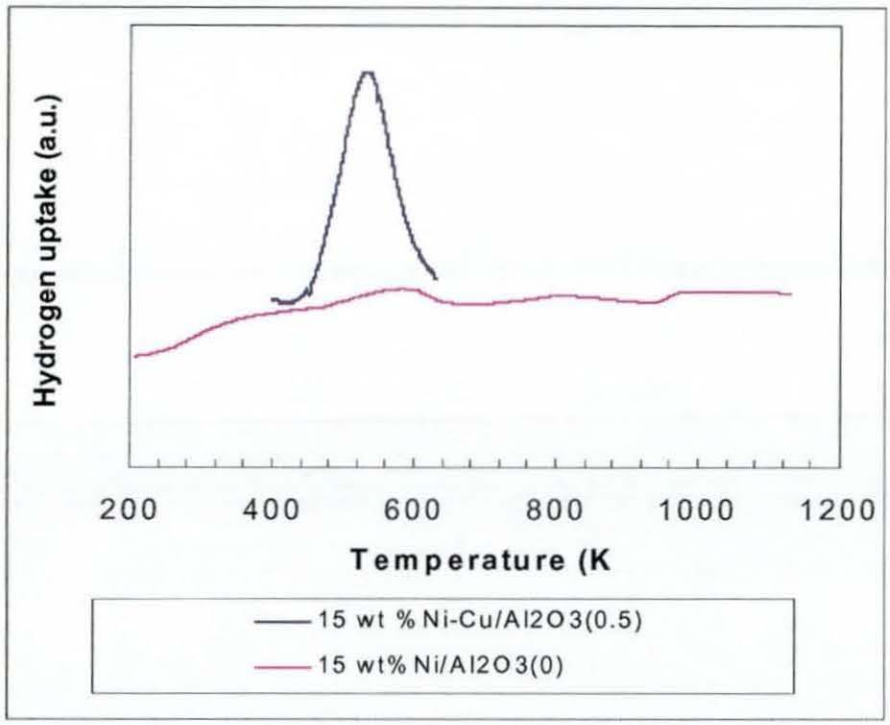

Figure 5.20 TPR profile of Ni/γ-Al_2O_3 and Ni-Cu/γ-Al_2O_3 (0.5 wt%)

5.8. Influence of reaction temperature of copper promoted catalyst on activity, WHSV = 19200 ml/hr g cat

Figures 5.21, 5.22 and 5.23 illustrates the influence of reaction temperature on CH_4, CO_2 conversion and CO yield at space velocity of 19200 ml/hr g cat over unpromoted catalyst and copper promoted Ni-Cu/γ-Al_2O_3 catalysts. The CH_4 conversion increases with increasing temperature for the 0.25 wt% and 1 wt% Cu promoted catalyst. On the other hand, a decline of CH_4 conversion was observed for both unpromoted and 0.5 wt% Cu promoted catalyst. As can be seen in Figure 5.21, no significant difference was observed in CH_4 conversion at lower temperatures < 973K. The Ni-Cu/γ-Al_2O_3 (1 wt%) showed higher CH_4 conversion at all temperatures except at 1023K. At 1023K, equal CH_4 conversion values were observed compared to the unpromoted catalyst. The Ni-Cu/γ-Al_2O_3 (0.25 wt%) also showed higher CH_4 conversion at 1073K compared to unpromoted catalyst. On the other hand, Ni-Cu/γ-Al_2O_3 (0.5 wt%) catalyst showed equal CH_4 conversion at 1073K.

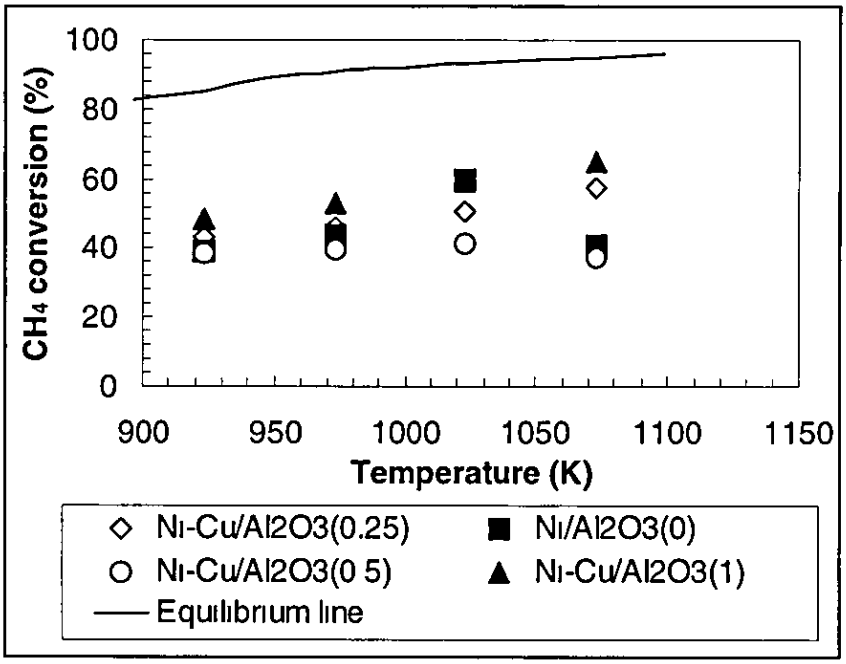

Figure 5 21 CH_4 conversion as function of temperature, WHSV = 19200 ml/hr g cat, $CH_4/CO_2 = 1$, P = 1 atm., catalyst weight = 50 mg

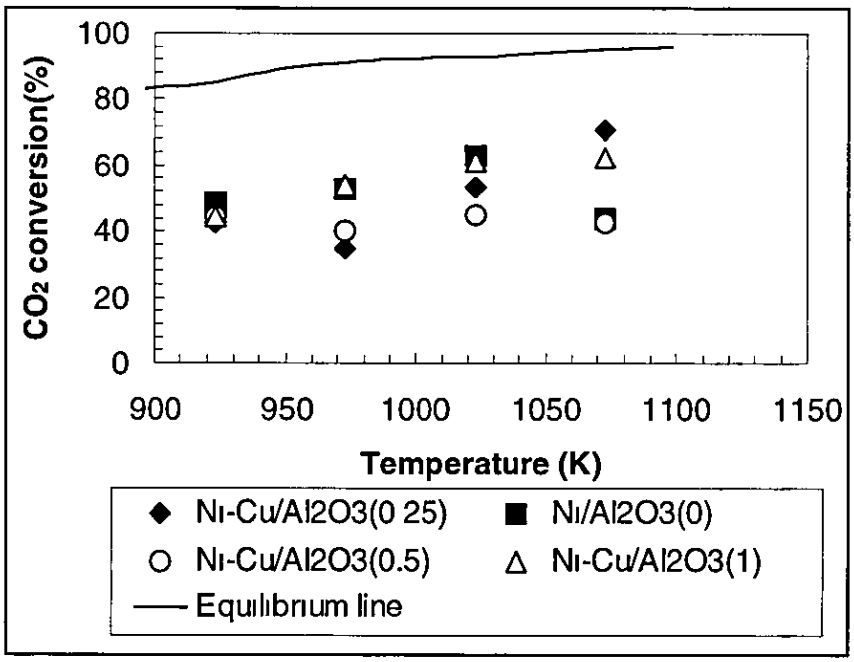

Figure 5 22 CO_2 conversion as a function of temperature, WHSV = 19200 ml/hr g cat, $CH_4/CO_2 = 1$, P = 1 atm , catalyst weight = 50 mg

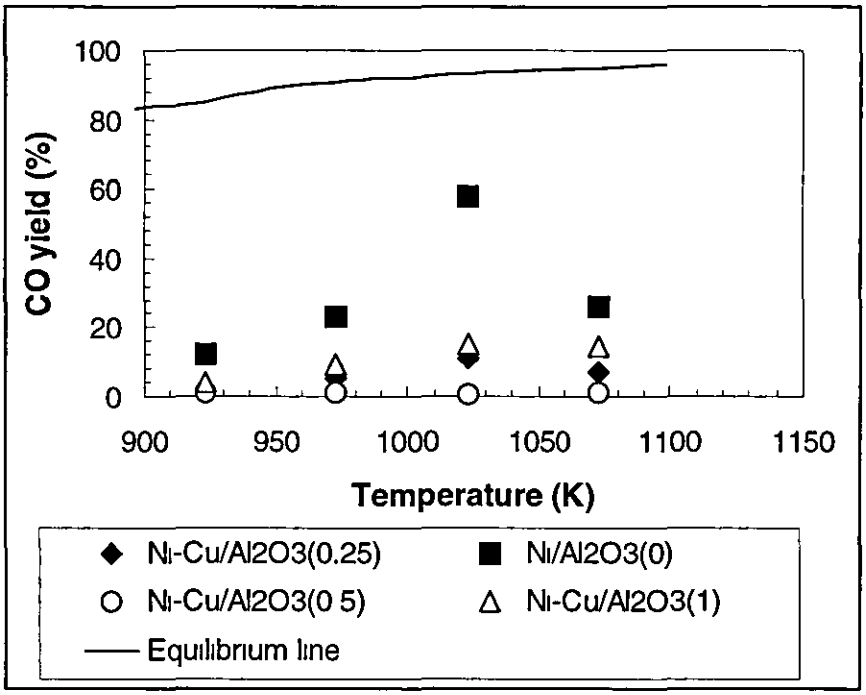

Figure 5.23 CO yield as a function of temperature, WHSV = 19200 ml/hr g cat, CH_4/CO_2 = 1, P = 1 atm , catalyst weight = 50 mg

The CO_2 conversion followed a similar trend to that of CH_4 conversion (see Figure 5.22), especially for the Ni-Cu/γ-Al_2O_3 (1 wt%) catalyst. However, equal CO_2 conversions were observed for 0 25 wt% and 1 wt% Cu at temperatures < 1023K. At 1073K the CO_2 The conversion was higher for Ni-Cu/γ-Al_2O_3 (1 wt%) compared to the unpromoted catalyst. The conversions for CH_4 and CO_2 of the unpromoted and 0.5 wt% Cu promoted catalysts showed lower values at 1073K compared to temperatures at 1023K which may be attributed to coke formation or sintering processes.

On the other hand, Ni-Cu/γ-Al_2O_3 (0 25 wt%) catalyst shows activity loss at lower temperatures in terms of CO_2 conversion but it was restored at temperatures > 1073K. The CO_2 conversion for Ni-Cu/γ-Al_2O_3 (0 25 wt%) was higher than that of CH_4 conversion at higher temperatures > 1073K which indicates significant RWGS reaction ($CO_2 + H_2 \leftrightarrow CO + H_2O$ It was also observed that CO_2 conversion at 923K was higher than that at 973K.

It may be speculated that the WGS reaction was significant since the CO yield was so minimal at this temperature. The CO yield for the unpromoted catalyst was higher than all Cu promoted catalysts The rate constant for CO formation (k_3 = $69*10^{-5}$ s^{-1}) for the unpromoted catalyst compared to the Cu promoted catalyst was (k_3 = $11*10^{-5}$ s^{-1}) which was consistent with the CO yield result. The activation energies for CO of the unpromoted catalyst and Ni-Cu/γ-Al_2O_3 (0.25 wt%) were 40 kJ and 64 kJ/mol respectively. The result indicates higher activity for the unpromoted catalyst at 1023K compared to the Cu promoted catalyst, which also confirmed in CO yield in Figure 5.23. The Cu promoted catalysts (Ni-Cu/γ-Al_2O_3 (1 wt%) showed the highest CO yield which may be due to significant RWGS reaction ($CO_2 + H_2 \leftrightarrow CO + H_2O$). The coke formation result conducted at 1073K appear to confirm the above observation because lower coke deposit was found on Ni-Cu/γ-Al_2O_3 (1 wt%) compared to others. Although high CO yield was observed for the unpromoted catalyst compared to the Cu promoted catalyst, coke formation was higher

However, comparing to Pd promotion, the CH_4 and CO_2 conversions for the Cu prompted catalyst was higher at lower temperatures < 923K and higher space velocities of 19200 ml/hr For example at 923K, the CH_4 and CO_2 conversions for the 0 25 wt% Cu promoted catalysts are 43.1% and 42 5% while CH_4 and CO_2 conversions of 42 3% and 37 9% were achieved At higher temperatures > 1073K, the Pd promoted catalyst exhibited higher conversions of 79.6% and 78.8%, whilst the Cu promoted catalyst showed conversions of 57 2% and 70 8% for CH_4 and CO_2 respectively The CO yield for the 0.25 wt % Cu promoted catalyst was higher (7 1%) compared to 0.25 wt% Pd promoted catalyst (0.83%). The higher CO yield may be due to significant occurrence of RWGS reaction ($CO_2 + H_2 \leftrightarrow CO + H_2O$) for the Cu promoted catalyst. The CO_2 conversion of the 0 25 wt% Cu promoted catalyst also confirms the above mechanism because it was higher than that of CH_4 conversion

At 13900 ml/hr g cat, the CH_4 conversion was higher at 1023K for the unpromoted catalyst compared to all the copper promoted catalysts although close ties were observed at higher temperatures (see Appendix IV, Figure A4.5 1). The CH_4 conversion of the unpromoted catalyst and Ni-Cu/γ-Al_2O_3 (1 wt%) catalyst showed almost equal values at 923K, 1023K and 1073K

On the other hand, Ni-Cu/γ-Al_2O_3 (0 5 w %) shows the lowest CH_4 conversion at all temperatures In the case of Ni-Cu/γ-Al_2O_3 (0 25 wt%), CH_4 conversion increases with increasing temperature. Apart from Ni-Cu/γ-Al_2O_3(0 5 wt%) all catalyst show close tie values at 1073K A similar trend was observed in CO_2 conversion except at 1073K, where the CO_2 conversion of Ni-Cu/γ-Al_2O_3 (1 wt%) catalyst was higher than that of the unpromoted catalyst (see Appendix IV, Figure A4 5.1)

The CO yield for the unpromoted catalyst was higher than that of all the copper promoted catalysts at all temperatures. The Ni-Cu/γ-Al_2O_3 (0 5 wt%) catalyst CO yield was higher among the Cu promoted catalyst at temperatures > 973K (see Appendix IV, Figure A4 5 1) At temperatures < 923K, no significant CO yield was observed for the copper promoted catalyst compared to the unpromoted catalyst.

The CH_4 conversion at space velocity of 7840 ml/hr g cat followed a similar trend observed under the condition of 13900 ml/hr g cat. For CO_2 conversion, the unpromoted catalyst (Ni/γ-Al_2O_3) showed almost the same value as that of the copper promoted catalysts at 923K, and 1023K The CO yield followed a similar trend to the observation made at space velocity of 9820 ml/hr g cat.

5 8 1 Effect of copper promotion on catalytic stability, WHSV = 19200 ml/hr g cat, T = 1073K

Figures 5 24, 5 25 and 5 26 illustrate the effect of copper on the catalytic stability as a function of time on stream for CO_2 reforming of CH_4 at 1073K and space velocity of 19200 ml/hr g cat over copper promoted Ni catalysts and unpromoted Ni/γ-Al_2O_3 catalyst. The Ni-Cu/γ-Al_2O_3 (1 wt%) and Ni-Cu/γ-Al_2O_3 (0 25 wt%) catalysts maintained initial catalytic activity for 250 minutes with CH_4 conversions of 54% and 59% The Ni-Cu/γ-Al_2O_3(0 5 wt%) catalyst shows lower activity but also maintained the initial activity with time on stream. In contrast, the unpromoted catalyst showed a gradual deactivation

The cause of deactivation for the unpromoted catalyst may be due to carbon deposition A similar trend was observed for the CO_2 conversion (see Figure 5 25) Carbon deposition of 0.14 g/g cat was obtained for the unpromoted catalyst while 0 09 g/g cat 0 06 g/g cat and 0 04 g/g cat were obtained for the Cu promoted catalyst with decreasing loading of 1 wt%, 0 5 wt% and 0.25 wt% respectively.

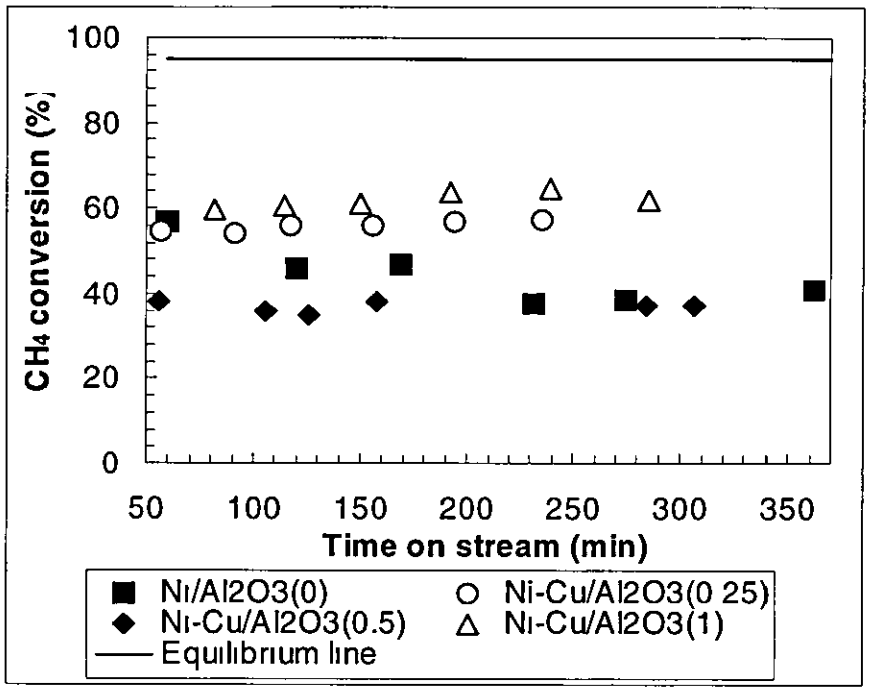

Figure 5.24 CH_4 conversion as a function of time, WHSV = 19200 ml/hr g cat, CH_4/CO_2 = 1, P = 1 atm , catalyst weight = 50 mg, T = 1073K

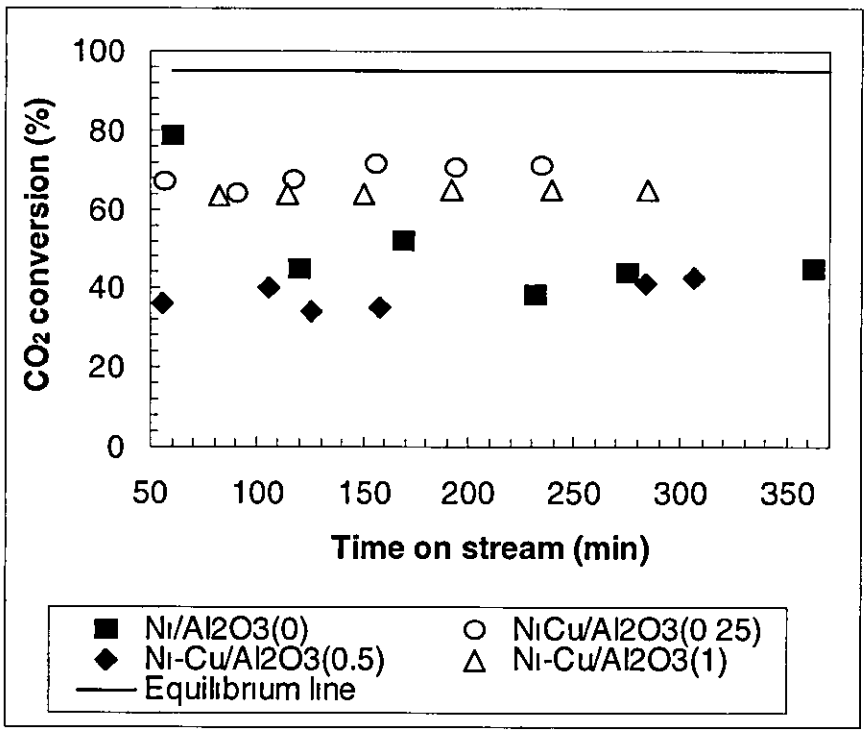

Figure 5.25 CO_2 conversion as a function of time, WHSV = 19200 ml/hr g cat, CH_4/CO_2 = 1, P = 1 atm , catalyst weight = 50 mg, T = 1073K

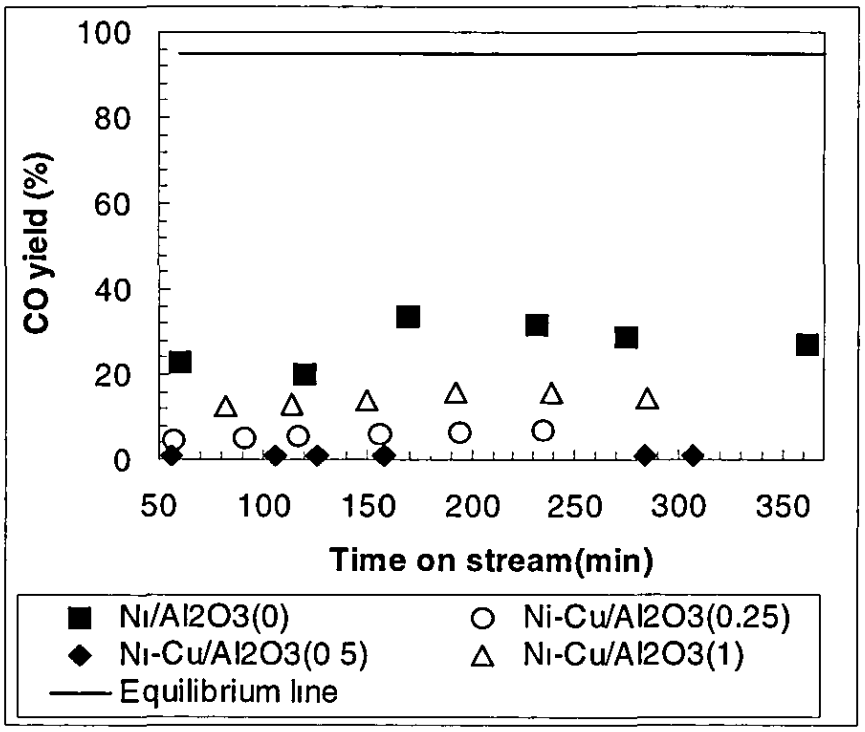

Figure 5 26 CO yield as a function of time, WHSV = 19200 ml/hr g cat, $CH_4/CO_2 = 1$, P = 1 atm , catalyst weight = 50 mg, T = 1073K

Apart from Ni-Cu/γ-Al_2O_3 (0.5 wt%) catalysts, the CO_2 conversion was higher than the CH_4 conversion for all other catalysts, which may be due to the occurrence of the reverse water-gas shift reaction ($CO_2 + H_2 \leftrightarrow CO + H_2O$) The results suggest that the RWGS reaction was favoured at this temperature.

In terms of CO yield, the unpromoted catalyst shows the highest value compared to all the Cu promoted catalyst which suggest that the three copper promoted catalysts show lower CO yield but maintained the initial activity with the following order Ni-Cu/γ-Al_2O_3 (1 wt%) > Ni-Cu/γ-Al_2O_3 (0.25 wt%) > Ni-Cu/γ-Al_2O_3 (0 5 wt%). The kinetic data showed higher rate constant for CO formation ($k_3 = 60*10^{-5}\ s^{-1}$) for the unpromoted catalyst compared to Cu promoted catalyst ($k_3 = 11*10^{-5}\ s^{-1}$).

The CO rate of formation for the unpromoted catalyst was higher than that of the copper promoted catalysts, which agreed with the kinetic results because the activity energies for CO production (40 kJ/mol) was lower for the unpromoted catalyst compared to (0.25 wt%) copper promoted catalyst (64.8 kJ/mol).

The catalytic activity observed at 13900 ml/hr g cat was different compared to the space velocity of 19200 ml/hr g cat The activity for Ni-Cu/γ-Al_2O_3 (1 wt%) catalyst decreases quickly from 85% to 80% but remain constant with time on stream (see Appendix IV, Figure A4.6 1) The CH_4 conversion for Ni-Cu/γ-Al_2O_3 (0.5 wt%) catalyst was also higher than that of the unpromoted catalyst. For the CO_2 conversion, both Ni-Cu/γ-Al_2O_3 (1 wt%) and Ni-Cu/γ-Al_2O_3 (0.5 wt%) catalysts and the unpromoted catalyst show activation with time on stream but all showed different initial CO_2 conversions of 54 4%, 16.1% and 50% respectively, which may be due to different induction periods

The Ni-Cu/γ-Al_2O_3 (0 25 wt%) catalyst shows an initial activity of 65.4% which stayed constant with time on stream The CO yield for the unpromoted catalyst increases with time on stream, showing a final value higher than that for all the promoted catalyst (see Figure A4 6 1, Appendix IV) In contrast, the Ni-Cu/γ-Al_2O_3 (1 wt%) and Ni-Cu/γ-Al_2O_3 (0.5 wt%) catalyst show constant CO yield while Ni-Cu/γ-Al_2O_3 (0.25 wt%) catalyst show little deactivation with time.

There was no significant difference in CH_4 conversion under the condition of 9820 ml/hr g cat compared to 13900 ml/hr g cat (see Figure A4 6 2, Appendix IV). The only observation was that the CH_4 conversion of Ni-Cu/γ-Al_2O_3 (0 25 wt%) was lower than that of the unpromoted catalyst. For the CO_2 conversion, a different trend was observed, because the unpromoted catalyst exhibits low initial activity but rapidly increases to 70 2% and remained stable with time on stream This occurrence may be due to initial carbon deposition at the initial stage of reforming of CH_4 All other catalyst show similar trend observed at space velocity of 13900ml/hr g cat The CO yield also followed a similar trend to the space velocity of 13900 ml/hr g cat except for the unpromoted catalyst that shows a different trend, with constant CO yield although still higher compared to the copper promoted catalysts

5 8.2 Effect of copper promotion on catalytic stability, WHSV = 19200 ml/hr g cat, T = 1023K

Figure 5 27 illustrates the catalytic stability of the unpromoted and copper promoted Ni catalyst as a function of reaction time during CH_4/CO_2 reforming at 1023K. For the unpromoted catalyst, it still exhibits a high initial conversion of CH_4 94.6% but stabilises to 59.9% after a period of about 300 minutes

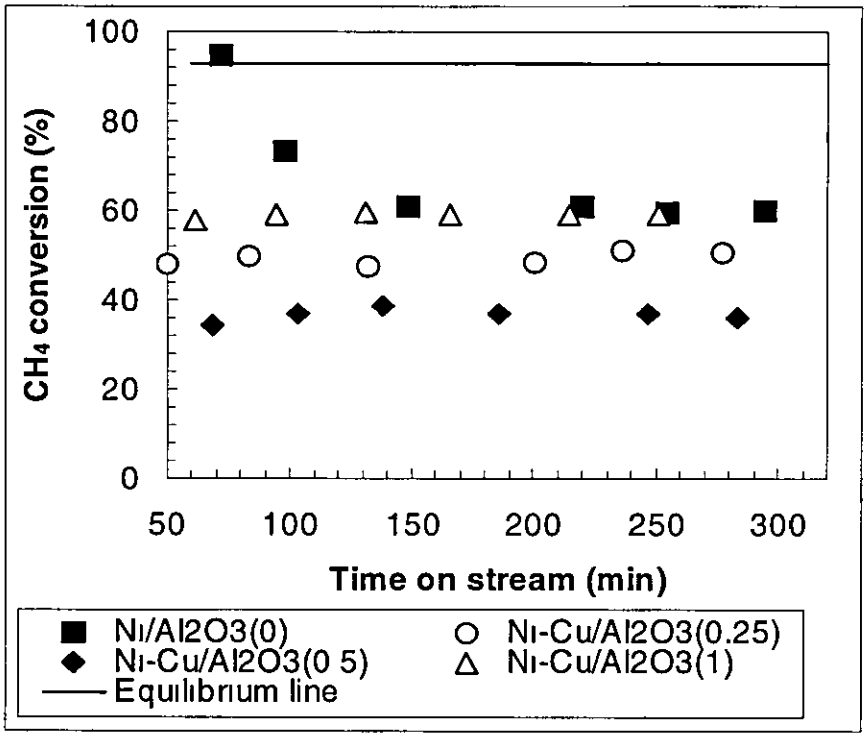

Figure 5 27 CH_4 conversion as a function of time, WHSV = 19200 ml/hr g cat, CH_4/CO_2 = 1, P = 1 atm., catalyst weight = 50 mg, T = 1023K

For the three copper promoted catalysts, Ni-Cu/γ-Al_2O_3 (0 25 wt %), Ni-Cu/γ-Al_2O_3 (0 5 wt%) and Ni-Cu/γ-Al_2O_3 (1 wt%) the initial conversions of CH_4 were 47 8%, 34.3% and 57.7%, lower than the unpromoted catalyst, however they maintained stability. A similar trend was observed for the CO_2 conversion as well as the CO yield for all the catalysts It appears that the Ni-Cu/γ-Al_2O_3 (0 5 wt%) catalyst exhibited the lowest activity among the promoted catalysts (Figure not shown).

Although the unpromoted catalyst showed deactivation, it exhibits the highest CO yield compared to the copper promoted catalysts. The addition of copper lowered the initial activity at this temperature and space velocity although stable activity was achieved. Also, the CO yield was not enhanced by the addition of copper. The performance of the unpromoted catalyst was different compared to the observation at the condition of 19200 ml/hr g cat. Almost equal activities were observed for both the unpromoted catalyst and that of Ni-Cu/γ-Al_2O_3 (1 wt%) but they all show stability.

The CH_4 conversion for Ni-Cu/γ-Al_2O_3 (0 25 wt %) catalyst was slightly lower but also shows stability while Ni-Cu/γ-Al_2O_3 (0 5 wt %) catalyst shows a slight activation with time on stream The CO_2 conversions follow a similar trend to CH_4 conversion as well as the CO yield for both catalysts (Figure not shown).

The activity and stability observed at 973K and 923K show no remarkable difference apart from slight differences observed at varying space velocities The entire set of experimental plots can be found in Appendix IV.

5 9 Coke deposition

As can be seen, there was no indication of filamentous carbon being formed on the catalysts (see Figure 5.28). No significant difference was also found on the catalyst surface After burn -off, the carbon formation order was found to be 0 14g/g cat > 0.09g/g cat > 0 06g/gcat > 0 04g/gcat for the unpromoted catalyst, Ni/γ-Al_2O_3 > Ni-Cu/γ-Al_2O_3 (0.25 wt%) > Ni-Cu/γ-Al_2O_3 (0 5 wt%) > Ni-Cu/γ-Al_2O_3 (1 wt%) respectively.

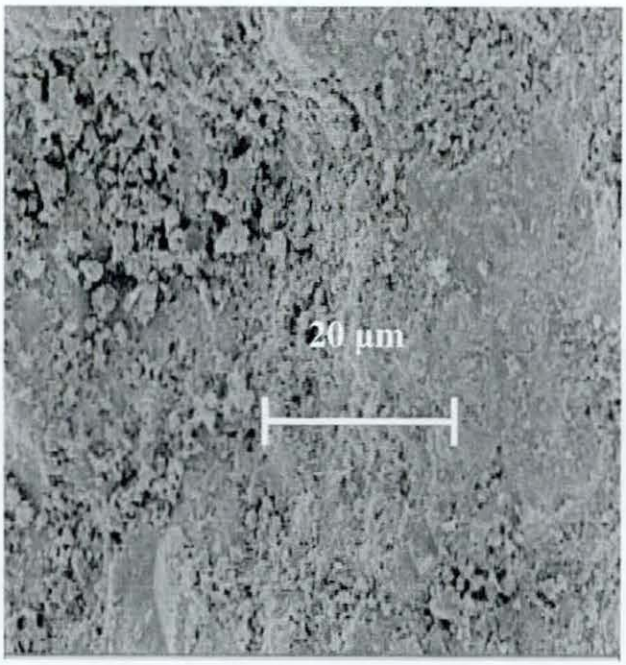

(a)

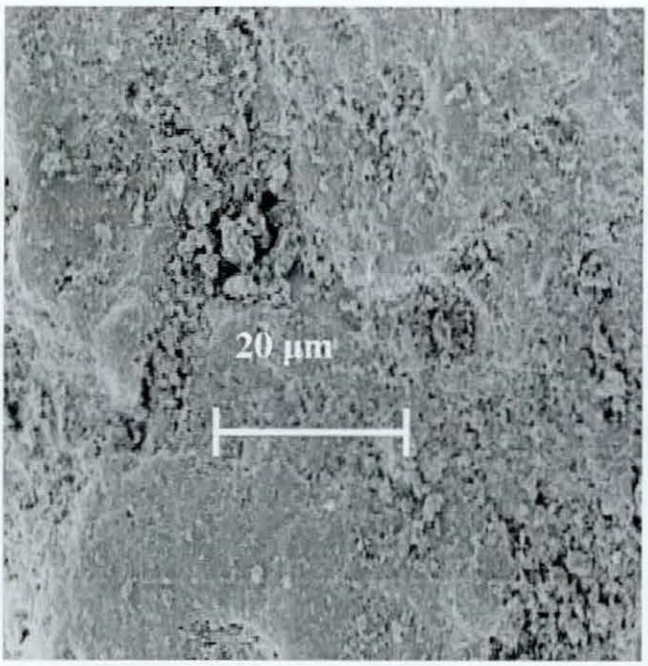

(b)

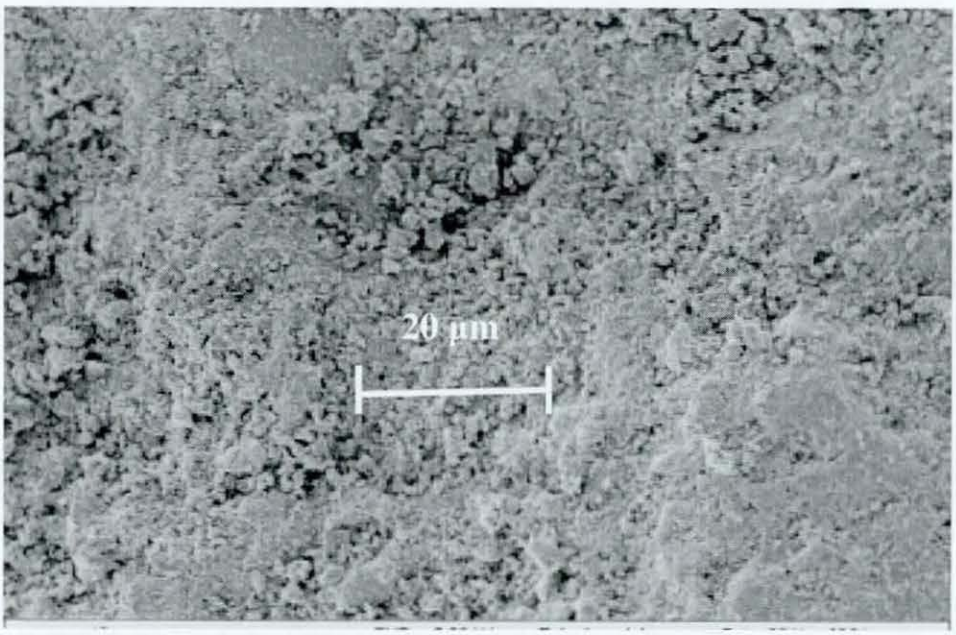

©

Figure 5.28 SEM images (a) Ni-Cu/γ-Al_2O_3 (1 wt%) (b) Ni-Cu/γ-Al_2O_3 (0.25 wt%) (c) Ni-Cu/γ-Al_2O_3 (0.5 wt%),WHSV=19200 ml/hr g cat, $CH_4/CO_2 = 1$, P = 1 atm., catalyst weight = 50 mg, T = 1073K

The amount of carbon deposits on the catalysts appears to agree with the higher CO yield observed for Ni-Cu/γ-Al_2O_3 (1 wt%) catalyst compared to others, where the carbon deposit was found to be the lowest among the copper promoted catalyst. The addition of copper appears to reduce the carbon deposition

Figure 5 29 illustrates the coke deposition with Pd and Cu loading. For Pd the coke deposition increased as the amount of Pd loading increased whilst coke deposition for the Cu promoted catalyst decreased with increasing Cu loading. The reason for this observation is not clear because higher CH_4 and CO_2 (79.6%, 85.2%) and (78 8%, 81.3%) conversions were achieved for 0 25 wt% and 0.5 wt% Pd promoted catalyst compared to that of the Cu promoted catalyst (57.2%, 37.2%) and (70 8%, 42 6%). For the 1 wt% Pd and Cu, conversions of 62% and 64 8% were achieved for CH_4 and CO_2, giving equal values of CO yield (14 6%).

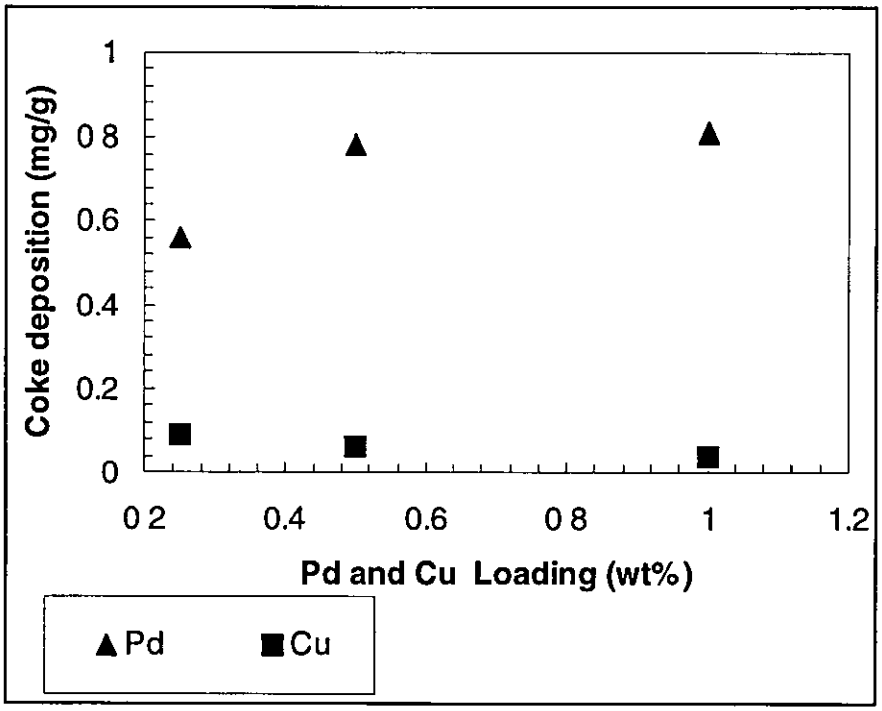

Figure 5 29 Coke deposition as a function of Pd and Cu Loading, WHSV = 19200 ml/hr g cat, CH_4/CO_2 = 1, P = 1 atm , catalyst weight = 50 mg, T = 1073K

For lower level loadings of 0 25 wt% and 0.5 wt% Cu, the CO_2 conversion were higher 70 8% and 42 6% whilst 57.2% and 37 2% were obtained for CH_4 which suggests a significant occurrences of RWGS reaction ($CO_2 + H_2 \leftrightarrow CO + H_2O$).

Higher CO yield (7.1%) was obtained compared to that of the 0 25 wt % Pd loading of 0.83%. On the other hand, for the Pd loading of 0 25 wt% and 0.5 wt%, the CO_2 conversions were lower (78.8%, 81.3%) and (79 6%, 85.2%) for CH_4 conversions The XRD results also showed an increase in crystallite sizes for the promoted catalysts, showing no dilution effect, although the increase in crystallite sizes were more pronounced for the Cu promoted catalyst which was reflected in the low dispersion (0.14%) result

However, the TPR results showed the lowered reduction temperature on the Cu promoted catalyst at 540K compared to the unpromoted catalyst at 974K which indicated that the Cu promoted catalyst could be activated in H_2 atmosphere during reforming, that can easily gasify carbon formed. It is also likely that Cu promoted catalyst promotes the RWGS reaction, which enhanced CO yield, especially at lower loadings compared to Pd. Further investigation is needed to study this observation.

5.9 Conclusions

Carbon dioxide reforming of methane was studied over copper promoted Ni catalysts, to gain insight into the modification of the active phase by copper atoms on a bimetallic catalyst. Based on the results of this work, the following conclusions can be drawn

Compared with the unpromoted catalyst, the activity and stability of Ni-Cu/γ-Al_2O_3 catalysts for CH_4/CO_2 reforming was enhanced remarkably at 1073K, WHSV = 19200 ml/hr g cat, although it negatively affected the initial activity. The reduced initial activity may be due to induction period at the start of reforming. The CO yield was not enhanced because all promoted catalysts show lower CO yield compared to the unpromoted catalyst The reason is not clear because Cu promoted catalyst reduced coke formation compared to the unpromoted catalyst Also, stability was achieved with the addition of Cu while the unpromoted catalyst deactivated with time on stream at higher temperatures > 1073K and space velocity of 19200 ml/hr g cat. The Pd promoted catalyst also enhanced stability, but coke deposition increased with increasing Pd loading whilst a decrease in coke deposition was observed with an increase in Cu loading

The rate constant for CO formation was higher ($k_3 = 60*10^{-5}\ s^{-1}$) than that of Cu promoted catalyst ($k_3 = 11*10^{-5}\ s^{-1}$).

The kinetic data agreed with the experimental results because higher CO yield was obtained for the unpromoted catalyst compared to the Cu promoted catalyst. Activation energies of 40 kJ/mol and 64 8 kJ/mol for CO were obtained for the unpromoted catalyst and Cu promoted catalyst respectively. It was found that the influence of copper on the nickel based catalyst depended strongly on the amount of copper added, temperature and space velocity.

CHAPTER 6

CATALYSTS POISONING WITH NH_3 AND H_2O

6.1 Introduction

Chapter 6 discusses all the experimental results obtained from the studies conducted using NH_3 as poison for four catalysts the unpromoted catalyst (Ni/γ-Al_2O_3), Ni/ZrO_2/γ-Al_2O_3, Ni-Pd/γ-Al_2O_3 (0 25 wt%) and Ni-Cu/γ-Al_2O_3 (0.25 wt%) catalysts Biogases contain traces of ammonia, hydrogen sulphide and water depending on the source e g. (1000-3000 ppm, 80-100 ppm) of ammonia (Cheremisinoff *et al* 1980, Effendi *et al.*, 2002). Among the support promoted catalysts, the ZrO_2 promoted catalyst showed an excellent performance in terms of both activity and stability for CO_2 reforming of methane. Therefore it was desirable to conduct poisoning experiments in order to ascertain if the trace compounds have any effect on the catalyst. In this study only NH_3 was selected for the poisoning experiments due to time constraint. Investigations were also carried out on the effect of H_2O activity and stability at 1073K and space velocity of 19200 ml/hr g cat; conditions far away from equilibrium. Although high conversions were obtained with the palladium promoted catalyst, a very low CO yield was observed with high carbon deposits compared to the unprompted catalyst. However, addition of 0 25 wt% palladium showed no appreciable change in surface area of the unpromoted catalyst (Ni/γ-Al_2O_3) which was also reflected in the dispersion result (see Table 5 1) Therefore Ni/ZrO_2/γ-Al_2O_3 and Ni-Pd//γ-Al_2O_3 (0.25 wt%) catalysts together with the unpromoted catalyst were selected for the NH_3 poisoning experiment. For good comparison, the Ni-Cu/γ-Al_2O_3 (0 25 wt%) catalyst was also selected, because less carbon deposition was found, although the surface area was reduced. The results obtained for the effect of NH_3 and H_2O on activity and stability for the individual catalysts are compared. The carbon deposition during reforming is also discussed.

6.2 Effect of NH_3 on catalytic activity of unpromoted Ni/γ-Al_2O_3 catalyst

6 2 1 Effect of NH_3, WHSV = 19200 ml/hr gcat, T = 923K-1073K

Figure 6 1 compares the catalytic activity of the unpromoted catalyst (Ni/γ-Al_2O_3) for dry reforming and NH_3 (3000 ppm) in the system at temperatures ranging from 923K-1073K and space velocity of 19200 ml/hr g cat

The CH_4 conversion was higher in the case of the NH_3 compared to that of the dry reforming. As can be seen in Figure 6.1, the increase in CH_4 conversion was more significant at higher temperatures, especially at 1073K, which almost doubled the CH_4 conversion compared to the dry reforming The CH_4 conversion increases with increasing temperature for the NH_3 system, which suggests that little sintering occurs at higher temperatures. A similar trend of CO_2 conversion to CH_4 conversion was observed (see Figure A5 1.1, Appendix V). However, a higher CO_2 conversion was observed for the dry reforming at 923K. The CO yield did not follow the trend to CH_4 and CO_2 conversion (see Figure A5.1 1, Appendix V). At 923K, the catalyst exhibited low CO yield in the dry reforming compared to that of the NH_3 system with higher CO_2 conversion But higher CO yield was observed for the NH_3 system at 1023K. The high conversion observed in the NH_3 system may be due to the decomposition of NH_3 at the temperature range employed It has been reported in literature that nickel catalyst is suitable for NH_3 decomposition at 1 atmospheric pressure and in the temperature range of 948K-1123K (Staniforth and Ormerod 2003; Yin *et al*, 2004) The process of nitrogen diffusion on to the metal surface to form nitrides after NH_3 decomposition may result in a decrease in surface energy of the metal, which may cause surface rearrangement of the catalyst surface, thus exposing active sites Therefore the increase in conversion observed at all temperatures for the NH_3 system may be due to the rearrangement of the Ni metal on the catalyst surface as a result of nitrogen diffusion due to NH_3 decomposition (Lif *et al*, 2004).

The many step decomposition mechanism of NH_3 at Ni (110) or Ni (100) have been proposed in literature (Cheng *et al*, 1995) NH_3 adsorption on Ni surfaces and forms an adsorbate NH_3(ad), and subsequent dissociation into NH_2(ad) and H(ad) occurs and eventually leading to N(ad) and H(ad) adatoms Nitriding processes have been studied by many research groups (Balker and Maciejewski 1984; Kodentsov *et al*, 1999).

Nitriding is as a result of diffusion of atomic nitrogen at the metal surface. Metal nitrides precipitate, once the nitrogen concentration in the metal exceeds the solubility limits Depending on the size of the fragments, the adsorption species may reside at different sites (Cheng *et al*, (1995). According to the report by Cheng *et al*, (1995) the 'on-top mode' is the most favourable adsorption pattern of NH_3 at the metal surfaces with nitrogen end on the metal atom and the three hydrogen atoms pointing away from the surface

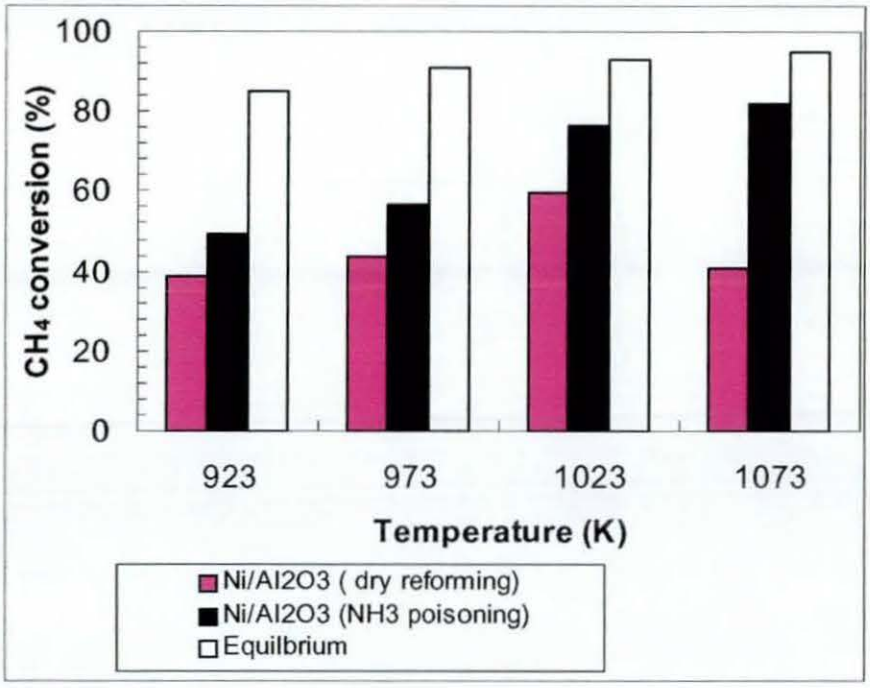

Figure 6.1 CH_4 conversion as a function of temperature, P = 1 atm, WHSV = 19200 ml/hr g cat, catalyst weight = 50mg

In the case of 13900 ml/hr gcat CH_4 conversion was lower for the NH_3 system compared to dry reforming at temperatures < 973K while similar observation was made at temperatures > 1023K in terms of CH_4 conversion for the NH_3 system. A similar trend was observed for CO_2 conversions to CH_4 at all temperatures in the two systems. Although CO_2 conversion was higher in the dry reforming at 973K, a lower CO yield was observed compared to the NH_3 system. The results can be found in Appendix V, Figure A5.1.2.

Reducing the space velocity to 9820 ml/hr g cat did not cause any difference in activity. However, the CH_4 conversion at 923K was lower in the NH_3 system (see Appendix V, Figure A5.1.3). Also lower CO_2 conversions were observed at 923K and 1023K. A difference in CO yield was observed at 1073K with a higher CO yield for the dry reforming compared to that at 19200 ml/hr gcat. The result suggests that the decomposition of NH_3 at lower temperatures < 923K was not significant as no difference in conversion was observed especially at higher space velocities > 13900 ml/hr gcat with the unpromoted catalyst. This result agreed with report in literature (Staniforth and Ormerod., 2003).

From the experimental findings, it was noted that higher CH_4 and CO_2 conversions were achieved at higher temperatures for the NH_3 system. High CO yield was observed at temperatures at 923K, 1023K and 1073K. Reducing space velocity and temperatures < 923K caused a significant difference in CO_2 conversion. The result suggests that significant water gas shift reaction was favoured at 1023K with the space velocity of 13900 ml/hr gcat because of the low CO observed.

6.2.2 Catalyst performance of unpromoted Ni/γ-Al_2O_3 catalyst with NH_3, dry reforming and mixed reforming, T = 1073K

Figures 6.2, 6.3 and 6.4 compares the catalytic activity of the unpromoted catalyst (Ni/γ-Al_2O_3), for varying space velocities at 1073K for the dry reforming, mixed reforming and the NH_3 system. As discussed earlier in section 6.2.1 higher CH_4 conversion was observed for the NH_3 system compared to both dry reforming and mixed reforming (see Figure 6.2). However, higher CH_4 conversion was achieved for the mixed reforming compared to dry reforming at space velocities > 9840 ml/hr gcat. But CH_4 conversions at space velocities < 7840 ml/hr g cat the CH_4 conversion was lower compared to the dry reforming.

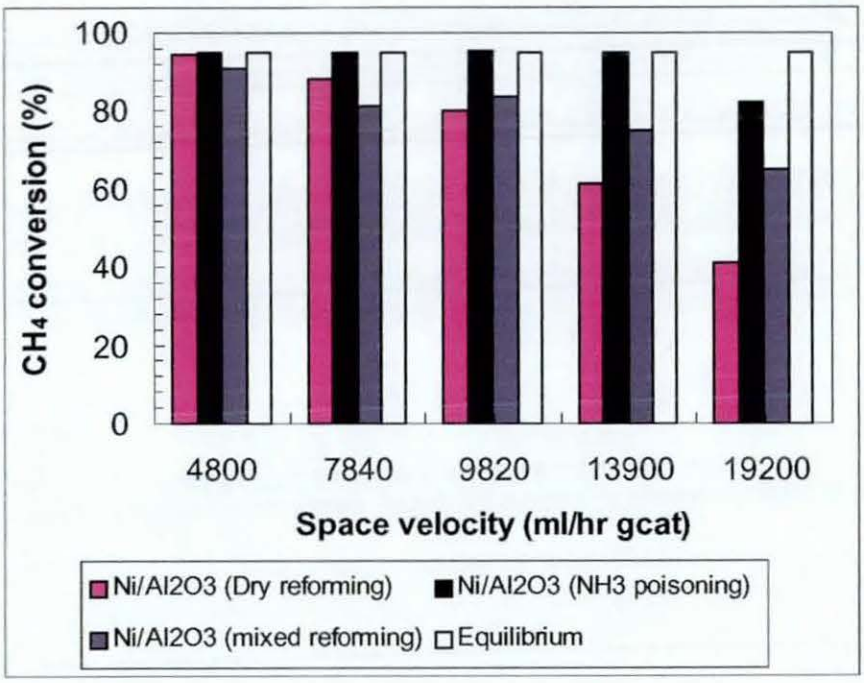

Figure 6.2 CH_4 conversion as a function of space velocity, P =1 atm, T = 1073K, catalyst weight = 50mg

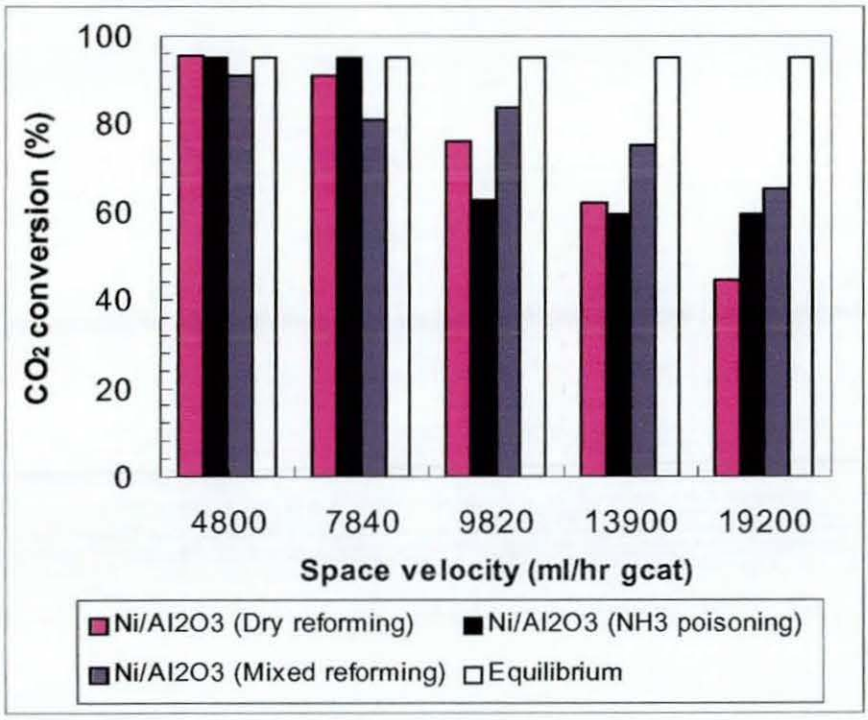

Figure 6.3 CO_2 conversion as a function of space velocity, P = 1 atm, T = 1073K, catalyst weight = 50mg

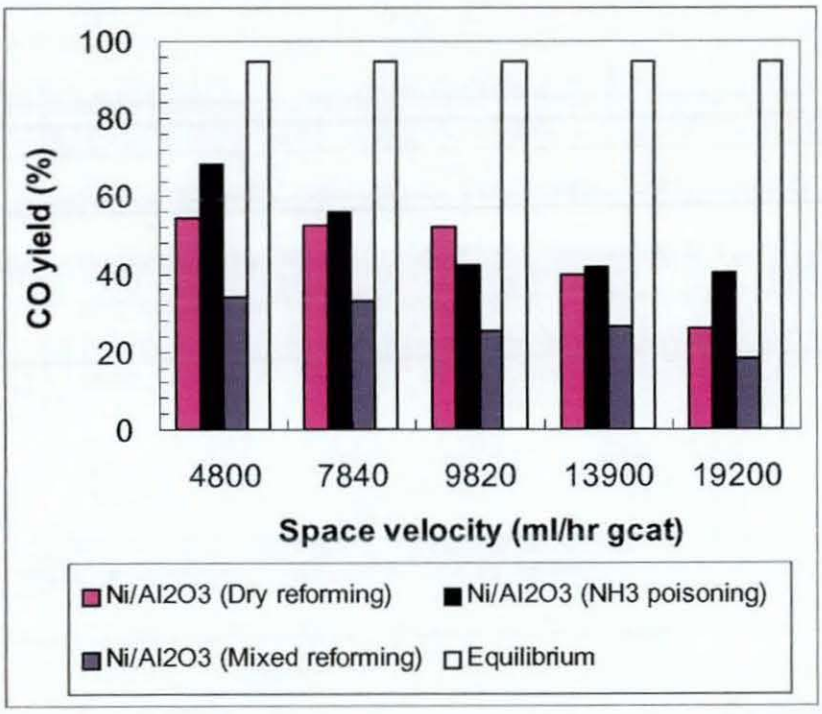

Figure 6.4 CO yield as a function of space velocity, P = 1 atm, T = 1073K, catalyst weight = 50mg

As can be seen in Figure 6.3 the CO_2 conversion for the NH_3 system was lower at space velocities of 9820 ml/hr g cat and 13900 ml/hr g cat compared to dry reforming On the other hand, lower CO_2 conversion was observed for the mixed reforming system except at 9820 ml/hr g cat compared to dry reforming and the NH_3 system. This lower CO_2 conversion may be due to the presence of water in the mixed reforming system, which also contributes to the reforming of CH_4 The presence of H_2O promotes oxidation of the catalyst that will result to the rearrangement of the catalyst which causes low adsorption capacity for CO_2, reducing the rate of CO_2 conversion (Chunshan and Wei 2004). But, the unusual behaviour at space velocity of 9820 ml/hr g cat indicating a very high CO_2 conversion is not clear. Another possible explanation may be due to the promotion of the WGS reaction ($CO + H_2O \leftrightarrow CO_2 + H_2$) which produces more of the CO_2 that cause a significant influence on the overall product distribution (Effendi *et al.*, 2002). In Figure 6 4 the CO yield is lower for the mixed reforming compared to the other two systems studied It is also interesting to note that conversion of CH_4 reached equilibrium values for the NH_3 system at space velocities < 13900 ml/hr g cat. For the dry reforming, equilibrium values were approached only at space velocities < 7840 ml/hr g cat, indicating a remarkable difference between the two systems for the same catalyst.

The presence of water in the system adversely affects the product distribution, as well as the CO_2 conversion, reducing the CO yield at all space velocities but increases CH_4 conversion at space velocity of 9820 ml/hr g cat. The amount of carbon deposits in the mixed reforming system was also larger compared to that of the dry reforming Apart from the space velocities of 9820 ml/hr g cat and 13900 ml/hr g cat the addition of NH_3 into the system enhances the conversion of CH_4 and CO_2.

6 2 3 Effect of NH_3 and H_2O on catalytic stability, T = 1073K, WHSV = 19200 ml/hr g cat

The stability of the unpromoted catalyst was studied for the two systems NH_3 system, and mixed reforming at 1073K under the condition of 19200 ml/hr g cat, for 6 hours and compared to that of dry reforming, since carbon deposition and sintering processes are mostly favoured at higher temperatures and significant differences in conversion were observed at higher space velocities.

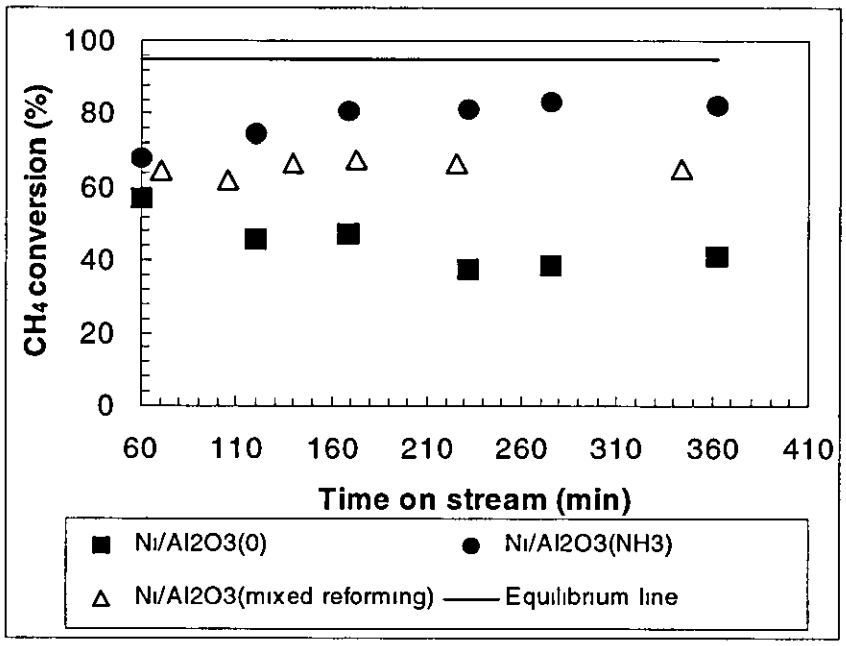

Figure 6.5 CH_4 Conversion as a function of time, P = 1 atm, T = 1073K, WHSV = 19200 ml/hr g cat, catalyst weight = 50mg, $CH_4/CO_2 = 1$

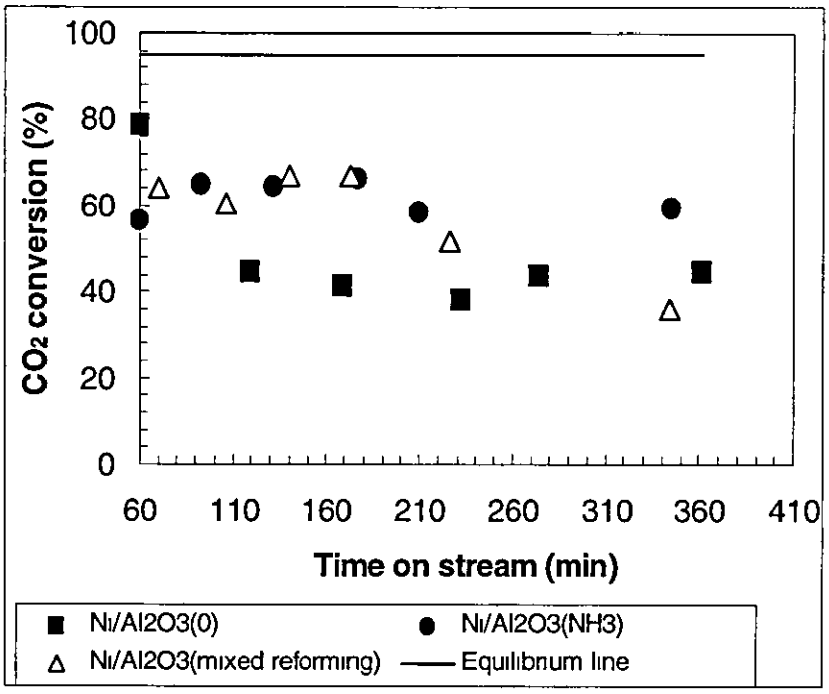

Figure 6.6 CO_2 Conversion as function of time, P = 1 atm, T = 1073K, WHSV = 19200 ml/hr g cat, catalyst weight = 50mg, $CH_4/CO_2 = 1$

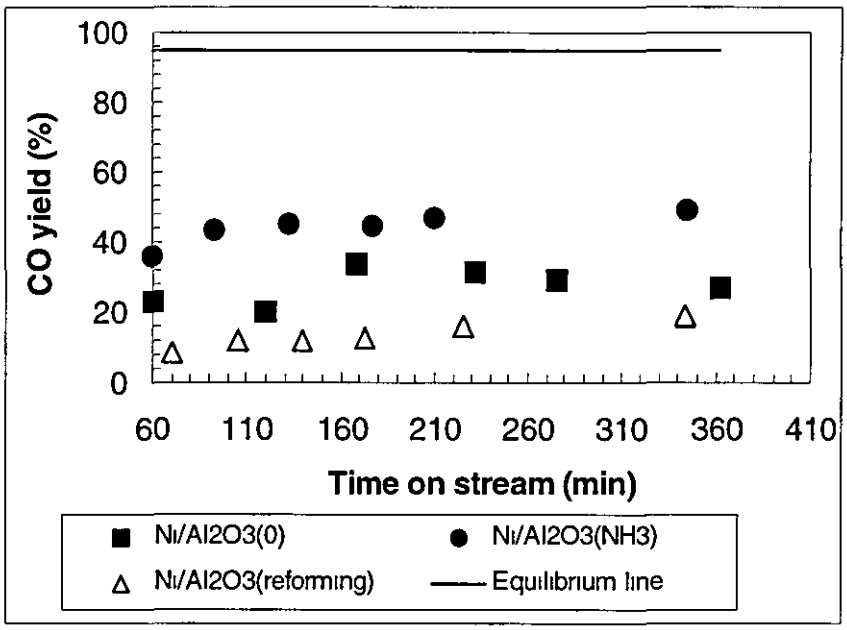

Figure 6.7 CO yield as a function of time, P = 1 atm, T = 1073K, WHSV = 19200 ml/hr gcat, catalyst weight = 50mg, $CH_4/CO_2 = 1$

The stability in terms of CH_4 conversion for the three systems, dry forming, mixed reforming and the NH_3 system are compared in Figures 6 5, 6 6 and 6.7. The unpromoted catalyst shows activity loss with increasing time, in terms of CH_4 and CO_2 conversions for the dry reforming as earlier discussed in Chapter 4 section 4 3.

In Figure 6 5 the initial activity (CH_4 conversion) of 62% was observed for the mixed reforming which fairly remained constant with increasing time on stream. The CH_4 conversion linearly increases from 69% to 80% as time increases. A similar initial CO_2 conversion was observed for the mixed reforming but it decreases to 40% after 340 minutes. As discussed earlier the CO_2 adsorption decreases due to the surface rearrangement of the catalyst because of the presence of H_2O. As a result the rate of CO_2 conversion decreases as time increases. On the other hand the constant CH_4 conversion observed may be due to the fact that there is also the possibility of steam reforming taking place. For this reason, the CH_4 conversion is always higher than that of CO_2 conversion in mixed reforming (Effendi *et al*, 2002). Figure 6.7 confirms the above argument because the CO yield is lower compared to the CO yield observed in dry reforming

The CO yield for the NH_3 system followed a similar trend to CH_4 conversion. The initial CO yield was 38% which linearly increases to 56% as time increases One speculation for such an improved conversion and CO yield is due to constant activation of the catalyst because of the surface rearrangement by nitrogen diffusion into the nickel surface, thereby creating the promotion of continuous rejuvenation of active sites Another speculation is that the surface rearrangement may have developed new active sites for reforming reaction In the mixed reforming, a very low initial CO yield 10% was observed but linearly increases to 20% with time on stream The CO yield in the NH_3 system was higher (see Figure 6.7) compared to the other systems studied The result obtained indicates that NH_3 in the system did not cause deactivation of the unpromoted catalyst under the conditions employed.

6 2 4 Morphology of spent catalysts and carbon deposits

Figure 6.8 and 6 9 compare the morphology of the spent catalyst (unpromoted catalyst) after 6 hours reforming for both mixed reforming and the NH_3 system in order to compare with that of dry reforming (see Chapter 4 section 4 9, Figure 4.26) There was not much difference found on the morphology of the catalyst between the two systems. No visible carbon fibre was observed. The morphology of the catalyst after NH_3 reforming appears to be very smooth compared to that of the mixed reforming It confirms the speculation that the catalyst surface may have been rearranged due to nitrogen diffusion as a result of NH_3 decomposition. The carbon deposits after the burn off exercise was 0 25g/g cat for the NH_3 system.

In the case of the mixed reforming (Figure 6.8) it appears some form of particle agglomeration has occurred on the catalyst surface The morphology of the spent catalysts after dry reforming for the same time period (6 hours) shows fibrous carbon deposits and cracks on the surface (see Chapter 4, section 4.9, Figure 4 26) The carbon deposited on the catalysts for the three systems: dry reforming, mixed reforming and NH_3 system after 6h reforming reaction, follow the order: 0.14g/g cat, < 0 19g/g cat < 0 25g/g cat. Regardless of the amount of coke deposited on the catalyst for the NH_3 system, no loss of activity was observed instead the activity increases during 6h on stream, indicating that part of this carbon was not poisonous during reforming

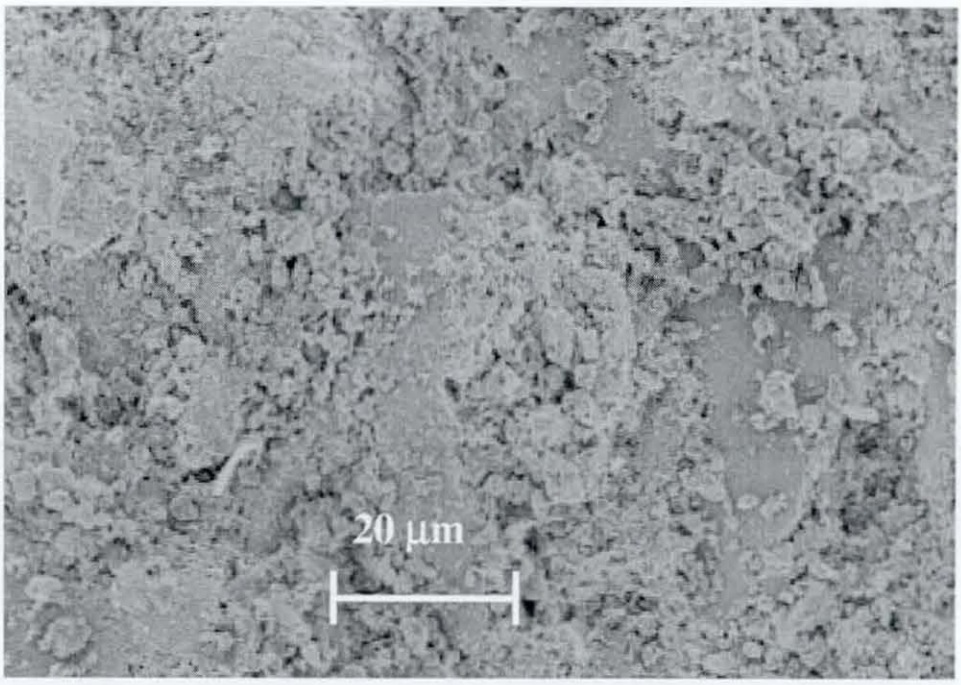

Figure 6.8 SEM image of Ni/γ-Al_2O_3 (0), Effect of H_2O at 1073K for 6hours, WHSV = 19200 ml/hr g cat

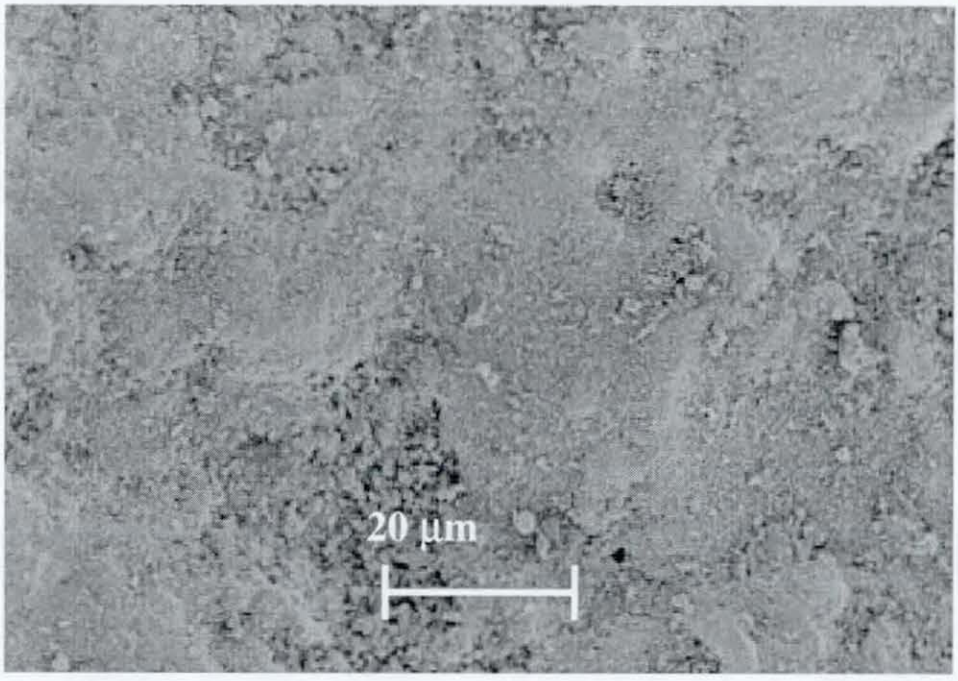

Figure 6.9 SEM image of Ni/γ-Al_2O_3 (0) catalyst, Effect of NH_3 at 1073K for 6 hours, WHSV = 19200 ml/hr g cat

The activity loss in the case of mixed reforming may be partly due to loss of Ni^0 active area due to oxidation because of the hydrothermal atmosphere. It is obvious from the findings of the study that the conditions employed and the environment can influence coke formation on the catalyst Although the coke formation on the NH_3 systems did not deactivates the catalyst, no further experiment was carried out to verify the type of coke formed on the catalyst for the systems.

6.3 Effect of space velocity on catalytic activity of Ni-Pd/γ-Al_2O_3 (0.25 wt%) catalyst

6 3 1 NH_3 system, dry reforming and mixed reforming, T = 1073K, WHSV = 4800-19200 ml/hr g cat

The catalytic activity of Ni-Pd/γ-Al_2O_3 (0 25 wt%) catalyst was studied at varying space velocities at 1073K. The CH_4 conversion was higher only at 9820 ml/hr g cat for the mixed reforming system among the three systems studied At all other space velocities, the CH_4 conversion was higher in dry reforming compared to the NH_3 system and mixed reforming On the other hand the CH_4 conversion shows higher values in mixed reforming compared to the NH_3 system at all space velocities. A similar trend was observed for CO_2 conversion at all space velocities. However, the difference in conversion for CH_4 and CO_2 was more significant between mixed reforming and the NH_3 system, while very close values were observed between dry reforming and mixed reforming. Although low conversion of CH_4 and CO_2 were observed in the NH_3 system, the CO yield was higher compared to both dry reforming and mixed reforming, at all space velocities except at 19200 ml/hr g cat, where the highest CO yield was observed in the mixed reforming. The catalyst shows a lower CO yield in the mixed reforming system at space velocities < 13900 ml/hr g cat

As can be seen in Figures 6.10, 6.11 and 6 12, CH_4 and CO_2 conversion are consistently lower in the NH_3 system compared to both dry and mixed reforming Ganley *et al.*, 2004 examined palladium among other metals for decomposition of NH_3 and found that palladium was not very active especially at conditions of (853K, 1 atm). On the other hand nickel was found to be an excellent catalyst for decomposition of NH_3 The results obtained confirm the observation made in literature (Granley *et al.*, 2004). The addition of palladium tends to reduce the rate of reaction for both CH_4 and CO_2 for the NH_3 system

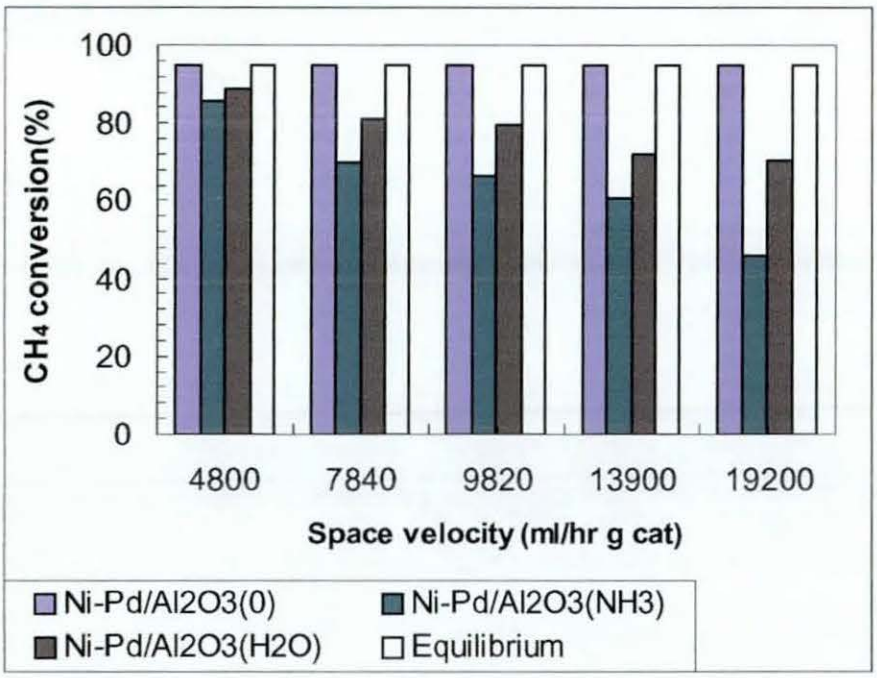

Figure 6.10 CH_4 conversion as a function of space velocity P = 1 atm, T = 1073K, catalyst weight = 50mg

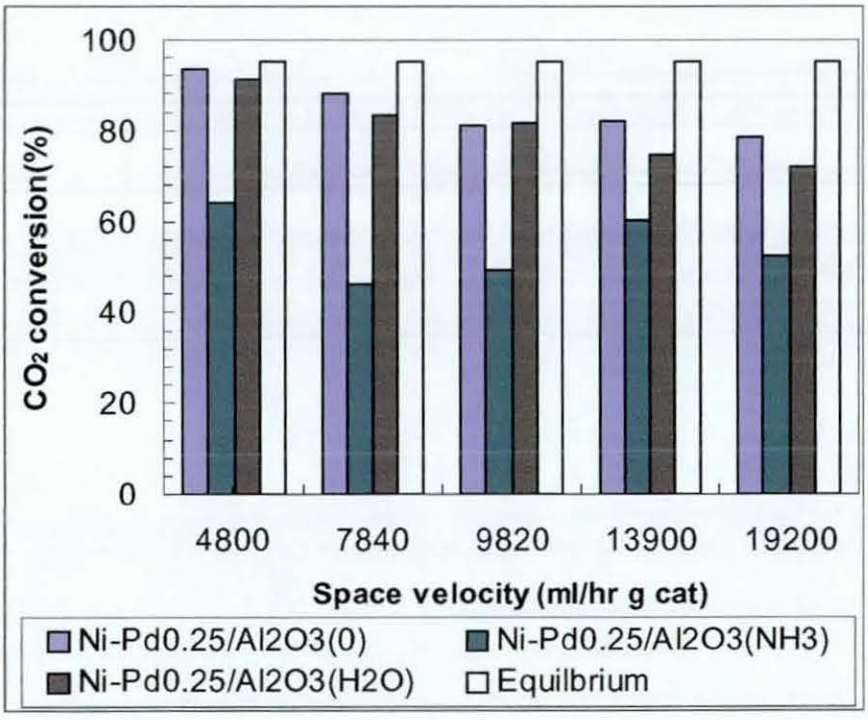

Figure 6.11 CO_2 conversion as a function of space velocity P = 1 atm, T = 1073K, catalyst weight = 50mg

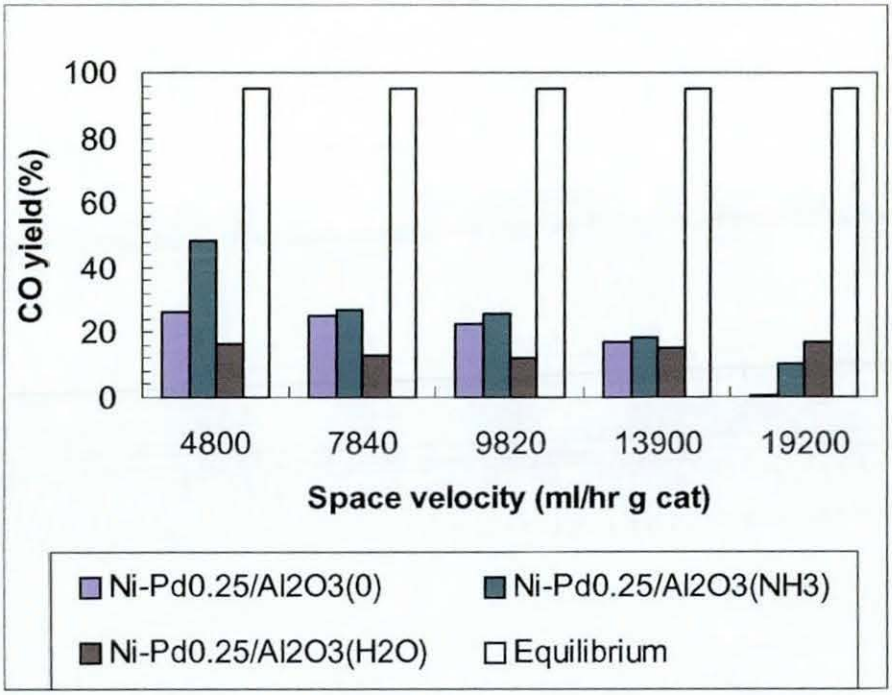

Figure 6.12 CO yield as a function of space velocity P = 1 atm, T = 1073K, catalyst weight = 50mg

The reduction in activity for Ni-Pd/γ-Al_2O_3 (0.25 wt%) catalyst observed for the NH_3 system may be due to changes in the electronic configuration of nickel with the addition of palladium which may have retarded the decomposition of NH_3.

One speculation may be due to formation of Pd-Ni alloy between the two metals which can also cause resistance to diffusion of N(ad). Another problem may be due to the adsorption of NH_3 on the catalyst surface which must have covered up most of the active sites since the rate of decomposition is low. Therefore one can speculate that one of the reasons for activity loss may have been caused by coverage of NH_3 on the active site. The result for coke deposits seems to confirm the above speculation because lower coke deposits were observed in the case of the NH_3 system compared to both dry reforming and mixed reforming.

As can be seen in Figure 6.10 and 6.11, low activities (CH_4 and CO_2 conversions) were observed for the mixed reforming compared to that of dry reforming.

However, the CO yield was improved compared to dry reforming and NH_3 system at 1073K which may be due to promotion of the RWGS reaction ($CO_2 + H_2 \leftrightarrow CO + H_2O$), which was also reflected in the CO_2 conversion (72 2%) higher than that of CH_4 conversion of (70.2%) (see Figure A5.3 1). The catalytic activity over palladium promoted catalyst for both dry reforming and the NH_3 system at varying temperature shows that CH_4 conversion was lower at all temperatures for the NH_3 system compared to dry reforming except at 923K space velocity of 19200 ml/hr g cat. A different conversion trend was observed in the case of CO_2, where no significant difference was observed at 973K but lower CO_2 conversions were observed at 923K, 1023K and 1073K for the NH_3 system. The rate of reaction increases with increasing temperature, but conversion of both CH_4 and CO_2 decreases as temperature increases in the NH_3 system (see Figure A5 3.1, Appendix V)

The conversions of CH_4 and CO_2 observed at space velocity of 13900 ml/hr g cat were not different compared to conversions at 19200 ml/hr g cat for the NH_3 system The CO yield followed a similar trend to CH_4 and CO_2 conversion. Although lower activity was observed for the NH_3 system, the rate of conversion increases with increasing temperature in terms of CH_4 conversion A decrease was observed at 1073K for CO_2 conversion and CO yield (see Figure A5 3 2, Appendix V). Decreasing the space velocity to 9820 ml/hr g cat did not change the trend of CH_4 conversion but a decrease was observed in CO_2 conversion at 1073K, showing that the rate of reaction was reduced (see Figure A5.3.3, Appendix V).

From the results obtained, it is obvious that palladium promoted catalysts did not favour decomposition of NH_3 but favoured the reverse water gas shift reaction because a higher CO yield was obtained despite lower conversions observed. For mixed reforming, very close conversions to that of dry reforming were achieved at all space velocities, especially at 1073K. The rate of CO yield was enhanced in the mixed reforming at higher temperatures

6 3 2 Effect of NH_3 and H_2O on catalytic stability for dry reforming, NH_3 system and mixed reforming, T = 1073K, WHSV = 19200 ml/hr gcat

Figure 6 13 and 6.14 compare the stability of palladium promoted nickel catalyst for the three systems studied at 1073K and space velocity of 19200 ml/hr g cat.

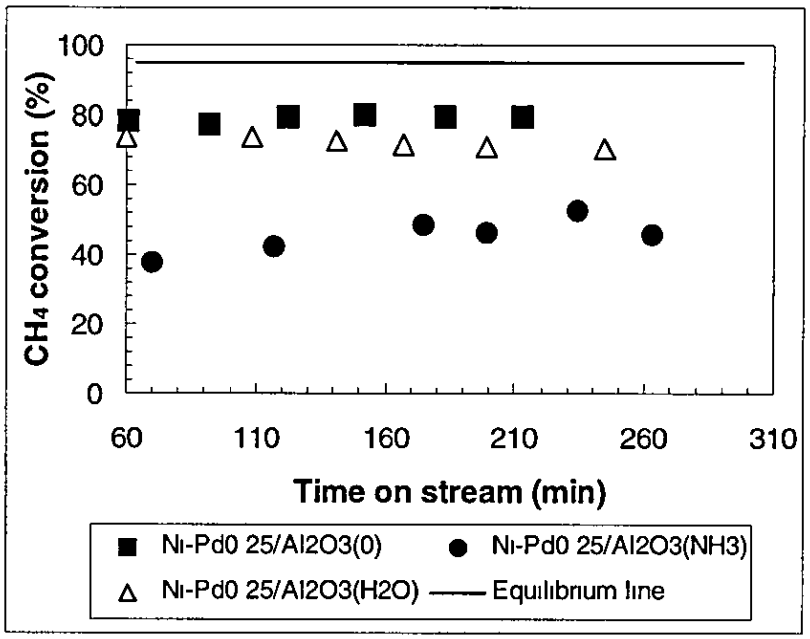

Figure 6.13 CH_4 Conversion as a function of time P = 1 atm, T = 1073K, WHSV = 19200 ml/hr g cat, catalyst weight = 50mg, $CH_4/CO_2 = 1$

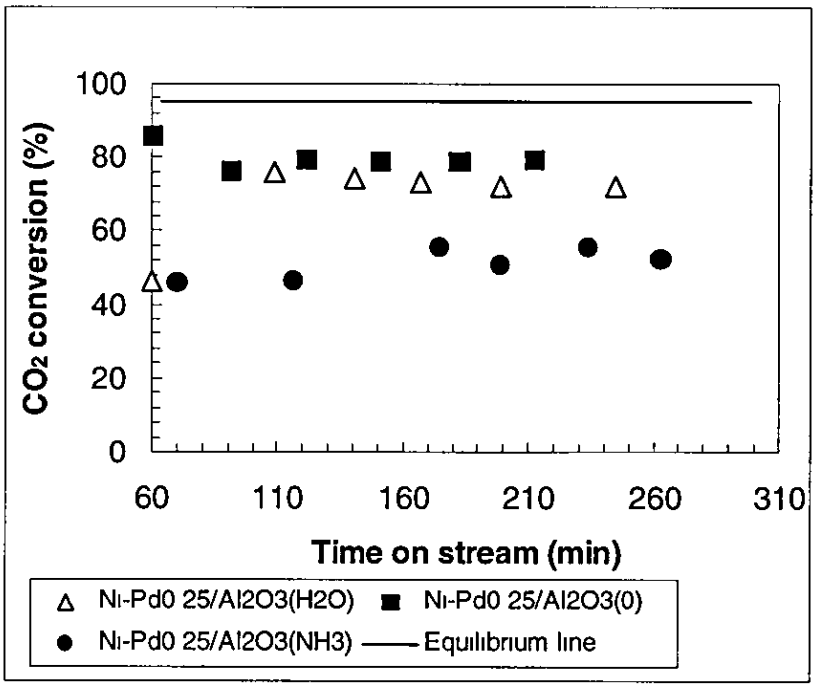

Figure 6.14 CO_2 conversion as a function of time P = 1 atm, T = 1073K, WHSV = 19200 ml/hr g cat catalyst weight = 50mg, $CH_4/CO_2 = 1$

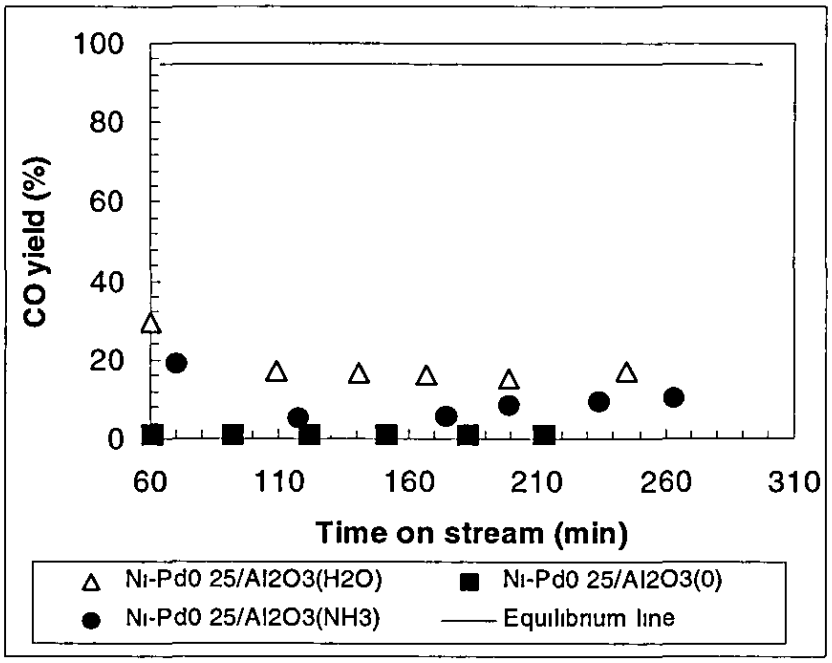

Figure 6.15 CO yield as a function of time P = 1 atm, T = 1073K, WHSV = 19200 ml/hr g cat catalyst weight = 50mg, CH_4/CO_2 = 1

The initial CH_4 conversion for both the dry reforming and mixed reforming were almost the same, 78.5% and 73 9% respectively. The CH_4 conversion for both systems maintained stability as time increases, apart from a slight decrease observed for the mixed reforming (73 2% to 70 2%).

A low initial CH_4 conversion (37.8%) was observed for the NH_3 system but increases to 45.8% with time on stream The CO_2 conversion followed a similar trend to the CH_4 conversion but the initial CO_2 conversion for the mixed reforming was very low i e 46 4% but rapidly increases to 75 2% which linearly stabilises at 72 2%. The initial CH_4 conversion was much higher than that of CO_2 in the mixed reforming which may be related to surface rearrangement of the catalyst due to the presence of H_2O that caused decrease in CO_2 adsorption. Higher initial CO yield of 26% and 18 8% were observed for both mixed and NH_3 system compared to the dry reforming. These values decrease rapidly to 16 9% and 5 3%, and stabilises to 10 3% for the NH_3 system while the mixed reforming remained stable at 16 9% with time on stream. As can be seen in Figure 6 15 the CO yield for the dry reforming was lower compared to all the other systems studied.

Although the activity of palladium promoted catalysts was adversely affected by NH_3 and water in the system, the catalyst appears to be stable both in CH_4 and CO_2 conversion with higher initial CO yield. However, the CO yield decreases rapidly at the start of the reforming which suggests significant water gas shift reaction.

Again the activity loss for the NH_3 system can not be attributed to the quantity of coke formed because less coke is formed compared to the dry reforming. Although, catalyst deactivation depends on the type of coke formed, no further experiment was carried out for confirmation.

6.3.3 Morphology of spent catalyst and carbon deposits

The morphology of the palladium promoted catalyst for the two systems; mixed reforming and NH_3 system are shown in Figure 6.16 and 6.17. No visible filamentous carbon was observed on the catalyst surface for both systems. However, the carbon deposits accumulated after reforming reaction for 6 hours shows higher carbon deposits on the catalyst for the mixed reforming compared to the both dry reforming and the NH_3 system.

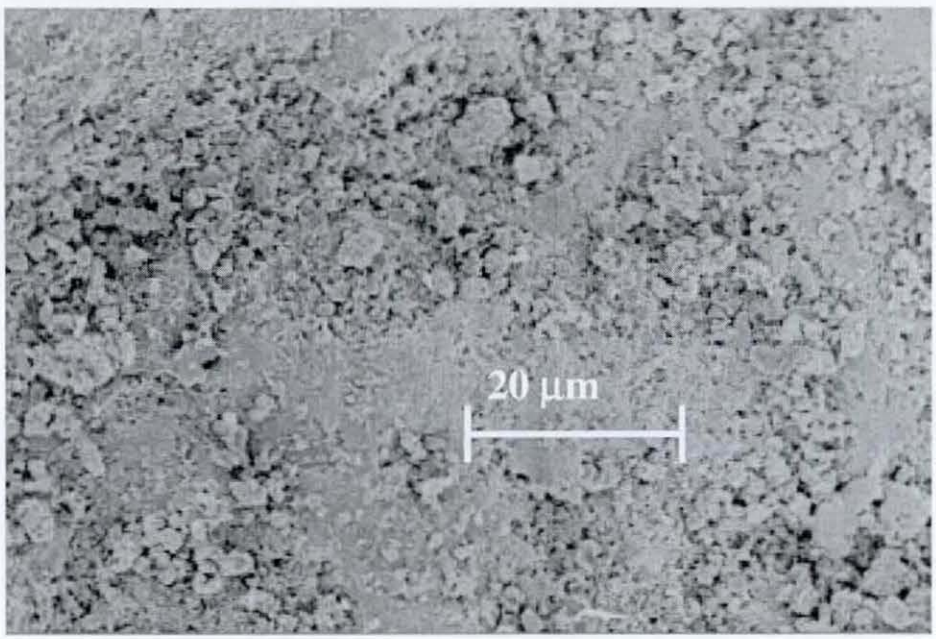

Figure 6.16 SEM image of Ni-Pd/γ-Al_2O_3 (0.25 wt%), effect of H_2O at 1073K, for 6hours , WHSV = 19200 ml/hr g cat

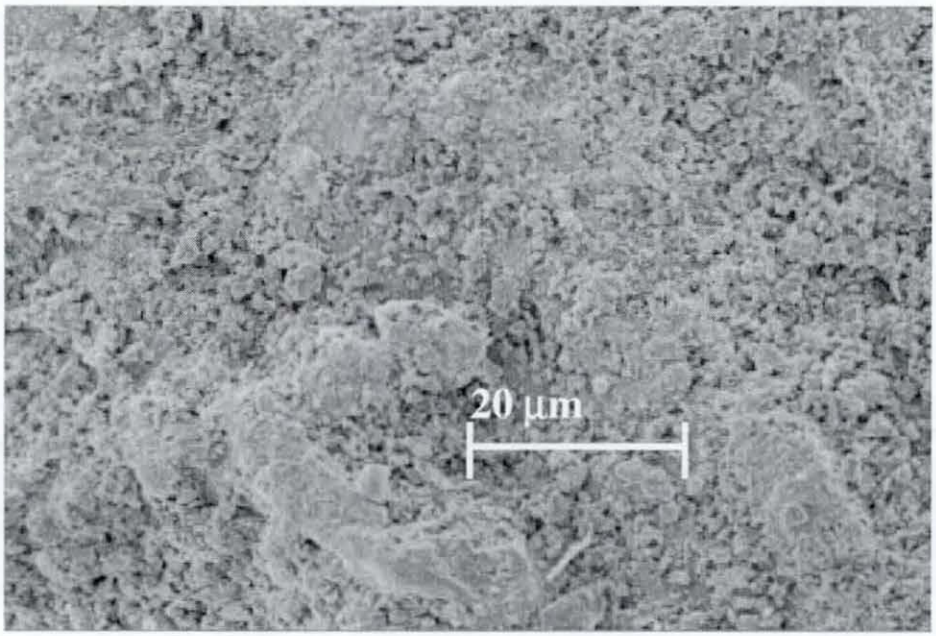

Figure 6.17 SEM image of Ni-Pd/γ-Al_2O_3 (0.25 wt%), effect of NH_3 at 1073K for 6hours, WHSV = 19200 ml/hr g cat

The carbon deposits of Ni-Pd/γ-Al_2O_3 (0.25 wt%) catalyst follow the order, 0.08g/g cat < 0.14g/g cat, < 0.41g/g cat for NH_3 system, dry reforming and mixed reforming respectively. In terms of catalytic performance, higher activity was observed for dry reforming followed by mixed reforming, but highest CO yield was found in the mixed reforming, although a rapid decrease was observed at the initial start of the reforming.

With the carbon accumulation result, it appears that the CO disproportionation reaction ($2CO \leftrightarrow C + CO_2$) was favoured at the initial stage of the reforming in the mixed reforming. The lowest activity was observed for the NH_3 system, although, the carbon deposit is lower compared to the other systems. Although tentative explanation for the loss in activity for the NH_3 system have been put forward, a detailed understanding is not yet possible.

It may be attributed to either coverage of active sites by NH_3, which may have contributed to reduced dispersion of Ni on the catalyst surface, or sintering processes or the type of carbon formed since the carbon deposit is very low. Therefore it is necessary to carry out further investigations in order to verify the actual cause for the loss in activity.

6.4 Effect of space velocity on catalytic activity over $Ni/ZrO_2/\gamma\text{-}Al_2O_3$ catalyst

6.4.1 NH_3 system, dry reforming and mixed reforming, T = 1073K, WHSV = 4800-19200 ml/hr g cat

As can be seen in Figure 6.18 and 6.19 the highest CH_4 conversion was observed in the dry reforming at all space velocities among the three systems studied. However, at space velocities of 13900 ml/hr g cat and 19200 ml/hr g cat, the CH_4 conversion was higher in the mixed reforming compared to the NH_3 system. At lower space velocities, < 9820 ml/hr gcat, the catalyst shows lower CH_4 conversion in the mixed reforming compared to the NH_3 system but exhibited almost the same conversion at the space velocity of 4800 ml/hr g cat. It then suggests that at lower space velocities the effect on the activity of $Ni/ZrO_2/\gamma\text{-}Al_2O_3$ catalysts in terms of CH_4 conversion was insignificant. The CO_2 conversion followed a similar trend to CH_4 conversion at higher space velocities > 9820 ml/hr gcat. At space velocities of 7840 ml/hr g cat and 4800 ml/hr g cat, the trend was different. As can be seen in Figure 6.19 the CO_2 conversion was higher in the mixed reforming among the three systems studied. However, the lowest CO_2 conversion was observed for the NH_3 system under the condition of 19200 ml/hr g cat. At space velocity of 9820 ml/hr g cat, the catalyst shows higher activity in terms of CH_4 conversion and CO yield for the NH_3 system. It is interesting to note that CH_4 conversions and CO yield for both systems decreases with increasing space velocity. The CO_2 conversion did not follow this trend, for the CO_2 conversion shows no consistency in decrease with increasing space velocity. For the mixed reforming, the activity appears to follow the trend to CH_4 conversion. The dry reforming shows restored activity at higher space velocities.

Figure 6.20 shows the comparable difference in CO yield exhibited by $Ni/ZrO_2/\gamma\text{-}Al_2O_3$ catalyst for dry reforming, NH_3 system and that of mixed reforming.

A very high CO yield was achieved in the case of the dry reforming Also lower CO yield was observed in the mixed reforming compared to the NH_3 system especially at lower space velocities < 9820 ml/hr g cat. At higher space velocities > 13900 ml/hr g cat, no significant difference of CO yield was observed between the mixed reforming and the NH_3 system.

The apparent loss in activity for both the mixed reforming and NH_3 system is not clear. However, one can speculate that modification of the catalysts support using ZrO_2 did not promote decomposition of NH_3, may be due to low dispersion of Ni active sites hence enhances the coverage of active sites by NH_3. The presence of water may have also caused rearrangement of the catalyst surface. The interaction between Al_2O_3 and H_2O present in the gas phase may cause the Al_2O_3 to migrate to the surface since the presence of H_2O causes a significant enrichment of Al in form of the oxide (Effendi *et al,* 2002). The above phenomenon may cause loss of surface nickel of the catalyst during reforming process.

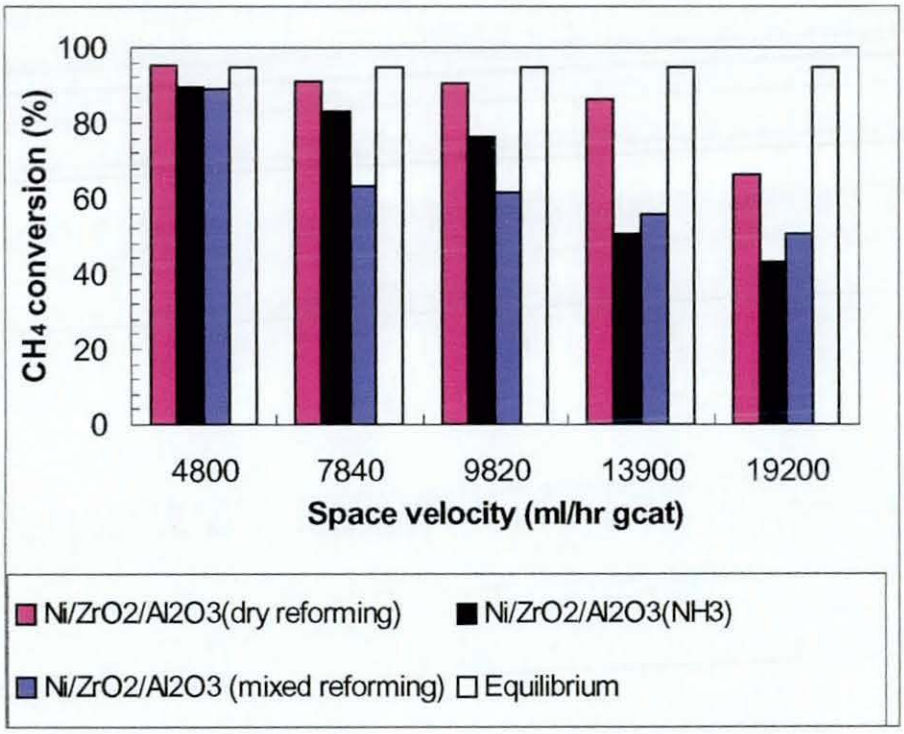

Figure 6.18 CH_4 conversion as a function of space velocity, P = 1 atm, T = 1073K, catalyst weight = 50mg

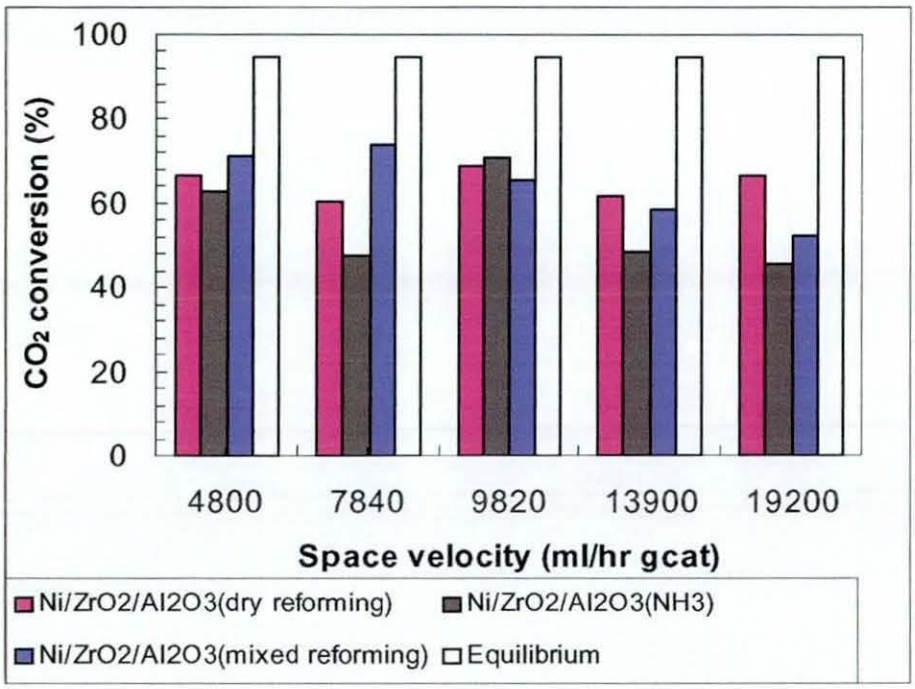

Figure 6.19 CO_2 Conversion as a function of space velocity, P = 1 atm, T = 1073K, catalyst weight = 50mg

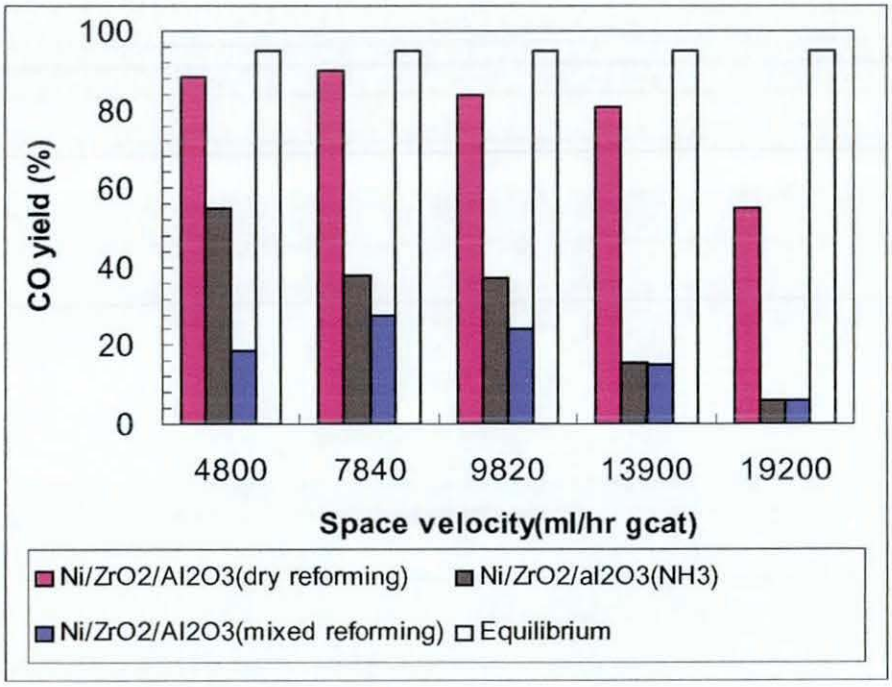

Figure 6.20 CO yield as function of space velocity, P = 1 atm, T = 1073K, catalyst weight = 50mg

From the result obtained, it suggests that the $Ni/ZrO_2/\gamma\text{-}Al_2O_3$ catalyst is a promising catalyst for the dry reforming of methane since the catalyst exhibits higher activity compared to the other systems studied at 1073K. The reasons for this excellent performance in the case of dry reforming have been discussed in Chapter 4 Although high conversions of CH_4 and CO_2 were observed at higher space velocities in case of mixed reforming compared to the NH_3 system, no significant difference was observed in CO yield

As can be seen the CH_4 conversion is close to the calculated equilibrium values for CH_4 conversion and CO yield even at higher space velocities. The activity of $Ni/ZrO_2/\gamma\text{-}Al_2O_3$ catalyst at different temperatures < 1073K and space velocity of 19200 ml/ hr g cat shows that higher CH_4 conversion were observed for NH_3 system at 923K, 973K and 1023K compared to dry reforming. The CO_2 conversion followed a similar trend to CH_4 conversion except at 1023K where the CO_2 conversion was lower. However it is very clear that the CO yield for the dry reforming were higher compared to the NH_3 system even at lower temperatures despites the higher conversions observed except at 1023K, where the CO yield was higher for the NH_3 system The rate of reaction for both CH_4 and CO_2 increases with an increasing temperature as well as CO yield for the dry reforming but it was not consistent for that of the NH_3 system. However, it appears to decrease at higher temperatures >1073K Several speculations may be put forward to explain the decrease in activity at this space velocity, either coke deposition or sintering processes because sintering can occur at higher temperatures (Rasmussen *et al*, 2004) due to nickel particle migration However, it is necessary to carry out further experiments for confirmation.

One possible reason for the low activity observed for the ZrO_2 promoted catalyst may be due to the acidic/basicity properties (Souza *et al* 2001). CO_2 is an acidic gas therefore higher adsorption is enhanced when the acidic nature of a support is lowered NH_3 and H_2O are basic so the adsorption capacity for the ZrO_2 promoted catalyst is lower compared to that of the dry reforming system Compared to the dry reforming, the $Ni/ZrO_2/\gamma\text{-}Al_2O_3$ was greatly affected by the NH_3 environment The results may suggest that there was adverse effect of NH_3 on the catalyst at higher temperatures > 1023K especially at this space velocity.

The reasons for low CO yield for the NH_3 system at 973K, despite the fact that higher CH_4 and CO_2 conversions were observed, may suggests a significant simultaneous occurrence of the water gas shift reaction at this temperature ($CO + H_2O \leftrightarrow CO_2 + H_2$). Similar conversions and CO yield were observed for the space velocity of 13900 ml/hr gcat (see Figure A5.2.2 Appendix V). Reducing the space velocity to 9820 ml/hr g cat did not make any significant difference in conversion compared to the space velocity of 19200 ml/hr gcat (see Figure A5.2 3).

At 1073K the CO_2 conversion was almost the same for the NH_3 system and dry reforming (see Figure 6 19). However, the CO_2 conversion was slightly higher for the NH_3 system compared to dry reforming. All other results for lower space velocities are presented in Appendix V

6 4.2 Effect of NH_3 on catalytic stability of $Ni/ZrO_2/\gamma\text{-}Al_2O_3$ catalyst, T = 1073K, WHSV = 19200 ml/hr g cat

A stability test was also carried out for the ZrO_2 promoted catalyst at 1073K and space velocity of 19200 ml/hr g cat since good comparison can be made at higher space velocities. The CH_4 conversions are compared in Figure 6 21 for the three systems The initial CH_4 conversion for both the dry reforming and mixed reforming were almost the same As can be seen in Figure 6 21 the catalyst shows an increase in activity in the CH_4 conversion for the dry reforming. The CH_4 conversion increases linearly from 48 8% to 50 3% with time on stream for the dry reforming A slight increase was also observed for the mixed reforming.

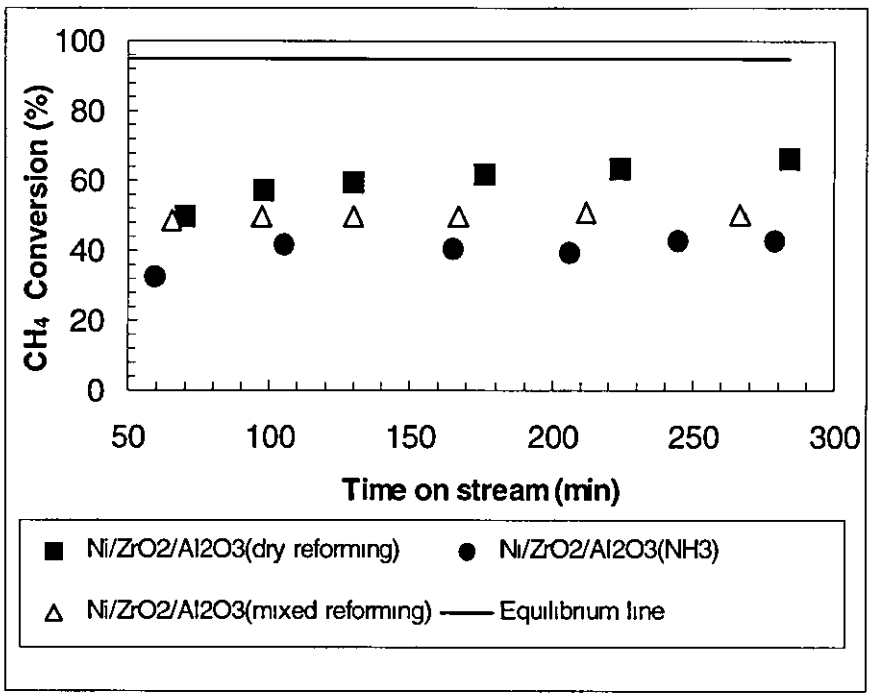

Figure 6.21 CH_4 conversion with time P = 1 atm, T = 1073K, WHSV = 19200 ml/hr g cat catalyst weight = 50mg

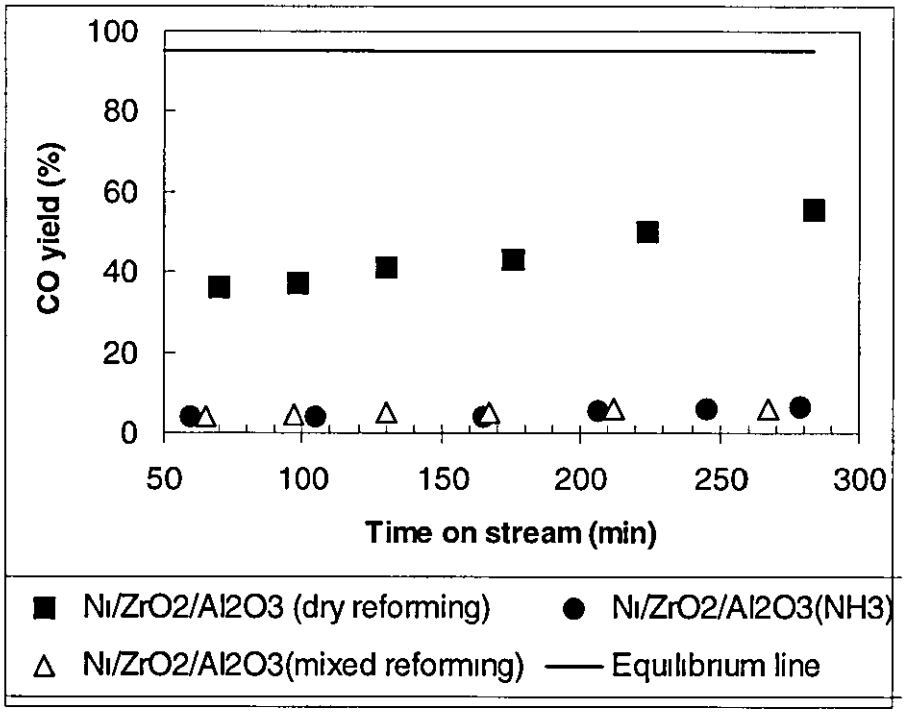

Figure 6 22 CO yield with time P = 1 atm, T = 1073K, WHSV = 19200 ml/hr g cat catalyst weight = 50mg

It clearly indicates that there is activation of the catalyst during reforming. For the NH_3 system, a constant activity was observed until the end of the experimental period (6 hours). However, the CH_4 conversion was lower in the mixed reforming than that of the dry reforming through out the period of 6 hours A much lower CH_4 conversion (32 8%) was observed for the NH_3 system, but increases to 43 1% with time on stream, showing a similar trend. A similar trend was observed for the CO_2 conversion to CH_4 conversion.

A similar trend was observed for the CO_2 conversion to CH_4 conversion. Although, very close initial CO_2 conversions were observed as 51.2% and 47.7% for the dry reforming and mixed reforming, the CO_2 conversion was higher in the dry reforming with time on stream There was a significant difference between the three systems, in the case of the CO yield especially for the dry reforming and the two systems, mixed reforming and the NH_3 system. While a higher initial CO yield of 36.1% was observed in the dry reforming, only 3.8% and 4 2% were observed in the case of the NH_3 and the mixed system.

However a similar trend of increasing CO yield with time was observed in all the three systems because final values of 55.2%, 6% and 6.3% were achieved for the dry reforming, mixed reforming and the NH_3 system respectively.

Although low activity was observed in the two systems compared to dry reforming, no deactivation was observed. Therefore the activity loss in the case of the mixed reforming and NH_3 system is not understood because carbon deposits accumulated in the case for the NH_3 system was even lower than that of the dry reforming. Therefore it is not possible to relate this observation to either coke formation or sintering processes, since further experiment was not conducted for verification.

The ZrO_2 support modified catalyst is a promising, excellent catalyst for dry reforming compared to the other systems studied Introduction of NH_3 and H_2O into the system reduces activity of the catalyst This observation may be due the acidic/basicity properties of ZrO_2 promoted catalyst compared to the unpromoted alumina support that is acidic (Souza *et al* 2001)

The basic nature of NH_3 and H_2O can cause less adsorption capacity for the ZrO_2 promoted catalyst compared to that of the dry reforming system, which is mainly CO_2.

6.4.3 Morphology and Carbon deposit on spent catalyst

Pyrolitic coke is produced on alumina, depending on the surface acidity and the component of the support (Martinez *et al.*, 2004). The addition of zirconia to the Ni/γ-Al_2O_3 sample would favour decrease in the coke formation as the support acidity is lower due to the basic/weak acidic properties of ZrO_2 (Roh *et a.l.*,2 001). The coke formation of Ni/ZrO_2/γ-Al_2O_3 catalyst for the three systems follows the order; 0.11g/g cat < 0.14g/g cat < 0.18g/g cat for NH_3 system, dry reforming and mixed reforming respectively. The activity loss of Ni/ZrO_2/γ-Al_2O_3 during reaction in the NH_3 system is clearly not related to coke formation. The coke formed on the catalyst in the NH_3 system was lower but there was a big difference in activity loss compared to the other systems, indicating that not all coke formed on the catalyst causes deactivation. It is also interesting to note that coke formed on the catalyst in the mixed reforming is more than that formed in NH_3 system, but the activity is higher in terms of CH_4 and CO (see Figure 6.21 and 6.22).

Figure 6.23 SEM image of Ni/ZrO_2/γ-Al_2O_3 catalyst, effect of NH_3 for 6 hours, WHSV = 19200ml/hr g cat

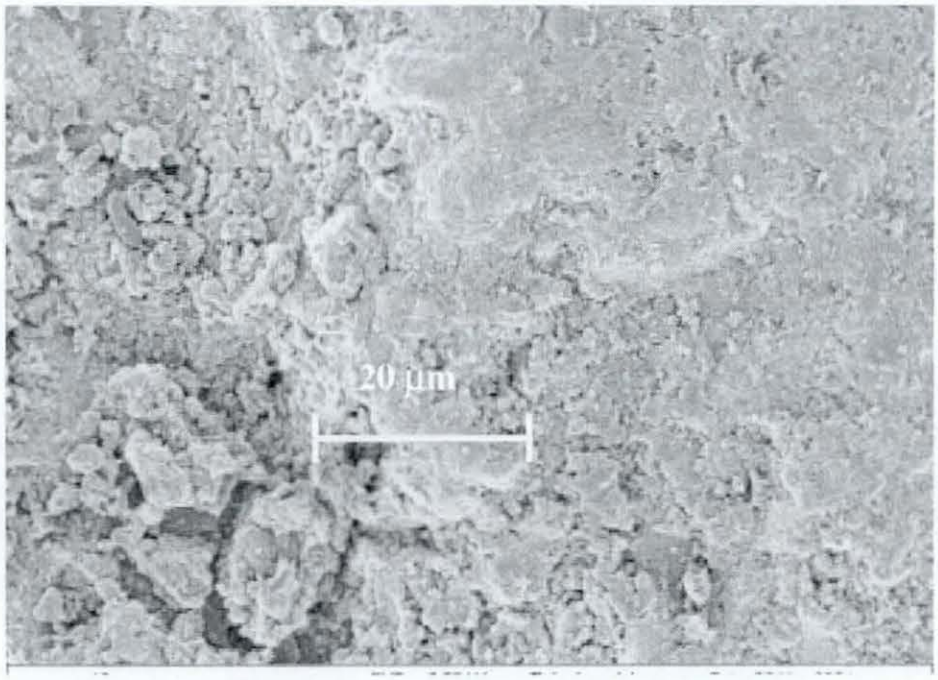

Figure 6.24 SEM image of $Ni/ZrO_2/\gamma\text{-}Al_2O_3$ catalyst, effect of H_2O for 6 hours, WHSV = 19200 ml/hr g cat

The addition of zirconia to the $Ni/\gamma\text{-}Al_2O_3$ sample would favour decrease in the coke formation as the support acidity is lower due to the basic/weak acidic properties of ZrO_2 (Roh *et a.l.*,2001). The coke formation of $Ni/ZrO_2/\gamma\text{-}Al_2O_3$ catalyst for the three systems follows the order; 0.11g/g cat < 0.14g/g cat < 0.18g/g cat for NH_3 system, dry reforming and mixed reforming respectively. The activity loss of $Ni/ZrO_2/\gamma\text{-}Al_2O_3$ during reaction in the NH_3 system is clearly not related to coke formation. The coke formed on the catalyst in the NH_3 system was lower but there was a big difference in activity loss compared to the other systems, indicating that not all coke formed on the catalyst causes deactivation. It also interesting to note that coke formed on the catalyst in the mixed reforming is more than that formed in NH_3 system, but the activity is higher in terms of CH_4 and CO_2 (see Figure 6.23 and 6.24). However, the mechanism of the catalyst poisoning process is not understood. It may be speculated that the presence of both NH_3 and H_2O causes rearrangement of the catalyst surface which may have caused reduction of surface active sites during reforming reaction.

6.5 Effect of space velocity on catalytic activity over Ni-Cu/γ-Al_2O_3 (0.25 wt%) catalyst

6.5.1 NH_3 system, dry reforming and mixed reforming, T = 1073K, WHSV = 4800-19200 ml/hr g cat

Figure 6.25 and 6.26 compare the CH_4 and CO_2 conversion with varying space velocities for the three systems studied at 1073K over Ni-Cu/γ-Al_2O_3 (0.25 wt%) catalyst. The catalyst exhibits high CH_4 conversion for the NH_3 system at lower space velocities < 7840 ml/hr gcat but low CH_4 conversion was observed at higher space velocities > 9820 ml/hr gcat compared to both dry reforming and mixed reforming. For the dry reforming the CH_4 conversion was higher than that of mixed reforming at lower space velocity < 7840 ml/hr gcat. While a decrease in conversion with increasing space velocities was observed for both the dry reforming and NH_3 system, the CH_4 conversion appears to be constant at all space velocities for the mixed reforming (see Figure 6.25). The CO_2 conversion followed a similar trend to CH_4 conversion in the case of the mixed reforming.

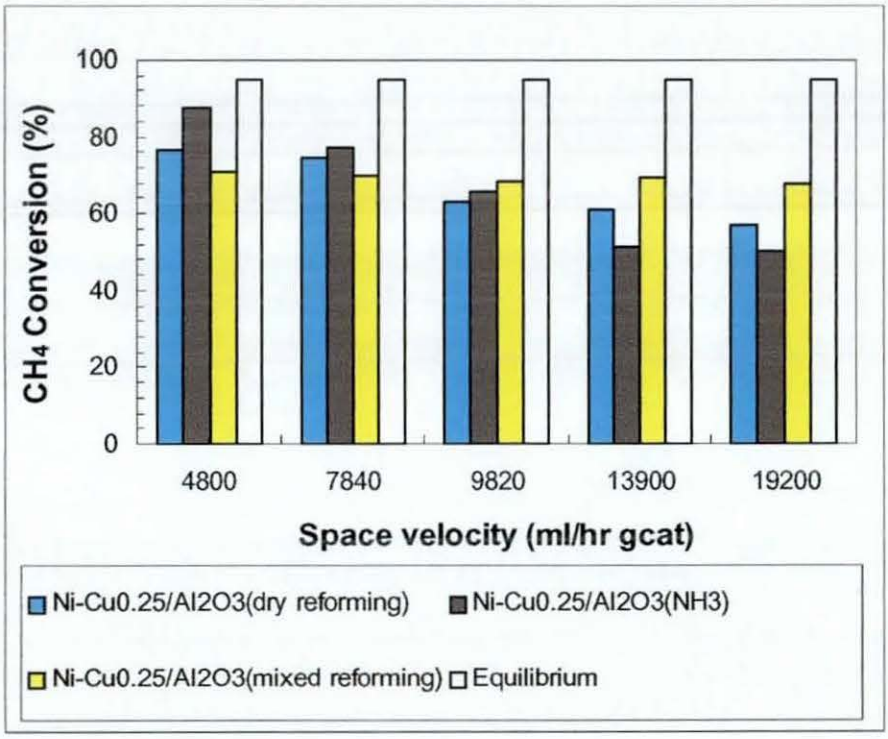

Figure 6.25 CH_4 Conversion as function of space velocity P = 1 atm, T = 1073K, catalyst weight = 50mg

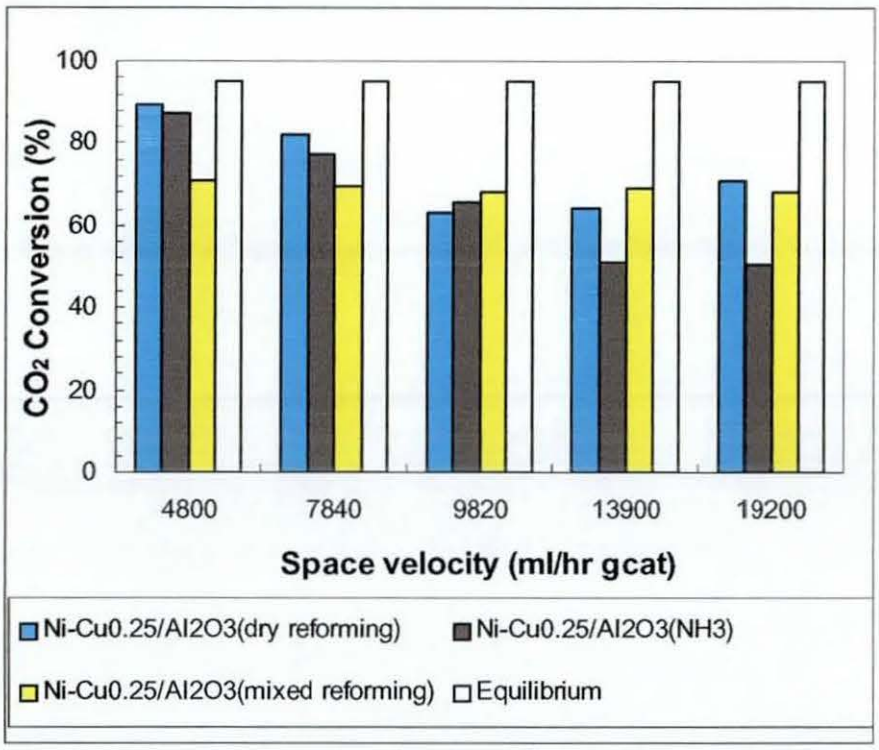

Figure 6.26 CO_2 conversion as a function of space velocity P = 1 atm, T = 1073K, catalyst weight = 50mg

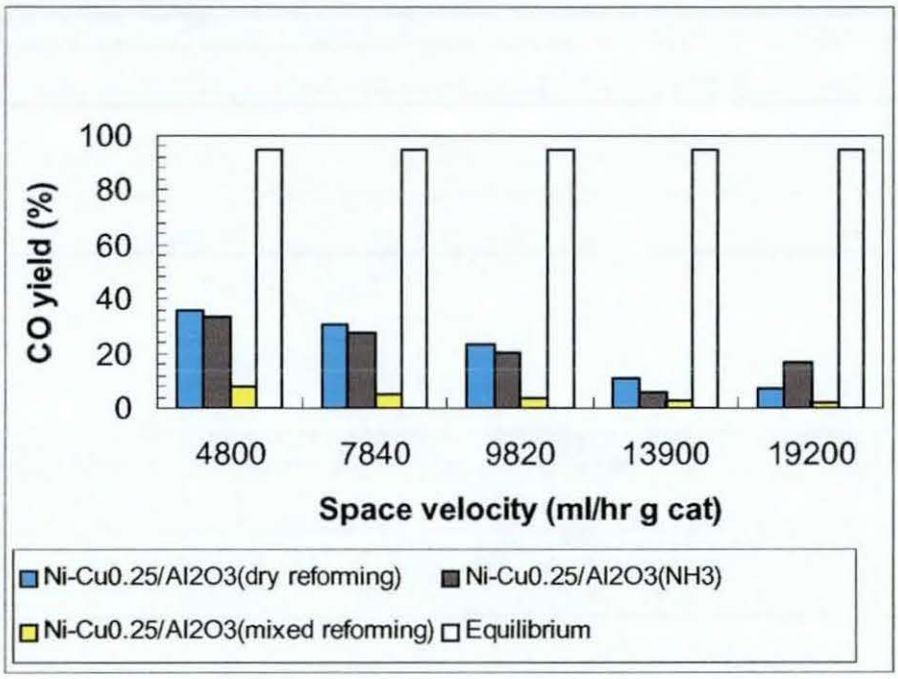

Figure 6.27 CO yield as a function of space velocity P = 1 atm, T = 1073K, catalyst weight = 50mg

However, low CO_2 conversion was observed for the NH_3 system at 4800 ml/hr g cat, 7840 ml/hr g cat 13900 ml/hr g cat and 19200 ml/hr g cat compared to dry reforming The conversion trend for both CH_4 and CO_2 were the same at space velocity of 9820 ml/hr g cat for all the three systems. The CO_2 conversion decreases with increasing space velocity but activity was slightly restored at space velocities > 13900 ml/hr g cat.

The catalyst exhibits higher CO yield for the dry reforming, followed by the NH_3 system at space velocities < 13900 ml/hr g cat At space velocity of 19200 ml/hr g cat, the CO yield was higher for the NH_3 system followed by dry reforming while the lowest CO yield was observed in mixed reforming. With the copper promoted catalyst, the highest activity was achieved at space velocity of 4800 ml/hr g cat and 7840 ml/hr g cat for the NH_3 reforming in terms of CH_4 conversion but the CO yield was still lower than that of the dry reforming It may be speculated that the rate of reaction was enhanced in the NH_3 environment for this catalyst. Also it appears that the copper promoted catalyst promotes decomposition of NH_3 at higher temperatures and lower space velocities

The reasons for the low CO yield may be due to simultaneous occurrence of the WGS reaction during reforming because the CO_2 conversion was lower than that of CH_4 conversion at this space velocity. On the other hand, the CO yield was higher than that of dry reforming at space velocity of 19200 ml/hr gcat even wt low conversions Also the coke formation observed for the NH_3 system was higher than that of dry reforming (see section 6.13) which should have caused a low CO yield. The reason for such unusual observation is not understood However, it is suggested that RWGS reaction was enhanced at this space velocity, increasing the rate of CO yield ($CO_2 + H_2 \leftrightarrow CO + H_2O$).

The effect of temperature on activity for both NH_3 and dry reforming shows no significant difference at 923K and 1023K and space velocity of 19200 ml/hr gcat between the two systems in terms of CH_4 conversion At 973K, the catalytic activity was higher for the NH_3 system while low CH_4 conversion (50.5%) was observed at higher temperatures > 1073K, compared to dry reforming (57.2%). The CO_2 conversion followed a similar trend to CH_4 conversion at 973K (see Figure A5.4 1, Appendix V)

However, a significant difference was observed at 923K and 1023K, where a higher CO_2 conversion was observed for the NH_3 system, but the CO_2 conversion was lower at the temperature of 1023K and 1073K. The CO yield was consistently lower for the NH_3 system at the temperature range of 923K-1023K but it shows an increase with increasing temperature. It is an indication that the rate of CO increases with increasing temperature. Although copper is among the metal that exhibits low activity for decomposition of NH_3 (Ganley *et al*, 2004) the copper promoted nickel catalyst shows higher activity for the NH_3 system especially at 973K in terms of CH_4 and CO_2 and highest CO yield at 1073K.

At 1023K and space velocity of 13900 ml/hr gcat low CH_4 conversion was observed for the NH_3 system. Similar results were observed at all other temperatures The CO yield did not actually follow the trend to CH_4 and CO_2 conversion. Very low CO yield was observed for the NH_3 system, except at 1023K, where the CO yield was higher compared to dry reforming. The CO yield at 1023K and 1073K did not follow the trend observed at the space velocity of 19200 ml/hr gcat. Higher CO yield was obtained for the NH_3 system at 1023K, while very low CO yield was observed at 1073K for the NH_3 system compared to dry reforming (see Figure A5 4 2, Appendix V).

At space velocity of 9820 ml/hr gcat CH_4 conversion (50 5%) for both CH_4 and CO_2 conversions were higher in the NH_3 system at all temperatures compared to that of 19200 ml/hr gcat (see Figure A5.4.3). The CO yield also followed a similar trend to conversions of CH_4 and CO_2 However, the CO yield showed higher values in the NH_3 system compared to the dry reforming at lower space velocities.

6 5 2 Effect of NH_3 and H_2O on catalytic stability over Ni-Cu/γ-Al_2O_3(0 25 wt%) catalyst, T = 1073K, with NH_3, dry reforming and mixed reforming

Stability test carried out over the Ni-Cu/γ-Al_2O_3 (0 25 wt%) catalyst shows that there was no significant deactivation during reaction with the three systems studied at 1073K and space velocity of 19200 ml/hr gcat. The CH_4 conversion was higher in the mixed reforming with initial CH_4 conversion of 68.7% with stable activity. The same observation was made for both dry reforming and the NH_3 system. The initial CO_2 conversion was higher in the dry reforming compared to mixed reforming and the NH_3 system but all the CO_2 conversions values for the three systems were converged at the end of the 6 hours run

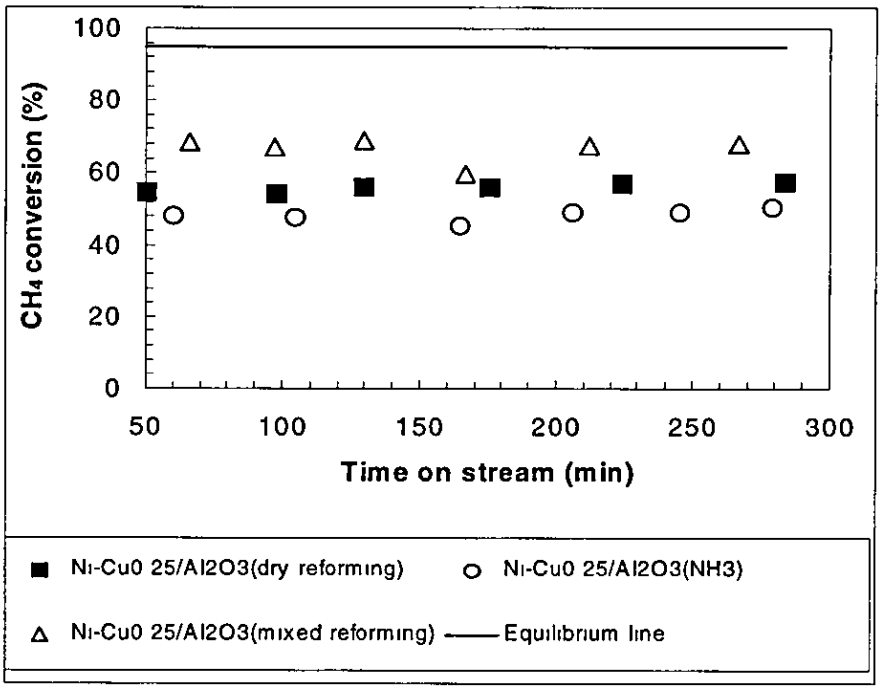

Figure 6 28 CH_4 conversion as a function of time P = 1 atm, T = 1073K, WHSV = 19200ml/hr g cat catalyst weight = 50mg

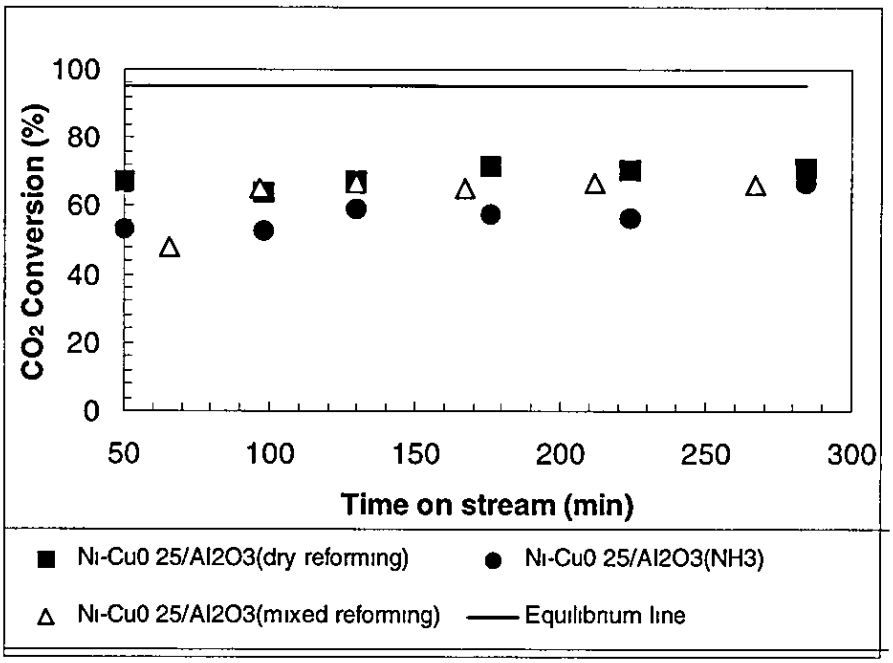

Figure 6.29 CO_2 conversion as a function of time P = 1 atm, T = 1073K, WHSV = 19200ml/hr g cat, catalyst weight = 50mg

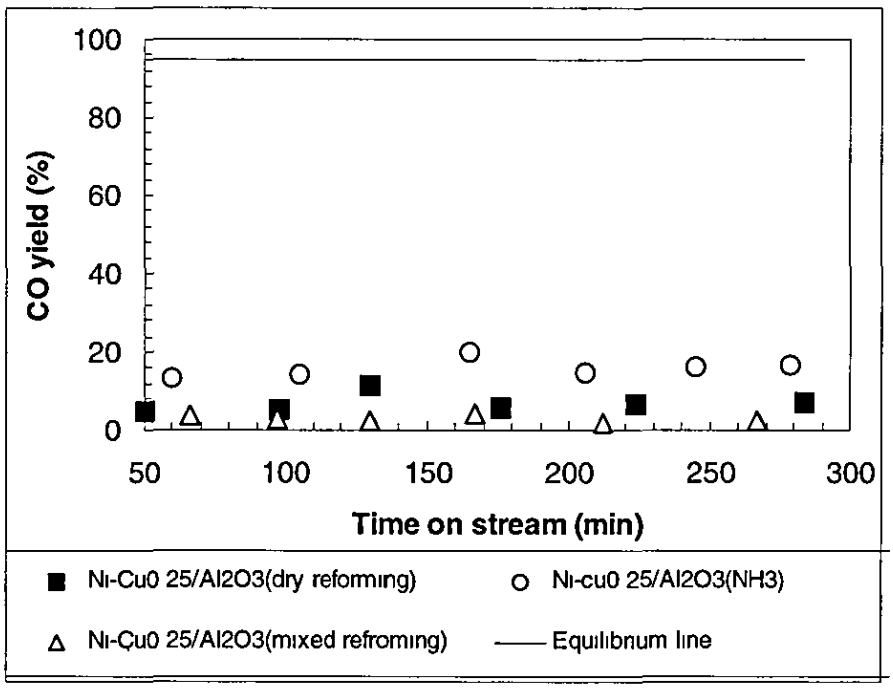

Figure 6.30 CO yield as function of time P = 1 atm, T = 1073K, WHSV = 19200ml/hr gcat catalyst weight = 50mg

Despite the fact that lower CH_4 and CO_2 conversions were observed for the NH_3 system, CO yield was higher than that of mixed and dry reforming. It then suggests that the rate of CO yield was enhanced in the NH_3 system, an indication of significant RWGS reaction ($CO_2 + H_2 \leftrightarrow CO + H_2O$). This is confirmed with the CO_2 conversion being higher than that of CH_4 conversion.

This is confirmed with the CO_2 conversion being higher than that of CH_4 conversion. However, a similar trend of CO yield for both NH_3 and dry reforming were observed with time on stream. However, the mixed reforming exhibits the lowest CO yield although higher conversions were observed It is possible that the WGS reaction was significant ($CO + H_2O \leftrightarrow CO_2 + H_2$.

6.5.3 Morphology of spent catalyst and carbon deposition

The coke formation of this catalyst follows the order 0.09g/g cat < 0.14g/g cat < 0.18g/g cat for dry reforming, NH_3 system and mixed reforming respectively. It shows that the coke accumulation is larger in the mixed reforming compared to the NH_3 system. Also the coke deposition is higher in NH_3 system compared to dry reforming. Although, the activity was lower in the NH_3 system, higher CO yield was observed in the NH_3 system. It suggests that the CO disproportionation reaction was favoured in the mixed reforming that must have lead to the high coke formation compared to the other systems.

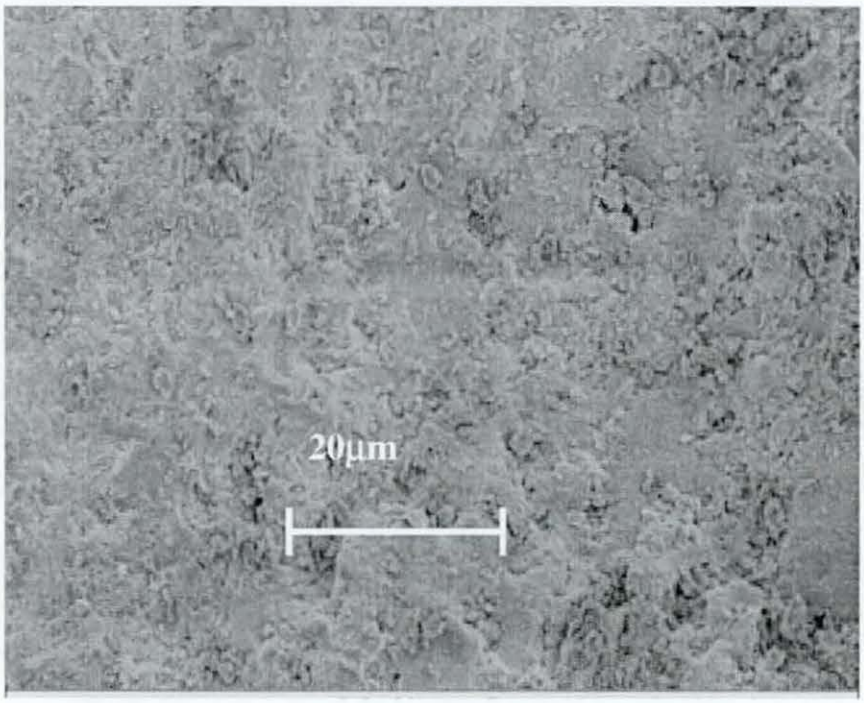

Figure 6.30 SEM image of Ni-Cu/γ-Al_2O_3 (0.25 wt%), effect of H_2O for 6 hours, WHSV = 19200ml/hr g cat, P = 1atm, T = 1073K

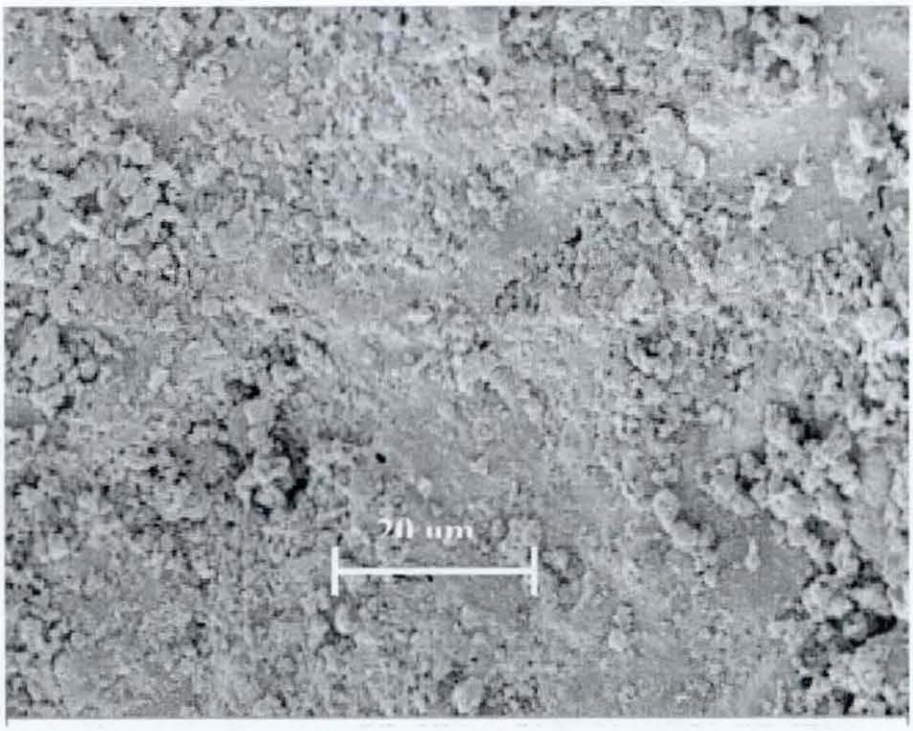

Figure 6.31 SEM image of Ni-Cu/γ-Al_2O_3 (0.25 wt %), Effect of NH_3 for 6h, WHSV=19200 ml/hr gcat, P=1atm, T=1073K

Although the catalyst exhibits lower activity in both dry reforming and NH_3 system, the high CO yield in these systems suggest that the reverse water gas shift reaction was favoured under the condition employed. At higher space velocity and temperature the rate of CO yield was increased.

6.14 Conclusion

The effect of NH_3 (3000 ppm) in the feed stream on unpromoted Ni/γ-Al_2O_3 catalyst, Ni-Pd/γ-Al_2O_3 (0.25 wt%), Ni-Cu/γ-Al_2O_3 (0.25 wt%) and Ni/ZrO_2/γ-Al_2O_3 have been investigated at temperatures ranging from 923K–1073K and varying space velocities of 4800–19200 ml/hr gcat.

The activity (CH_4 conversion) of the unpromoted Ni/γ-Al_2O_3 catalyst was higher at all temperatures and space velocities studied with the NH_3 system.

Catalyst activation was observed during reforming with NH_3 feed, due the diffusion of nitrogen in to the surface of nickel catalyst, which must have caused more surface active sites. The introduction of NH_3 in the feed stream has enhanced both the activity and stability of the unpromoted catalyst. On the other hand, H_2O in the feed stream also increases the CH_4 conversion at higher space velocities of > 9820 ml/hr g cat and 13900 ml/hr g cat compared to the dry reforming. However lower CO_2 conversions were observed which agrees with reports in literature (Effendi *et al.*, 2002)

No visible carbon deposits were observed with the unpromoted catalyst but the burn off revealed carbon deposition on the catalyst for all the three systems The carbon deposits for the NH_3 system was higher compared to both dry reforming and mixed reforming, but did not have any effect on the activity and stability. It may be due to the type of carbonaceous species formed on the catalyst during reforming that can not cause deactivation. The NH_3 in the system did not only improve activity and stability but may have also caused changes in structure of carbon formed on the catalyst.

In the case of Ni-Pd/γ-Al_2O_3 (0 25 wt%) catalysts, there was activity loss at all temperatures and space velocities employed for the NH_3 system. The carbon deposition in the NH_3 system was lower compared to the other systems but that not withstanding, the catalyst exhibits low activity. It suggests that the type of carbon formed deactivates the catalyst or the catalyst surface have been covered up by adsorbed NH_3 species It needs further investigation to verify the above speculation. Although the activity was low for the mixed reforming, highest CO yield was attained at 19200 ml/hr gcat and temperatures of 1073K, followed by the NH_3 system. There was also a slight decrease in activity in the presence of H_2O in the feed and lower CO yield compared to dry reforming except at 19200 ml/hr gcat and temperature of 1073K. Although there was loss in activity, the presence of NH_3 and H_2O in the feed stream did not affect the stability of the catalysts under the conditions employed. The highest carbon deposition was found in the mixed reforming

Among the three systems studied the $NiZrO_2$/γ-Al_2O_3 catalyst exhibits the highest activity in dry reforming Compared to NH_3 system, the activity was higher in mixed reforming at 13900 ml/hr gcat and 19200 ml/hr gcat at 1073K. However, the carbon deposition on the catalyst was lower in the NH_3 system compared to the other systems.

It then suggest that the low activity may not be related to carbon deposition. The $Ni/ZrO_2/\gamma$-Al_2O_3 catalyst is also not a promising catalyst in the presence of water but excellent for dry reforming. It can promote the reverse water gas shift reaction, which can result in the stoichiometric product ratio of 1 0 for down stream application.

For Ni-Cu/γ-Al_2O_3 (0.25 wt%) catalyst excellent performance was observed at 973K and space velocity of 19200 ml/hr gcat in NH_3 system, although the CO yield is slightly lower than that of dry reforming At 1073K, the CO_2 and CH_4 conversions were lower in NH_3 system compared to dry reforming but higher CO yield was achieved. This is a clear indication of significant RWGS reaction because with in the NH_3 system, CO_2 conversion was higher than that of CH_4 conversion The catalytic performance of the catalyst depends on the space velocity, because, at the same temperature activity varies with varying space velocity.

CHAPTER 7

CONCLUSIONS AND RECOMMENDATIONS

7.1 Conclusions

A reactor for conducting the reforming of simulated biogas (CH_4/CO_2 as model gas) over Ni-based supported catalysts was assembled and commissioned. Provision for direct injection of products into a Gas Chromatograph equipped with a thermal conductivity detector (on-line analysis) was included. Process conditions (temperature and pressure) were predicted (1073K and 1atm) and the values were used to determine the equilibrium mole fractions of both reactants and products The equilibrium constants and rate constants for the three independent reactions considered for CO_2 reforming were also determined. Furthermore, a model was developed to estimate the rate constants for the three independent reactions considered for CO_2 reforming

Ni-based supported catalysts such as $Ni/\gamma\text{-}Al_2O_3$ (reference catalyst), $Ni/ZrO_2/\gamma\text{-}Al_2O_3$, $Ni/MgO/\gamma\text{-}Al_2O_3$ and $Ni/La_2O_3/\gamma\text{-}Al_2O_3$ were prepared using the incipient wetness impregnation technique Further catalysts included Ni/Pr_2O_3, and Ni-promoted catalysts ($Ni\text{-}Pd/\gamma\text{-}Al_2O_3$ and $Ni\text{-}Cu/\gamma\text{-}Al_2O_3$) From the experimental results of CO_2 reforming of methane on the support promoted catalyst, it was found that modification of support has enhanced both the activity and stability. The transition oxide promoted catalysts exhibited stability compared to unpromoted catalysts ($Ni/\gamma\text{-}Al_2O_3$) at temperatures > 973K and higher space velocities. The activity of $Ni/ZrO_2//\gamma\text{-}Al_2O_3$ and $Ni/La_2O_3/\gamma\text{-}Al_2O_3$ increased with increasing temperature while the activity for the unpromopted catalyst $Ni//\gamma\text{-}Al_2O_3$ (the reference catalyst) and $Ni/MgO/\gamma\text{-}Al_2O_3$ decreased at temperatures above 1073K, and space velocity of 19200 ml/hr g cat due to carbon deposition The unpromoted catalyst showed deactivation during a reaction time of 6 hours compared to the support promoted catalysts The ZrO_2–containing catalyst showed the highest CO yield, at all space velocities at 1073K The amount of carbon deposits observed on the catalysts surface revealed that catalyst deactivation depends on the type of carbon formed. This is confirmed with the observation in this study over $Ni/ZrO_2/\gamma\text{-}Al_2O_3$ and the unpromoted catalyst. Although they have the same amount of carbon deposited, only the latter showed deactivation

The rate constant for the $Ni/ZrO_2/\gamma\text{-}Al_2O_3$ catalyst was higher compared to the unpromoted catalyst. However, high CO activation energy (89 kJ/mol) was obtained for the $Ni/ZrO_2//\gamma\text{-}Al_2O_3$ catalyst whilst activation energy of 40 kJ/mol was obtained for the unpromoted catalyst.

Activation energies of CH_4 and CO_2 are 29 8 kJ/mol, 26 kJ/mol and 33 kJ/mol, 29.9 kJ/mol for $Ni/ZrO_2/\gamma\text{-}Al_2O_3$ and the unpromoted catalyst respectively. Several authors have indicated that deactivation is attributed to carbon formation surrounding the metal-support perimeter (Souza *et al.*, 2002). The high CO yield may be due to interfacial sites on $Ni\text{-}ZrO_x$ which are active for CO_2 dissociation, providing active species of oxygen that may react with carbon formed by CH_4 decomposition. Additionally, the ZrO_2 promoted support can actively participate in the catalytic reaction by oxidizing or reducing reaction intermediates (redox properties). Also, the lack of significant concentration of strong Lewis acid sites may cause less deactivation of the catalyst because carbon hardly forms at all on ZrO_2 (Nagaoka *et al*, 2001) The Ni/Pr_2O_3 catalyst showed activity at higher temperatures but no significant activity was observed at lower temperatures. This poor performance may be attributed to the reduced surface area which may have been caused by sintering during heat treatment

The palladium promoted catalysts ($Ni\text{-}Pd/\gamma\text{-}Al_2O_3$) exhibited higher catalytic activity and stability especially at higher temperatures compared to the unpromoted Ni catalysts ($Ni/\gamma\text{-}Al_2O_3$). The activation energy for CH_4 and CO_2 for the palladium promoted catalyst were 11 kJ/mol and 6 6 kJ/mol whilst 32 9 kJ and 29.8 kJ were obtained for the unpromoted catalyst. The activity decreases with increasing palladium loading in terms of CO_2 and CH_4 conversions. The catalyst promoted with low levels of palladium (0.25 wt% and 0.5 wt%) showed similar activities while lower activity was observed over $Ni\text{-}Pd/\gamma\text{-}Al_2O_3$ (1 wt%) catalyst. However, CO yield was highest for the unpromoted catalysts. Promotion with low level of palladium caused a drastic decrease in CO yield With increasing palladium loading, CO yield increases, although a high coke deposition was observed The reason why high coke deposition of $Ni\text{-}Pd/\gamma\text{-}Al_2O_3$ (1 wt%) associated with a higher CO yield among the promoted catalysts is unclear. Less coke deposition is usually caused by suppression of the Boudouard reaction.

Small levels of palladium appear to promote this behaviour. Calculation of individual rate constants quantified this effect but it is also unclear what type of interaction between Ni and Pd is responsible for this effect Although, addition of palladium increases activity, it did not actually reduce the coke formation compared to the unpromoted catalyst despite stability recorded with the promoted catalysts.

The BET surface area decreased with increasing palladium content, which subsequently led to a decrease in dispersion. This might also have an effect on the activity since accessibility of reactants to active sites is high on meso-porous supports which maintain dispersion and hence increase in the adsorption of CO_2 for high reactivity.

Compared with the unpromoted catalyst, the activity and stability of copper promoted catalyst (Ni-Cu/γ-Al_2O_3) for CH_4/CO_2 reforming was enhanced remarkably at 1073K, WHSV = 19200 ml/hr g cat, although it negatively affected the initial activity. The copper promoted catalysts exhibited lower initial activities, compared to the unpromoted catalyst. The low initial activity may be due to slower rate of CH_4 consumption. The CO yield was lower for all copper promoted catalysts compared to the unpromoted catalyst. The rate of CO formation was higher for the unpromoted catalyst compared to copper promoted catalyst

It was found that the influence of copper on the nickel based catalyst depended strongly on the amount of copper added, temperature and the space velocity. The Ni-Cu/γ-Al_2O_3 (1 wt%) catalyst indicates the highest CO_2 and CH_4 conversion at all temperatures > 1073K where decrease in conversion was observed which may be due to carbon deposits or sintering processes at a space velocity of 19200 ml/hr g cat. No further experiments were conducted to verify this speculation especially for the sintering processes. The CO yield for Ni-Cu/γ-Al_2O_3 (1 wt%) catalyst was high at 1073K compared to the other copper promoted catalysts but no significant CO yield was observed at 973K and 1023K. At 1073K, the Ni-Cu/γ-Al_2O_3 (0.25 wt%) catalyst showed the highest CO_2 conversions but lower CO yield was observed while the lowest conversion in terms of CH_4 and CO_2 was observed for Ni-Cu/γ-Al_2O_3 (0.5 wt%) at all temperatures.

Coke deposition increases as the amount of copper decreased which also agrees with the CO yield results. It shows that the rate of CO formation increases with increasing amount of copper, which indicates significant occurrence of the RWGS reaction.

Coke deposition for Pd promoted catalyst increased with increasing Pd loading, while a decrease in coke formation was observed for the Cu promoted catalyst. The decrease in coke formation for Cu promoted catalyst may be due to high reduction in H_2 atmosphere, which can contribute to rapid gasification of coke formed during reforming.

The effect of NH_3 (3000 ppm) in the feed stream on unpromoted $Ni/\gamma\text{-}Al_2O_3$ catalyst, $Ni/Pd/\gamma\text{-}Al_2O_3$ (0.25 wt%), $Ni\text{-}Cu/\gamma\text{-}Al_2O_3$ (0 25 wt%) and $Ni/ZrO_2/\gamma\text{-}Al_2O_3$ catalysts investigated at temperatures ranging from 923K–1073K and space velocities of 4800–19200 ml/hr g cat show increase in activity especially for the unpromoted catalyst.

The activity (CH_4 conversion) of the unpromoted $Ni/\gamma\text{-}Al_2O_3$ catalyst was higher at all temperatures and space velocities with NH_3 addition compared to dry CO_2 reforming The catalyst activation observed with NH_3 feed, may be due to the diffusion of nitrogen at the surface of nickel, which causes mobility that may lead to exposure of more surface active sites.

The stability of the umpromoted catalyst was also enhanced. The presence of H_2O also increased the CH_4 conversion at higher space velocities > 9820 ml/hr g cat and 13900 ml/hr g cat compared to the dry reforming. However lower CO_2 conversions were observed which agrees with reports in literature (Effendi *et al* , 2002)

No visible carbon deposits were observed with the unpromoted catalyst but the burn-off method revealed carbon deposition on the catalyst for all three systems. The carbon deposits for the NH_3 system was higher compared to both dry reforming and mixed reforming, which shows that the carbon deposits have no effect on the activity and stability It appears that the presence of NH_3 also affect the type of carbon deposit formed on the catalyst. Catalyst deactivation depends on the type of coke formed.

From these findings, it is clear that the coke formed on the unpromoted catalyst for the NH_3 system is different from that for the dry reforming since deactivation was only observed for the latter. Further investigation is needed to verify this claim.

In the case of Ni-Pd/γ-Al_2O_3 (0 25 wt%) catalysts, there was activity loss at all temperatures and space velocities employed for the NH_3 system. Carbon deposition in the NH_3 system was lower compared to the other systems but that not withstanding, the catalyst exhibits low activity. It suggests that the activity loss may be due to the type of carbon formed or that the catalyst surface may have been covered up by adsorbed NH_3 species. It appears the addition of palladium has retarded the decomposition of NH_3. It needs further investigation to verify the above speculation.

Although the activity was lower for the mixed reforming, highest CO yield was attained at 19200 ml/hr g cat and at a temperatures of 1073K, followed by the NH_3 system There was also a slight decrease in activity in the presence of H_2O in the feed and lower CO yield compared to dry reforming except at 19200 ml/hr g cat and at a temperature of 1073K. Although there was loss in activity, the presence of NH_3 and H_2O in the feed stream did not affect the stability of the catalysts under the conditions employed. The highest carbon deposition was found in the mixed reforming

Among the three systems studied, the NiZrO_2/γ-Al_2O_3 catalyst exhibits the highest activity in dry reforming. Compared to the NH_3 system, the activity was higher in mixed reforming at space velocities of 13900 ml/hr g cat and 19200 ml/hr g cat at 1073K. However, the carbon deposition on the catalyst was lower in the NH_3 system compared to the other systems. It then suggests that the low activity may not be related to carbon deposition The Ni/ZrO_2/γ-Al_2O_3 catalyst is also not a promising catalyst in the presence of water but excellent for dry reforming It can promote the reverse water gas shift reaction, which can result in the stoichiometric product ratio of 1 0 for down stream application.

For the copper promoted Ni-catalyst (Ni-Cu/γ-Al_2O_3 (0.25 wt%), excellent performance was observed at 973K and space velocity of 19200 ml/hr gcat in NH_3 system, although the CO yield is slightly lower than that of dry reforming.

At 1073K, the CO_2 and CH_4 conversions were lower in NH_3 system compared to dry reforming but higher CO yield was achieved. This is a clear indication of significant RWGS reaction because with the NH_3 system, CO_2 conversion was higher than that of CH_4 conversion.

7.2 Recommendations and Further work

One aspect of the present study that should be looked into is the experimental arrangement; the gas chromatograph (Shimazdu 8A instrument with a TCD detector) used for the exit gas analysis could not analyse H_2 which is one of the products of reforming Therefore calculations for H_2 yield were based on mass balance. A modification on the current experimental set up is therefore suggested, which should include an additional GC (Hp-3392 integrator). Also, the thermocouple arrangement allowed only temperature measurements outside the wall of the reactor for the catalyst bed A thermocouple within a thermo-well be could be used for direct contact to the catalyst–bed in order to measure the temperature.

The present work focused on simulated biogas (CH_4/CO_2 as model gas). Future studies should employ biogas produced by gasification of wood or from anaerobic digestion of organic waste materials. The need for further study on biogas production is clearly identified In particular, detailed information is required on the composition of biogas with respect to catalyst poisoning. As shown in (Table 1.1), not much information is available on biogas composition in literature This limited study may be due to the fact that biogas produced, has been used mainly for energy consumption in which detail composition data was not necessary. Gas composition may be by source as well as the process condition For example, wood gas produced by gasification (wood waste) differs from digester gas (domestic/industrial waste) in that its main fuel energy component is hydrogen rather than methane (White and Plaskett 1981). Moreover, compositions may vary from site to site. From the study on catalyst poisoning it has been clearly identified that activities vary depending on the interaction of NH_3 with the catalyst. Although the cause of this varying performance is unclear, the fact remains that trace amounts of NH_3 can cause significant effect on the catalyst activity.

Such studies will lead to better understanding of the composition of biogas as it affects the reforming performance of a catalyst, especially the CH_4/CO_2 ratio, and trace amount of components

The nickel crystallite size depends on the method of catalyst preparation employed The present study used the incipient wetness impregnation technique (Ni crystallite sizes ranging from 26 nm-38 nm were obtained which fall within the range of 2 nm-50 nm nickel crystallites sizes mainly for meso pores for the support modified catalysts The crystallites sizes can be reduced using other techniques such as the co–precipitation method (Hou *et al,* 2003) Increasing the calcination temperature will strengthen the interaction between Ni and the support that leads to spinel formation The reduction of spinel at higher temperature results in smaller Ni crystallites sizes which also contributes to retarding of catalysts sintering It is therefore recommended that future studies should also investigate the effect of calcination temperature. Nickel loading affects activity and coke deposition In this study, nickel loading as well as oxide promotion used was conducted at fixed values i.e. 15 wt% Ni and 5 wt% oxide respectively. Catalysts with varying loading of Ni and oxide promotion should be prepared in order to investigate the effect of loading on dispersion, surface area as well as catalytic activity.

Catalyst deactivation is mainly caused by coke deposition and sintering Sintering occurs at higher temperatures as a result of migration of nickel particles within the catalyst. In the present study, the only method used to estimate the amount of coke deposited was burn-off method. This burn-off method could not give a clear picture of the type of coke formed, which also affects the activity and stability of the catalyst. Therefore, further characterisation is recommended to investigate coke formed on the catalyst

As mentioned earlier the present investigation did not present a clear picture of the correlation between the high activity and stability observed on the palladium promoted catalyst and coke deposition. Therefore, spent catalysts characterisation should be extended to thermo-gravimetric analysis method and temperature programmed oxidation (TPO). These experiments will lead to the understanding of the oxidation state of nickel and the nature of carbonaceous species formed during reforming

Also future studies on characterisation of catalyst by X-ray diffraction (XRD), surface area as well as TPR should be conducted, so that better conclusions are drawn on catalyst deactivation if it is caused by sintering or coke deposition.

The present studies on catalyst poisoning are limited to NH_3. The unusually high activity observed for the unpromoted catalyst in the NH_3 system is not well understood. On the other hand, ZrO_2-promoted catalysts as well as nickel promoted catalyst with palladium and copper show loss of activity at most of the temperatures investigated. Although it has been speculated that one possible reason may be due to decomposition of NH_3 by nickel and rearrangement at the catalyst surface by the diffusion of N_2, no further studies have been conducted to understand the reaction mechanisms involved Therefore, future work is recommended to look into the mechanism of this reaction, for better understanding

For mixed reforming (effect of H_2O), experiments were limited to a temperature of 1073K and a space velocity of 19200 ml/hr g cat, in order to compare with the other systems of reforming, due to limited time. Future work should be extended to lower temperatures and space velocities which may also help to draw reasonable conclusions.
Biogas composition includes trace amounts of H_2S (1000-3000 ppm) The present experimental set-up is limited to only NH_3, in which it was fed into the system by saturation. Therefore, future work should include modification of the experimental rig, to provide a possible channel to introduce H_2S.

The kinetic study in this work could not render a complete data for proper validation of the process. The data obtained from the model equations were used to only calibrate the experiment data. Although, the general stepwise mechanism has been proposed by many research groups (e g Souza *et al.*, 2001) where in the rate determining step CH_4 decomposed to H_2 and active carbon, followed by direct and fast conversion of this carbon with CO_2 to CO. Other research groups (ref) have proposed mechanism based on CH_4 activation forming CH_x and CH_x O decomposition as the slow kinetic steps with the fact that CO_2 takes part in the reaction mechanism only through the RWGS reaction to produce surface OH groups that react with the adsorbed CH_x to yield formate species. The present study did not present a clear picture of this mechanism since the support played a vital role in the activity and stability

Therefore, future study should extend the kinetic study to investigate the TAP experiments, especially with the zirconia promoted catalyst for more understanding of the presence of oxygen pool The high activation energy barrier for CO formation with the high CO yield observed for the zirconia promoted catalyst is also unclear

Finally, a new catalyst (Ni-Pd/CeO_2) is proposed for future study. The palladium promoted catalyst showed high activity in terms of CH_4 and CO_2 but high coke deposition was observed. Cerium oxide is one of the best supports in Ni-based for CO_2 dry reforming (Roh *et al* , 2004) because of the oxygen storage capacity. This new catalyst may cause less coke formation with high activity.

REFERENCES

Aparico, L. M. (1997), "Transient isotopic studies and micro kinetic Modelling of methane Reforming over Nickel catalyst," *Journal of Catalysis,* **165,** pp 262–274

Asami, K. Li, X. Fujimoto, K. Koyama, Y. Sakurama, A Kometani, N and Yonezawa, Y. (2003), "CO2 reforming of CH4 over ceria-supported metal catalysts," *Catalysis Today,* **84**, 27-31

Ashcroft, A.T. Cheetham, A.K. Foord, J S. Green M.L.H Grey, C.P Murrel, A J and Vernon, P D F. (1990), "Selective oxidation of methane to synthesis gas using transition metal catalyst," *Nature,* **344**, pp 319-321

Ashcroft, A.T. Cheetham, M.L.H Green and Vernon P D F, (1991), "Partial oxidation of methane to synthesis gas using carbon dioxide," *Letters to Nature,* **352**, p 224 (1991)

Bartholomew, C.H. (1984), "Catalyst deactivation," *Chem. Energy*, 91 pp 96-112

Balker, A. and Maciejewski, M. (1984), "Formation and Thermal Stability of copper and Nickel Nitride," J Chem Soc , Faraday Trans, **80,** pp 2331-2341

Basini, L and Sanfilippo, D (1995), "Molecular Aspects in Syngas production: The CO_2 Reforming reaction case," *Journal of Catalysis,* **157,** pp 162–178

Bitter, J.H, Seshan, K; and Lercher, J A; (1997), "The state of ZrO_2 supported platinum catalyst for CO_2 /CH_4 reforming," *Journal of Catalysis,* **171**, pp 279 –286

Bitter, J.H. Seshan, K. and Lercher, J A (1999), "Deactivation and coke accumulation during CO_2/CH_4 reforming over Pt catalyst," *Journal of catalysis* **183**, p336

Blander, M, (1999), "Biomass gasification as a means for avoiding fouling and corrosion during combustion," *Journal of Molecular Liquids,* **83**, pp 323-328

Blom, R. Dah, I M. Slagtern, D.I M. Soortland, B. Spjelkavik, A. and Tangtad, E. (1994), "Carbon dioxide reforming of methane over lanthanum-modified catalysts in a fluidised–bed reactor," *Catalysis of Today,* vol. **21,** pp 535 -543

Bridgwater, A.V. (1984), "Thermochemical processing of Biomass", Publishers, ButterWorth and Co Ltd, London First Edition, pp 35

Boyle, D (1984), "Bio-Energy Technology, Thermodynamic and costs," Publishers, Ellis Horwood, Chichester, England, First Edition p 67

Bradford, C J and Vannice, M.A. (1996a)," Catalytic reforming of methane with carbon dioxide over nickel catalysts 1 Catalyst characterisation and activity," *Applied Catalysis A· General* **142** pp 73-96

Bradford, C J and Vannice, M A (1996b)," catalytic reforming of methane with carbon dioxide over Nickel catalysts II Reaction kinetics," Applied Catalysis A: general **142** pp 97-122

Bradford, M C J and Vannice, M.A. (1998), "CO_2 reforming of CH_4 over supported Pt catalysts," *Journal of Catalysis*, 173, pp 157-171

Bradford, M C J and Vannice, M A. (1999), "The role of metal-support interactions in CO_2 reforming of CH_4," *Catalysis Today*, 50, pp 87-96

Chang, J-S, Park, S-E , Yoo, J W and Park, J-N , (2000), "Catalytic behaviour of supported KNiCa catalysts and mechanistic condensation fro carbon dioxide Reforming of methane," *Journal of Catalysis,* **195,** pp1-11

Chen, Y and Wang, W; (2000), "Carbon dioxide reforming of methane to synthesis gas over Ni/MgO-Al_2O_3-$AlPO_4$ catalyst," *Abstracts of papers of the America chemical Society 219 PETR PART 2* **26**

Chen, Z.X Zhao, X G. Li, J.L. and Zhu, Q.M (2001), "Role of support in CO_2 reforming of CH_4 over a Ni/Al_2O_3 catalyst," *Applied Catalysis A. General,* **205,** pp 31-36

Chen, Y-Z. Liaw, J-B.and Lai, H-W. (2002), "ZrO_2/SiO_2 and La_2O_3/Al_2O_3- supported platinum catalysts for CH_4/CO_2 reforming," *Applied Catalysis A. general* **230** pp73-83

Claridge, J B. green, M.L. H. and Tsang, S.C. (1994), "Methane conversion to synthesis gas by partial oxidation and reforming over rhenium catalysts," *Catalysis Today,* **21,** pp 455–460

Cheremisinoff, N P. (1979), "Gasohol for Energy production," Energy Technology Series, Ann Arbor Science, Michigan, United State of America First Edition pp 3

Cheng, Z.X. Zhao, X.G. Li, J L. and Zhu, Q M (2001), "Role of support in CO_2 reforming of CH_4 over a Ni/Al_2O_3 catalyst," *Applied Catalysis A: General,* **205,** pp 31-36

Cheng, H Reiser, D B Mathias, M P. Baumert, K and Dean, Jr. S W (1995), "Investigation of Nitriding mechanism at Transition metal surfaces: NH_3 Adsorption and Decomposition on Fe(100), Ni(100), and Cr(100)" *J Phys Chem.,* **99,** pp 3715-3722

Choudhary, V.R, Mamman, A. S. and Uphade B, (2001), "Steam and oxy-steam reforming of methane to syngas over $Co_xN_{1-x}O$ supported on MgO precoated SA–5205,"*AIChE Journal,* **45,** pp 1632–1637

Choudhary V.R. Banerjee, S. and Rajput, A.M. (2002), "Hydrogen from step-wise steam reforming of methane over Ni/ZrO_2: factors affecting catalytic methane decomposition and gasification by steam of carbon formed on the catalyst," *Applied Catalysis A: General* **234** pp 259-270

Cracium, R Daniell, W. and Knozinger, H. (2002), "The effect of CeO_2 structure on the activity of supported Pd catalysts used for methane steam reforming," *Applied Catalysis A· General,* **230** pp153-168

Crisafulli, C Scrie, S. Minico, S and Solarino, L (2002), "Ni-Ru bimetallic catalysts for the CO_2 reforming of methane," *Applied Catalysis A: General,* **225,** pp 1-9

Demirbas, A (2001), "Biomass resource facilities and biomass conversion processing for fuels and chemicals," *Energy Conversion and Management,* **42** pp 1357-1378

Dias, J A.C. and Assaf, J M. (2003)," Influence of calcium content in $Ni/CaO/Al_2O_3$ catalysts for CO_2 reforming," *Catalysis Today,* **85,** pp59-68

Dalai, .A K Sethuraman, R . Bakhshi, N N. Idem, R O and Katikaneni, S P.R (2001), "Performance evaluation of sulphated-TiO_2 as a modifier to Co-Ni-ZrO_2 catalyst in a dual-bed reactor for the selective production of C_4 hydrocarbons from syngas," *Energy and Fuel,* pp A-I

Dissanayake, D Rosynek, P.M. Kharas, and Lunsford J H (1991), "Partial oxidation of methane to Carbon Monoxide and Hydrogen over a Ni/Al_2O_3 catalyst," *Journal of Catalysis,* **132,** 117-127

Effendi, A. Zhang, Z G and Yoshida, T. (2000), "A comparative Study on CO_2–CH_4 Reforming using Fixed and Fluidised–bed reactors," *Abstracts of papers of the America Chemical Society* 219 50 PETR PART 2, **26**

Effendi, A Zhang, Z-G. Hellgardt, K. Honda, K. and Yoshida, T. (2002), "Steam reforming of a clean model biogas over Ni/Al_2O_3 in fluidized- and fixed-bed reactors," *Catalysis Today,* **77,** pp181-189

Effendi, A Hellgardt, K. Zhang, Z-G. and Yoshida, T (2003), "Characterisation of carbon deposits on Ni/SiO_2 in the reforming of CH_4-CO_2 using fixed–and fluidised–bed reactors," *Catalysis Communication* **4,** pp 203-207

Efsthiov, A M, Kladi, A, Tsipouriari, V A & Verykios, X. E,(1996), " Reforming of methane with carbon dioxide to synthesis gas over supported rhodium catalyst.11 A Steady–State tracing analysis: Mechanistic Aspect of the carbon and oxygen Reaction pathway to form CO," *Journal of Catalysis* **158,** pp 64–75

Erdohelyi, A; Cserenyi, J, and Solymosi, F; (1993) Activation of CH_4 and its reaction with CO_2 over supported Rh catalysts," *Journal of Catalysis,* **141,** page 287

Ermakova, M.A. Ermakov, D.Y Kuvshinov, G G and Plyasova, L M. (1999), "New nickel catalysts for the formation of filamentous carbon in the reaction of methane decomposition," Journal of catalysis, 187 pp 77-84

Ferreira-Aparicio, P Rodriguez-Ramaos, I. and Guerrero-Ruiz, A (2002), "On the applicability of membrane technology to the catalysed dry reforming of methane," Applied Catalysis A General, **237** pp 239-252

Flynn, P C and Wanke, S E; (1975), "Experimental studies of sintering of supported Platinum catalysts," *Journal of Catalysis,* **37,** pp 432-448

Frusteri, F Arena, F. Calogero, G. Torre, T. and Parmaliana, A. (2001), Potassium-enhanced stability of Ni/MgO catalysts in the dry-reforming of methane," *Catalysis Communications,* **2,** pp 49-56

Gadalla, A M and Bower, B. (1988), "The role of catalyst support on the activity of nickel for reforming methane with CO_2," *Chemical Engineering Science* **43,** p 3049-3062

Gates, C B. (1991), "*Catalytic Chemistry,*" Wiley and Sons Inc. United State of America, New York pp 1-7

Ganley, J C Thomas, F S. Seebauer and Masel, R.I. (2004), "A priori catalytic activity correlation· the difficult case of hydrogen production form ammonia," *Catalysis Letter* 96 117-122

Goula, M A., Lemonidou, A A and Efststhiou, A. M. (1996), "Characterisation of carbonaceous species formed during reforming of CH_4 with CO_2 over Ni/CaO-Al_2O_3 Catalyst studied by various transient techniques," *Journal of Catalysis,* **161,** pp 626

Guerrro-Ruiz, A, Sepulveda–Escribano, A Rodriguez-Ramos, I, (1994), "Cooperative action of cobalt and MgO for the catalysed reforming of CH_4 with CO_2," *Catalysis Today,* **21,** pp 545–550

Guo, J. Lou, H Zhao, H. Chai, D. and Zheng, X. (2004), "Dry reforming of methane over nickel catalysts supported on magnesium aluminate spinels," *Applied Catalysis A: General* **273**, pp 75-82

Hao, Z. Zhu, H.Y and Lu, G.O. (2003), "Zr-Laponote pillared clay-based nickel catalysts for methane reforming with carbon dioxide," *Applied Catalysis A: General,* 242, pp 275-286

Hayashi, H, Murata, S; Togo, T, Kishida, M; and Wakabayashi, K; (2001), "Low carbon deposition on CO_2 reforming of methane over Ni/Al_2O_3 catalysts prepared using w/o microemulson," *Journal of Japanese Petroleum Institutes,* **44,** pp334 -337

Hong, S, Oh, S Park, D and Kim, G (2001), " The methane Reforming with carbon dioxide on Ni catalyst Activated by a D C–Pulsed Corona discharge," *Ind. Eng Chem,* **7**, pp 410–416

Hou, Z. and Yashima, T. (2004), "Meso-porous Ni/Mg/Al catalysts for methane reforming with CO_2," *Applied Catalysis A general,* vol **261**, pp 205-209

Ikenga, N Nakagawa, K Hideshima, S. Akamatsu, N.M. and Suzuki, T. (2000), "CO_2 Reforming of methane over Ru-loaded lanthanoid oxide catalysts," *Abstracts of Papers of the America chemical Society 219: PETR PART 2,* **26**

Inui, T. (2001), "Rapid catalytic reforming of methane with CO_2 and its application to other reactions," *Applied Organmetallic Chemistry,* **15,** pp 87–94

Joo, O-S and Jung, K-D. (2002), "CH_4 dry Reforming on alumina-supported nickel catalyst," *Bull Korean Chem. Soc*, **23**, p1149-1153

Juan-Juan, J Martinez-Roman, M.C. and Gomez-Ilian, M.J. (2004), "Catalytic activity characterization of Ni/Al_2O_3 and NiK/Al_2O_3 catalyst for CO_2 methane reforming," *Applied Catalysis A· General*, **264** pp 169-174

Lee, J-H. Lee, E-G Joo, O-S and Jung, K-D (2004), "Stabilization of Ni/Al_2O_3 catalyst by Cu addition for CO_2 reforming of methane," *Applied Catalysis A: General*, **269**, pp 1-6

Lemonidou, A.A. and Vasalos, A (2002)" Carbon dioxide reforming of methane over 5 wt % Ni/CaO/al2O3 catalyst," *Applied catalysis A· General*, **228** pp 227-235

Keulen, A N.J. Seshan, K Hoebink, J.H B J and Ross J.R H. (1997), "Tap investigation of the CO_2 reforming of CH_4 over Pt/ZrO_2," *Journal of Catalysis*, **166**, pp 306-314

Lif, J MSkoglundh, Mand Lowendahi (2004)" Stablising alumina supported nickel particles against sintering in ammonia/hydrogen atmosphere," *Applied Catalysis A General*, **274** pp 61-69

Kirk and Othmers (1980), "Encyclopaedia of chemical Technology" John Wiley and sons, New York Fourth Edition pp 902-910

Kodentsov, A A. Van Dal, M J H. Cserhati, C Daroczi, L. and Van Loo, F.J J (1999), "Permeation of nitrogen in solid nickel and deformation phenomena accompanying Internal Nitridation," *Acta mater*, **47**, pp 3169-3180

Kroll, V C H. Swaan, H M and Mirodatos, C. (1996), "Methane reforming reaction with carbon dioxide over Ni/SiO_2 catalyst: Deactivation studies," *Journal of Catalysis*, **161**, pp. 409- 422

Kroll ,V.C.H Swaan, H.M. Lacombe, S. and Mirodas, C. (1997), "Methane reforming reaction with carbon dioxide over Ni/SiO_2 catalyst 11 A Mechanistic study," *Journal of Catalysis,* **164,** pp 387 -398

Mark, F; and Maier, W.F; (1996), "CO_2 Reforming of methane on supported Rh and Ir catalysts *Journal of catalysis,* **164,** pp 122-130

Martinez, R Romero, E. Guimon, C and Bilbao, R (2004), "CO_2 reforming of methane over coprecipited Ni-Al catalyst modified with lanthanum" *Applied Catalysis A. General,* **274,** pp 139-149

Michael, C J B. Fanning, P E and Vannice, M.A. (1997), "Kinetic of NH_3 decomposition over well dispersion RU," Journal of Catalysis, **172,** pp 479-484

Missien, R.W. Mims, C A and Saville, B.A (1999), "Introduction to Chemical Reaction Engineering and Kinetics," John Wiley and Sons Inc, New York Pp 215-216

Nakagawa, K. Nishimoto, H Kikuchi, Maski and Egashira, S (2003), "Synthesis Gas Production from Methane using oxidized –diamond-supported Group VIII Metal catalysis" *Energy and Fuels,* **17,** pp 971-976

Nagaoka, K. Seshan, K. Aika, K. and Lercher, J.A. (2001), "Carbon deposition during carbon dioxide reforming of methane-comparison between Pt/Al_2O_3 and Pt/ZrO_2," *Journal of Catalysis,* **197,** 34-42

Nwanchukwu, C C and Lewis, C. (2000), A net Energy Analysis of fuel from Biomass The case of Nigeria," *Energy,* **11,** p 276

Ogawa, Y Toba, M and Yoshimura, Y. (2003), "Effect of lanthanum promotion on the structural and catalytic properties of nickel-molybdenum/alumina catalysts," *Applied Catalysis A: General,* **246,** pp 213-225

Olsbye, U Moen, O Slagton, A and Dahl, I.M (2002), "An investigation of the coking properties of fixed and fluid bed reactors during methane–to-synthesis gas reactions," *Applied Catalysis A· General* **228**, pp 289-303

Parvary, M. Jazayeri, S.H. Taeb, A Petit, C. and Kiennemann, A. (2001), "Promotion of active nickel catalysts in methane dry reforming reaction by aluminium addition," *Catalysis Communication*, **2,** pp 357-362

Qin, D and Lapszewicz, J. (1994) Study of mixed steam and CO_2 reforming of CH_4 to syngas on MgO–supported metals," *Catalysis of Today,* **21,** pp 551 -560

Qin, D , Lapsezwicz, J. and Jiang, X. J. (1996) Comparison of partial oxidation and steam-CO_2 mixed Reforming of CH_4 to Syngas on MgO-supported metals," *Journal of Catalysis,* **159,** 140

Rasmussen, F B. Sehested, J, Teunissen H.T (2004), "Sintering of Ni/Al_2O_3 catalysts studied by anomalous small angle X-ray scattering," *Applied Catalysis A: General,* **267,** 165-173

Richardson, J T. and Paripatyadar, S A. (1990), "Carbon dioxide reforming of methane with Supported rhodium," *Applied Catalysis,* **61,** pp 293–309

Roh, H-S. Jun, K-W. Dong, W-S. Park, S-E. Baek, Y-S (2001), "Highly stable catalyst supported on Ce-ZrO_2 for oxy-steam reforming of methane," *Catalysis Letters*, **74,** 31-36

Roh, H-S Potdar, H.S and Jun, K-W (2004), "Carbon dioxide reforming of methane over co-precipited Ni-CeO_2, Ni-ZrO_2 and Ni-Ce-ZrO_2 catalysts," *Catalysis Today*, 93-95 pp 39-44

Rostrup-Nielsen, N.R. and Hansen, J-H.B. (1993), "CO_2 reforming of methane over transition metals," *Journal of Catalysis,* **144**, p38

Rostrup–Nielsen, J.R. (1993), "Production of synthesis gas," *Catalysis Today,* **21,** pp 305–324

Rostrup–Nielsen, J. R, (1994), "Sulfur–passivated nickel catalysts for carbon -free steam reforming of methane," *Journal of Catalysis,* **85,** pp 31-43

Ruckenstein, E and Hu Y.H (1995), "Carbon dioxide reforming of methane over nickel alkaline earth metal oxide catalyst," *Applied Catalysis A: General,* **133,** pp 149-161

Ruckenstein, E and Hu Y.H (1996), "Role of support in CO_2 Reforming of CH_4 to Syngas over Ni catalyst," *Journal of Catalysis,* **162,** pp 230–238

Ruckenstein and Wang (2001), "Combined catalytic partial oxidation and CO_2 reforming of methane over supported cobalt catalyst," *Catalysis Letter,* 73 pp 99 –105

Ruckenstein, E., and Wang, H Y , (2002), "Carbon deposition and deactivation during CO_2 reforming of CH_4 over Co/Y- Al_2O_3 catalyst," *Journal of Catalysis,* **205,** pp 289–293

Sandler, S I (1989),"Chemical and Engineering Thermodynamics," Wiley series in chemical Engineering, Second Edition, pp 263-266 and pp 494–536

Seshan K. Ten Barge, H.W. Hally, W Van Keulen, A N J and Ross, J R.H. (1994), "Carbon dioxide reforming of methane in the presence of nickel and platinum catalysts supported on ZrO_2," *Study of Surface Science Catalysis,* **81,** pp 285

Sethuraman, Y, Kroll, V C H, Ferreira–Aparico, P and Mirodas, C, (1997), "Use of Transient kinetic Technique for studying the methane Reforming by carbon dioxide," *Catalysis Today,* **38,** pp 129–135

Sethuraman, R. Bakhshi, N N. Katikaneni and Idem, R O. (2001), " Production of C_4 hydrocarbons form Fisher-Tropsch synthesis in a follow bed reactor consisting of Co-Ni-ZrO_2 and sulphated –ZrO_2 catalyst beds

Shimizu T. Shimizu, K Kitayama Y and Kodama, T. (2001), "Thermo chemical methane reforming using WO_3 as an oxidant below 1173K by a solar furnace simulator," *Solar Energy,* **71,** pp 315–324

Shishido, T. Sukenobu, M. Morioka, H. Furukawa, R Shirahase, H. and Takehira, K. (2001)," CO_2 reforming of CH_4 over Ni/Mg-Al oxide catalysts prepared by solid phase crystallization method from Mg-Al hydrotalcite-like precursors," *Catalysis Letters,* **73,** pp 26

Slessers, M. and Lewis, C. (1981)," Biological Energy Resources," Publisers, Accademic press London p 53

Solymosi, F. Cserenyi, J. (1994), "Decomposition of CH_4 over supported Ir catalysts," *Catalysis Today,* **21,** pp 561–569

Song, C and Pan, W (2004), "Tri-reforming methane: a novel concept for catalytic production of industrially useful synthesis gas with desired H_2/CO ratios," *Catalysis Today* **98,** pp 463-484

Souza, M.M.V.M. Aranda, D.A.G Schmal, M (2001), "Reforming of methane with carbon dioxide over Pt/ZrO_2/Al_2O_3 Catalysts," *Journal of Catalysis,* **204,** pp 498-511

Souza, M M.V.M. Aranda, A G. Schmal, M (2002), "Coke formation on Pt/ZrO_2/Al_2O_3 Catalysts during CH_4 reforming with CO_2," *Ind. Eng Chem Res.* **41,** pp 4681-4685

Souza, M M.V.M Clave, L. Dubois, V. Perez, C.A.C. and Schmal, M. (2004), "Activation of supported nickel catalysts for carbon dioxide reforming of methane," *Applied Catalysis A· General,* **272,** pp 133-139

Staag, S.M, Romeo E, Padro, C; and Resasco, D.E; (1998), "Effect of promoter with Sn on supported Pt catalyst for CO_2 reforming of CH_4," *Journal of Catalysis,* **178,** pp 137-145

Staniforth, J and Ormerod, R.M. (2003), "Clean destruction of waste ammonia with consummate production of electrical power within a solid oxide fuel cell system," *Green Chem*, **5**, 606-609

Swaan, H M; Kroll, VC.H; Martin G A and Mirodatos, C; (1994), "Deactivation of supported Nickel catalysts during the reforming of methane by carbon dioxide," *Catalysis of Today*, **21**, p 571

Teixeira A C S C. and Giudici R (2001), "A Monte Carlo model for the sintering of Ni/Al_2O_3 catalysts," *Chemical Engineering Science*, **56**, pp 789–798

Tomishige, K Chen, Y and Fujimoto, K, (1998), "Studies on carbon Deposition in CO_2 reforming of CH_4 over Nickel-Magnesia solid solution catalysts," **181**, p 91

Tsipouriari, V.A Efstathoiu, Z I. Zhang, X E. Verykios, X E (1994), " Reforming of methane with carbon dioxide to synthesis gas over supported Rh catalysts," *Catalysis Today*, **21**, pp 579–587

Theron, J.N Fletcher T J.C Q. O'Connor C T (1994), "Oxidative reforming of methane to Syngas over a NiO - CaO catalysts," *Catalysis Today*, **21**, pp 489–494

Tomishige, K, Matsuo, Y, Sekine Y, Fujimoto K (2001), "Effective methane reforming with CO_2 and O_2 under pressurized condition using NiO-MgO and fluidized bed reactor," *Catalysis Communications*, **2**, pp 11-15

Tol, M F H. Gielbert, A & Nieumenhuys, B E (1993), "The adsorption and dissociation of CO_2 on Rh," *Applied Surface Science*, **67**, pp 166–178

Udengaard, N.R. BakHansen, J.H. Harison, D C. Stal, J A. (1992), "Sulfur passivated reforming process lowers syngas H_2/CO ratio," *Oil and Gas Journal*, **8**, pp 62–67

Valentini, A. Carreno, N.L.V. Probst, L F.D. Lisboa-Filho, P.N Schreiner, W H Leite, E.R. and Longo, E. (2003), "Role of vanadium in Ni:Al_2O_3 catalysts for carbon dioxide reforming of methane," *Applied Catalysis A. general,* **255**, pp 211-220

Wang , S.and Lu, G Q. (1996), "Carbon dioxide reforming of methane to produce synthesis Gas over metal-supported catalyst state of the Art," *Energy and Fuels,* **10,** pp 896-904

Wang, S and Lu, G Q (1998a), "Role of CeO_2 in Ni/CeO_2-Al_2O_3 catalysts for carbon dioxide reforming of methane," *Applied Catalysis* B. *Environmental,* **19,** pp 267-277

Wang, S and Lu, G.Q (1998b)," Reforming of methane with carbon dioxide over Ni/Al_2O_3 catalysts Effect of nickel precursor," *Applied catalysis A: General,* **169** pp 271-280

Wang, J.B. Tai, Y-L. Dow, W-P and Huang, T-J (2001), "Study of ceria-supported nickel catalyst and effect of yttria doping on carbon dioxide reforming of methane," Applied Catalysis A General, 218 69-79

Wang, J S Kuo, L-E. and Huang, T-J (2003a),"Study of ceria-supported nickel catalyst and effect of yttria doping on carbon dioxide reforming of methane," *Applied Catalysis A General,* **218**, pp 69-79

Wang, J S Kuo, L-E. and Huang, T-J (2003b), "Study of carbon dioxide reforming of methane over bimetallic Ni-Cr/yttria-dopped," *Applied Catalysis A· general,* **249**, pp 93-105

Wei, J. Xu, B Li, J. Chen, Z and Zhu (2000), "Highly Active abs carbon-resistant catalyst for CH_4 reforming with CO_2–Nickel supported on an ultra fine ZrO_2," *Abstracts of Papers of the America chemical Society 219: PETR PART 2,* **26**

White, L P, and Plaskett, L G. (1981)," Biomass as Fuel," Publisers , Accademic press, New York Second Edition, p 40

Xu, Z. Yumin, L Zhang, J Chang, L. Zhou, R and Duan, Z. (2001), "Ultra fine NiO-La_2O_3-Al_2O_3 aerogel a promising catalyst for CH_4/CO_2 reforming," *Applied Catalysis A· General,* **213,** pp 65-71

Xiao, T. Suhartanto, T. York A.P.E. Sloan, J and Green, M.L H. (2003), "Effect of molybdenum additives on the performance of supported nickel catalysts for methane dry reforming," *Applied Catalysis A· General,* **253,** pp 225-235

Valentini, A Carreno, N.L.V. Probst, L F D. Lisboa-Filho, P N Schreiner, W.H. Leite, E.R. and Longo, E. (2003), "Role of vanadium in Ni:Al_2O_3 catalysts for carbon dioxide reforming of methane," *Applied Catalysis A. general,* **255**, pp 211-220

Yin, S F Xu, B Q. Zhou, X P and Au, C.T (2004), "A mini-review on ammonia decomposition catalysts for on-site generation of hydrogen for fuel cell application," *Applied Catalysis A· General* 277 pp 1-9

Zhang, Z.I. and Verykios (1994), "Carbon dioxide reforming of methane to synthesis gas over supported Ni catalysts," *Catalysis Today,* **21,** pp 589-595

Zhang, Z. and Verykios, X E. (1996)," Carbon dioxide reforming of methane to synthesis gas over Ni/La_2O_3 catalysts," *Applied Catalyst A: General,* 138 pp 109-133

Zhang, Z L. Tsipouriari V.A. Efstathiou, A.M. and Verykios, X E (1996), Reforming of methane with carbon Dioxide to synthesis Gas over supported Rhodium catalysts: Effects of support and metal crystallite size on reaction Activity and deactivation characterisation," *Journal of Catalysis,* **158**, pp 51-63

Appendix 1 Calibration

A1.1 Carbon dioxide and methane flow rate calibration

Apparatus: (1) Methane cylinder (2) Carbon dioxide cylinder (3) Graduated burette (40 Stopwatch and soap solution

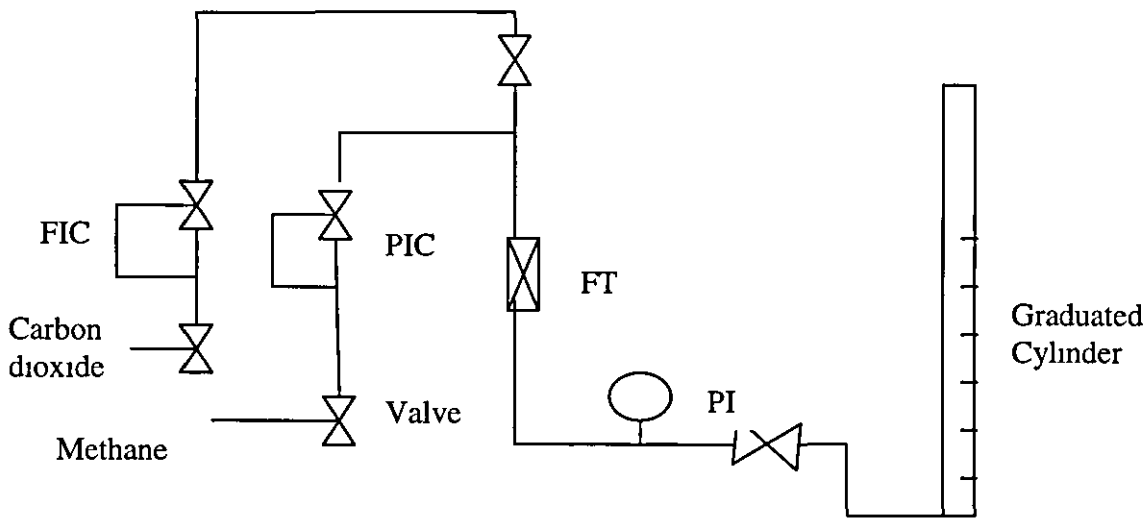

Figure A1.1 Schematic diagram for methane and carbon dioxide calibration

The experimental set up is as shown in figure A1.1. Soap solution was prepared and poured into the burette fixed to a rubber bulb tube Pressure was set at 5 bar and carbon dioxide cylinder valve was opened for gas flow The mass flow controller was set at zero and gradually increased to 10 5 and steady state was attained. Gas bubble was allowed to pass through the graduated burette of 25 ml by opening all the line valves. The time taken for a gas bubble to rise up to the mark at 25ml was recorded using a stopwatch. For every fixed mass flow, five readings were taken and at the increment of 5ml, data for volumetric flow rate calculation was collected. An average time was used for the calculation for accuracy. This was repeated for also methane gas The data obtained is presented in table 5 and calibration curves for both carbon dioxide and methane are presented in figure 2 and 3 which would be used to determine the space velocity of the system

Precautions·

(1) Check for gas leaks in all valves (2) Switch on extractor of fume cupboard (3) Set mass flow controller at steady state and keep fume cupboard shutters down during experiment

Carbon Dioxide				Methane			
Mass Flow controller	ml	Ave time	Volume. Flow rate	Mass Flow	ml	Average time	Volume Flow rate
10 5	25	3 292	7 594	10 6	25	3.206	7 800
15 5	25	2.170	11 520	15.1	25	2 226	11.231
203	25	1 484	17 265	20 2	25	1.430	17 483
25 7	25	1.210	20 661	25.5	25	1.226	20 391
30 3	25	1 094	22.852	30.4	25	1 086	23 020
35 0	25	0.990	25.250	35.5	25	0 969	25 792
40.2	25	0 859	29.104	40 0	25	0 855	29.240
45.2	25	0 742	33.693	45 9	25	0 751	33 285
50.1	25	0.674	37 091	50.2	25	0.677	36 928
55.1	25	0 605	41.295	55 5	25	0 607	41.186
60 2	25	0 546	45 700	60 2	25	0 551	45 372
65 9	25	0.494	50 607	65.5	25	0 502	49 801
70 1	25	0 416	54 230	70.1	25	0 470	53.191
75.6	25	0 424	58.962	75 8	25	0 427	58 548
80 4	25	0.391	63 939	80 8	25	0.393	63 678
85 4	25	0 363	68 871	85.7	25	0.368	67 861
90 2	25	0.340	73.529	90 2	25	0.339	73 746
95.5	25	0 320	78.125	95 6	25	0 318	78 616
100 2	25	0 302	82 780	100 3	25	0 295	84 750

Table A1 1 Mass flow controller data for Methane and Carbon dioxide

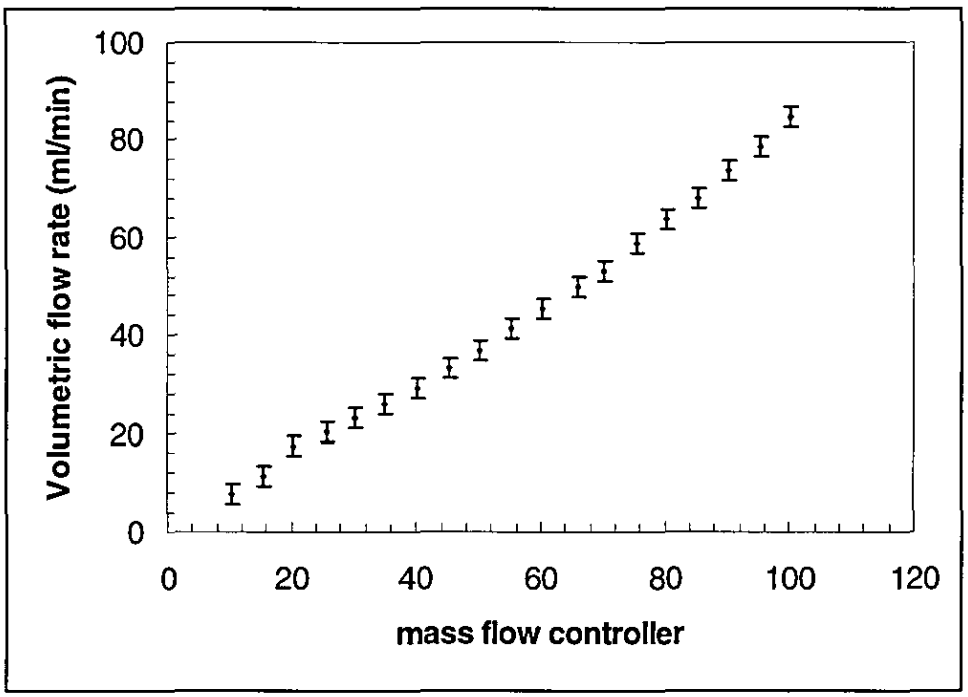

Figure A1 2 Mass flow controller calibration curve for methane.

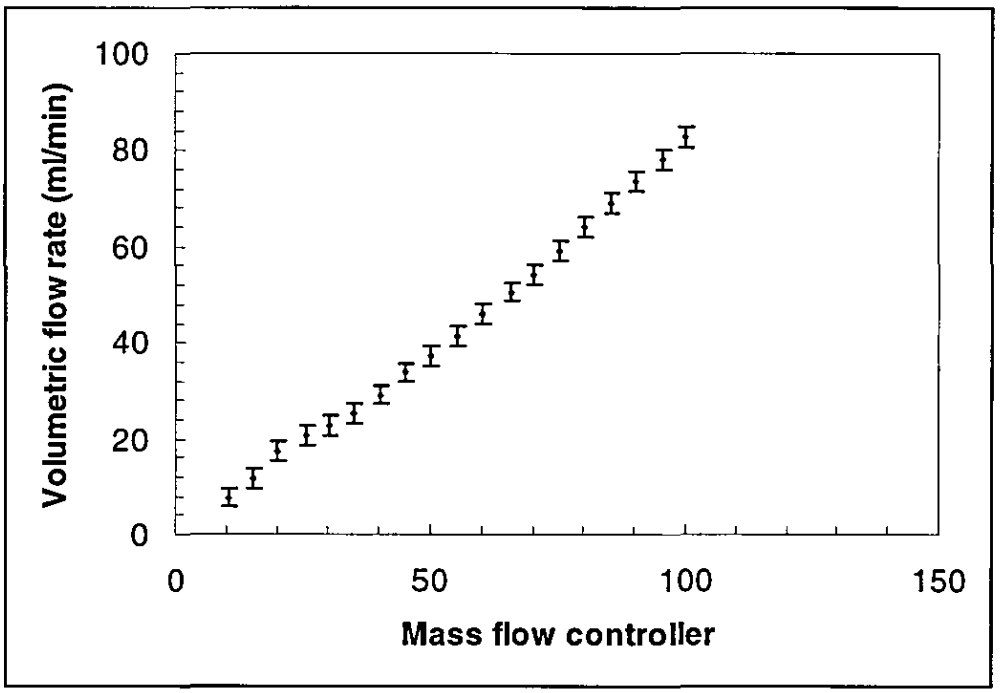

Figure A1.3 Mass flow controller calibration for carbon dioxide

A1.2 GC calibrations data for methane

Concentration (mol/L)	Response area		
	1st Run	2nd Run	3rd Run
0 00E+00	0.00E+00	0 00E+00	0.00E+00
2 23E-05	6.70E+06	7 43E+6	7 15E+06
4 46E-05	2.00E+07	1.50E+07	1 66E+07
6 69E-05	2.50E+07	2.4E+07	2 82E+07
8.93E-05	3.10E+07	3 5E+07	3 56E+07

Table A1.2 GC calibration data for methane

A1.3 GC calibration data for carbon dioxide

Concentration (mol/L)	Response area		
	1st Run	2nd Run	3rd Run
0 00E+00	0 00E+00	0 00E+00	0 00E+00
2 23E-05	7 00E+06	5.75E+06	5.78E+06
4 46E-05	1 09+07	1 31E+07	8 86E+07
6 69E-05	2 20+07	2 32E+07	1 84E+07
8 93E-05	3 10E+07	2 80E+07	2 61+07

Table A1 3 GC calibration data for carbon dioxide

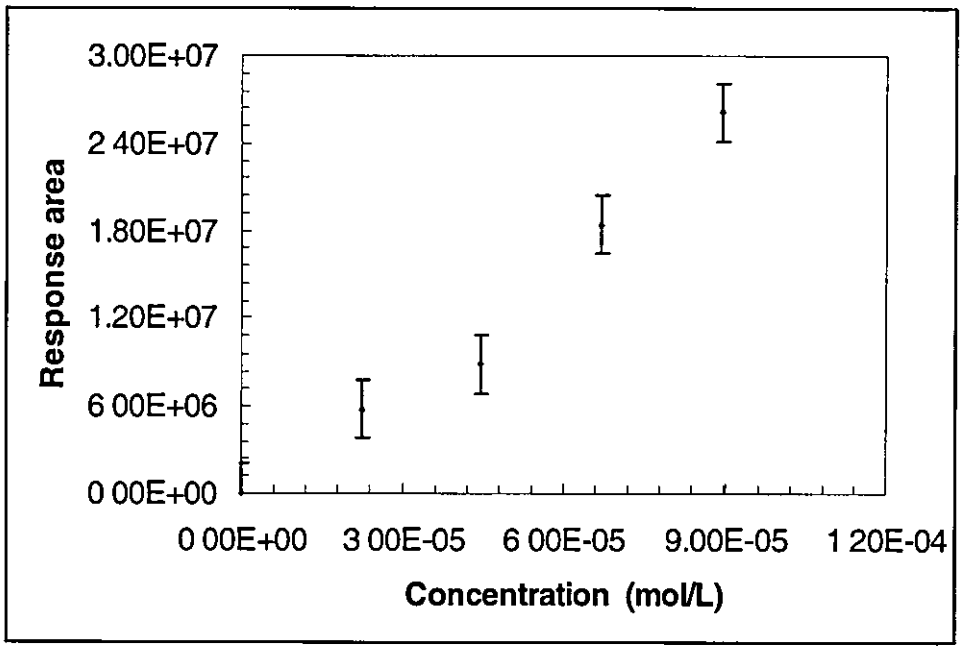

Figure A 1.4 GC calibration for methane

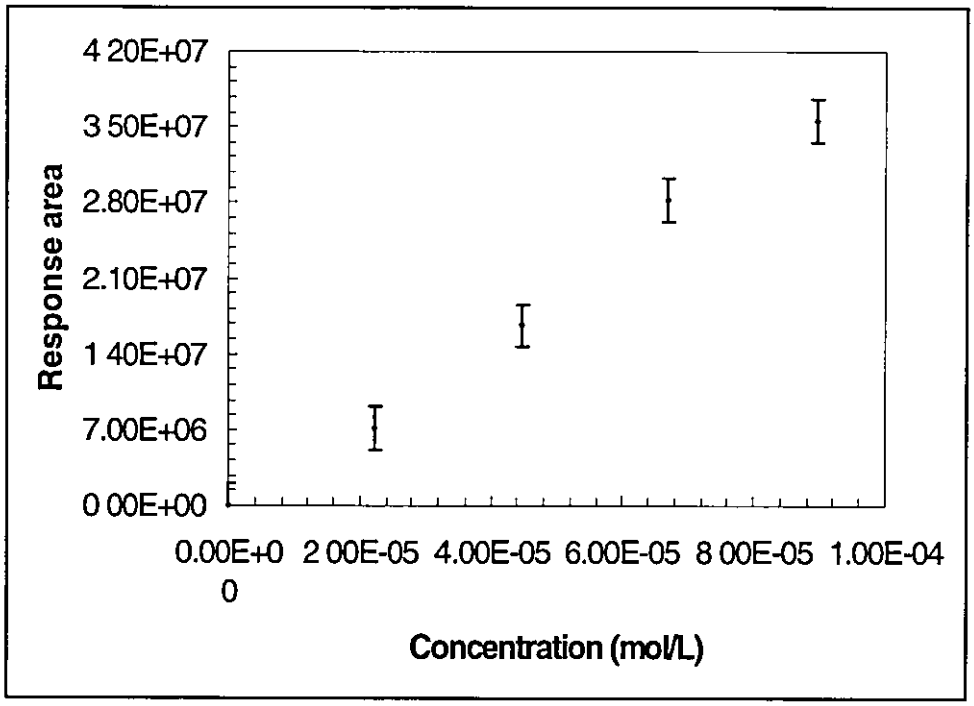

Figure A 1.5 GC calibration for carbon dioxide

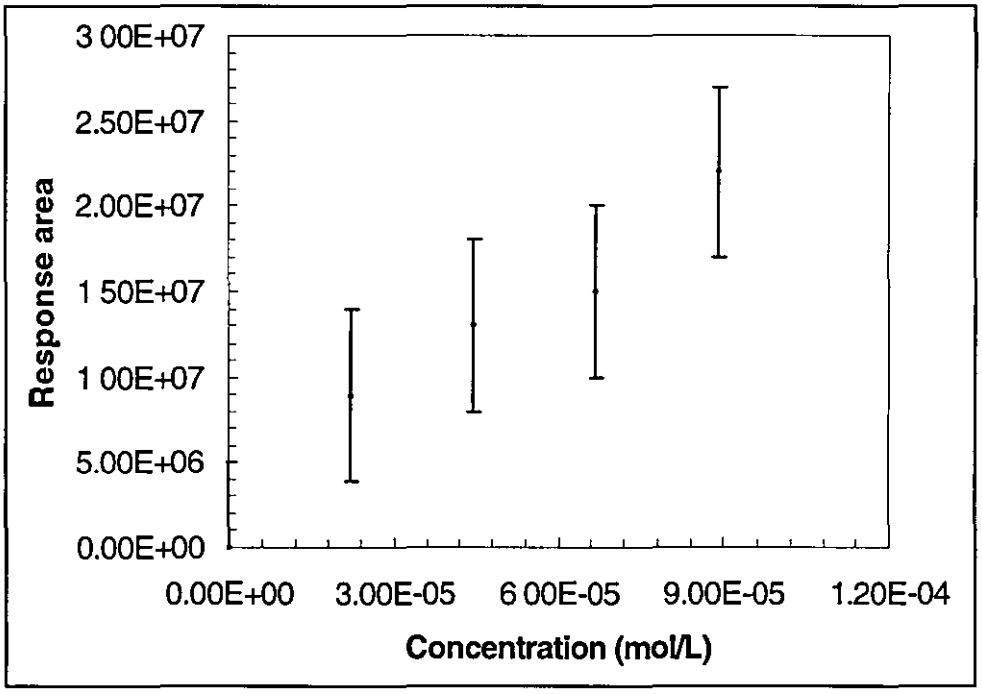

Figure A 1 6 GC calibration for carbon monoxide

A1.4 Reactor temperature profile

Length of reactor (cm)	Temperature (K)				
	1173	1073	973	872	773
7	707	665	619	564	539
12	742	680	629	582	549
17	912	805	733	670	624
22	1046	948	872	796	725
27	1112	1014	933	845	763
32	1143	1046	958	865	779
37	1152	1055	963	868	781
42	1145	1051	954	855	757
47	1127	1034	933	829	730
52	1088	1007	895	790	686
57	1039	959	842	734	634
62	952	892	768	561	561
67	844	807	655	567	477
72	530	592	478	431	376
77	487	429	397	366	335

Table A1.4 Data for reactor temperature profile

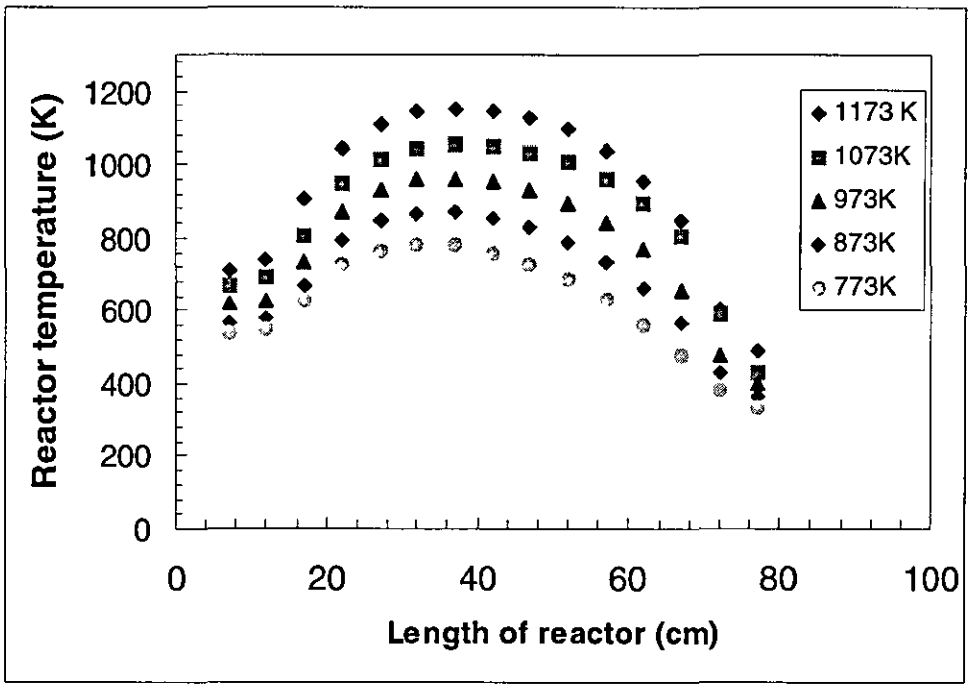

Figure A1 7 Reactor temperature profile

A1.5 Calibration for NH_3

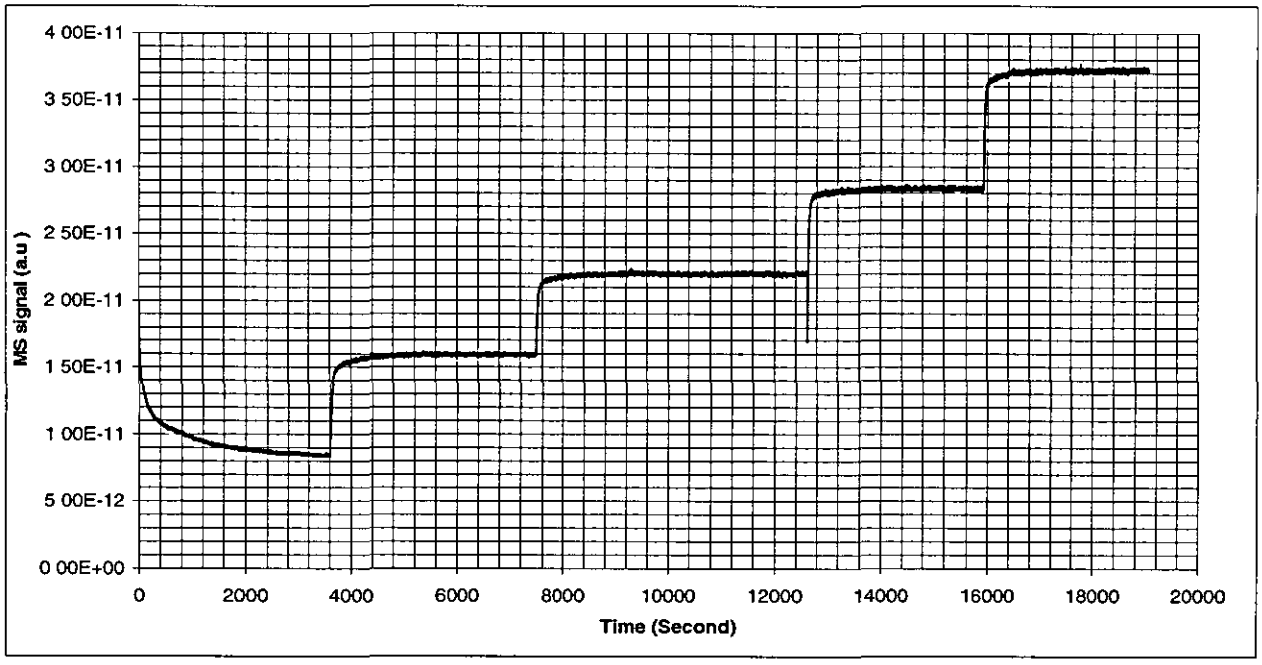

Figure A1 8 NH_3 trace, 3000 ppm at varying flow rates

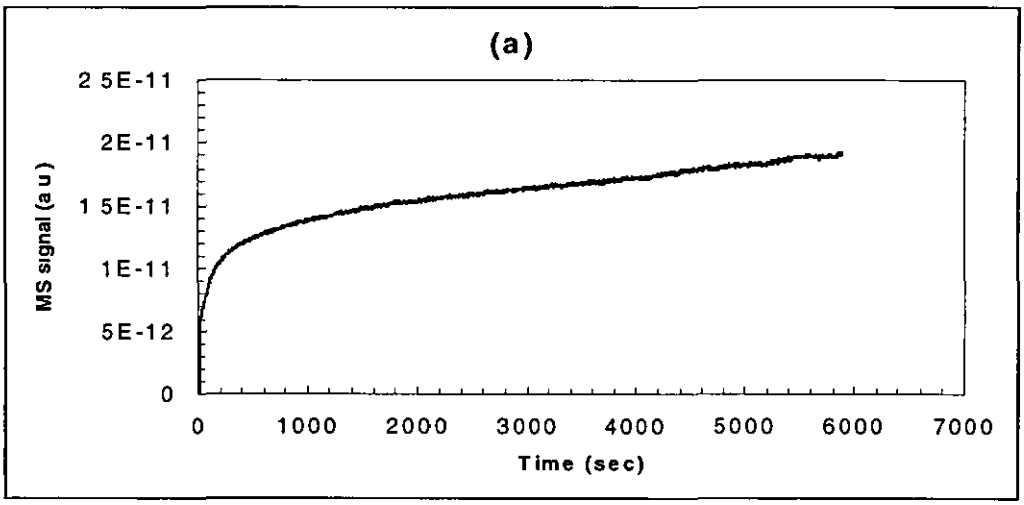

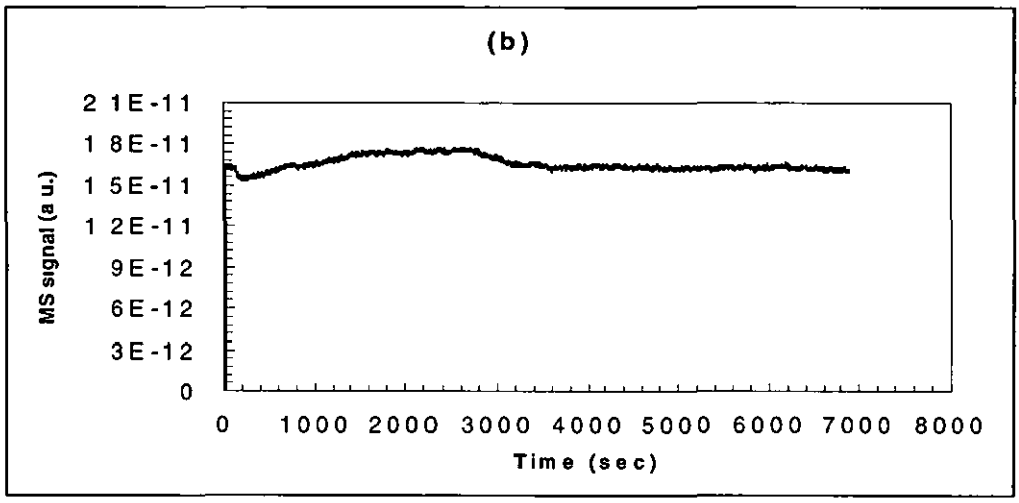

Figure A1 9 NH_3 trace (a) 3000 ppm (b) 1000 ppm at 80 ml/min

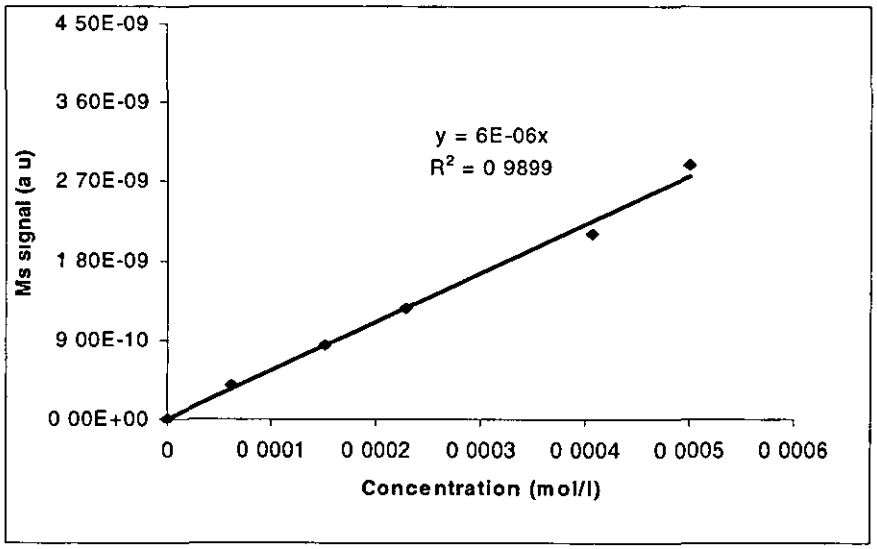

Figure A1.10 NH_3 calibration curve

A1.5 Absorption-desorption isotherm for surface area

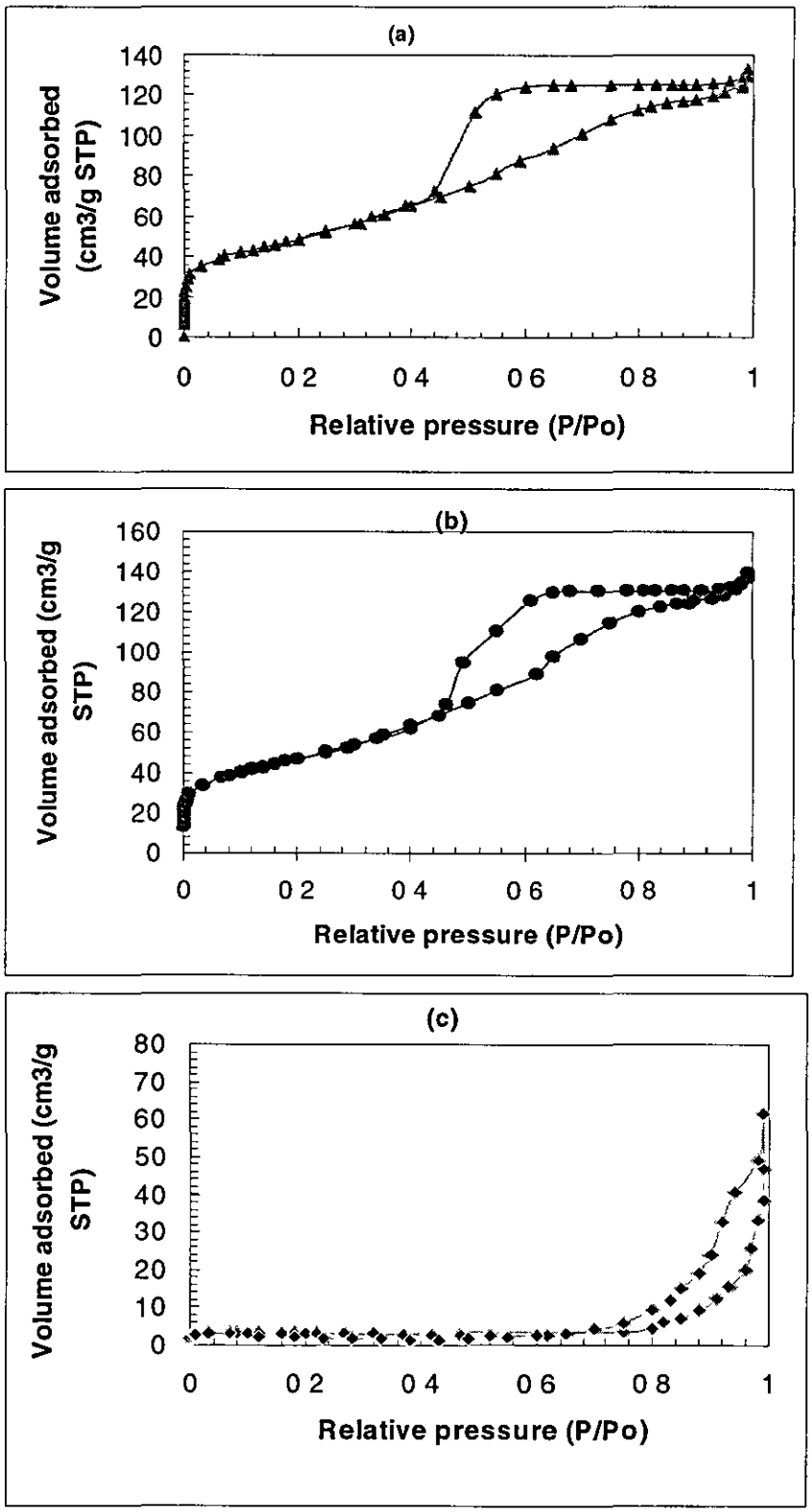

Figure A1.11 Absorption-desorption Isotherm (a) $Ni/\gamma\text{-}Al_2O_3$ (b) $Ni/ZrO_2/\gamma\text{-}Al_2O_3$ (c) $Ni/\gamma\text{-}Pr_2O_3$

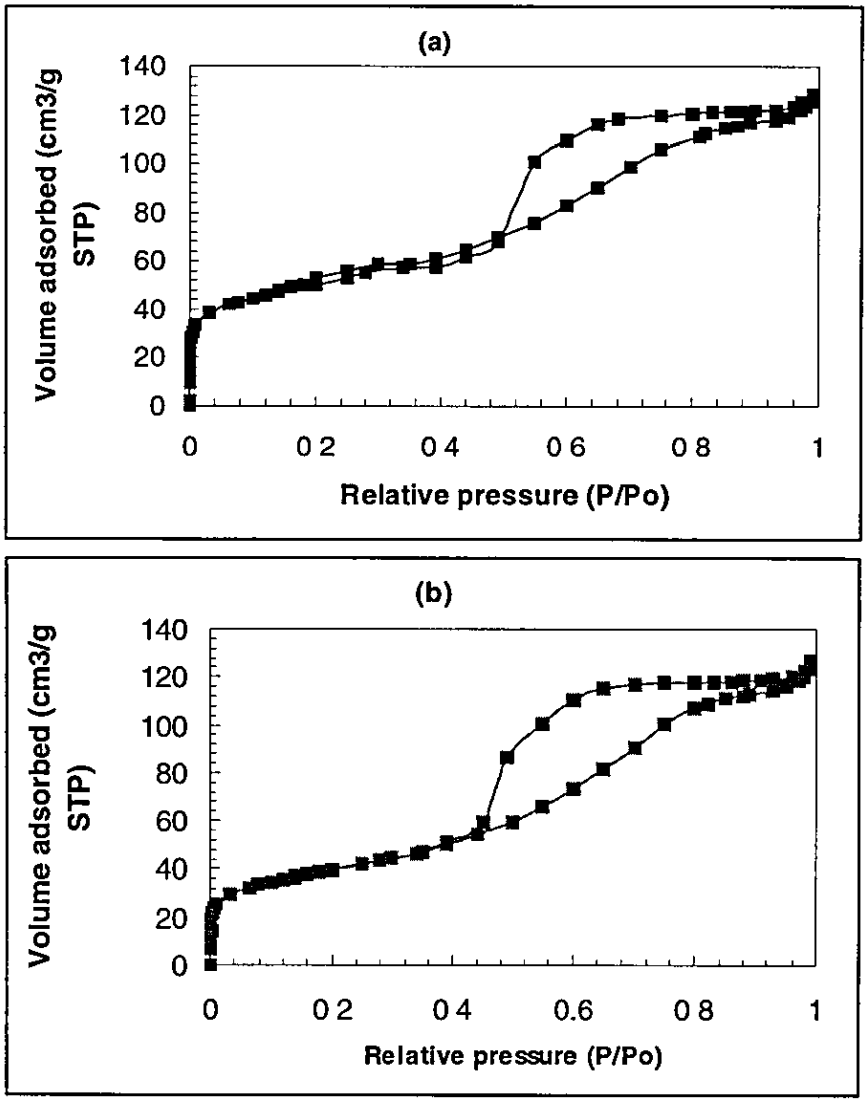

Figure A1 12 Absorption-desorption Isotherm (a) Ni-Pd/γ-Al_2O_3 (0 25 wt%) (b) Ni-Cu/γ-Al_2O_3 (0 25 wt%)

A.1.6 CO chemisorption

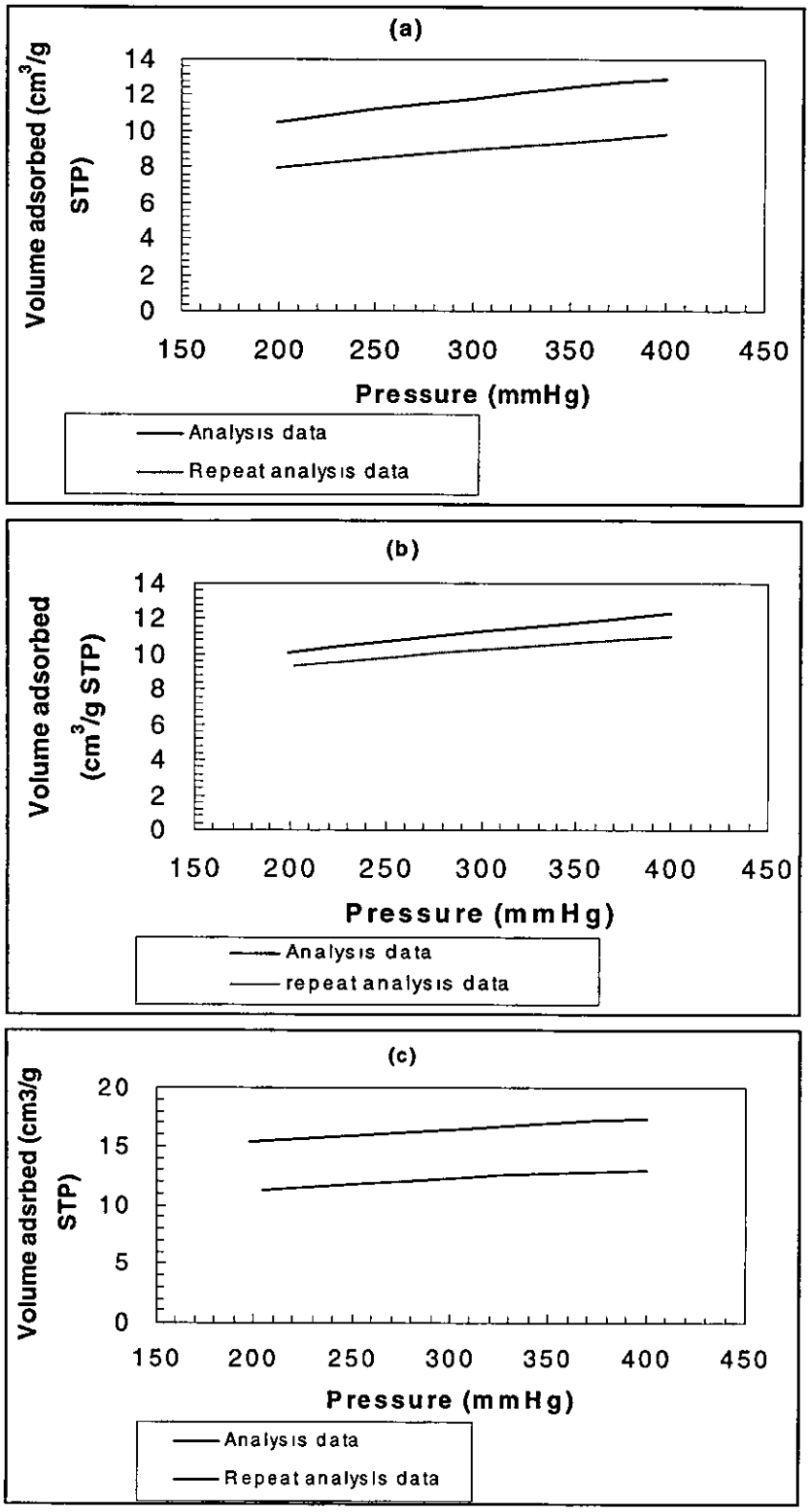

Figure A1.13 CO chemisorption curve (a) Ni/γ-Al_2O_3 (b) Ni/ZrO_2/γ-Al_2O_3 (c) Ni-Pd/γ-Al_2O_3(0.25 wt%)

A1.7 Peakfit TPR curves

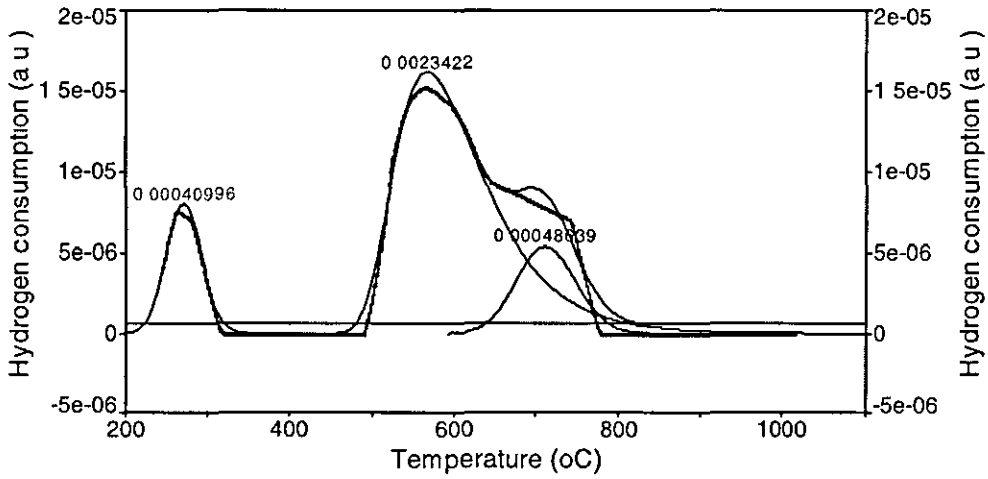

Figure A1.14 TPR curve for $Ni/ZrO_2/\gamma\text{-}Al_2O_3$ catalyst

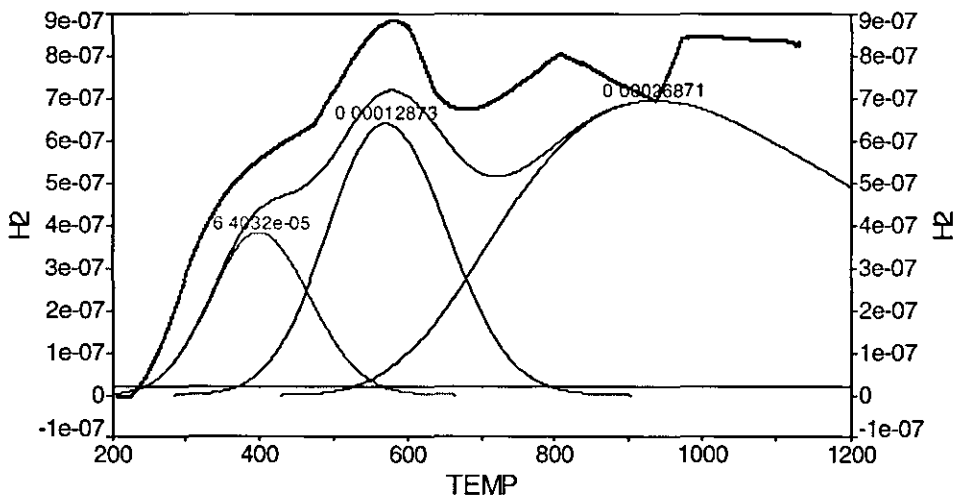

Figure A1 15 TPR curve for $Ni/\gamma\text{-}Al_2O_3$ catalyst

Appendix II Equilibrium constant and mole fraction data

Temp(° K)	Y H_2O	Y CO	Y H_2	YCO_2	Y CH_4
600	0 55071	0 006345	0 045171	0 21288	0 19061
650	0.50485	0 002482	0 085131	0 22443	0 18311
700	0 5142	0 007946	0 14283	0 23262	0 16518
750	0 38892	0 021547	0 21562	0.23547	0 13844
800	0 31821	0 050533	0 29519	0 22920	0 10687
850	0 24297	0 10336	0 36927	0 20868	0 075722
900	0 16982	0 18380	0 42623	0 17068	0 049466
950	0 10713	0 28171	0 46087	0 11993	0 030353
1000	0 061381	0.37212	0 47753	0 070838	0 018132
1050	0 033073	0 43443	0 48520	0 036341	0 010957
1100	0 017550	0 46849	0 48970	0 017434	0 0068277
1150	0 009480	0 48494	0 49284	0 0083452	0 0043975
1200	0 005295	0 49262	0 49504	0 0041251	0 0029195
1250	0 003072	0 49626	0 49654	0 0021322	0 0019922
1300	0 001850	0 49804	0 49756	0 0011548	0 0013939
1350	0 001155	0 49894	0 49825	0 00065400	0 00099766
1400	0 007446	0 49941	0 49873	0 00038603	0 00072903
1450	0 004945	0 49967	0 49906	0 00023662	0 00054286
1500	0 003374	0 49981	0 49929	0 00015009	0 00041120
1550	0 002359	0 49989	0 49946	0 000098220	0 00031635
1600	0 001687	0 49994	0 49958	0 000066120	0 00024683

Table A2.1 Equilibrium mole fractions of reactants and products at various temperatures

Temp(° K	K_1	K_2	K_3
600	001432208114	00040520436358	93 41604144
650	0 006381496168	0 000418644766	25 26566426
700	0 02328855805	0 0020251444177	8 097001438
750	0 07237429313	0 01194537506	2 977606550
800	0.1972299406	0 04687613461	1 226523764
850	0 48202288208	0 1574846244	0.5552974516
900	1 075182313	0 4613178658	0 2722850210
950	2 219453091	1 211874131	0 142905210
1000	4 287448282	2 894984450	0 07951583220
1050	7 821187209	6 373234617	0 04654203622
1100	13 57364629	13 07220761	0 02847163645
1150	22.55013043	25 20844254	0 01810524181
1200	36 04727711	46 05060268	0 01191346388
1250	55 68770631	80 20129325	0 00880285925
1300	83 4470152	133 8838684	0 00563020869
1350	121.6837334	215 217170	0 004018629753
1400	173.1361900	334 4614413	0.002931023323
1450	240 9451225	504 2202719	0 00219638939
1500	328 6433861	739 5866064	0 0011649477266
1550	440 1489182	1058 223926	0 001268144146
1600	579 7502226	1480 377861	0 0009890034578

Table A 2 2 Equilibrium constants

Catalyst	Component	Experimental	Model	Rate constant $*10^5\ s^{-1}$
Ni-Pd/γ-Al_2O_3 (0 25 wt%)	CO_2 CH_4 CO H_2	0.39 0.28 0.06 0 33	0 40 0.33 0 05 0.33	k1=69 k3=19 k5=3
Ni-Cu/γ-Al_2O_3 (0 25 wt%)	CO_2 CH_4 CO H_2	0 38 0.33 0.04 0.20	0.43 0.33 0 05 0 21	k1=24 k3=11 k5=7

Table A2.3 Kinetic data for palladium and Cu promoted catalysts

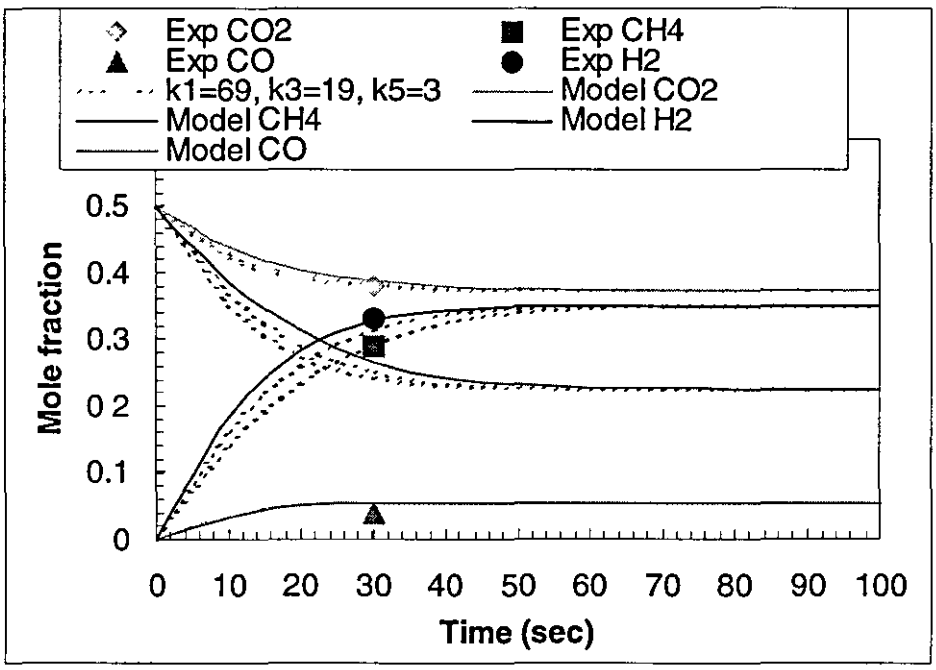

Figure A2 1 Model plot for Ni-Pd/γ-Al_2O_3(0 25 wt%)

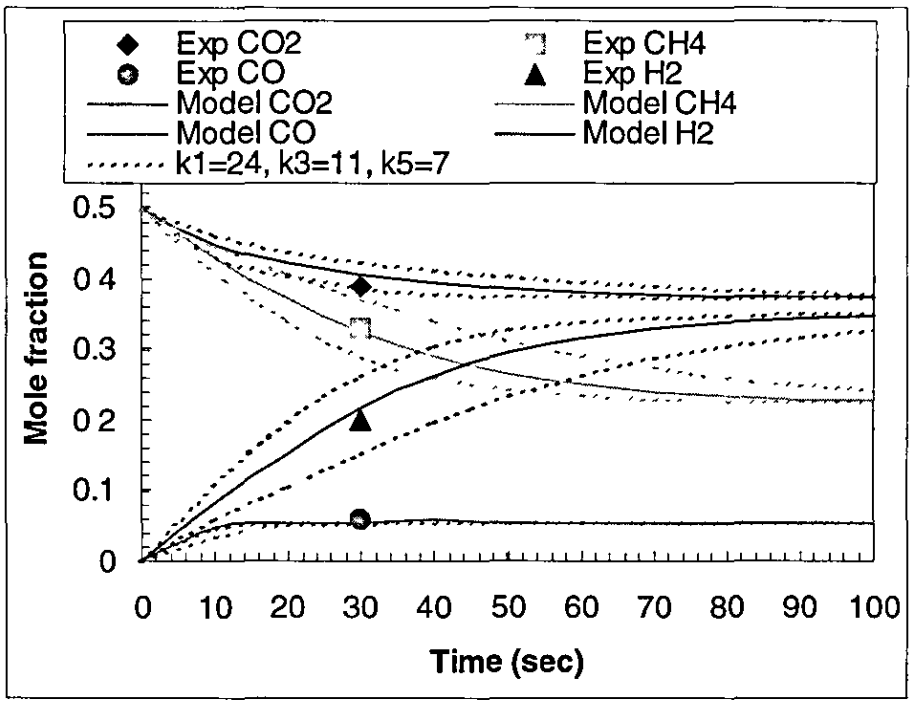

Figure A2 2 Model plot for Ni-Cu/γ-Al_2O_3(0.25 wt%)

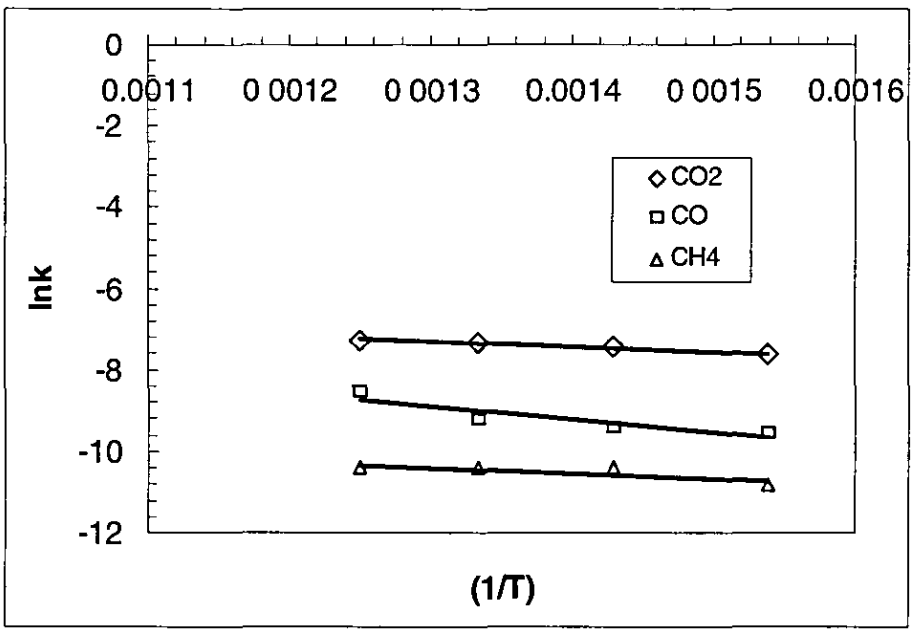

Figure A2 3 Activation plot for Ni-Pd/γ-Al_2O_3 (0 25 wt%)

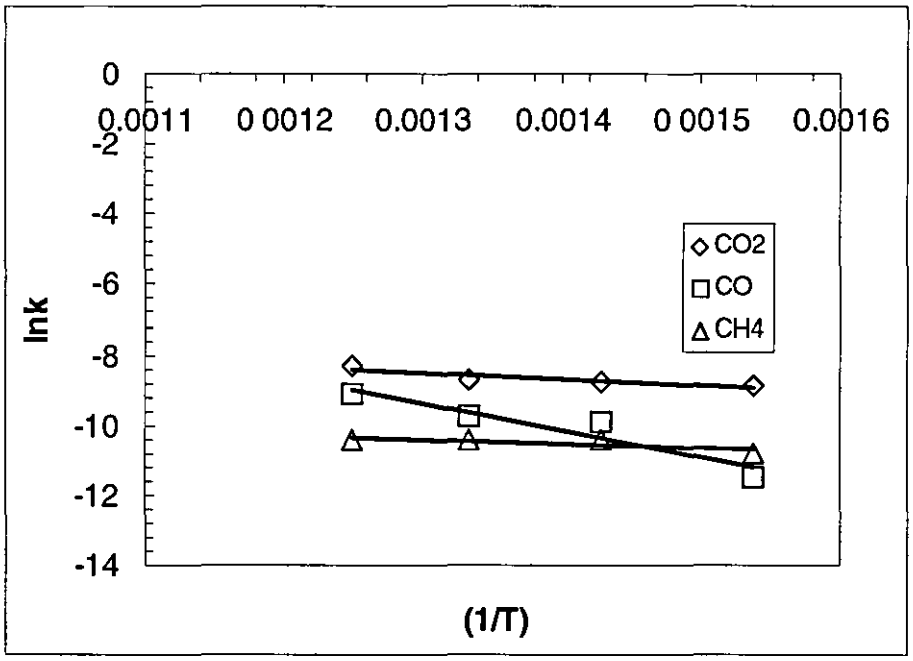

Figure A2.4 Activation plot for Ni-Cu/γ-Al_2O_3 (0 25 wt%)

Appendix III Effect of support

A3.1 Experimental plots for effect of support on catalytic activity

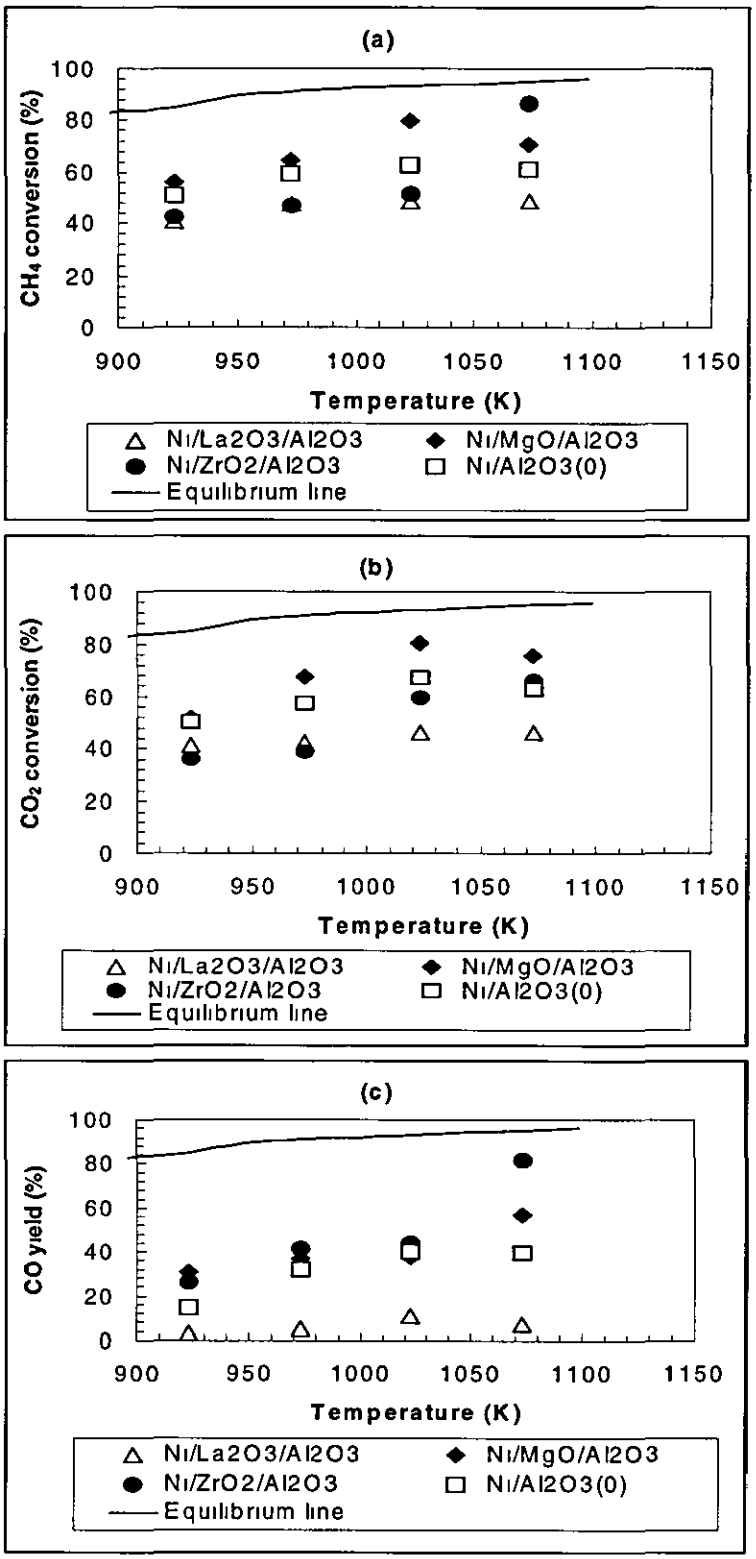

Figure A3 1 Conversion and yield as a function of temperature (a) CH_4 (b) CO_2 and (c) CO, 6h, P = 1 atm, WHSV = 13900 ml, hr g cat, catalyst

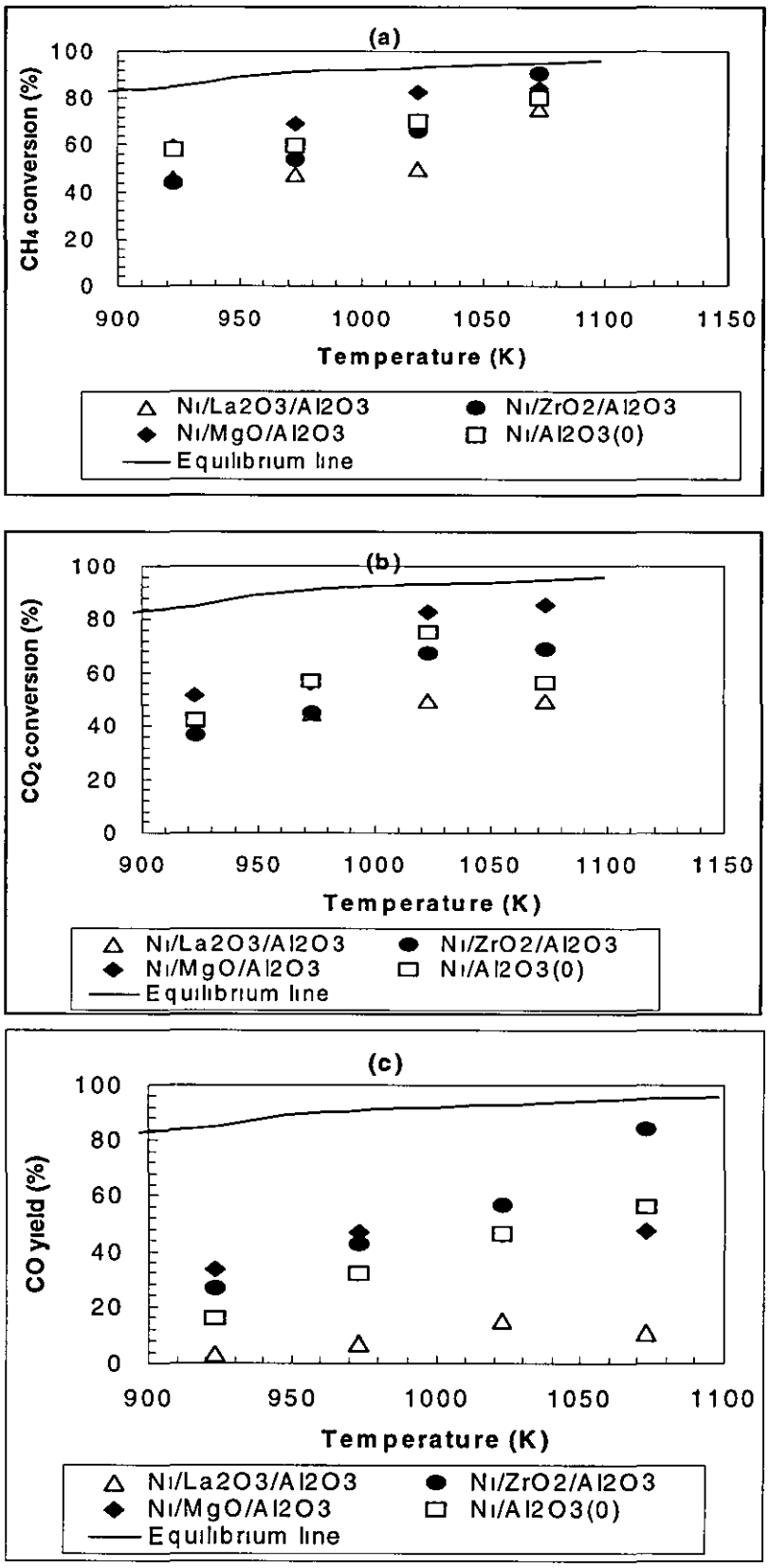

Figure A3 2 Conversion and yield as a function of temperature (a) CH_4 (b) CO_2 and (c) CO, 6h, P = 1 atm, WHSV = 9820 ml, hr g cat, catalyst

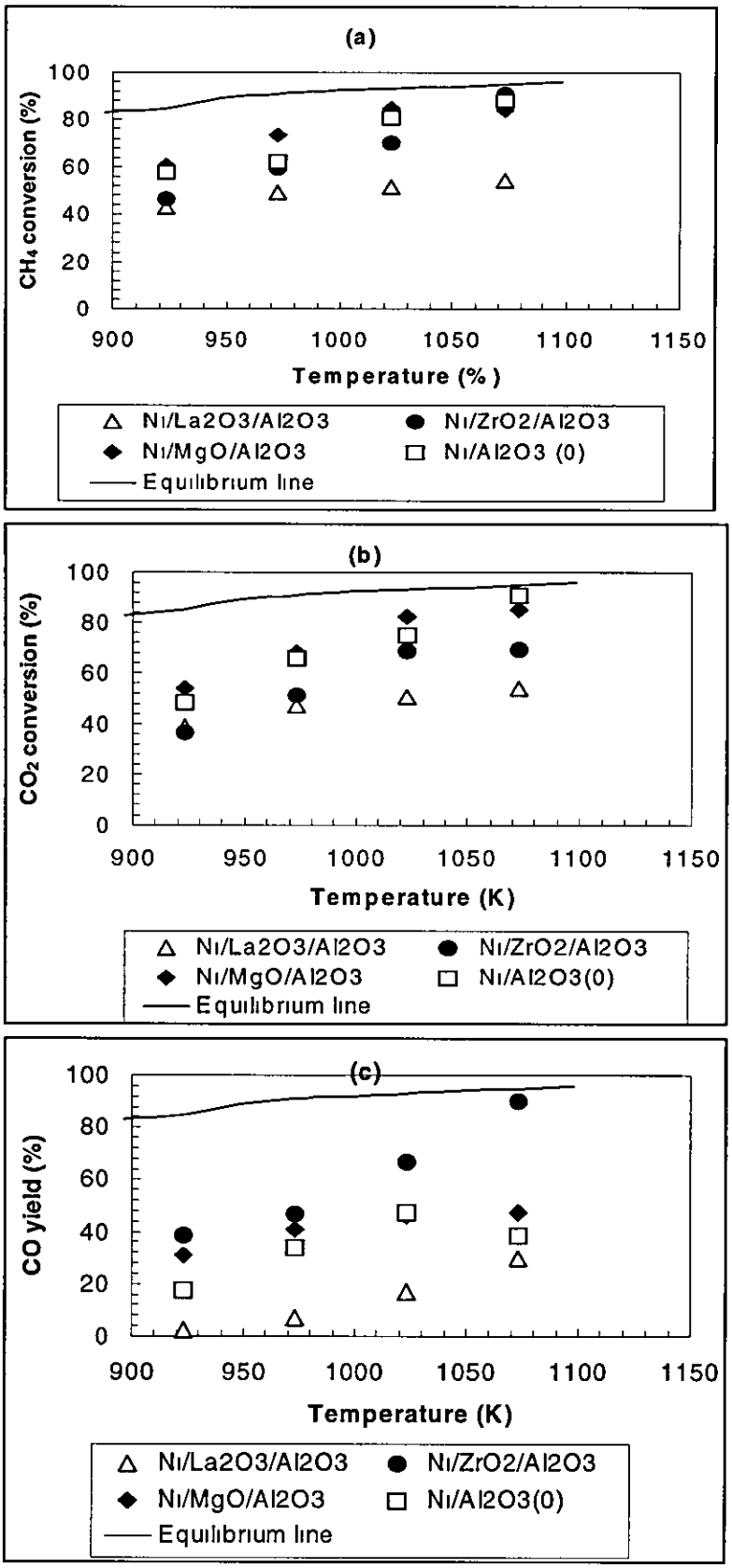

Figure A3.3 Conversion and yield as a function of temperature (a) CH_4 (b) CO_2 and (c) CO, 6h, P = 1 atm, WHSV =7 840 ml, hr g cat, catalyst

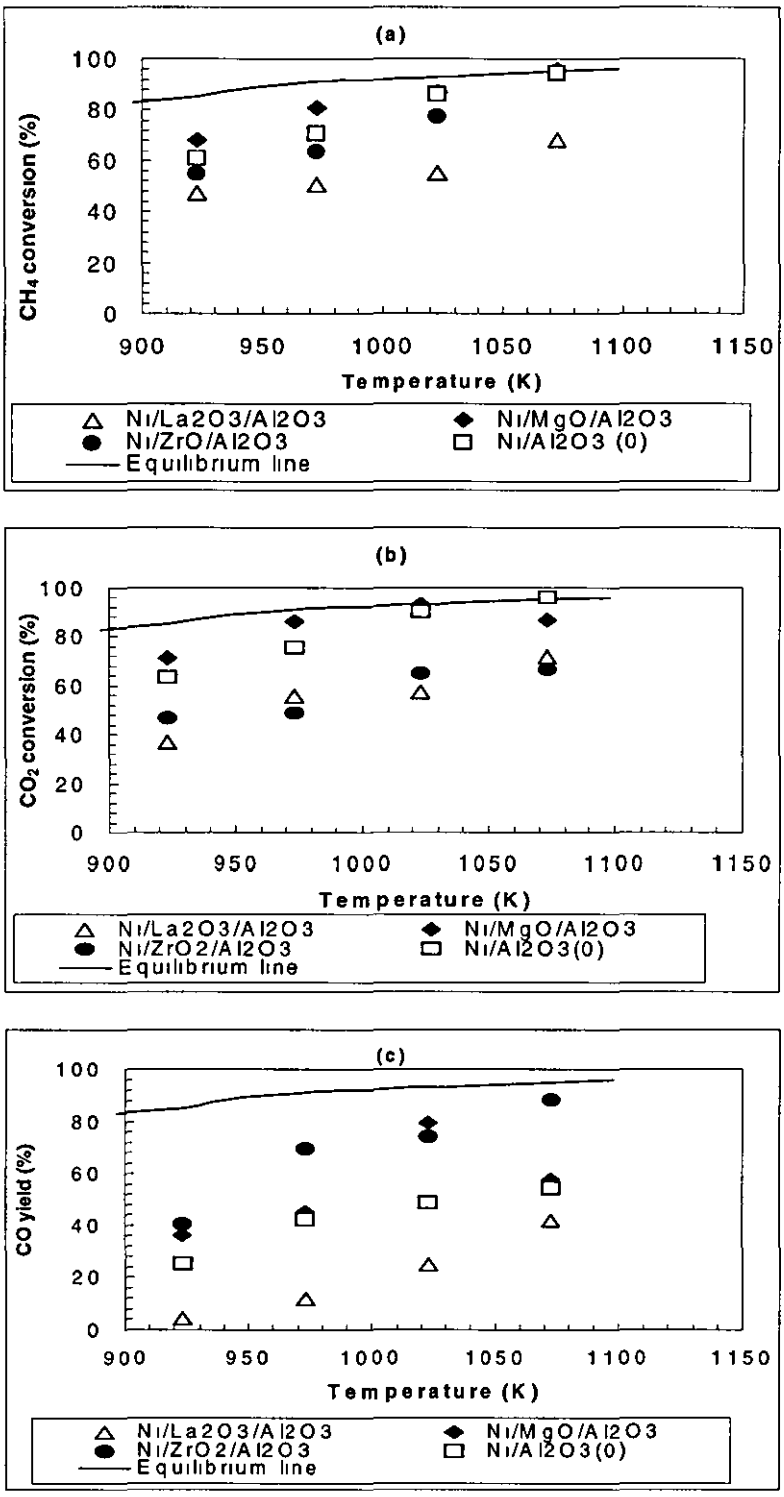

Figure A3.4 Conversion and yield as a function of temperature (a) CH_4 (b) CO_2 and (c) CO, 6h, P = 1 atm, WHSV = 4800 ml, hr g cat, catalyst

A3.2 Experimental plots for effect of support for Ni catalyst on stability, T=1073K

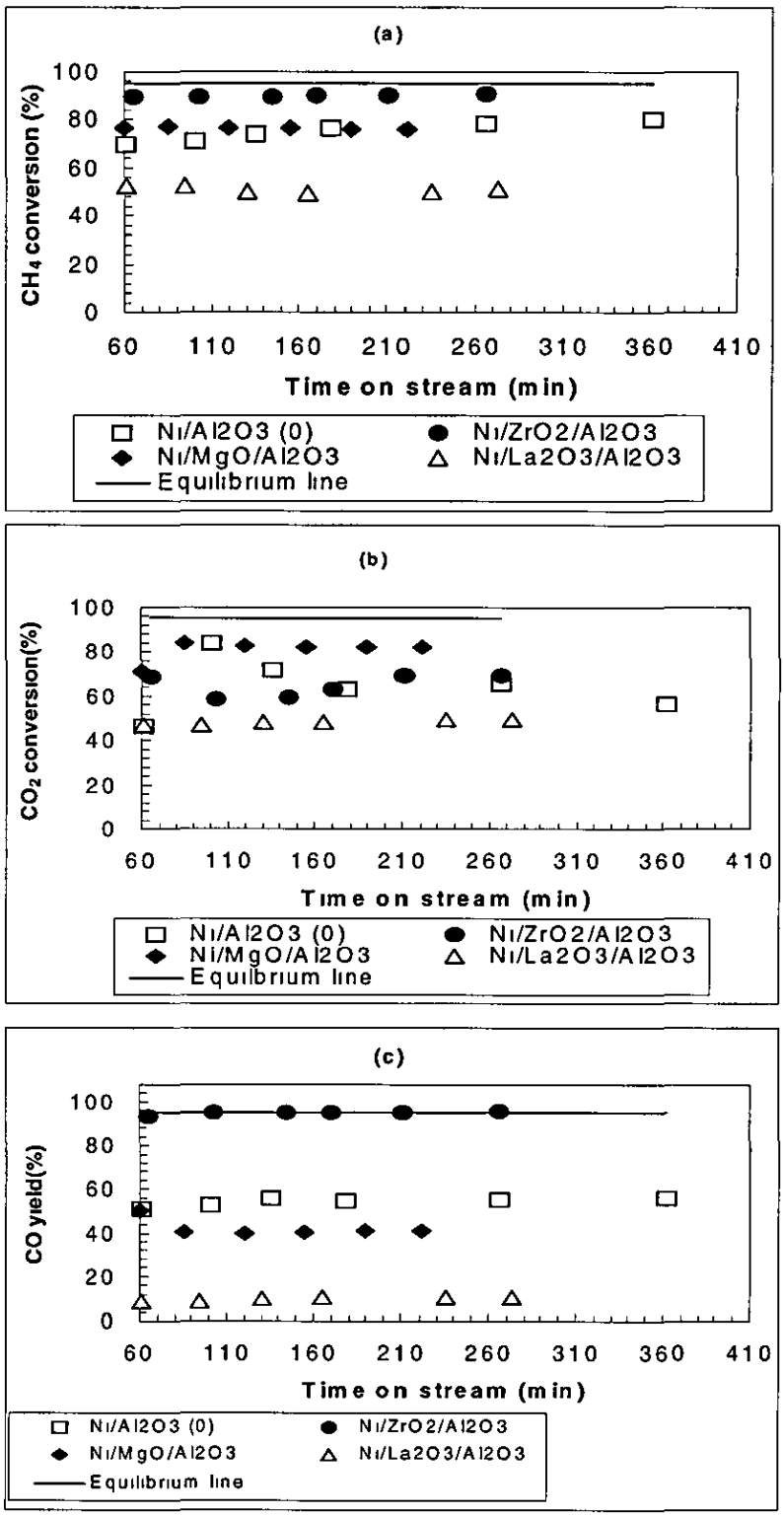

Figure A3 2.1 Conversion and yield as a function of time (a) CH_4 (b) CO_2 and (c) CO, 6h, P = 1 atm, WHSV = 9820 ml, hr gcat, catalyst

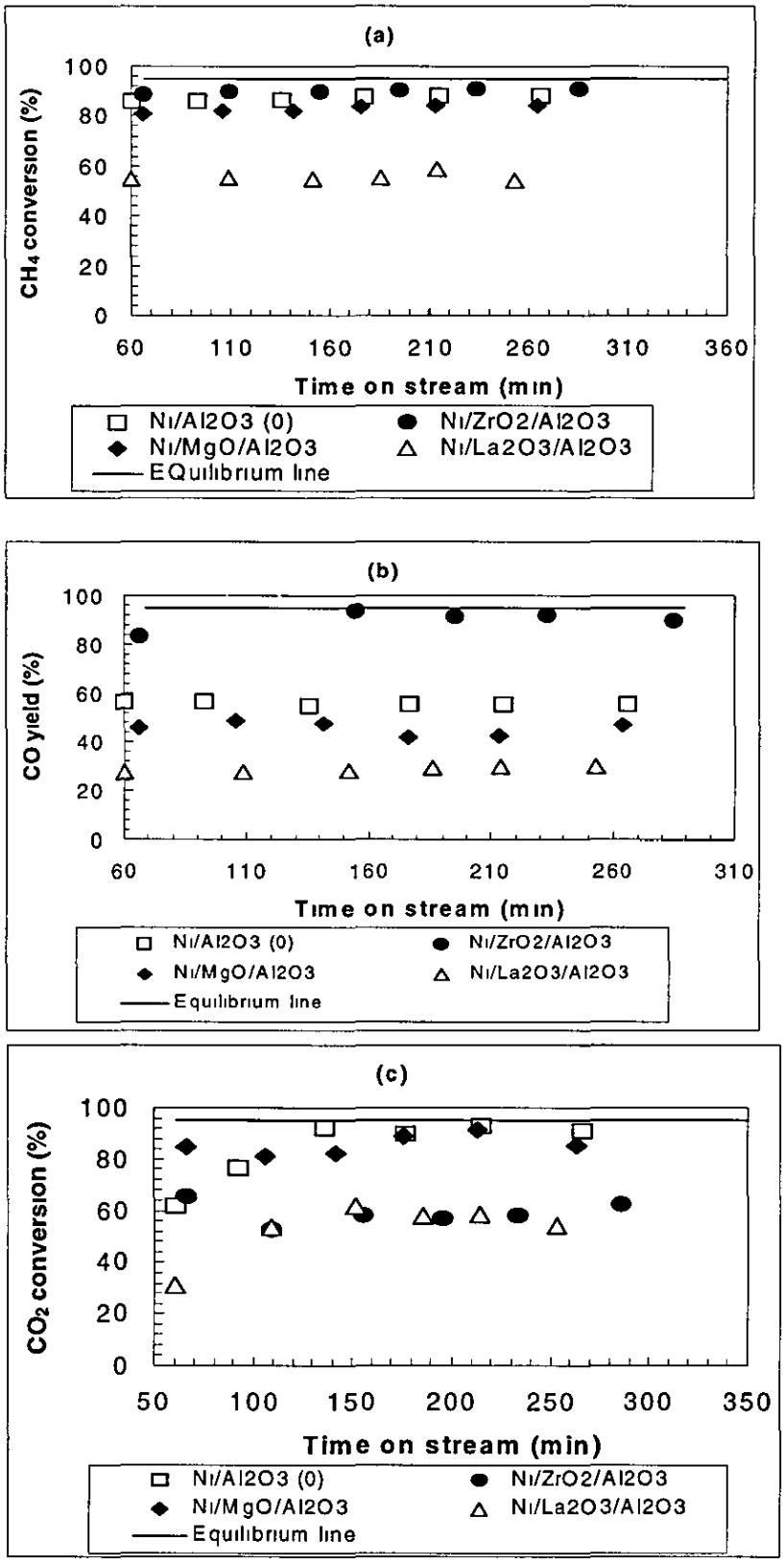

Figure A3.2 2 Conversion and yield as a function of time (a) CH_4 (b) CO and (c) CO_2, 6h, P = 1 atm, WHSV = 7840 ml, hr g cat, catalyst

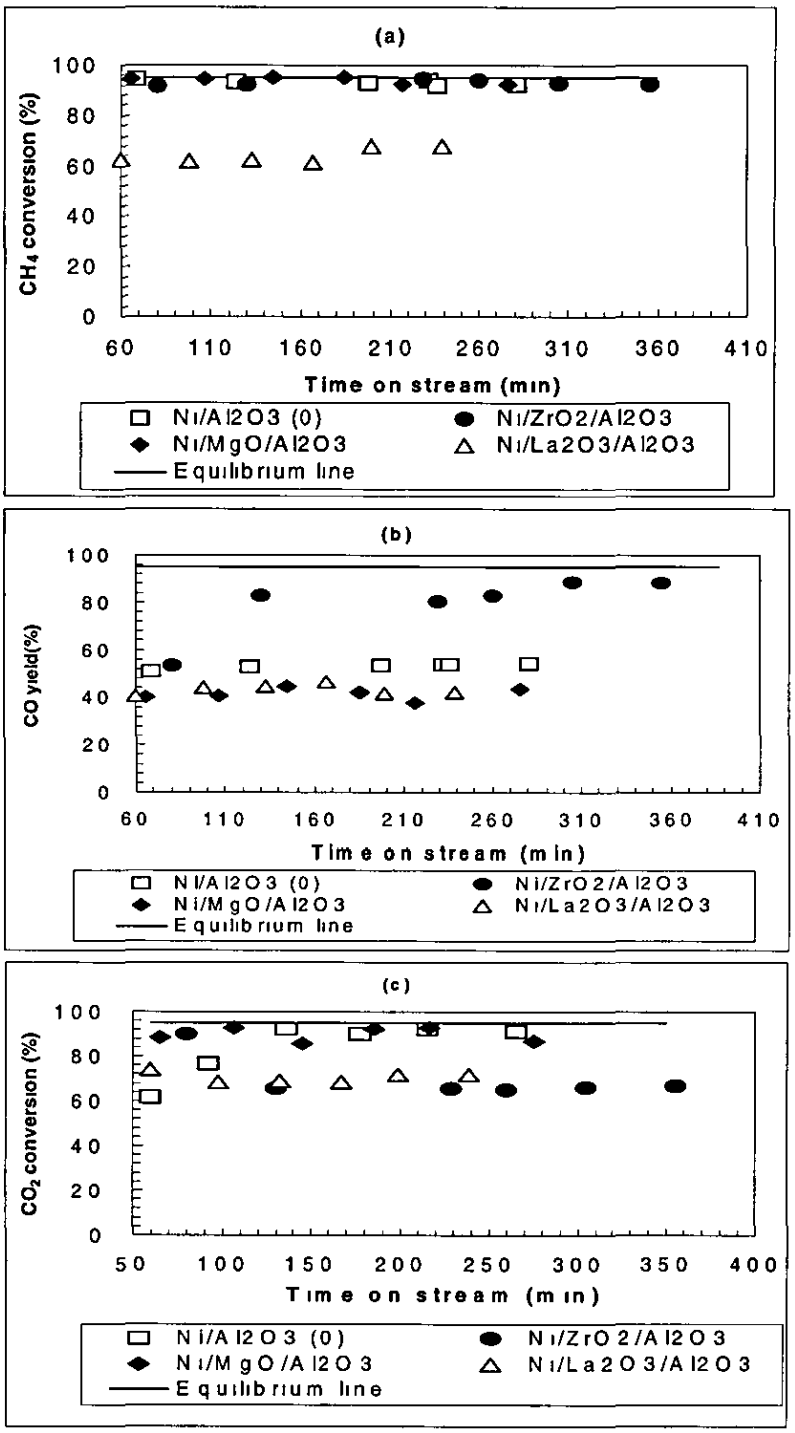

Figure A3.2 3 Conversion and yield as a function of time (a) CH_4 (b) CO and (c) CO_2, 6h, P = 1 atm, WHSV = 4800 ml, hr g cat, catalyst

A3.3 Experimental plots for effect of support for Ni catalyst on stability, T=1023K

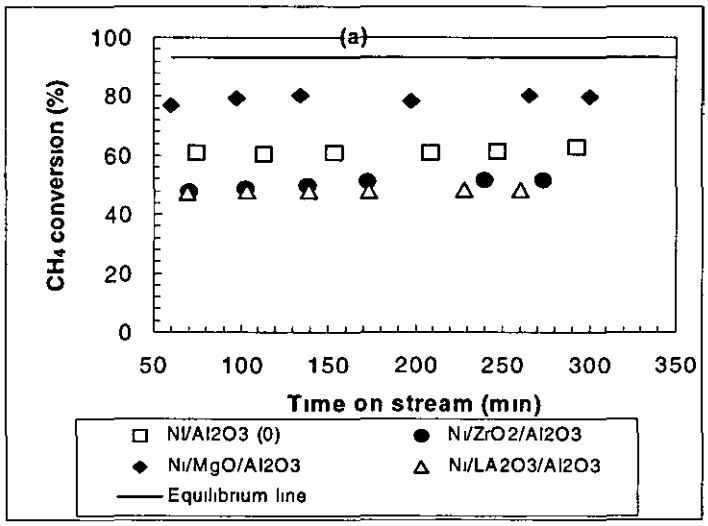

Figure A3 3.1 CH_4 conversion as a function of time, 6h, P = 1 atm, WHSV = 13900 ml, hr g cat, catalyst

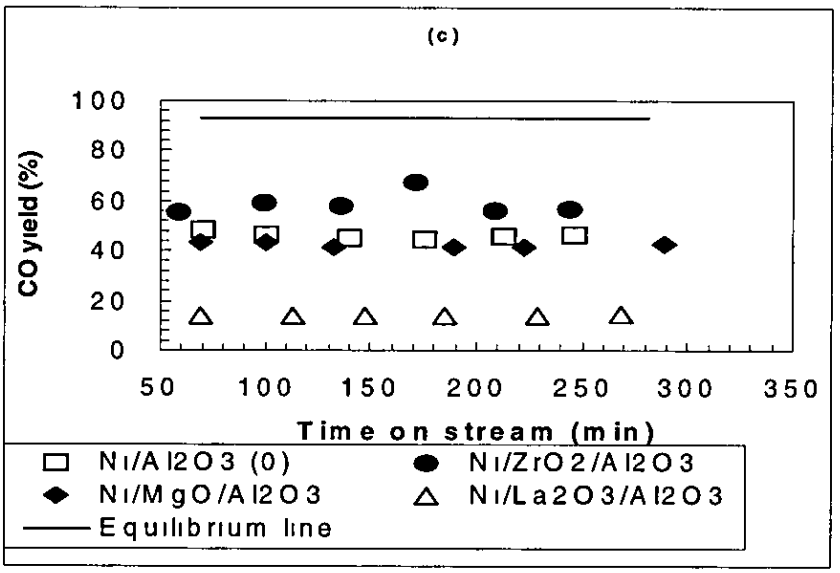

Figure A3 3.2 CO yield as a function of time, 6h, P = 1 atm, WHSV = 9820 ml, hr g cat, catalyst

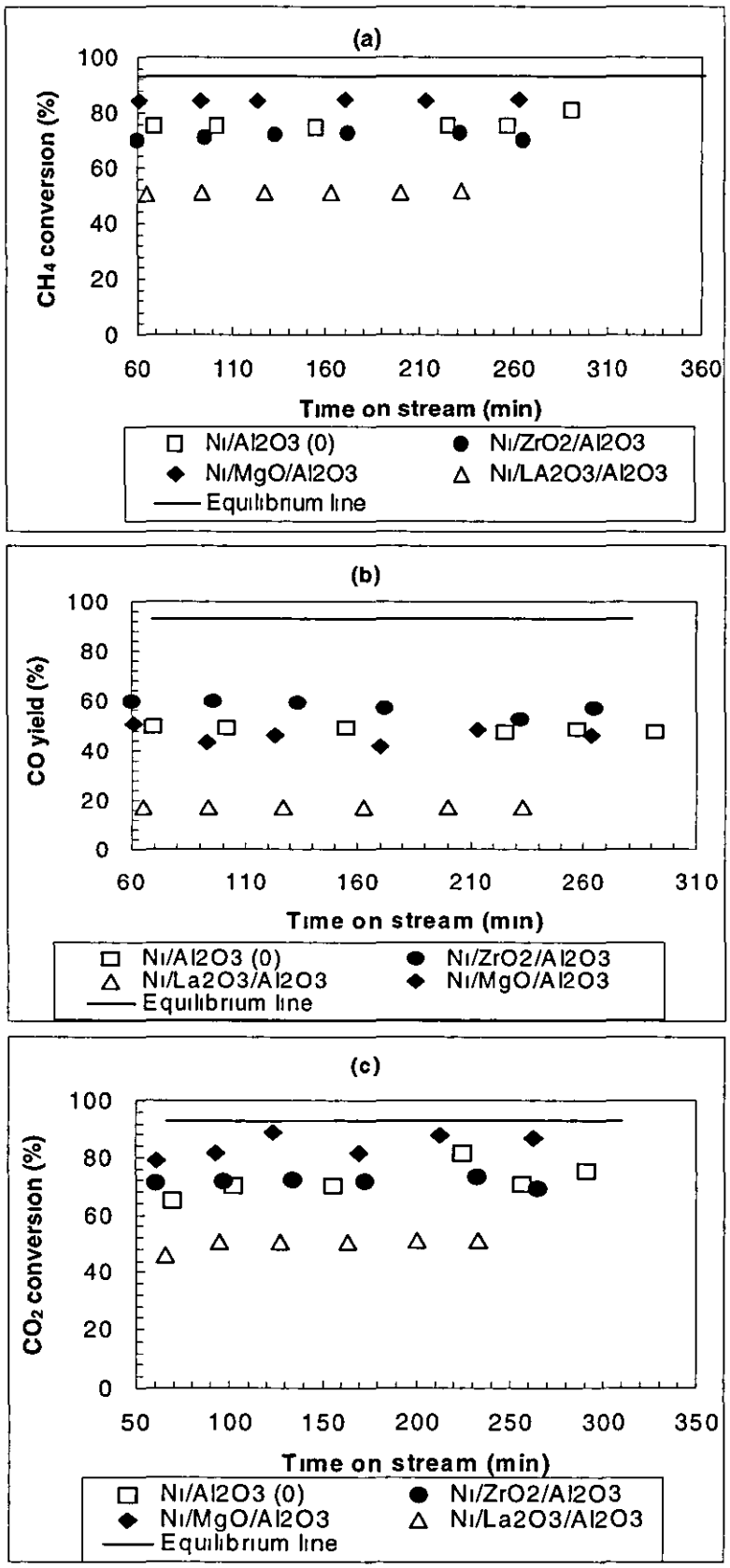

Figure A3.3 3 Conversion and yield as a function of time (a) CH_4 (b) CO and CO_2, 6h, P = 1 atm, WHSV = 7840 ml, hr gcat, catalyst

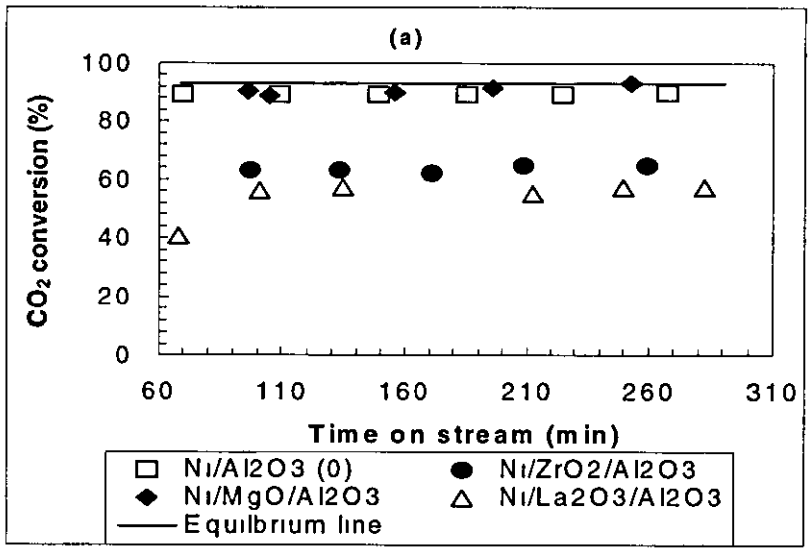

Figure A3.3 4 CO_2 conversion and yield as a function of time 6h, P = 1 atm, WHSV = 4800 ml, hr g cat, catalyst

A.3.4 Experimental plots for effect of support, T = 973K

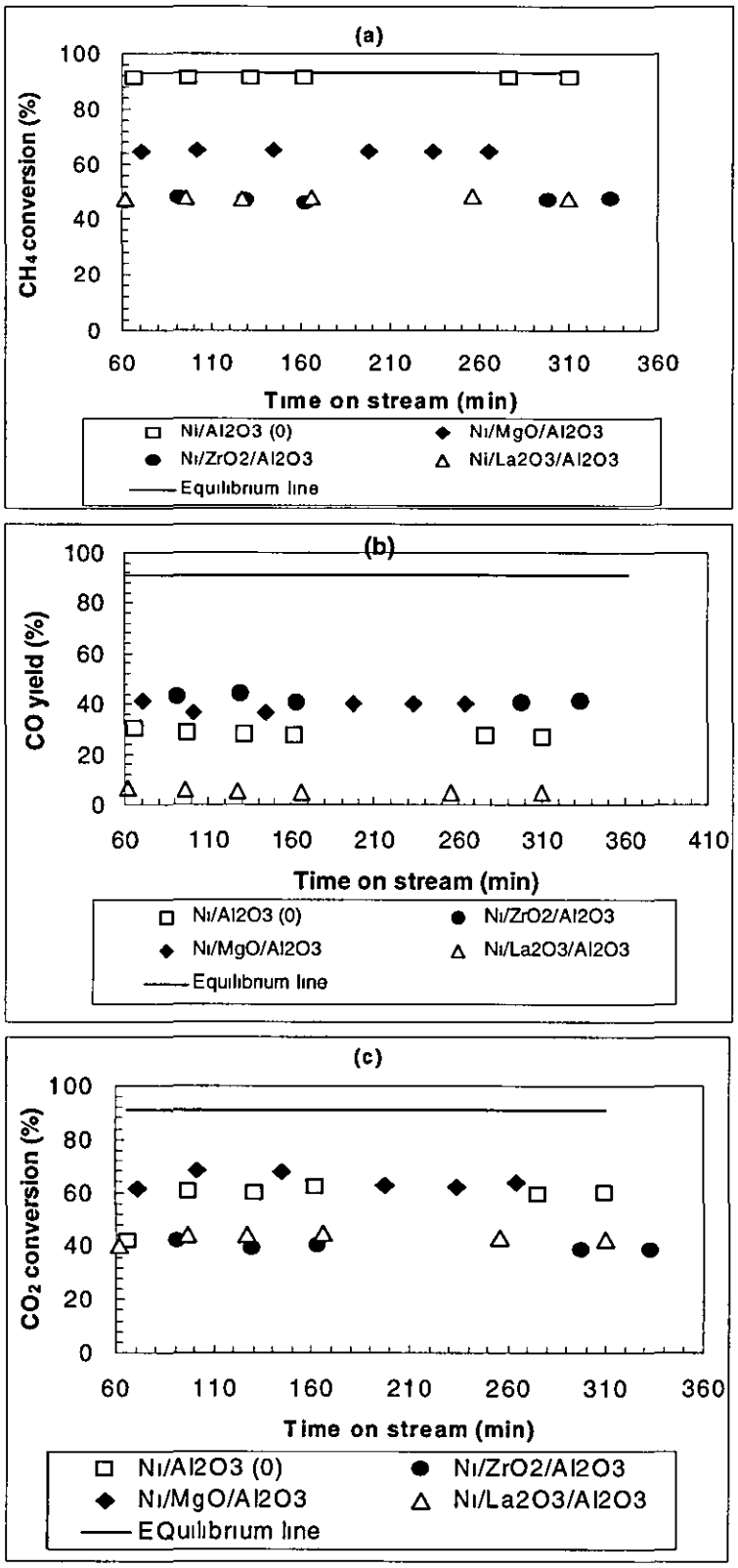

Figure A3 4 1 Conversion and yield as a function of temperature (a) CH_4 (b) CO, (c) CO_2 6h, P = 1 atm, WHSV = 13900 ml, hr gcat, catalyst

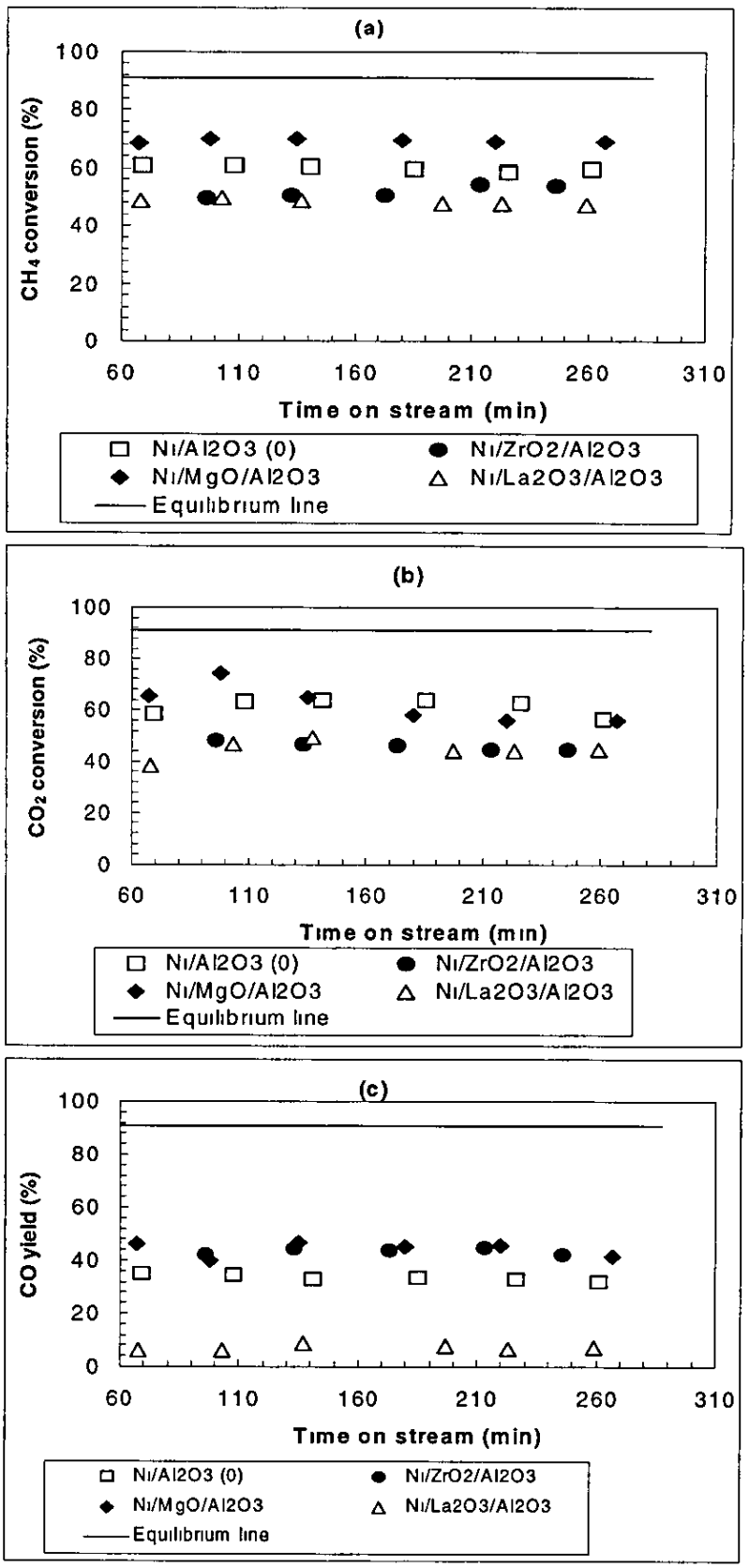

Figure A3 4 2 Conversion and yield as a function of temperature (a) CH_4 (b) CO_2, (c) CO 6h, P = 1 atm, WHSV = 9820 ml, hr g cat, catalyst

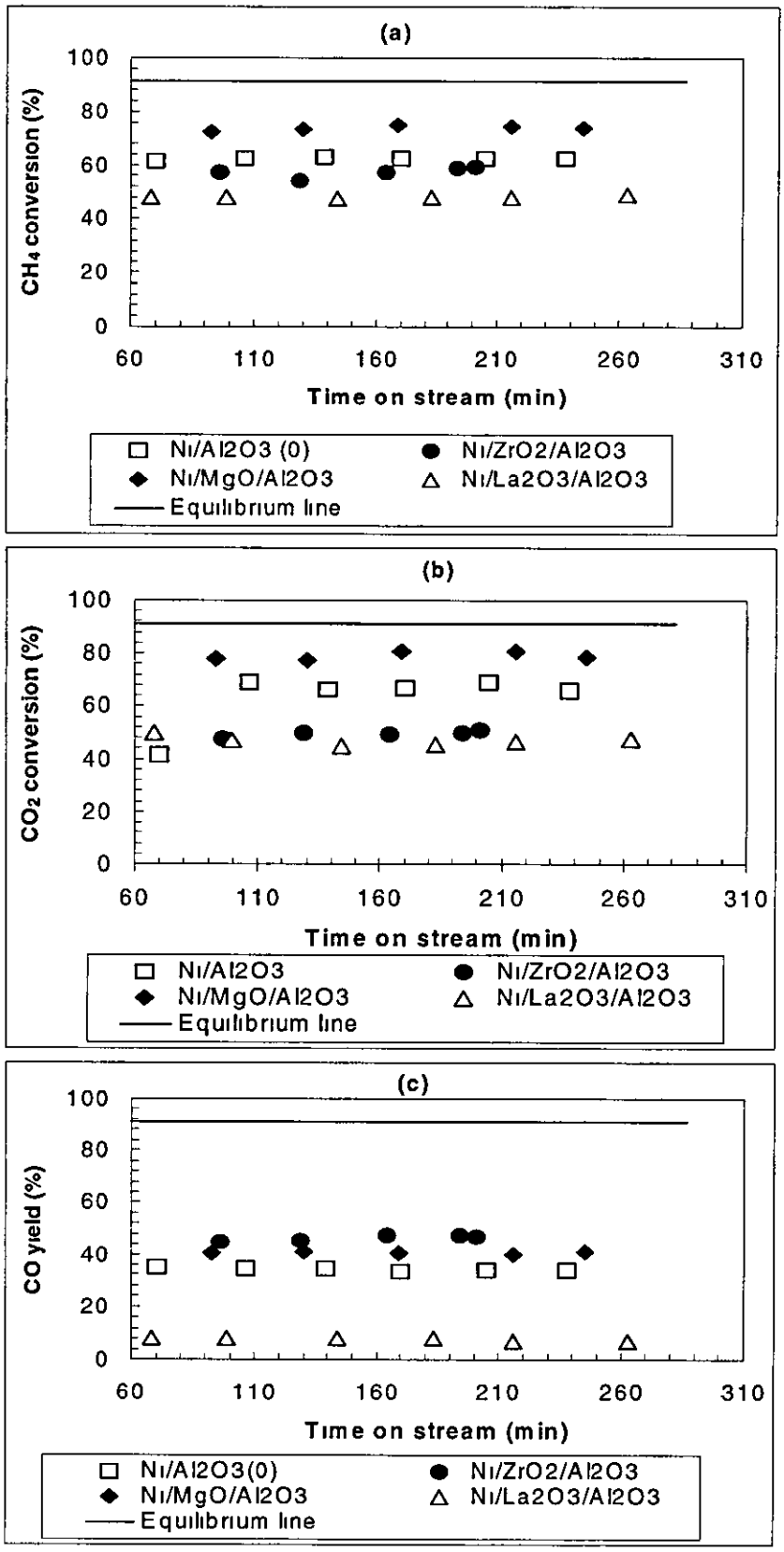

Figure A3 4 3 Conversion and yield as a function of temperature (a) CH_4 (b) CO_2, (c) CO 6h, P = 1 atm, WHSV = 7840 ml, hr gcat, catalyst

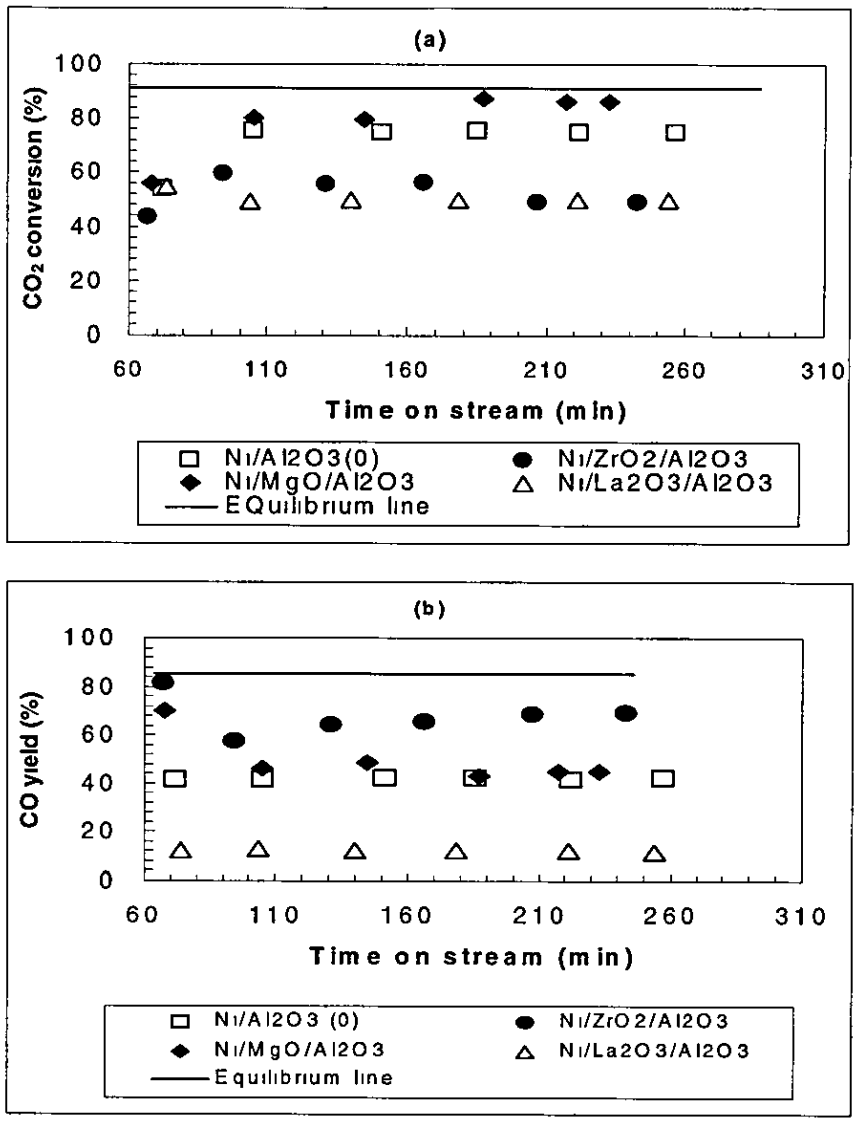

Figure A3.4.4 Conversion and yield as a function of temperature (a) CO_2, (b) CO 6h, P = 1 atm, WHSV = 4800 ml, hr gcat, catalyst

A3.5 Experimental plots for effect of support, T = 923K

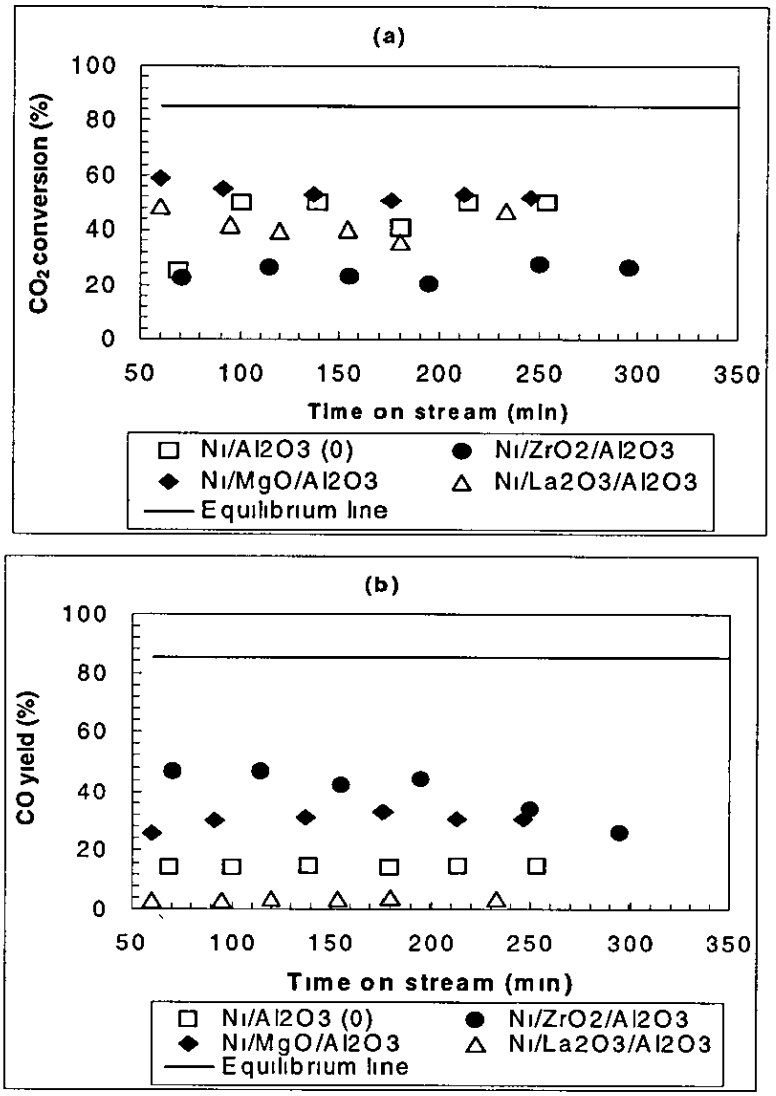

Figure A3 5.1 Conversion and yield as a function of temperature (a) CO_2, (b) CO 6h, P = 1 atm, WHSV = 13900 ml, hr g cat, catalyst

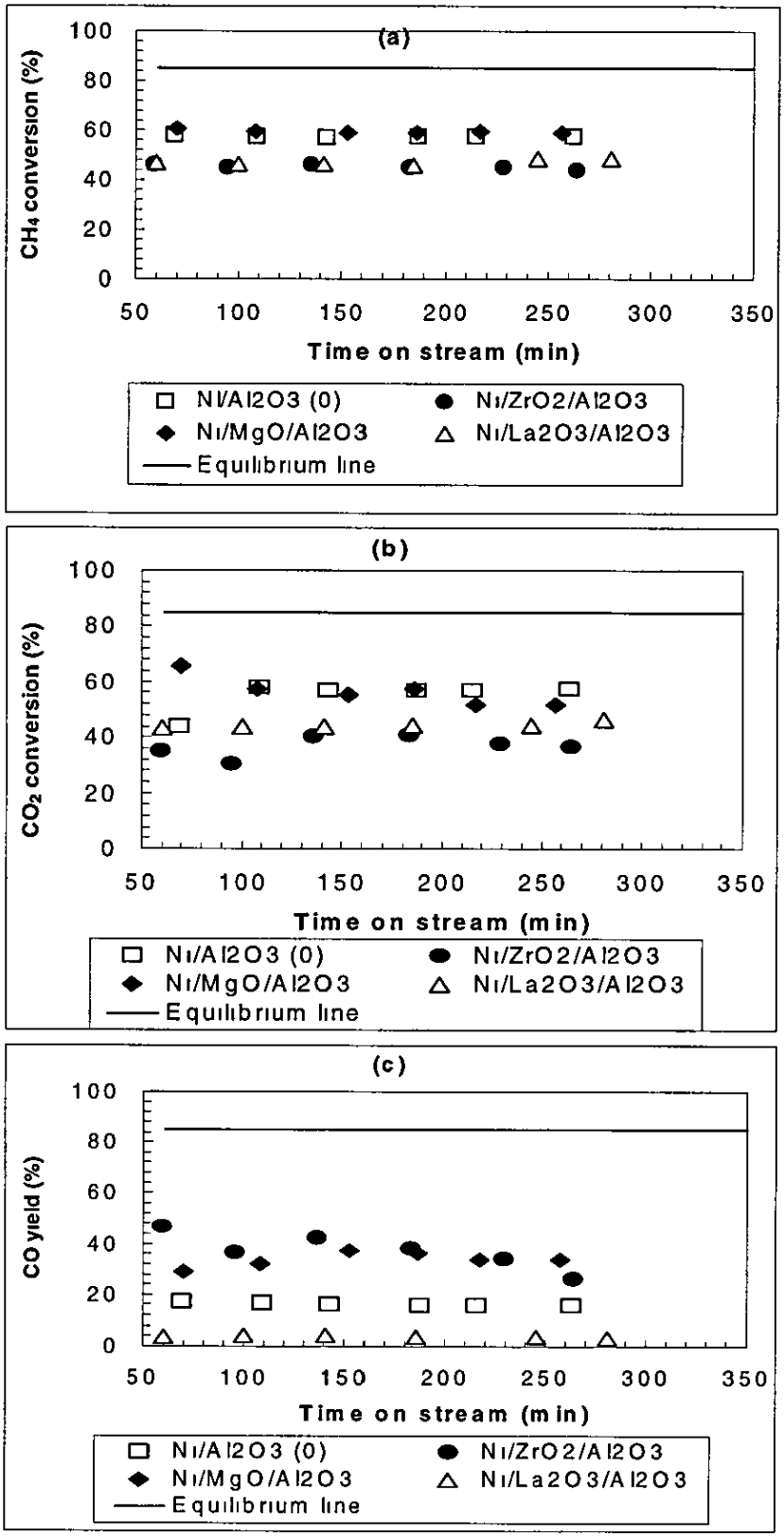

Figure A3.5 2 Conversion and yield as a function of temperature (a) CH_4 (b) CO_2, (c) CO, 6h, P = 1 atm, WHSV = 9820 ml, hr gcat, catalyst

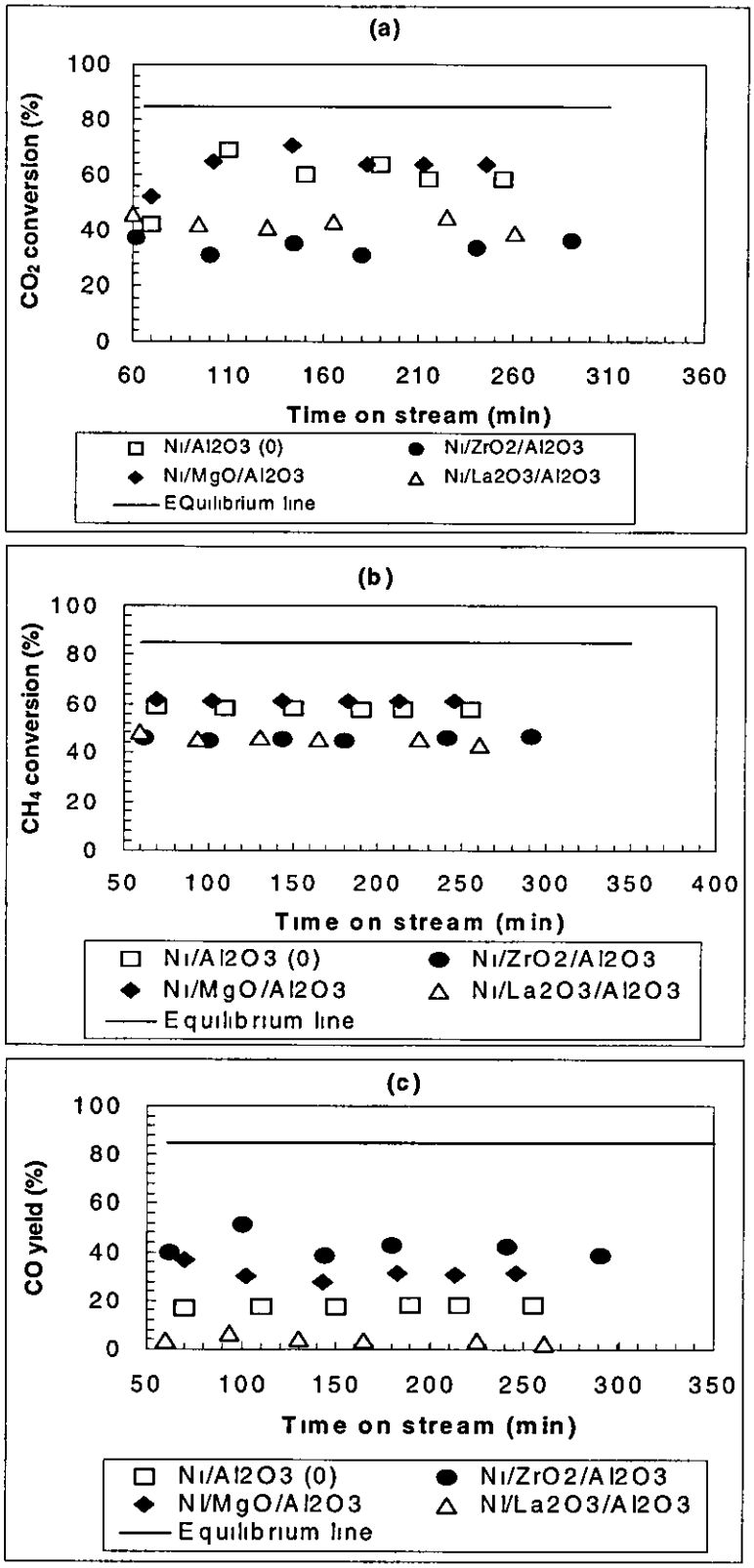

Figure A3.5 3 Conversion and yield as a function of temperature (a) CO_2, (b) CH_4 (c) CO 6h, P = 1 atm, WHSV = 7840 ml, hr gcat, catalyst

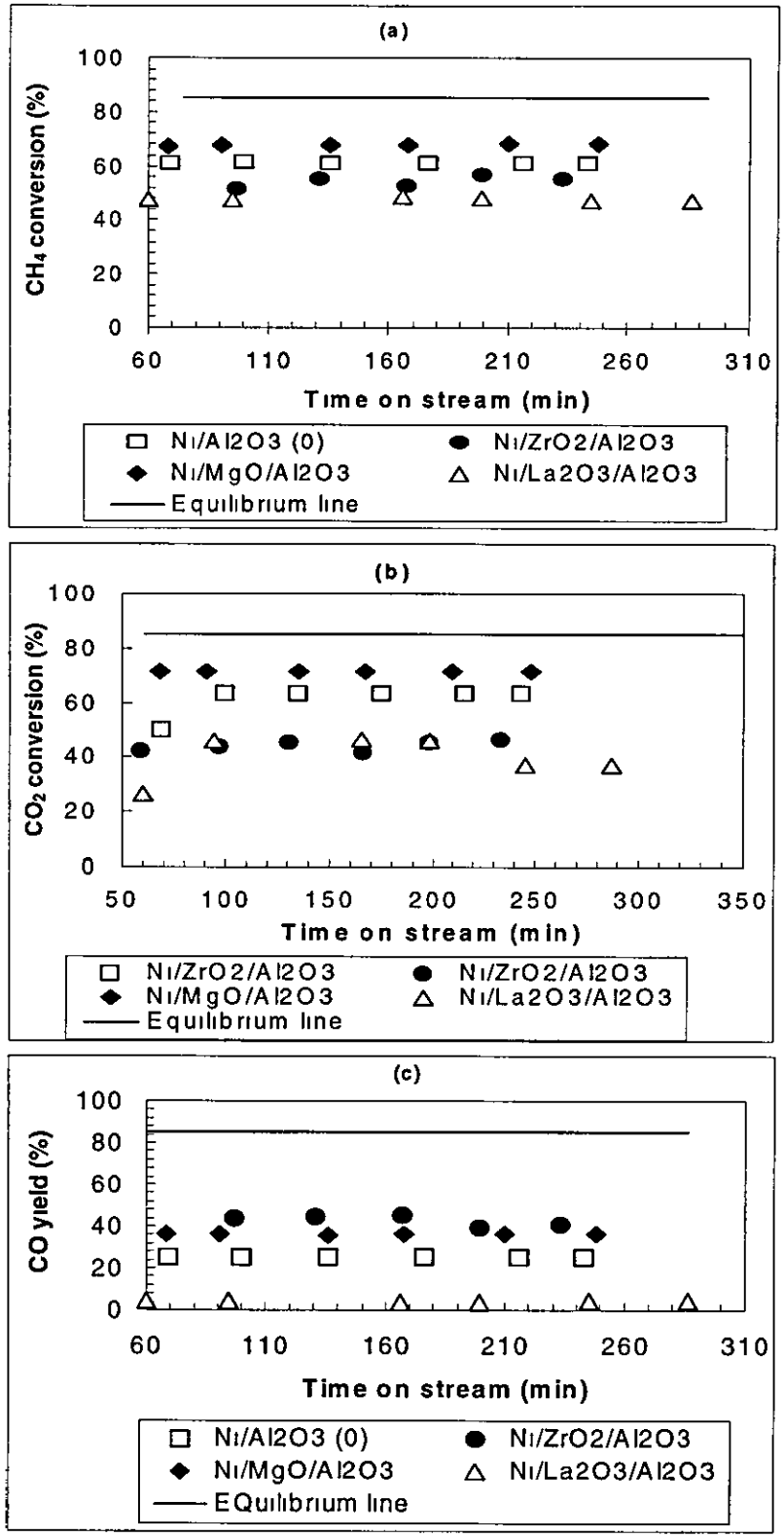

Figure A3.5 4 Conversion and yield as a function of temperature (a) CO_2, (b) CH_4 (c) CO, 6h, P = 1 atm, WHSV = 4800 ml, hr gcat, catalyst

A4.1 Appendix IV

A4.1.1 Experiment plots for effect of palladium on catalytic activity

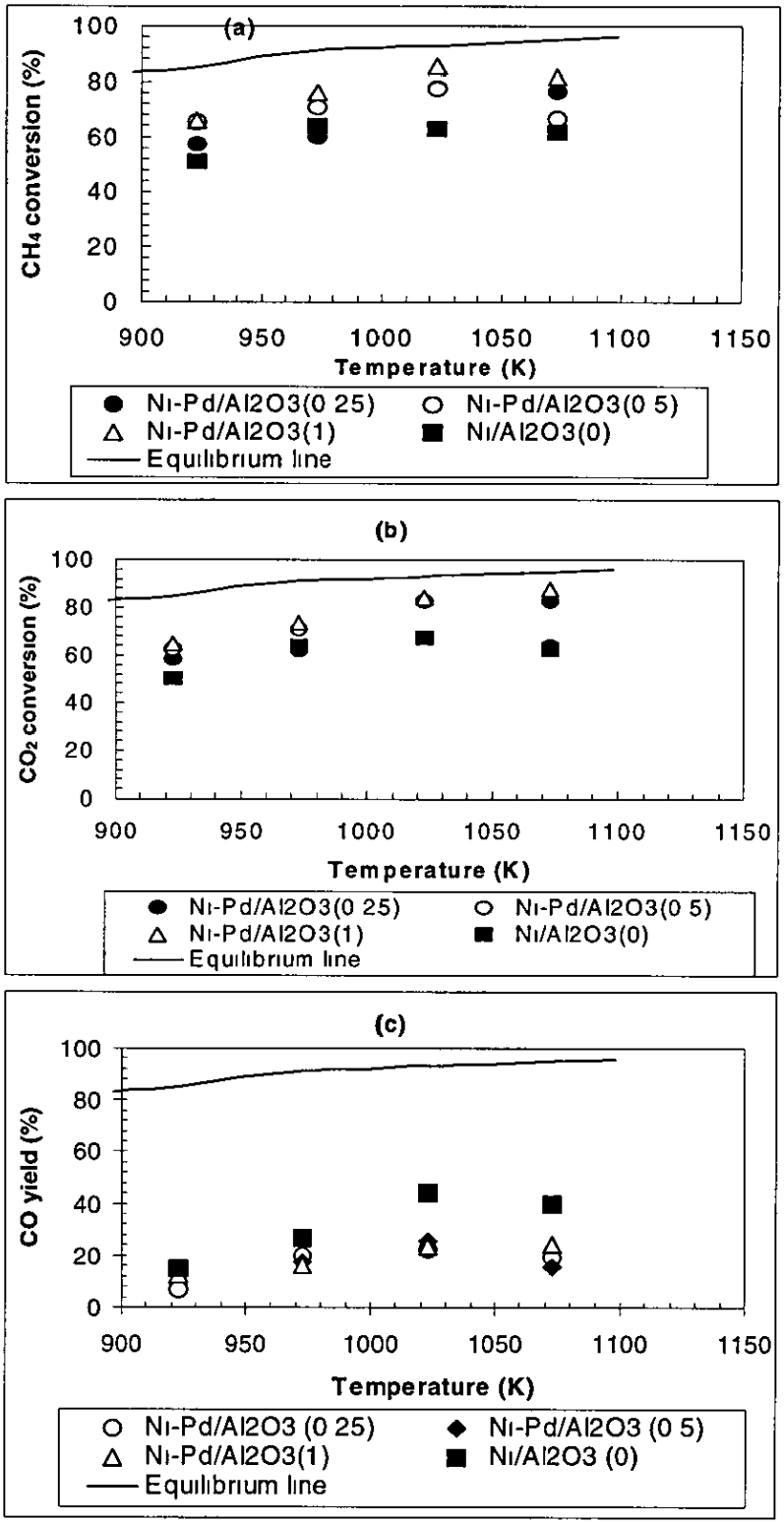

Figure A4.1 1 Conversion and yield as a function of temperature (a) CH_4 (b) CO_2 and (c) CO, 6h, P = 1 atm, WHSV = 13900 ml, hr g cat, catalyst weight = 50 mg

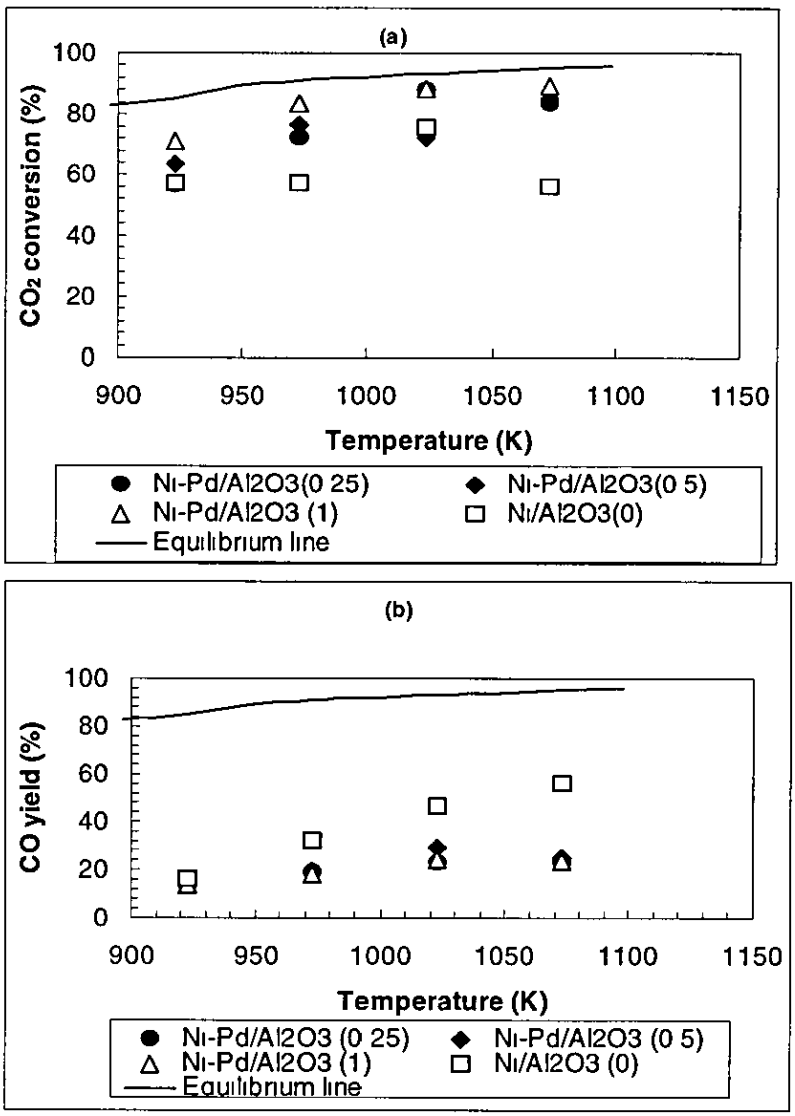

Figure A4.1 2 Conversion and yield as a function of temperature (a) CO_2 (b) CO, T = 1023K, 6h, P = 1 atm, WHSV = 9820 ml, hr g cat, catalyst weight = 50 mg

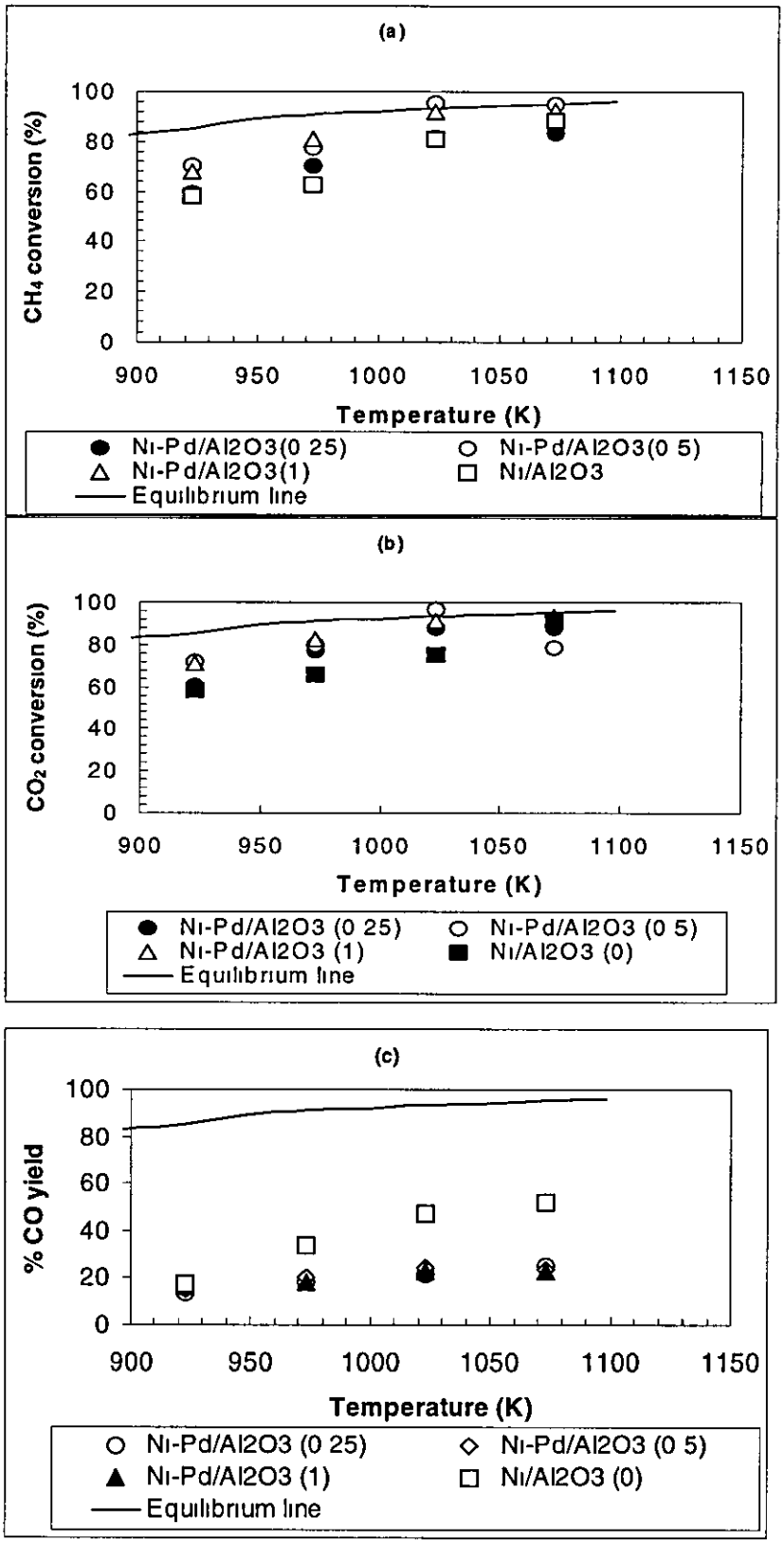

Figure A4.1 3 Conversion and yield as a function of temperature (a) CH_4 (b) CO_2 and (c) CO, T = 1023K, 6h, P = 1 atm, WHSV = 7840 ml, hr g cat, catalyst weight = 50 mg

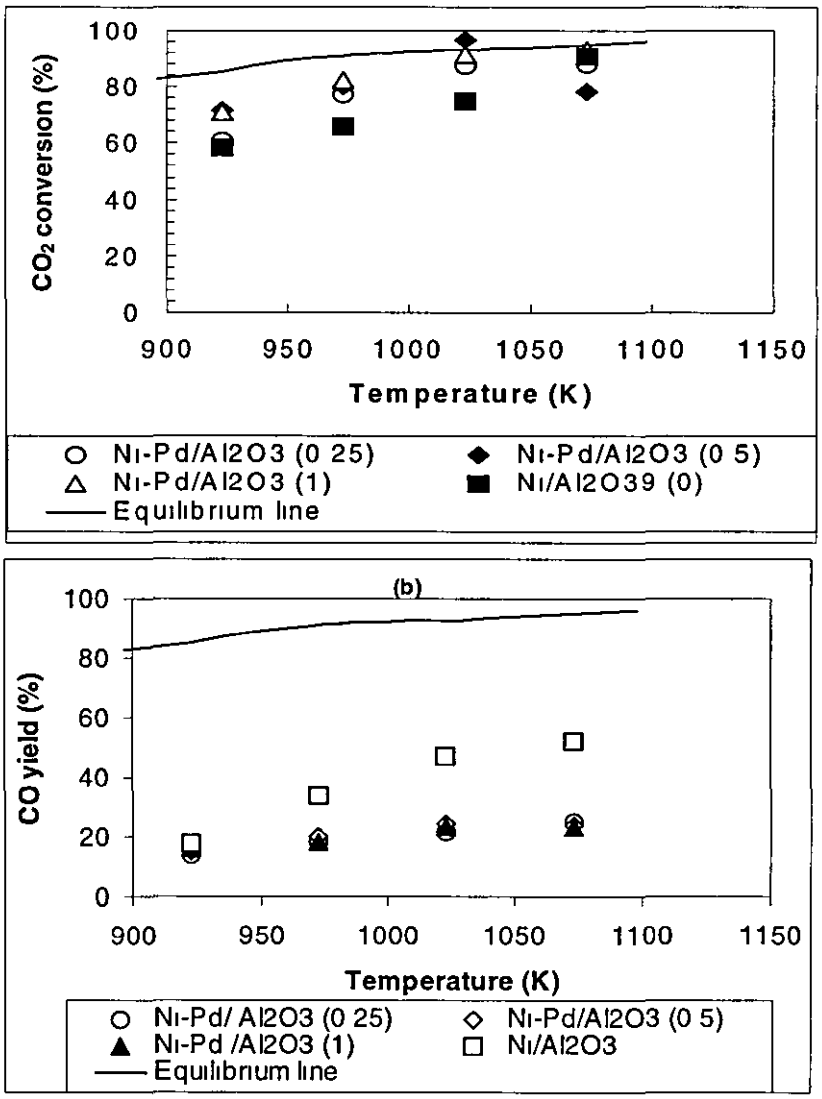

Figure A4.1 4 Conversion and yield as a function of temperature (a) CO_2 and (c) CO, T = 1023K, 6h, P = 1 atm, WHSV = 4800 ml, hr g cat, catalyst weight = 50 mg

A4.2 Experimental plots for effect of palladium promoted Ni catalyst on stability, T = 1023K

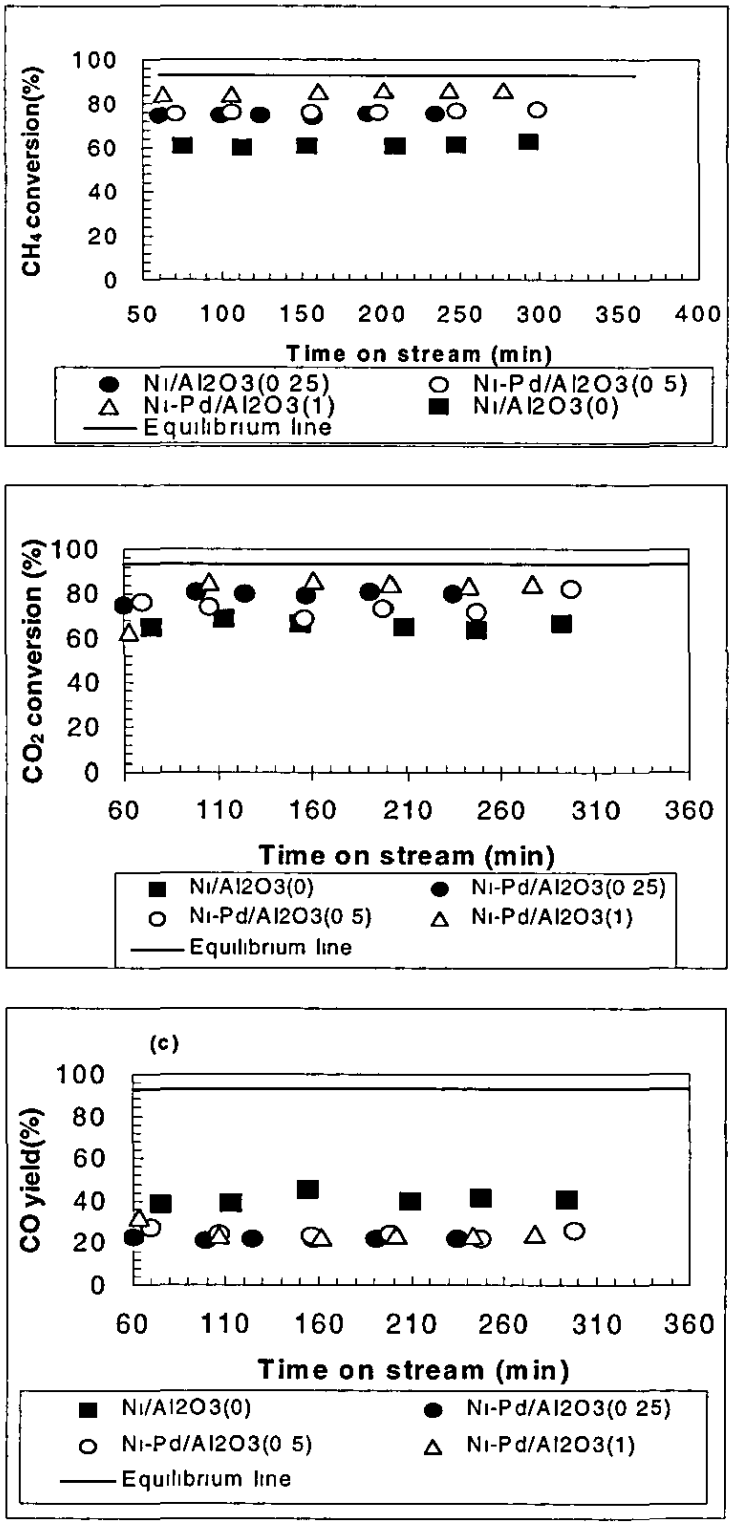

Figure A4 2 1 Conversion and yield as a function of time (a) CH_4 (b) CO_2 and (c) CO, T = 1023K, 6h, P = 1 atm, WHSV = 13900 ml, hr g cat, catalyst weight = 50 mg

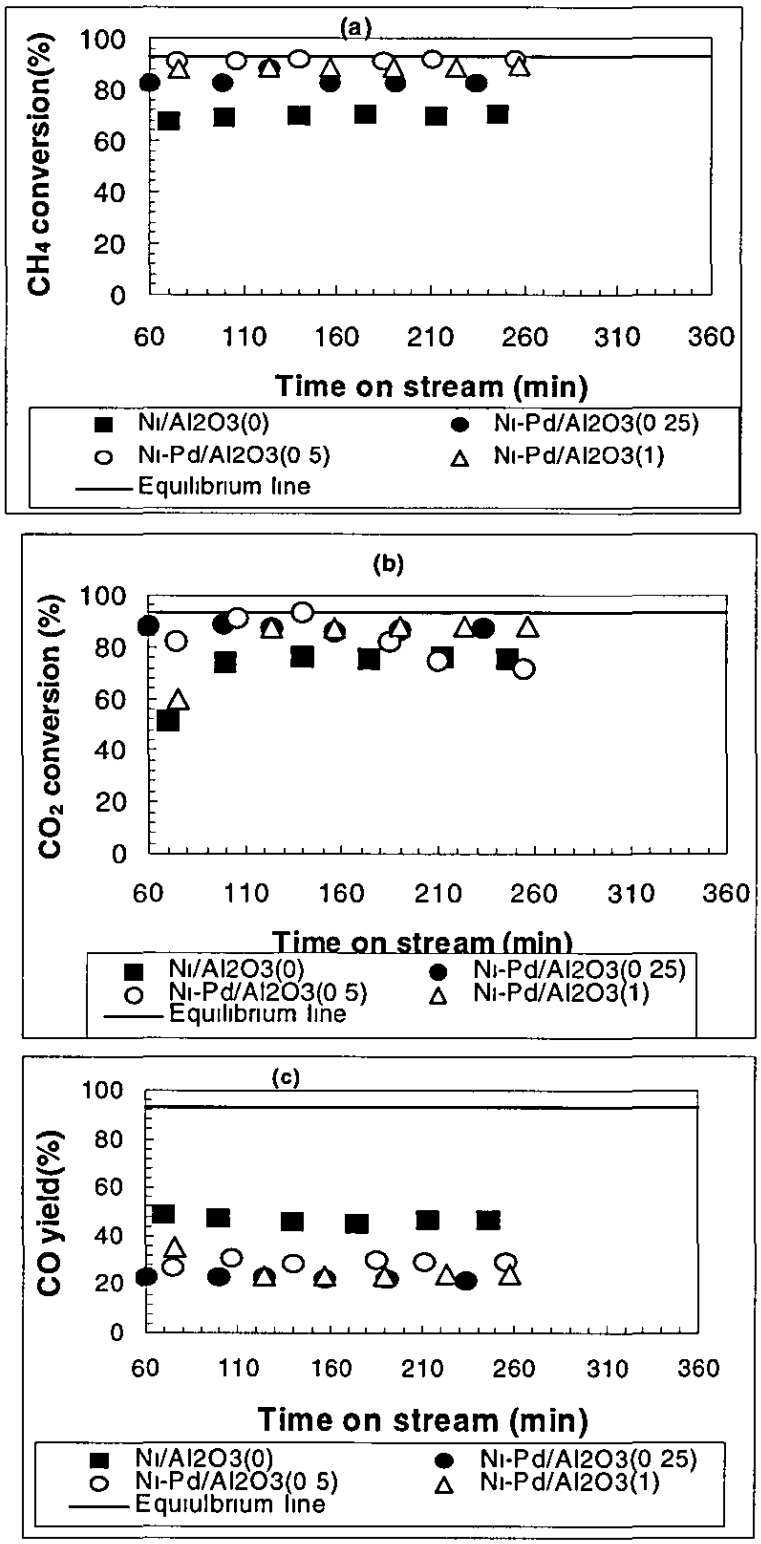

Figure A4 2.2 Conversion and yield as a function of time (a) CH_4 (b) CO_2 and (c) CO, T = 1023K, 6h, P = 1 atm, WHSV = 9820 ml, hr g cat, catalyst weight = 50 mg

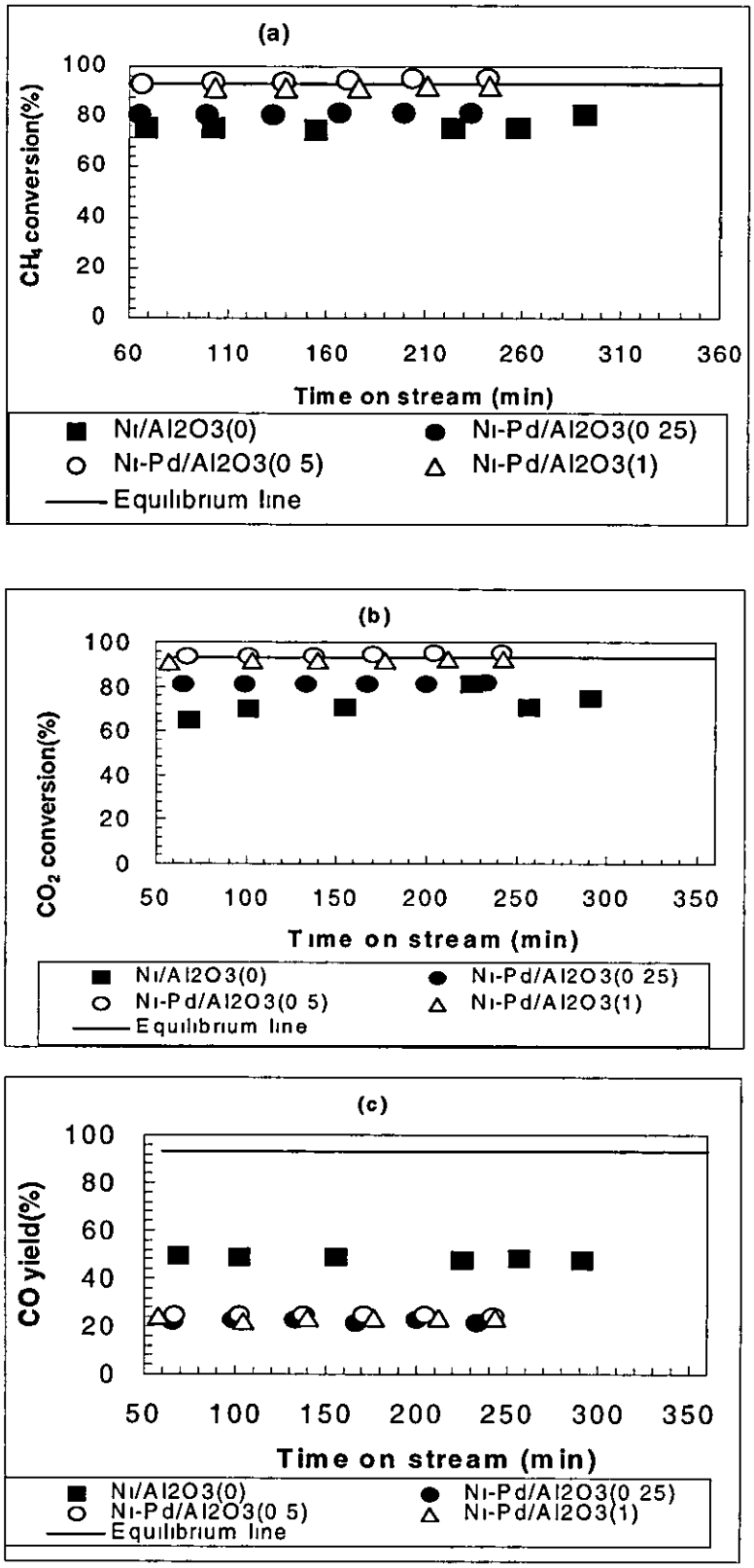

Figure A4 2.3 Conversion and yield as a function of time (a) CH_4 (b) CO_2 and (c) CO, T = 1023K, 6h, P = 1 atm, WHSV = 7840 ml, hr g cat, catalyst weight = 50 mg

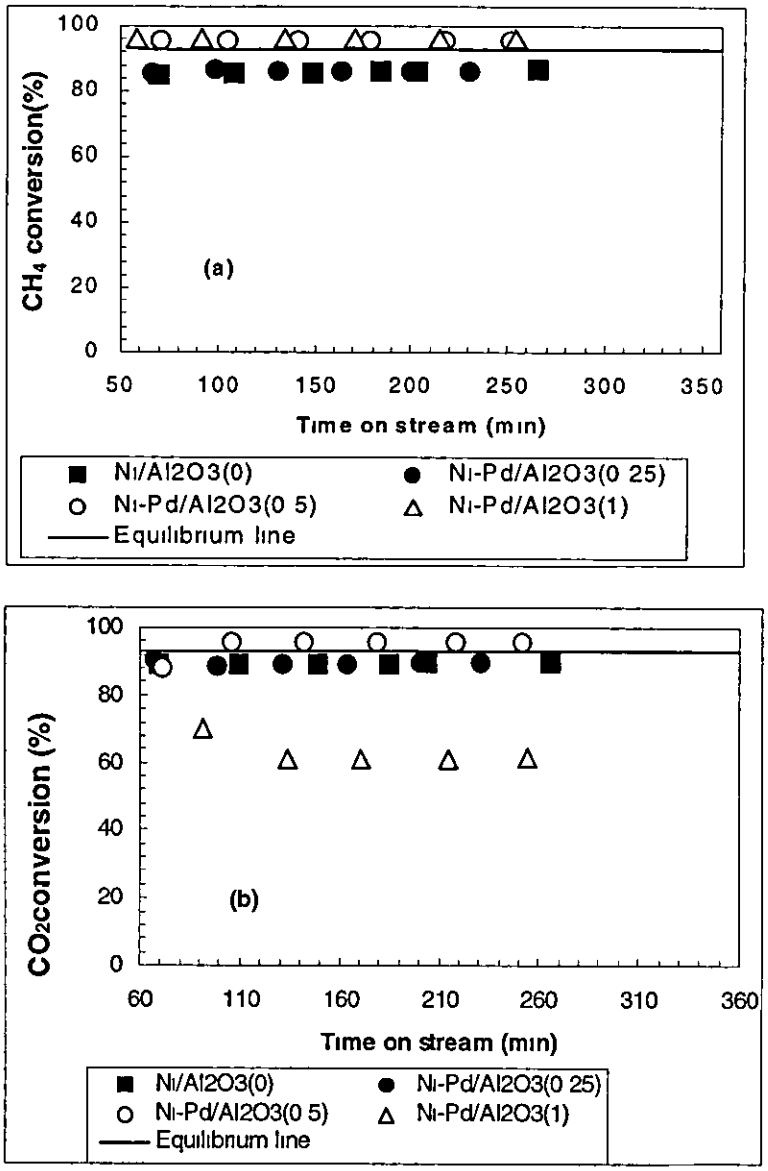

Figure A4.2.4 Conversion as a function of time (a) CH_4 (b) CO_2 and T = 1023K, 6h, P = 1 atm, WHSV = 4800 ml, hr gcat, catalyst weight = 50 mg

A4.3 Experimental plots for effect of palladium promoted Ni catalyst on stability, T = 973K

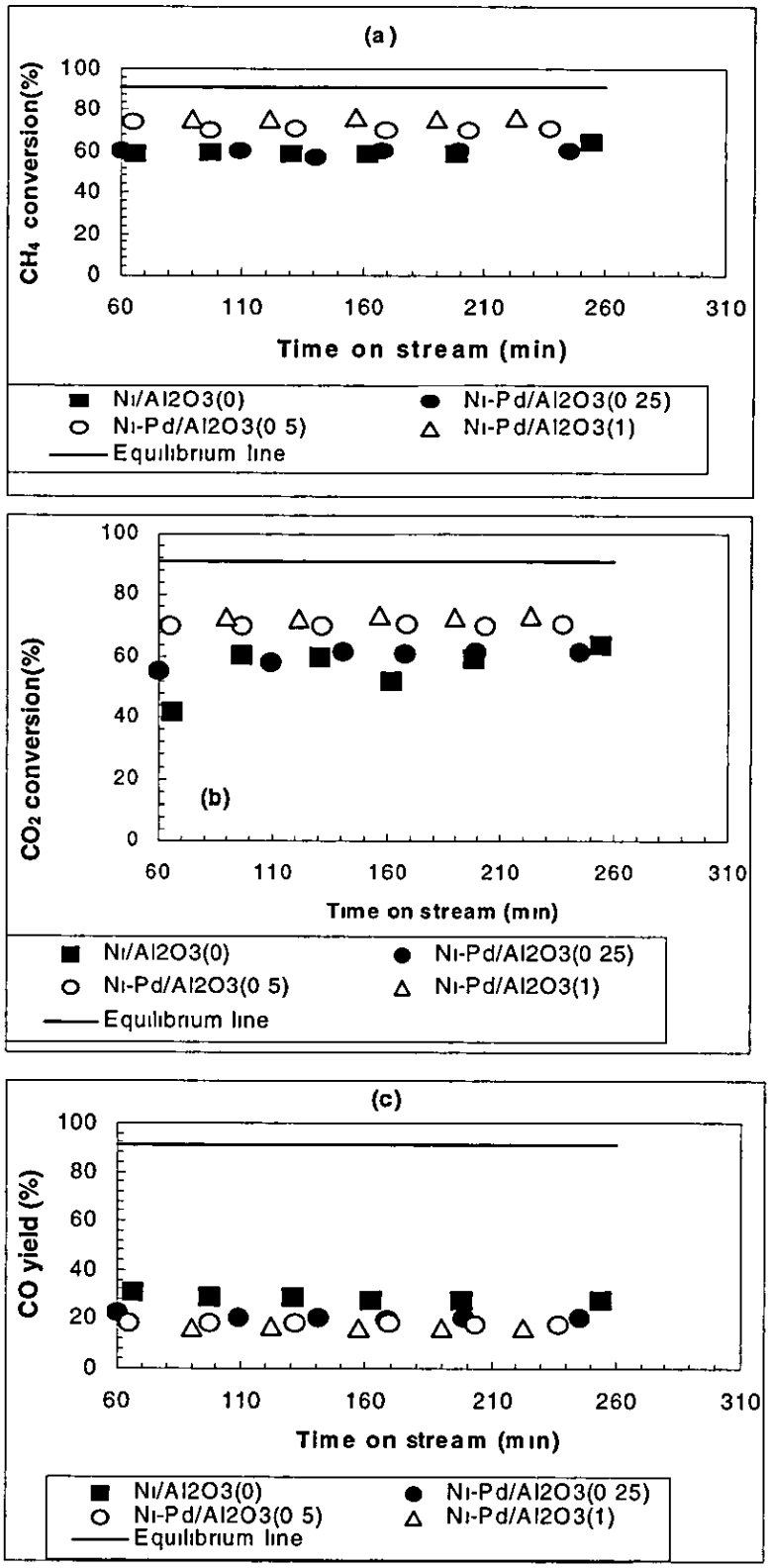

Figure A4 3.1 Conversion as a function of time (a) CH_4 (b) CO_2 and (c) CO, T = 973K, 6h, P = 1 atm, WHSV = 13900 ml, hr g cat, catalyst weight = 50 mg

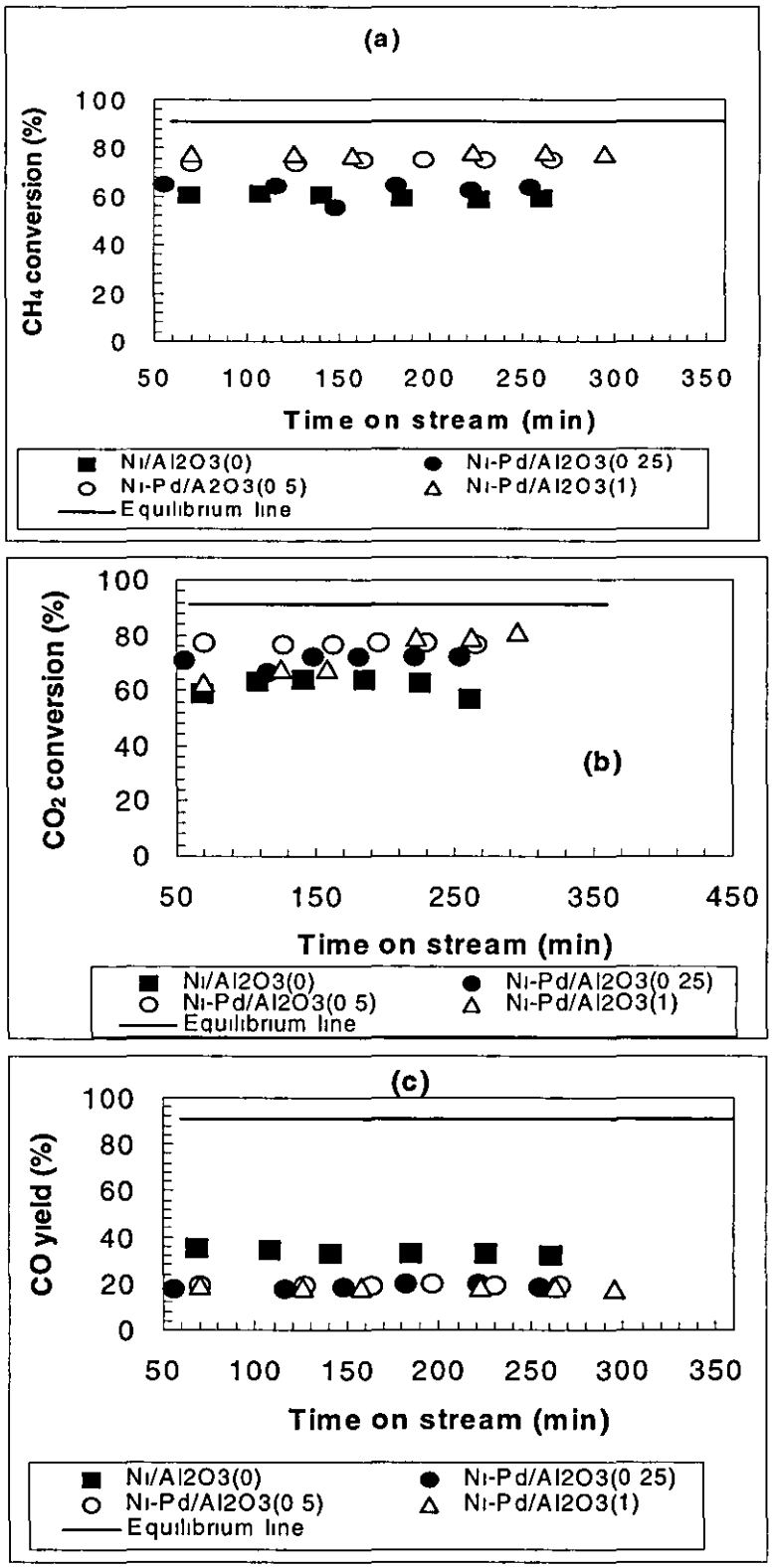

Figure A4.3.2 Conversion as a function of time (a) CH_4 (b) CO_2 and (c) CO, T = 973K, 6h, P = 1 atm, WHSV = 9820 ml, hr g cat, catalyst weight = 50 mg

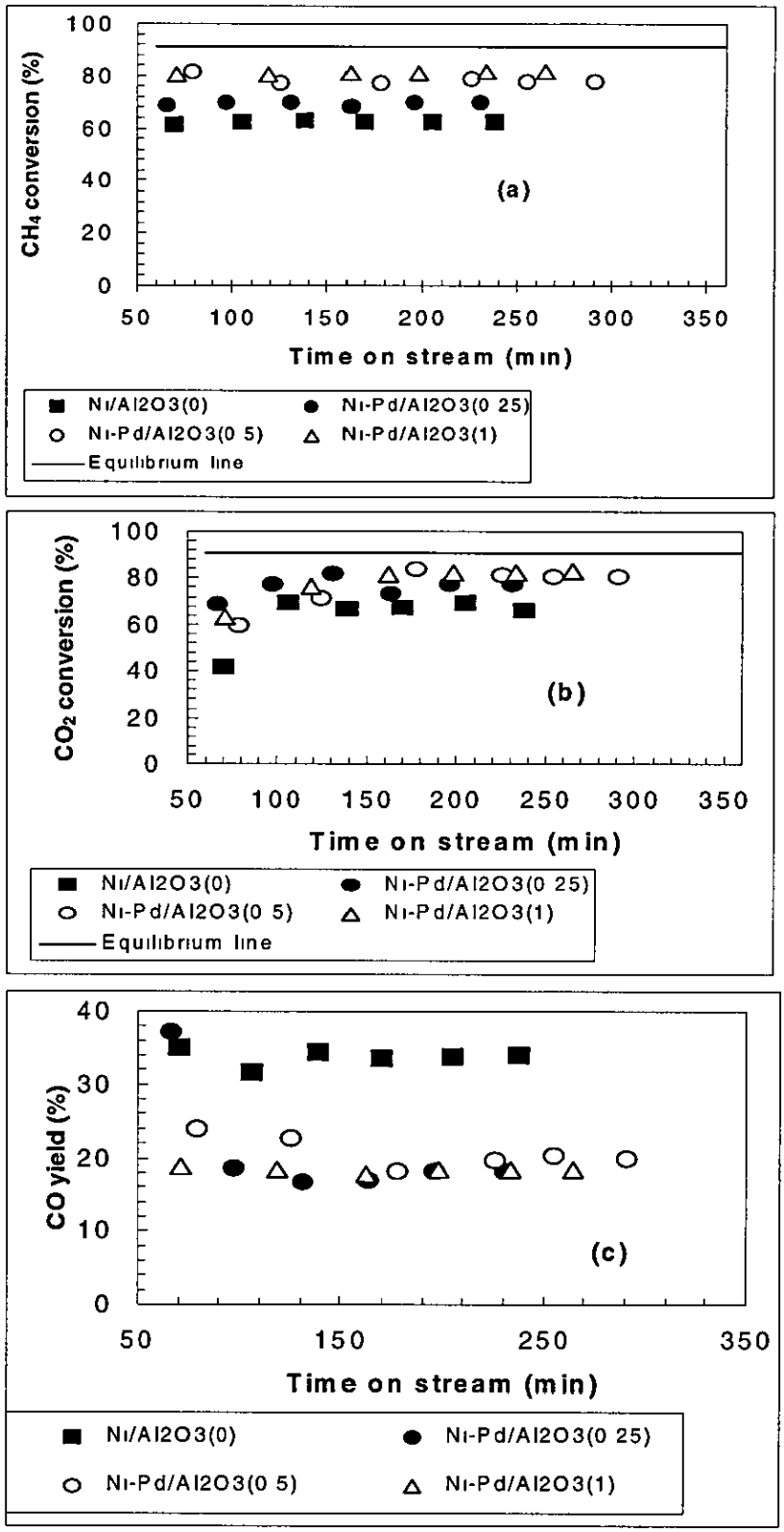

Figure A4 3.3 Conversion as a function of time (a) CH_4 (b) CO_2 and T = 973K, 6h, P = 1 atm, WHSV = 7840 ml, hr g cat, catalyst weight = 50 mg

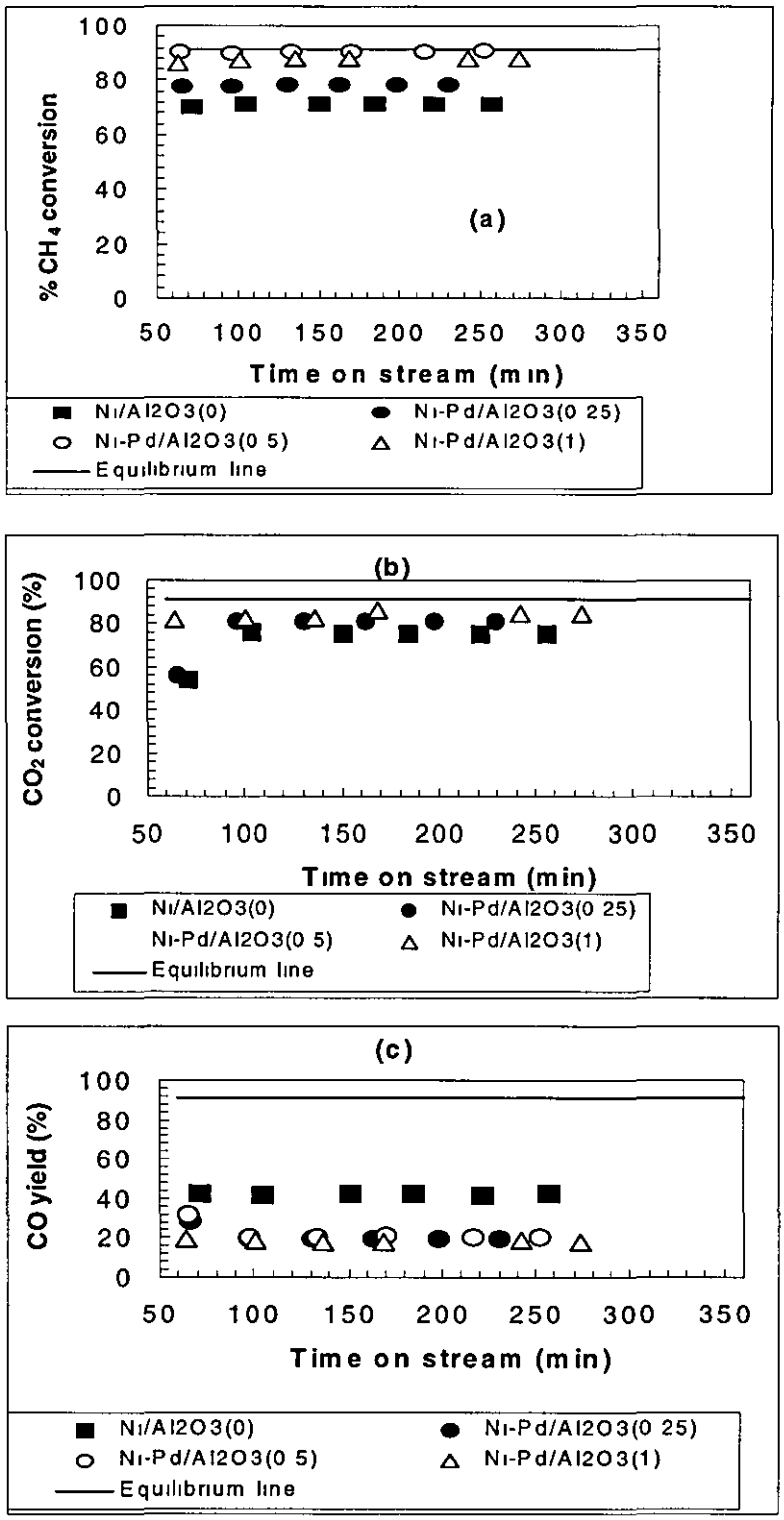

Figure A4.3.4 Conversion and yield as a function of time (a) CH_4 (b) CO_2 and (c) CO T = 973K, 6h, P = 1 atm, WHSV = 4800 ml, hr gcat, catalyst weight = 50 mg

A4.4 Experimental plots for effect of palladium promoted Ni catalyst on stability, T = 923K

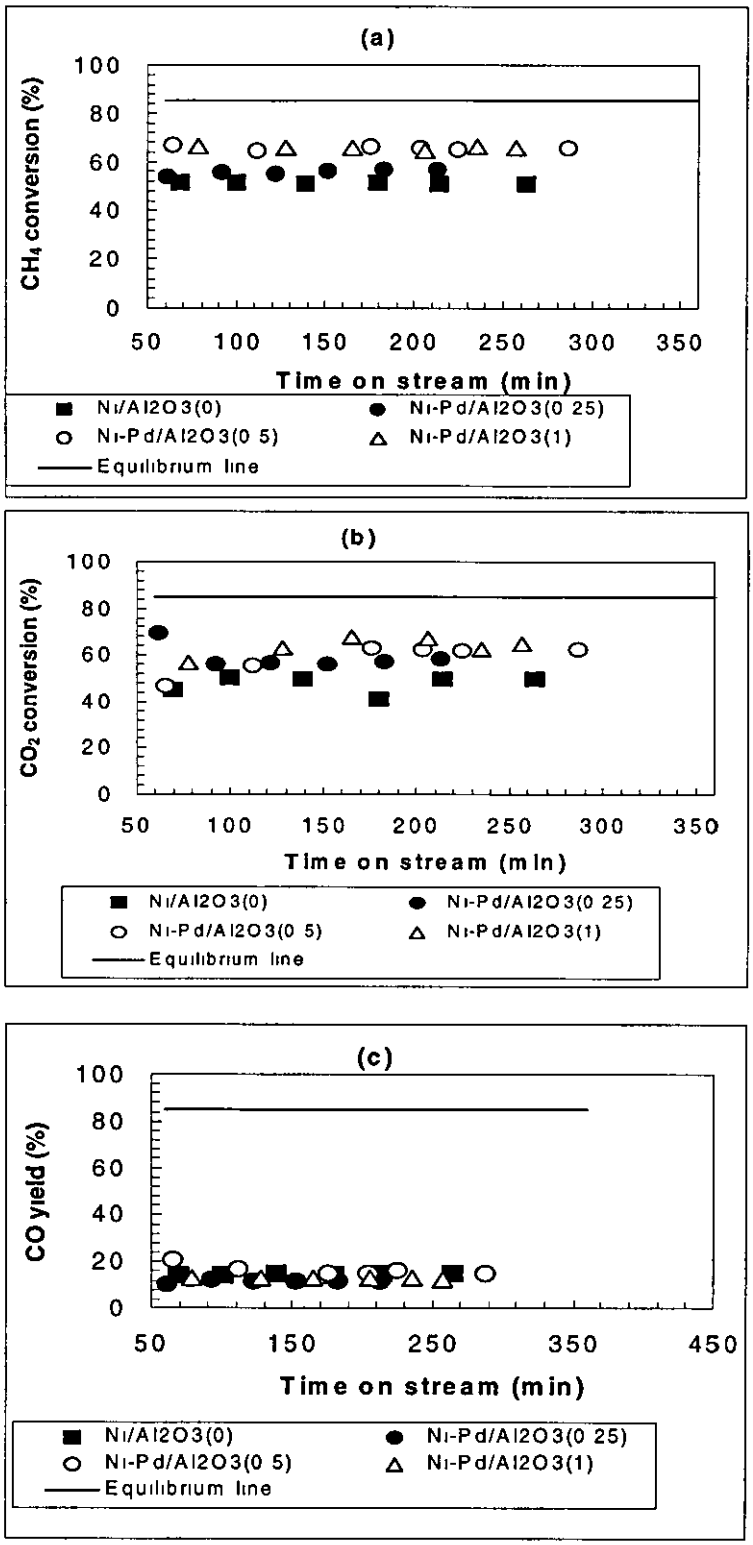

Figure A4 4 1 Conversion and yield as a function of time (a) CH_4 (b) CO_2 (c) CO T = 923K, 6h, P = 1 atm, WHSV = 13900 ml, hr g cat, catalyst weight = 50 mg

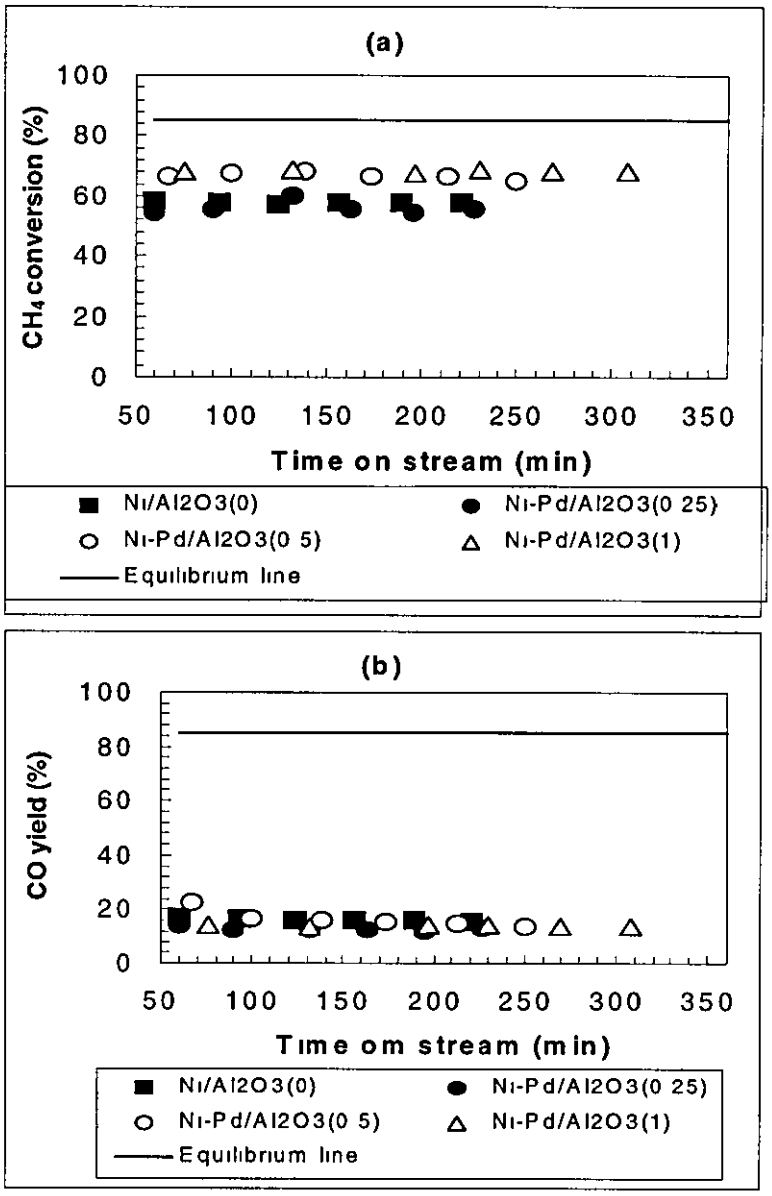

Figure A4 4 2 Conversion and yield as a function of time (a) CH_4 (b) CO and T = 923K, 6h, P = 1 atm, WHSV = 9820 ml, hr g cat, catalyst weight = 50 mg

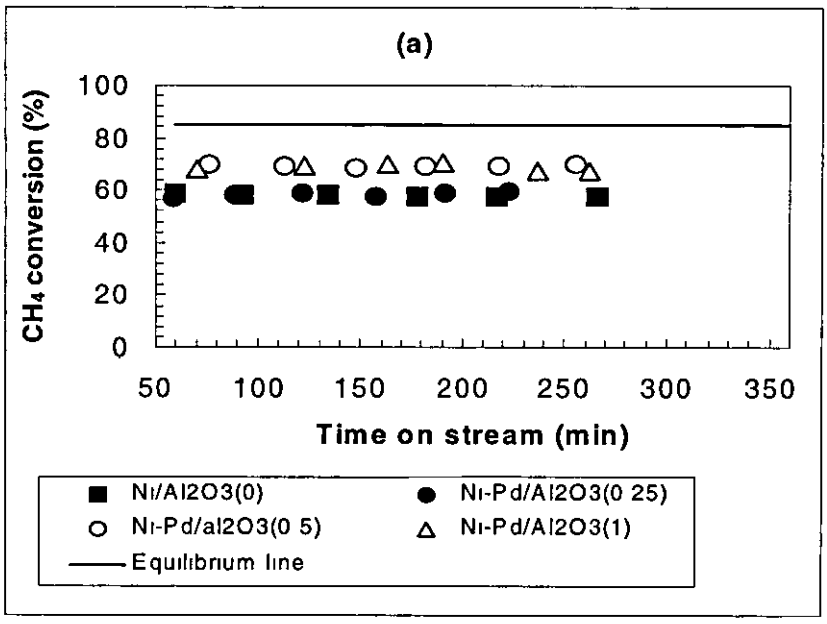

Figure A4.4.3 Conversion and yield as a function of time (a) CH_4, T = 923K, 6h, P = 1 atm, WHSV = 7840 ml, hr g cat, catalyst weight = 50 mg

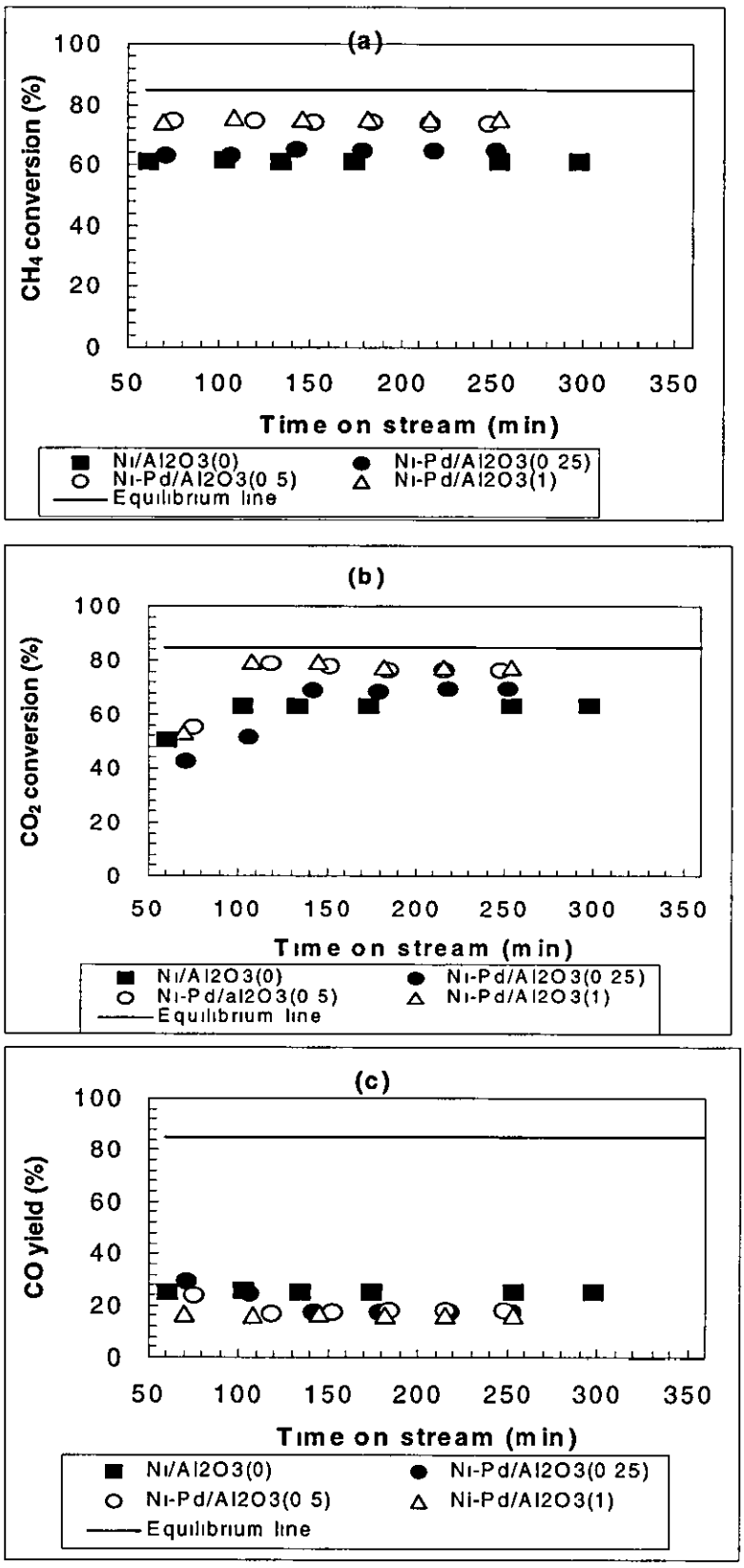

Figure A4 4 4 Conversion and yield as a function of time (a) CH_4 (b) CO_2 and (c) CO, T = 923K, 6h, P = 1 atm, WHSV = 4800 ml, hr g cat, catalyst weight = 50 mg

A4.5 Experimental plots for effect of copper on activity

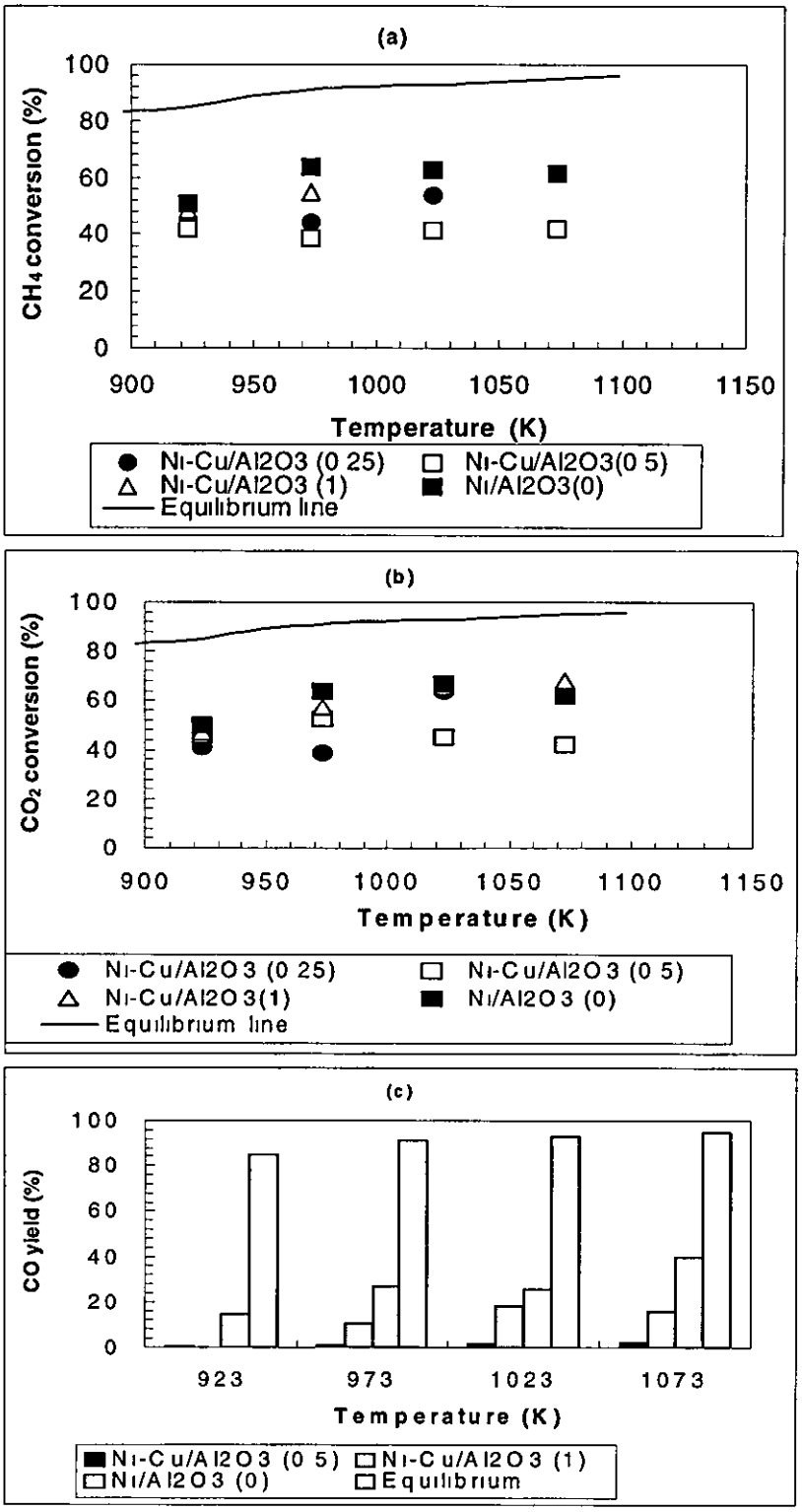

Figure A4 5 1 Conversion and yield as a function of temperature (a) CH_4 (b) CO_2 and (c) CO, 6h, P = 1 atm, WHSV = 13900 ml, hr g cat, catalyst weight = 50 mg

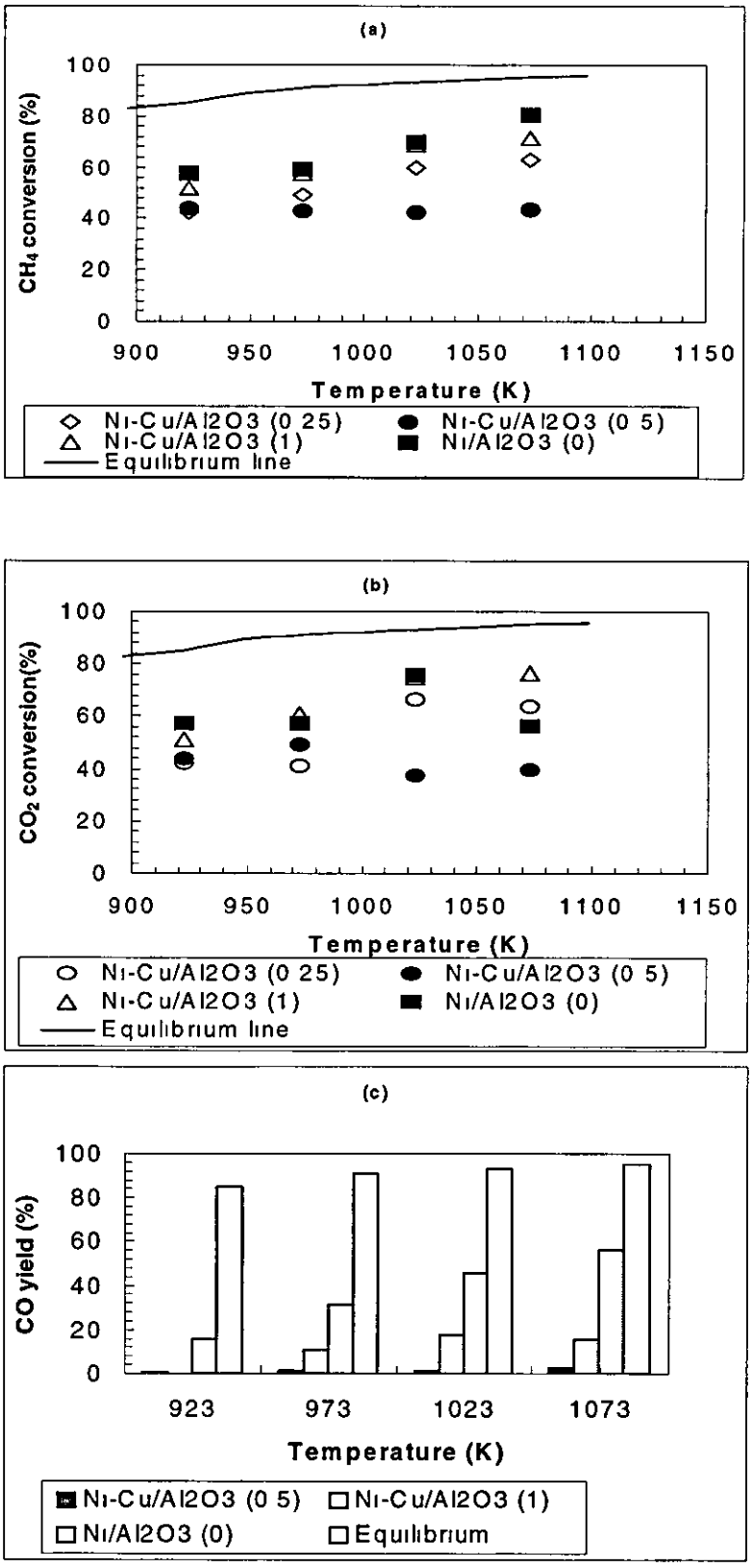

Figure A4.5 2 Conversion and yield as a function of temperature (a) CH_4 (b) CO_2 and (c) CO, 6h, P = 1 atm, WHSV = 9820 ml, hr g cat, catalyst weight = 50 mg

A4.6 Experimental plots for effect of copper promoted Ni catalyst on stability, T = 1073K

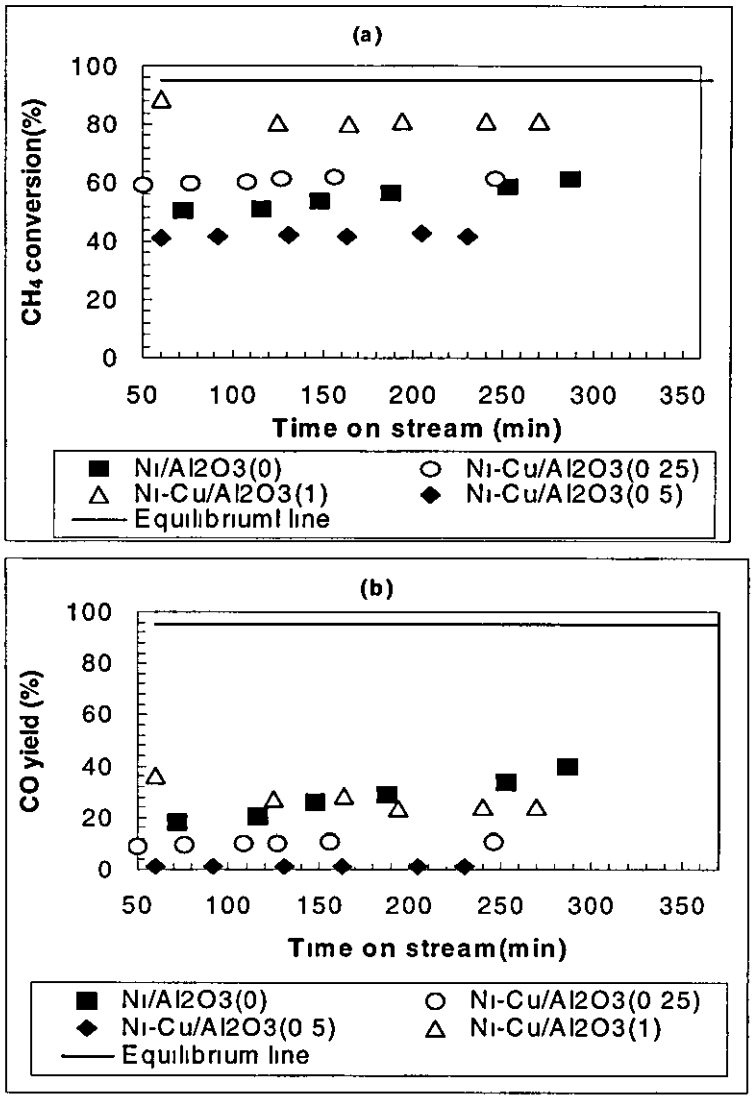

Figure A4.6.1 Conversion and yield as a function of time (a) CH_4 (b) CO, 6h, P = 1 atm, WHSV = 13900 ml, hr gcat, catalyst weight = 50 mg, T = 1073K

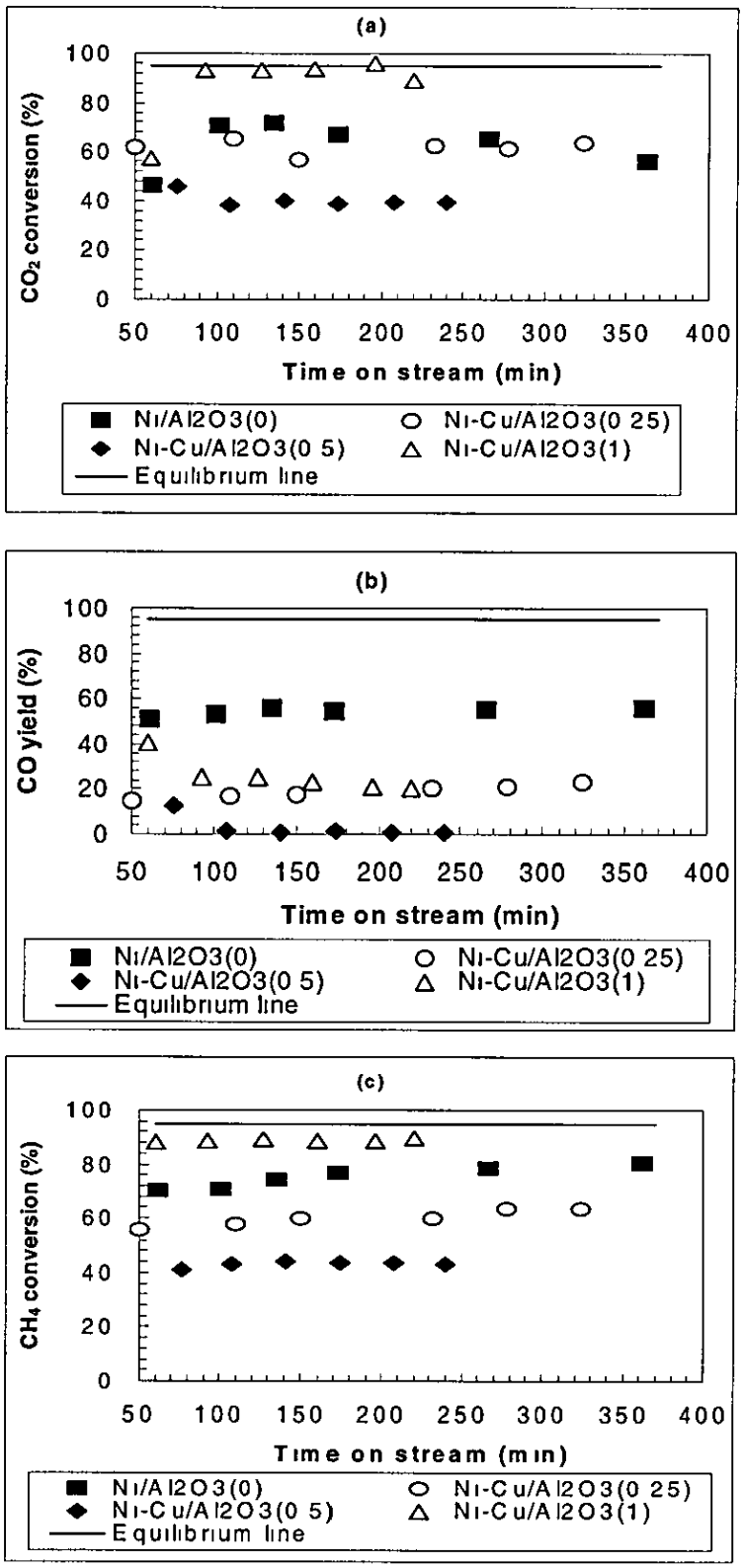

Figure A4 6 2 Conversion and yield as a function of time (a) CO_2, (b) CO (c) CH_4, 6h, P = 1 atm, WHSV = 9820 ml, hr g cat, catalyst weight = 50 mg, T = 1073K

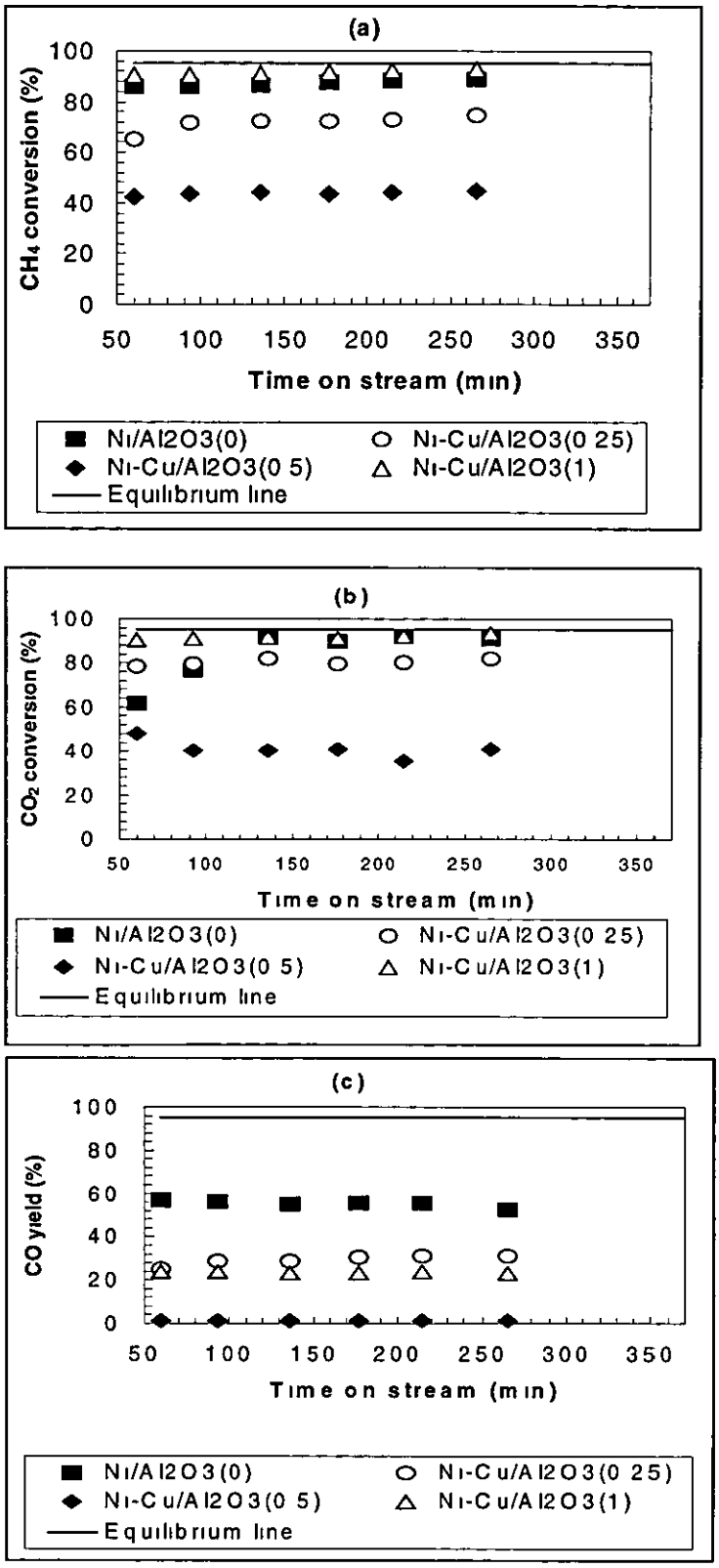

Figure A4 6 3 Conversion and yield as a function of time (a) CH_4 (b) CO_2, (c) CO, 6h, P=1 atm, WHSV=7840 ml, hr gcat, catalyst weight=50 mg, T = 1073K

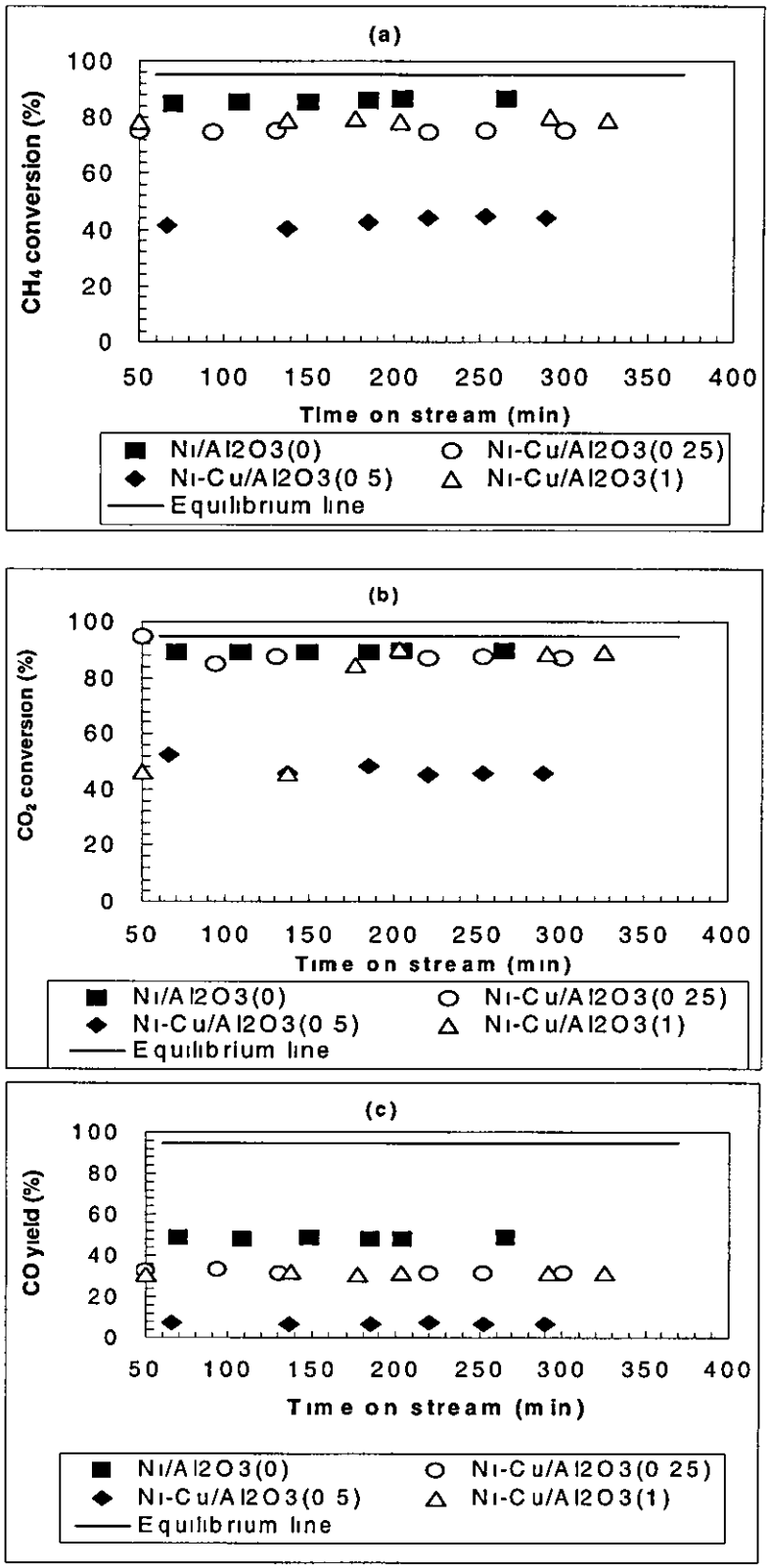

Figure A4 6 4 Conversion and yield as a function of time (a) CH_4 (b) CO_2, (c) CO, 6h, P = 1 atm, WHSV = 4800 ml, hr gcat, catalyst weight = 50 mg, T = 1073K

A4.7 Experimental plots for effect of copper promoted Ni catalyst on stability, T = 1023K

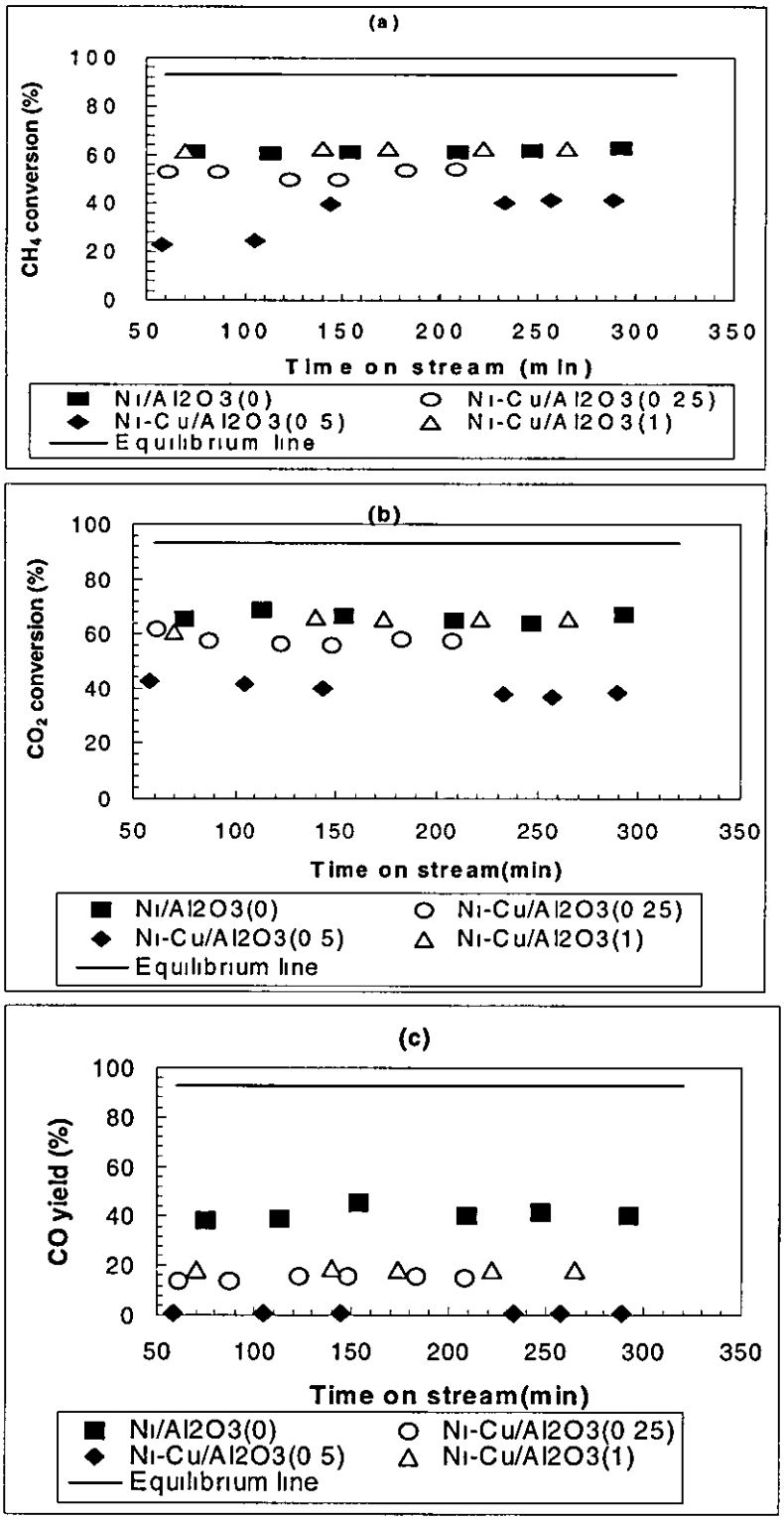

Figure A4 7 1 Conversion and yield as a function of time (a) CH_4 (b) CO_2, (c) CO, 6h, P = 1 atm, WHSV = 13900 ml, hr g cat, catalyst weight = 50 mg, T = 1023K

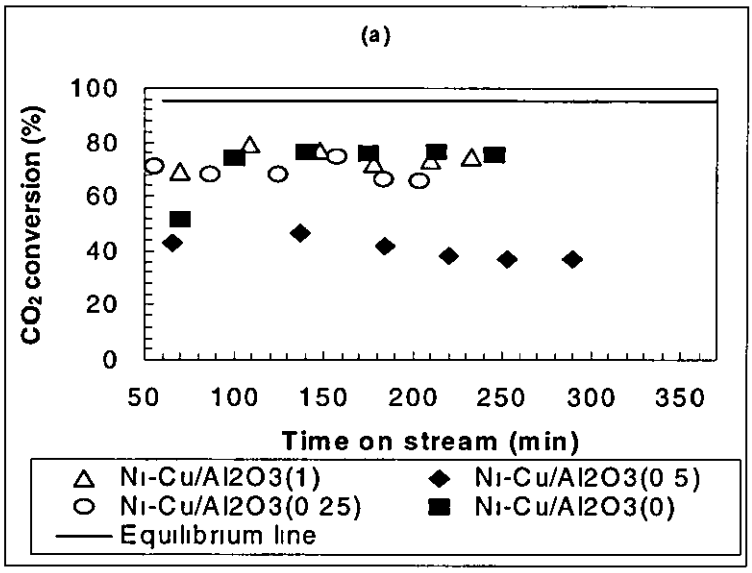

Figure A4.7 2 Conversion and yield as a function of time (a) CO_2, 6h, P = 1 atm, WHSV = 9820 ml, hr g cat, catalyst weight = 50 mg, T = 1023K

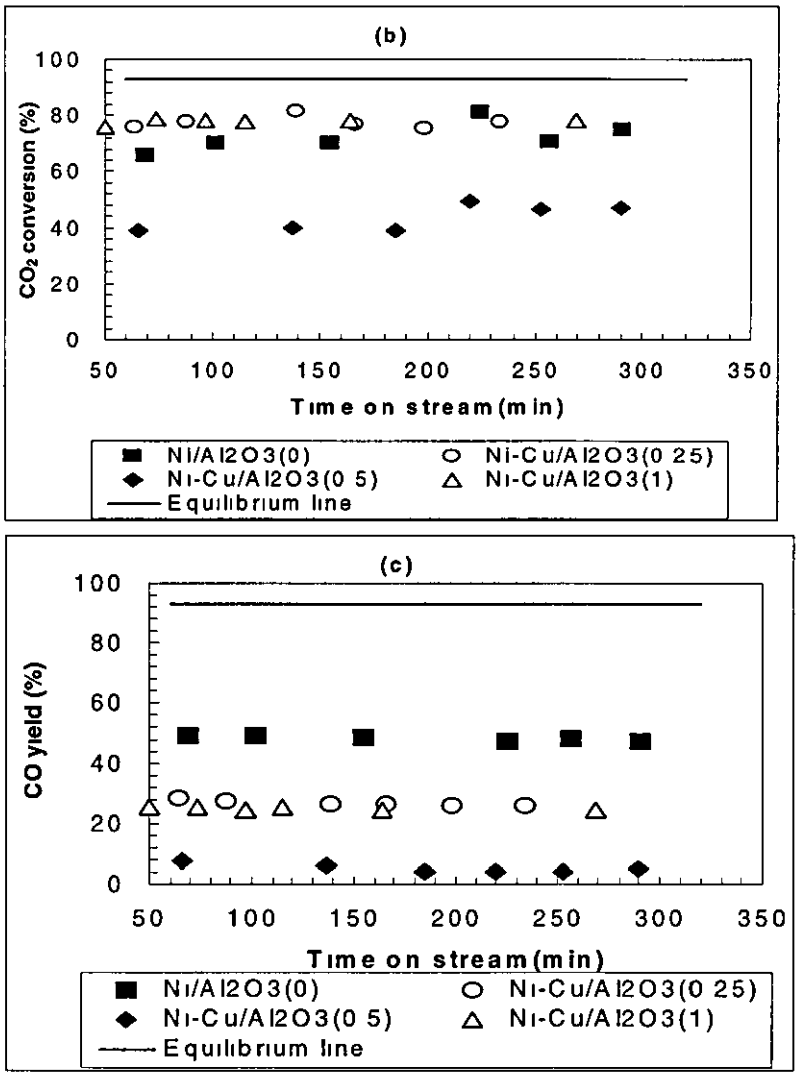

Figure A4.7.3 Conversion and yield as a function of time (a) CH_4 (b) CO_2, (c) CO, 6h, P = 1 atm, WHSV = 7840 ml, hr g cat, catalyst weight = 50 mg, T = 1023K

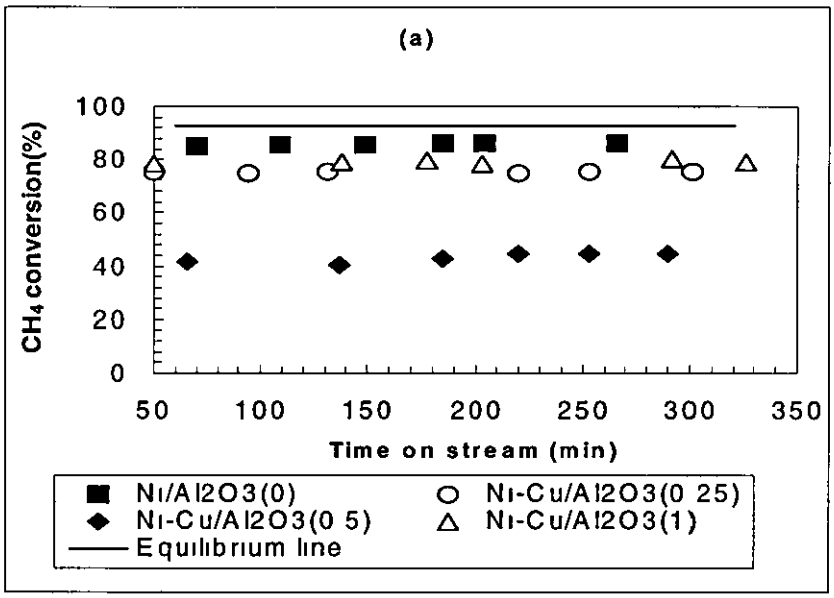

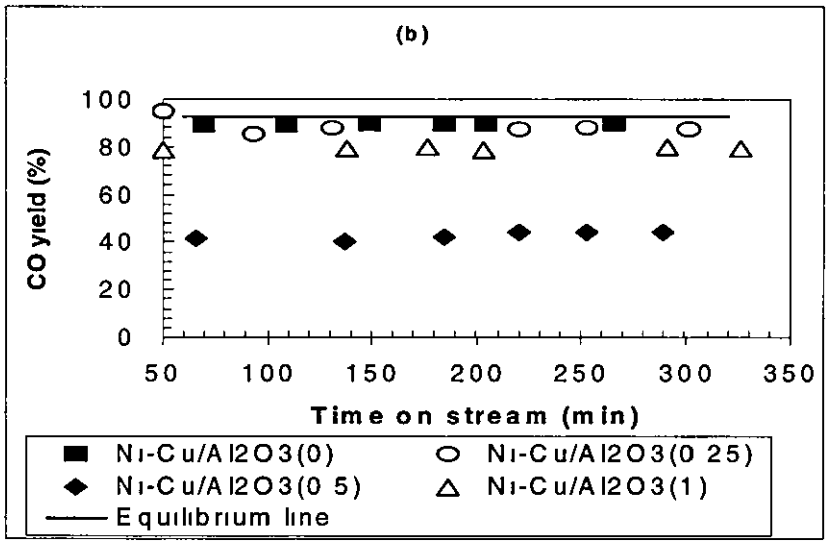

Figure A4.7.4 Conversion and yield as a function of time (a) CH_4 (b) CO, 6h, P = 1 atm, WHSV = 4800 ml, hr g cat, catalyst weight = 50 mg, T = 1023K

A4.8 Experimental plots for effect of copper promoted Ni catalyst on stability, T = 973K

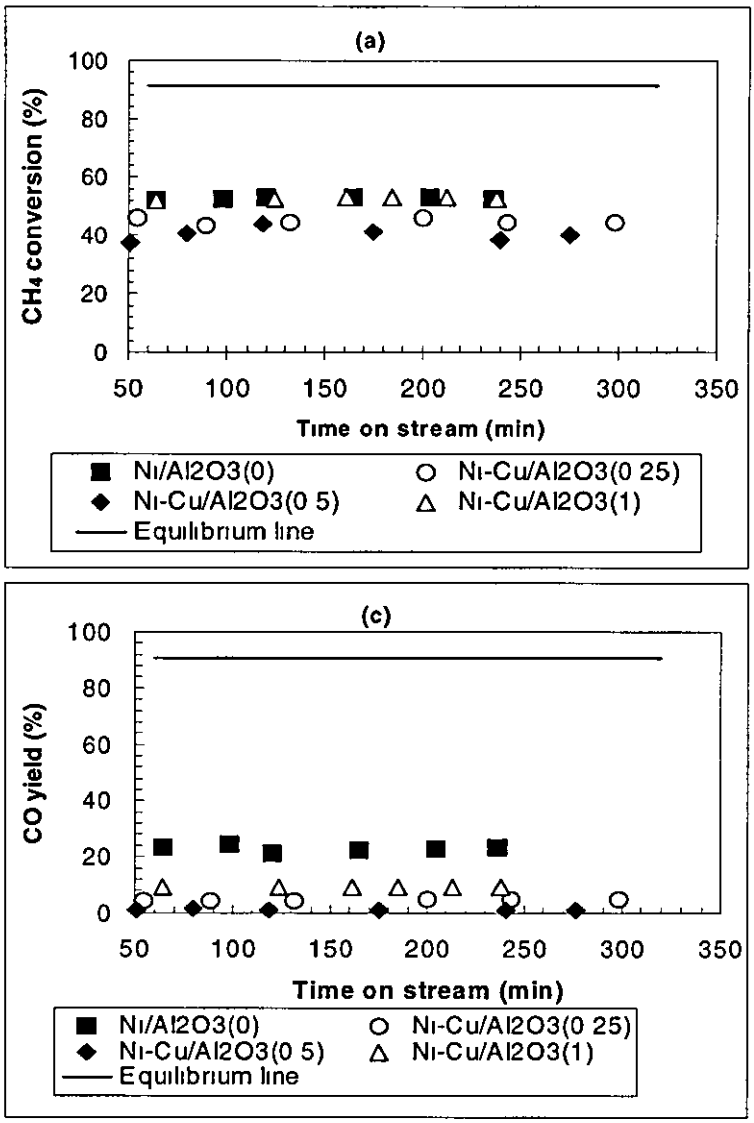

Figure A4 8.1 Conversion and yield as a function of time (a) CH_4 (b) CO, 6h, P = 1 atm, WHSV = 19200 ml, hr g cat, catalyst weight = 50 mg, T = 973K

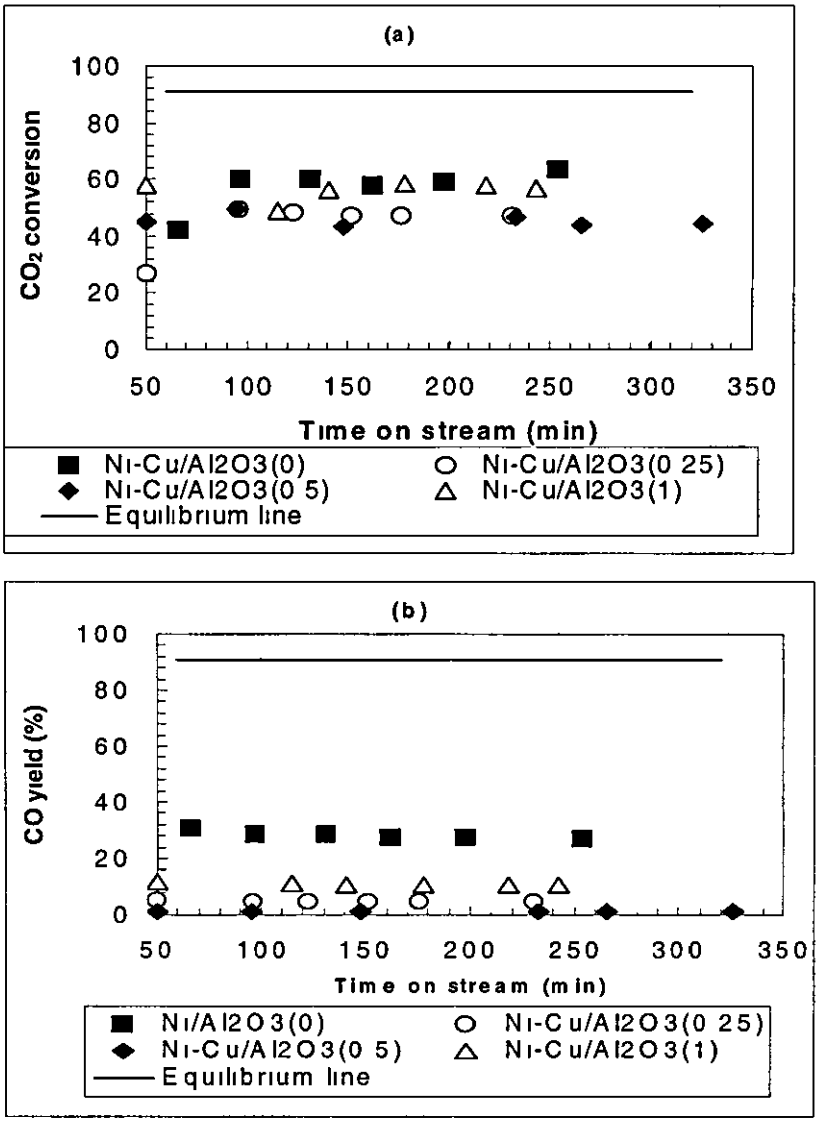

Figure A4.8 2 Conversion and yield as a function of time (a) CH_4 (b) CO, 6h, P=1 atm, WHSV = 13900 ml, hr g cat, catalyst weight = 50 mg, T = 973K

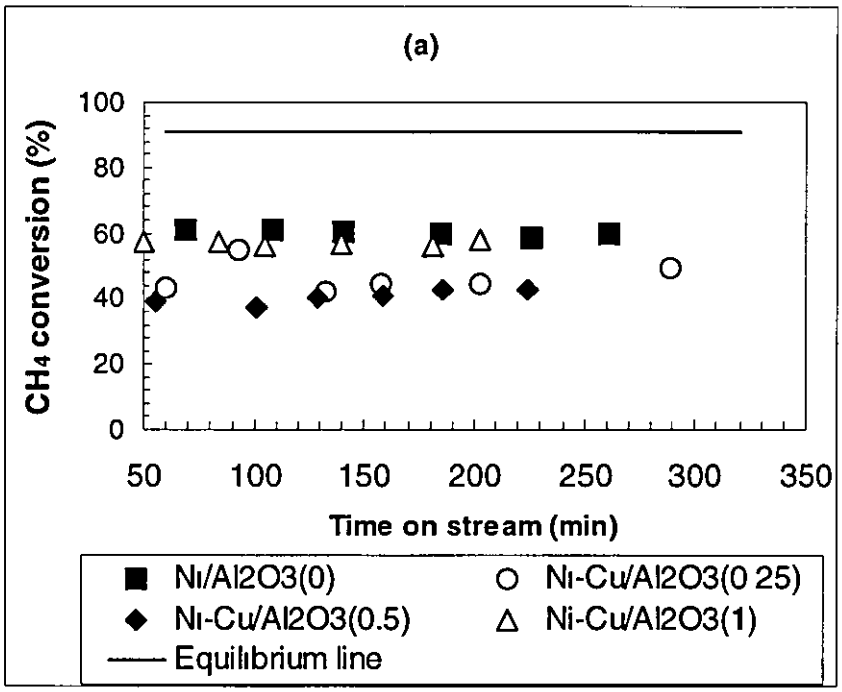

Figure A4.8.3 Conversion and yield as a function of time (a) CH_4 (b) CO, 6h, P=1 atm, WHSV = 9820 ml, hr g cat, catalyst weight = 50 mg, T = 973K

A4.9 Experimental plots for effect of copper promoted Ni catalyst on stability, T=923K

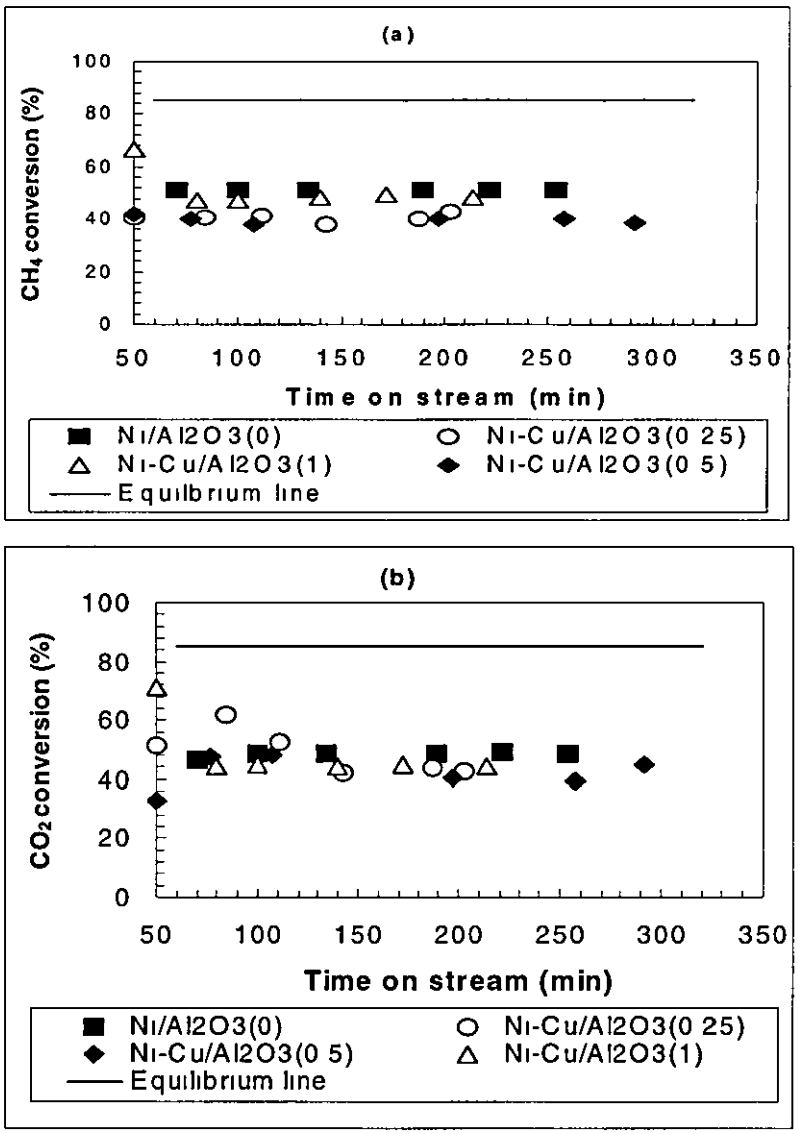

Figure A4 9.1 Conversion and yield as a function of time (a) CH_4 (b) CO_2, 6h, P = 1 atm, WHSV = 19200 ml, hr g cat, catalyst weight = 50 mg, T = 923K

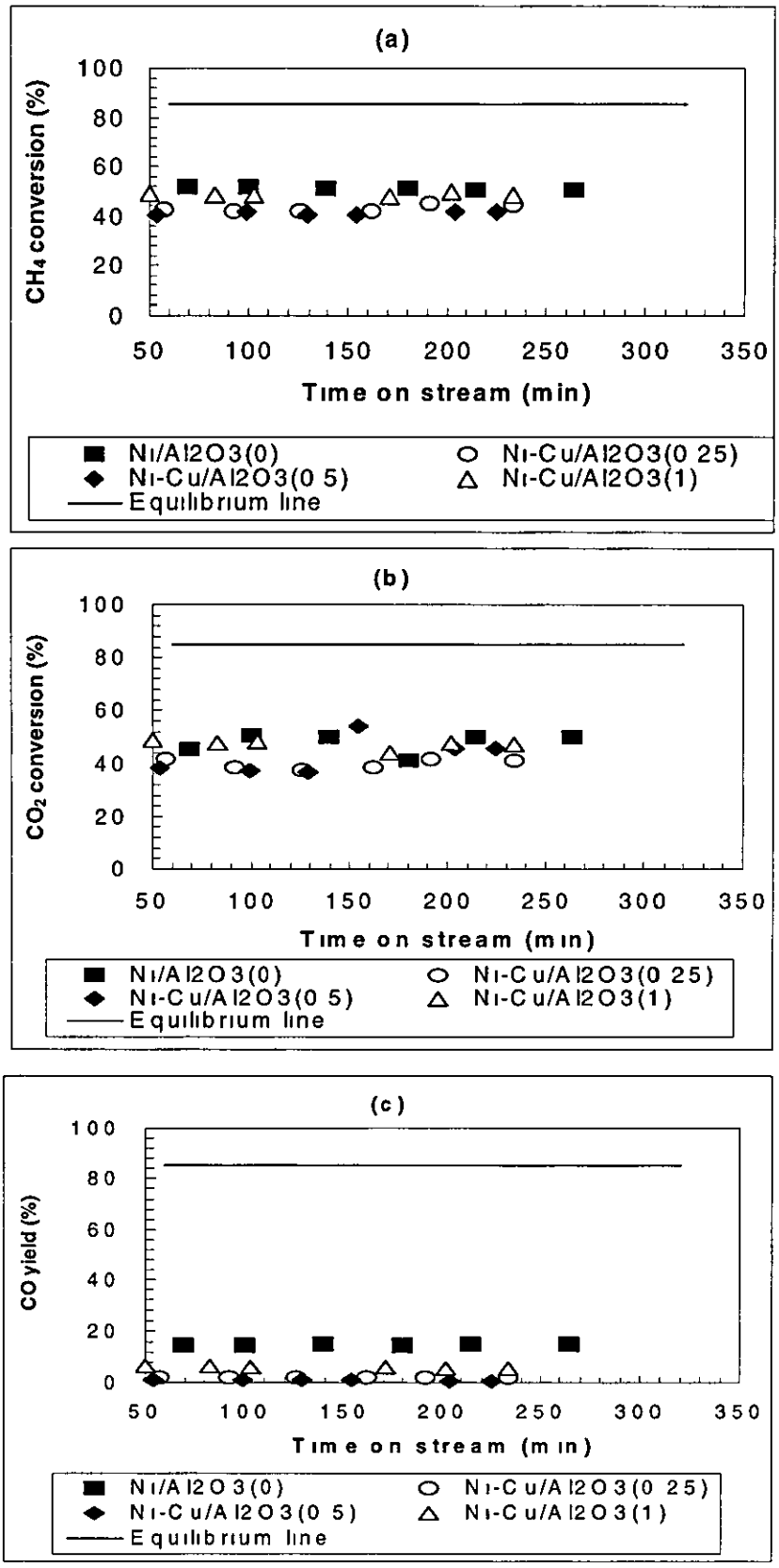

Figure A4.9.2 Conversion and yield as a function of time (a) CH_4 (b) CO_2 (c) CO, 6h, P = 1 atm, WHSV = 13900 ml, hr g cat, catalyst weight = 50 mg, T = 923K

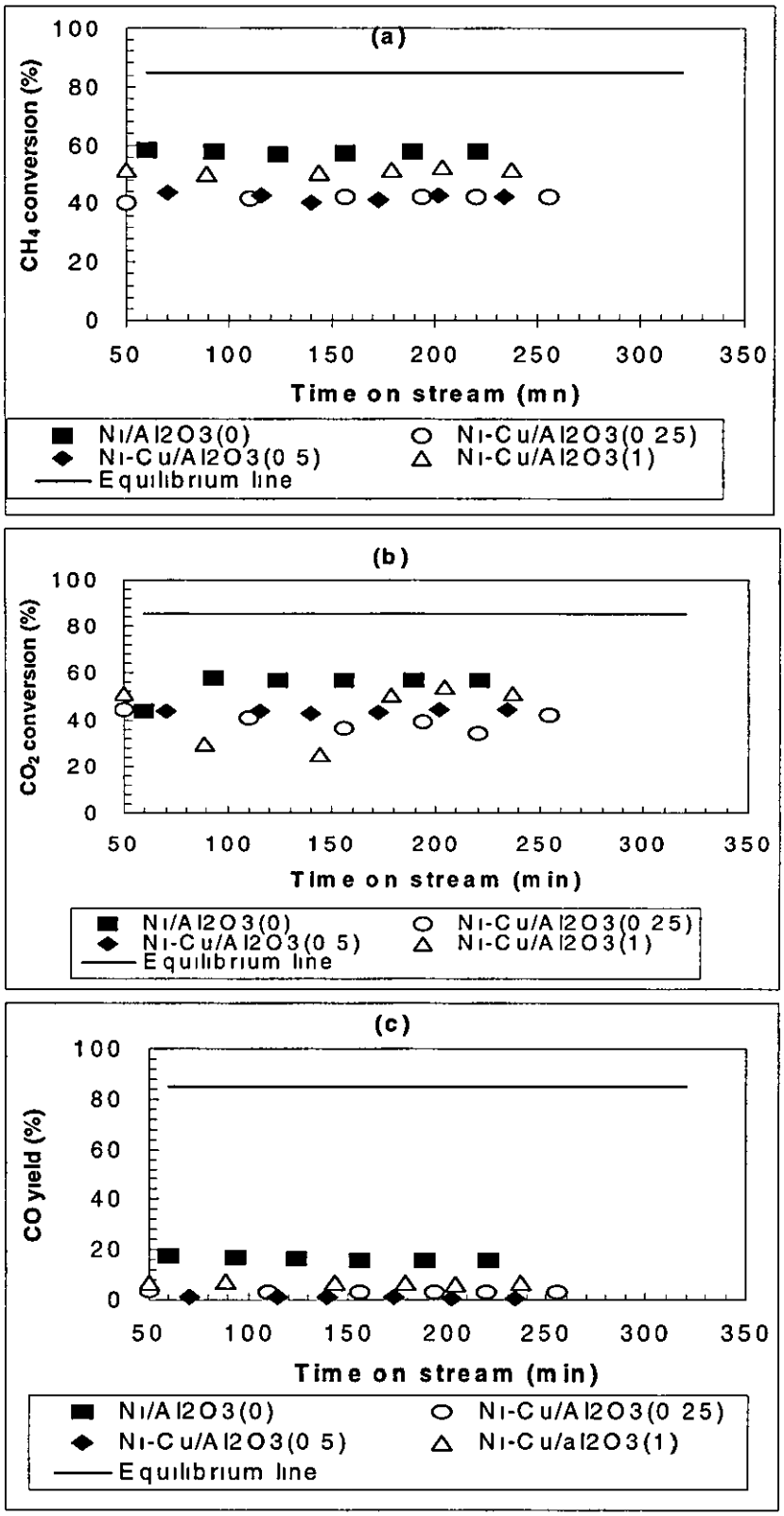

Figure A4.9 3 Conversion and yield as a function of time (a) CH_4 (b) CO_2 (c) CO, 6h, P = 1 atm, WHSV = 9820 ml, hr g cat, catalyst weight = 50mg, T = 923K

A5.1 Appendix V

A5.1.1 Experimental plots for effect of NH_3 on activity (Ni/Al_2O_3) catalysts

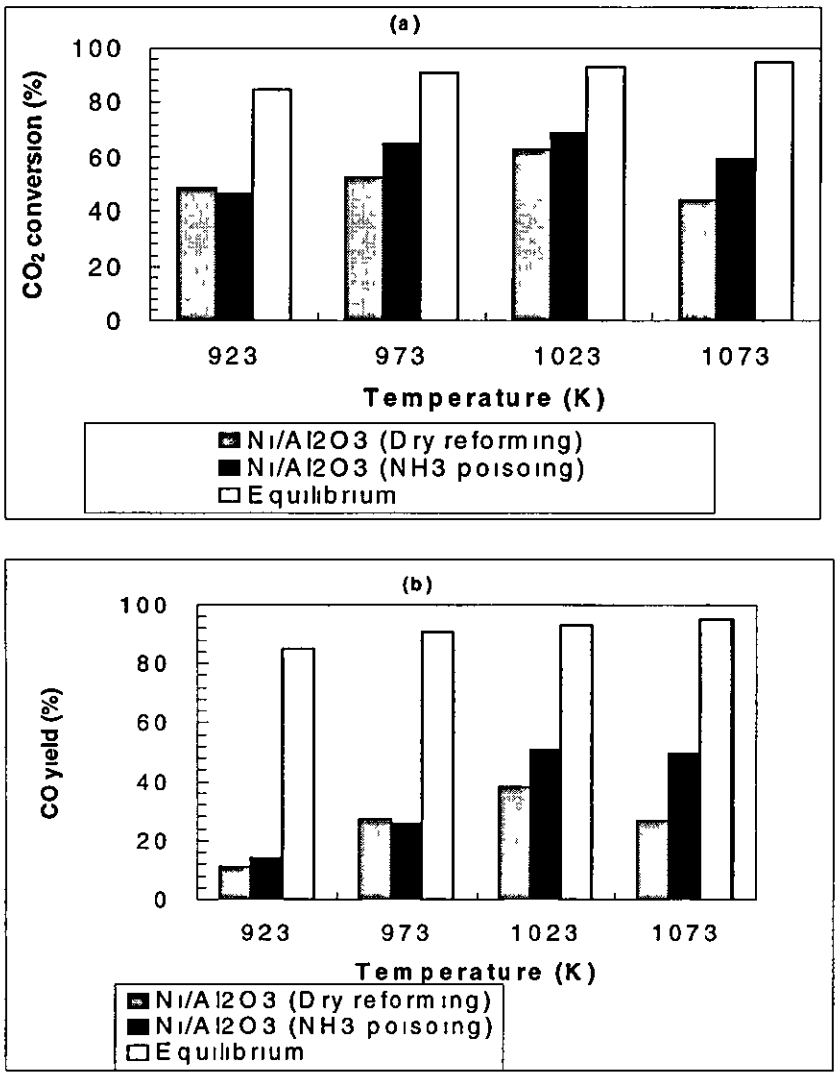

Figure A5 1.1 Conversion and yield as a function of temperature (a) CO_2 and (b) CO, 6h, P = 1 atm, WHSV = 19200 ml, hr g cat, catalyst weight = 50 mg

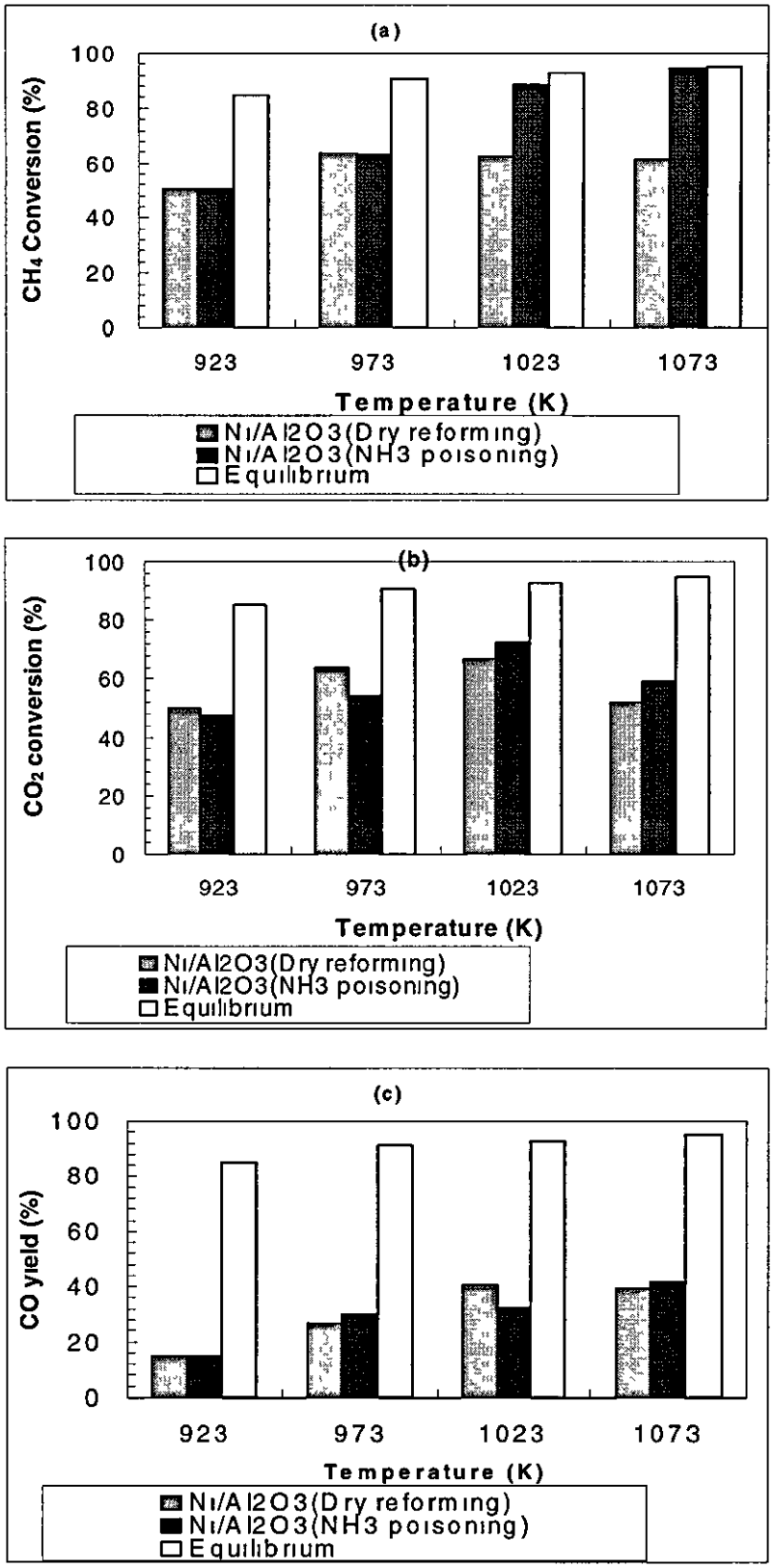

Figure A5 1 2 Conversion and yield as a function of temperature (a) CH_4 (b) CO_2 and (c) CO, 6h, P = 1 atm, WHSV = 13900 ml, hr gcat, catalyst weight = 50 mg

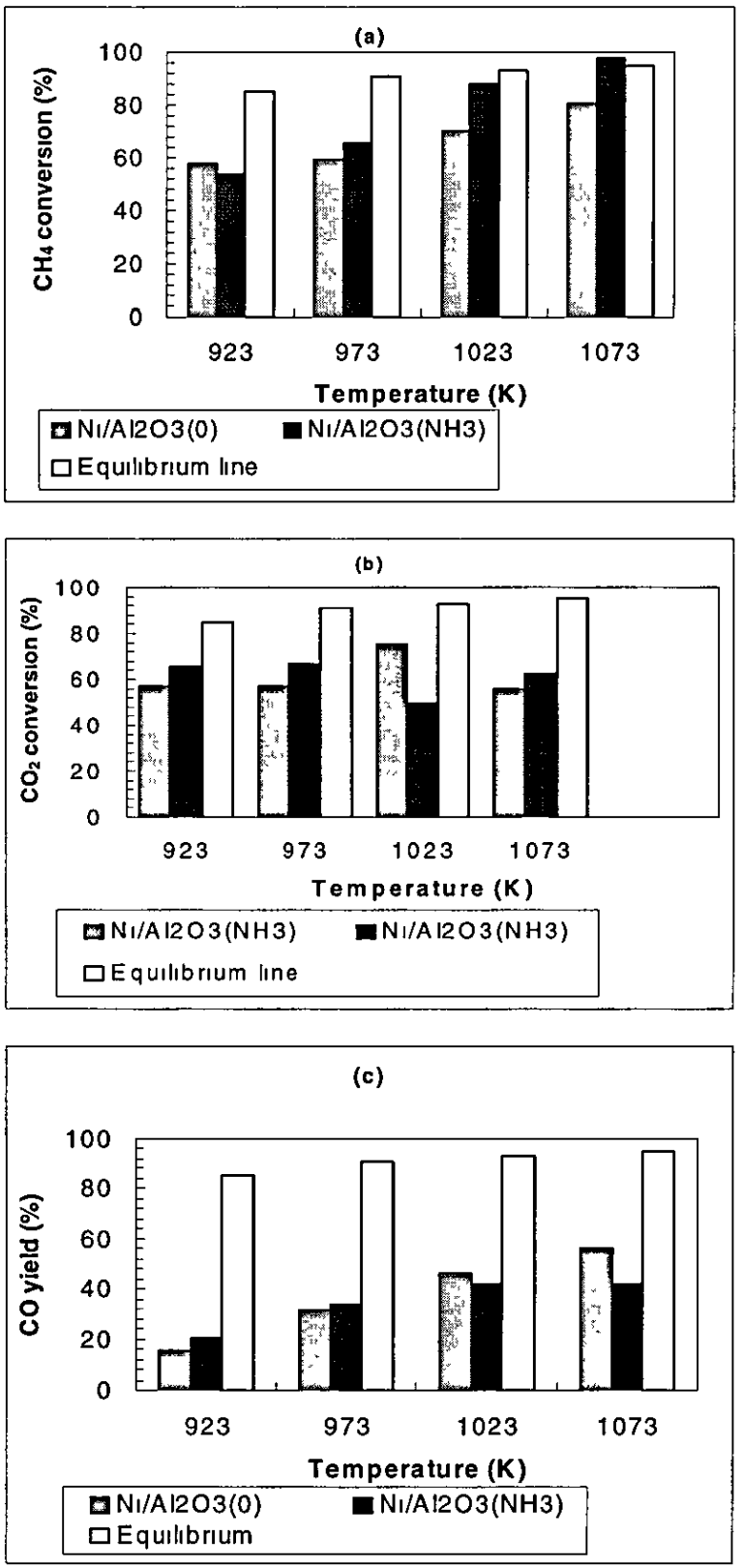

Figure A5.1 3 Conversion and yield as a function of temperature (a) CH_4 (b) CO_2 and (c) CO, 6h, P = 1 atm, WHSV = 9820 ml, hr g cat, catalyst weight = 50 mg

A5.2 Experimental plots for effect of NH_3 on activity ($Ni/ZrO_2/Al_2O_3$) catalysts

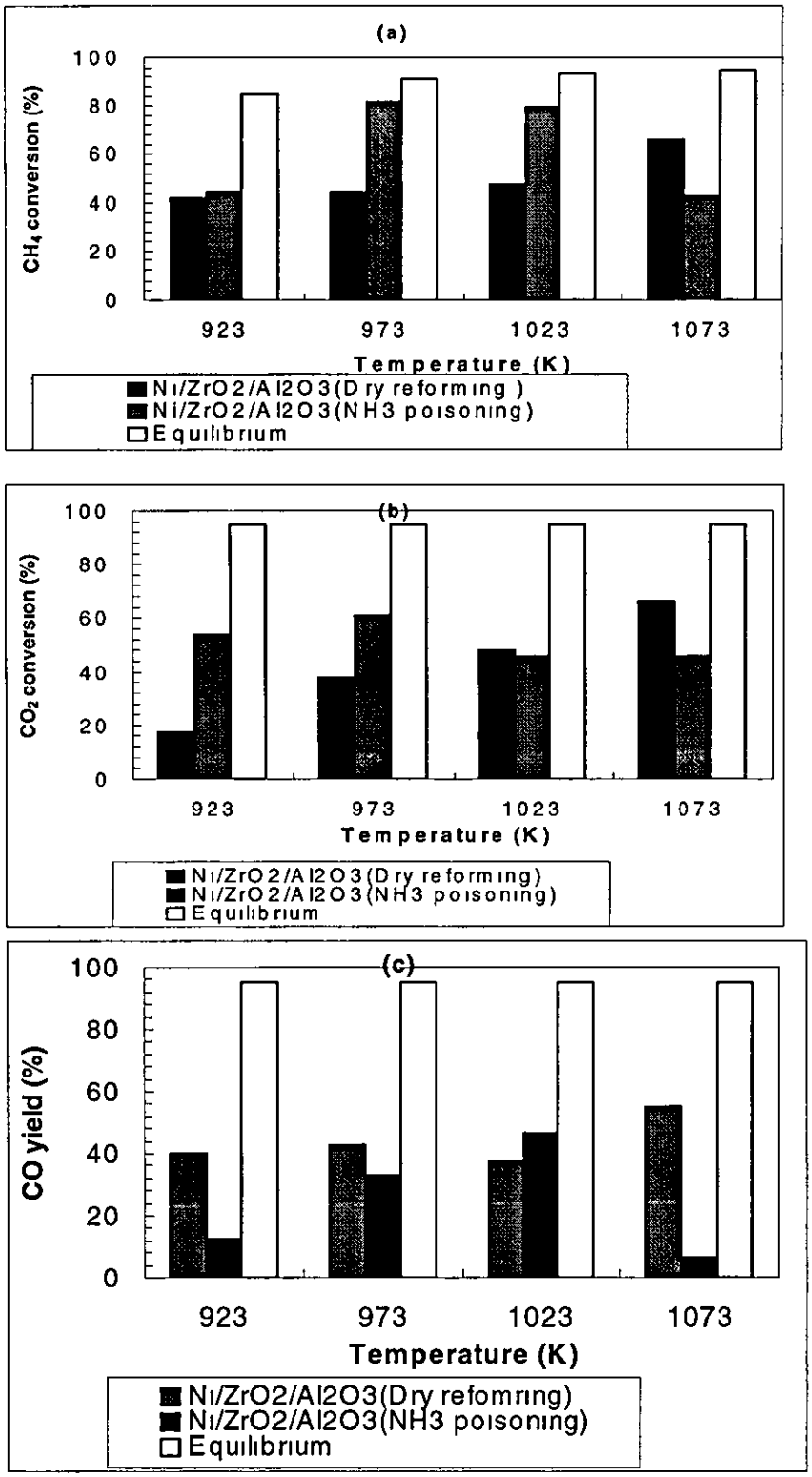

Figure A5 2.1 Conversion and yield as a function of temperature (a) CH_4 (b) CO_2 and (c) CO, 6h, P = 1 atm, WHSV = 19200 ml, hr g cat, catalyst weight = 50 mg

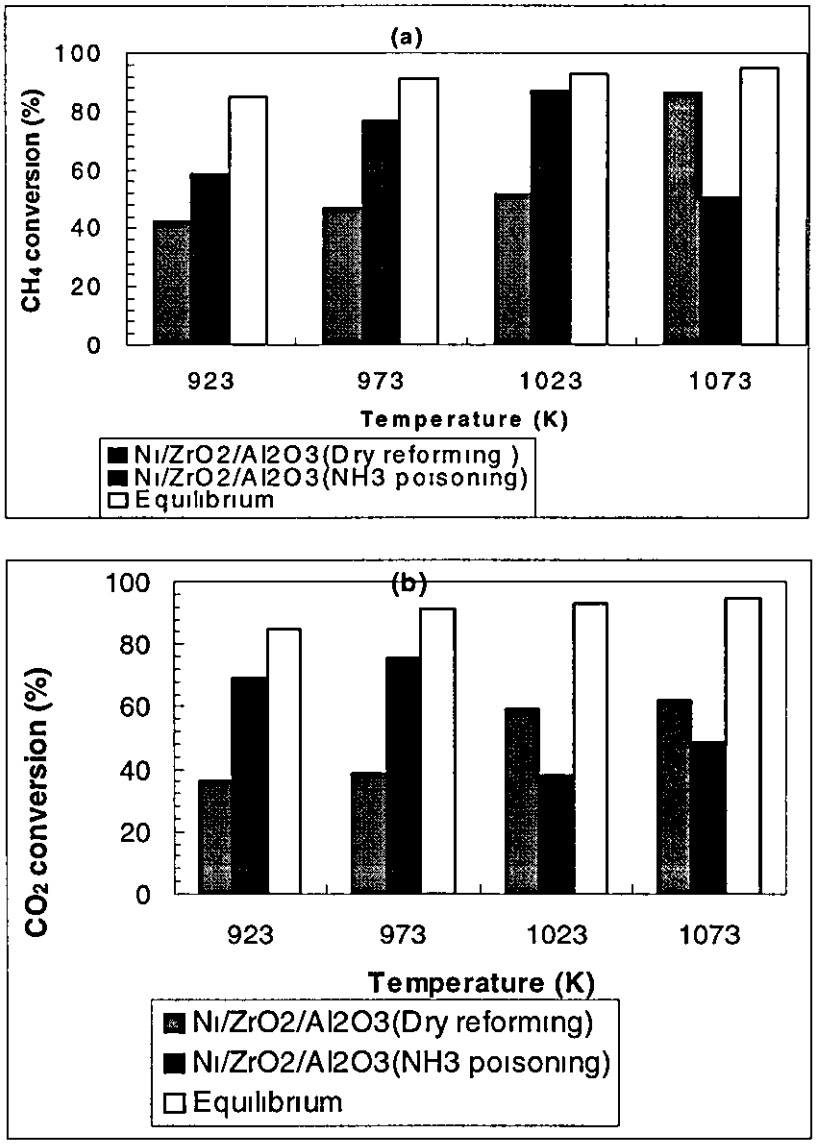

Figure A5 2.2 Conversion and yield as a function of temperature (a) CH_4 (b) CO_2, 6h, P = 1 atm, WHSV = 13900 ml, hr g cat, catalyst weight = 50 mg

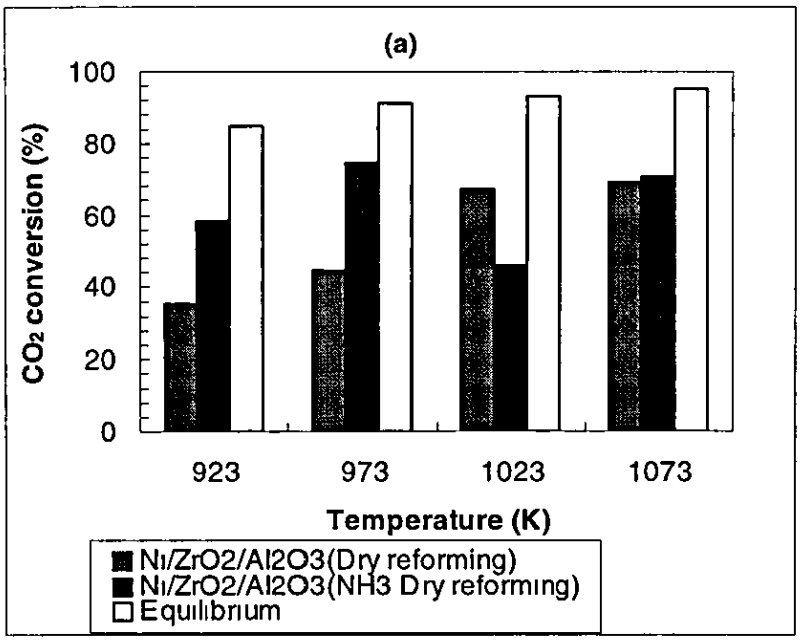

Figure A5.2.3 Conversion and yield as a function of temperature (a) CH_4 (b) CO_2, 6h, P = 1 atm, WHSV = 9820 ml, hr g cat, catalyst weight = 50 mg

A5.3 Experimental plots for effect of NH_3 on activity ($Ni\text{-}Pd/Al_2O_3$ (0.25 wt%) catalysts

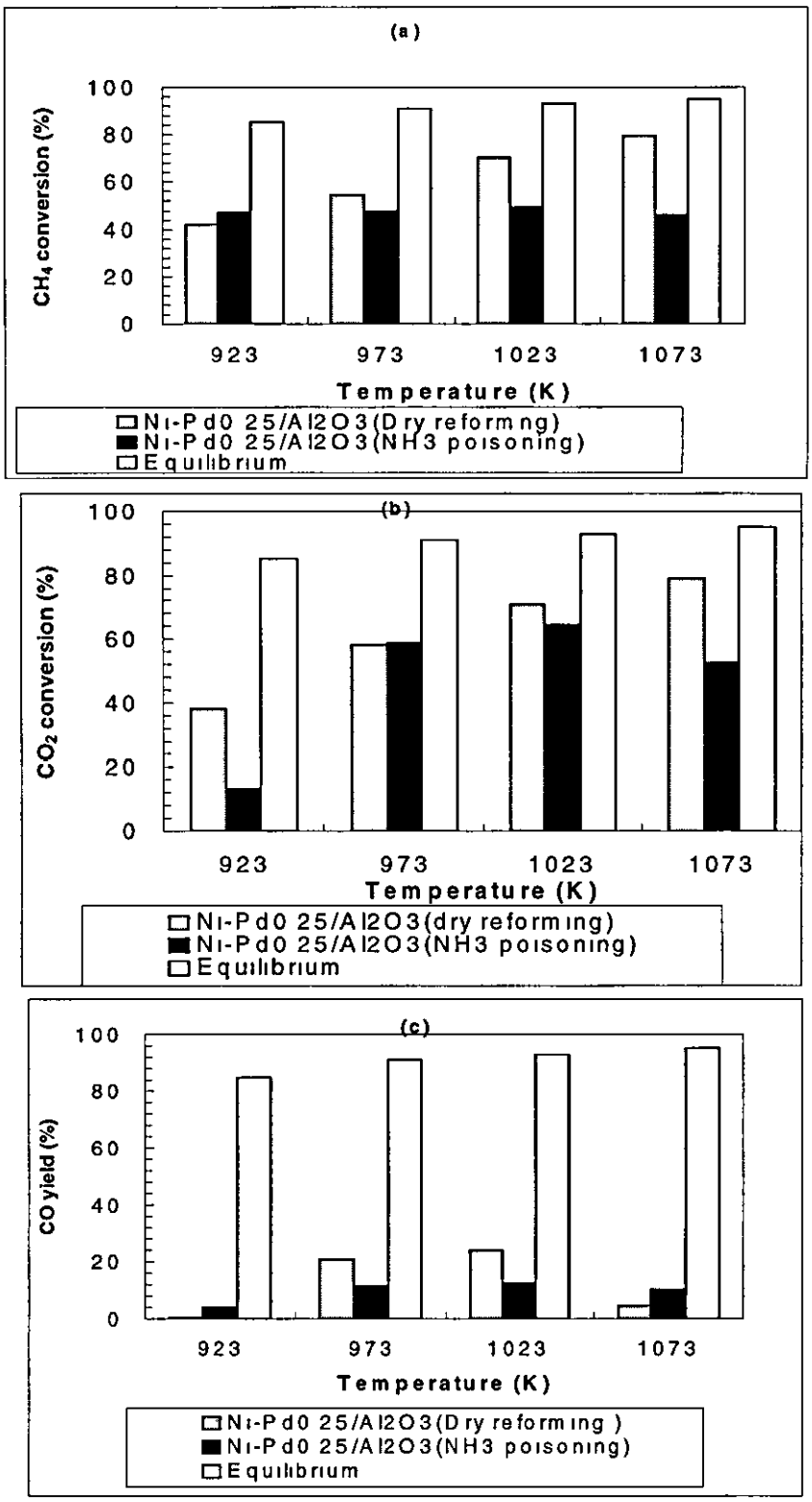

Figure A5.3.1 Conversion and yield as a function of temperature (a) CH_4 (b) CO_2, and (c) CO, 6h, P = 1 atm, WHSV = 19200 ml, hr g cat, catalyst weight = 50 mg

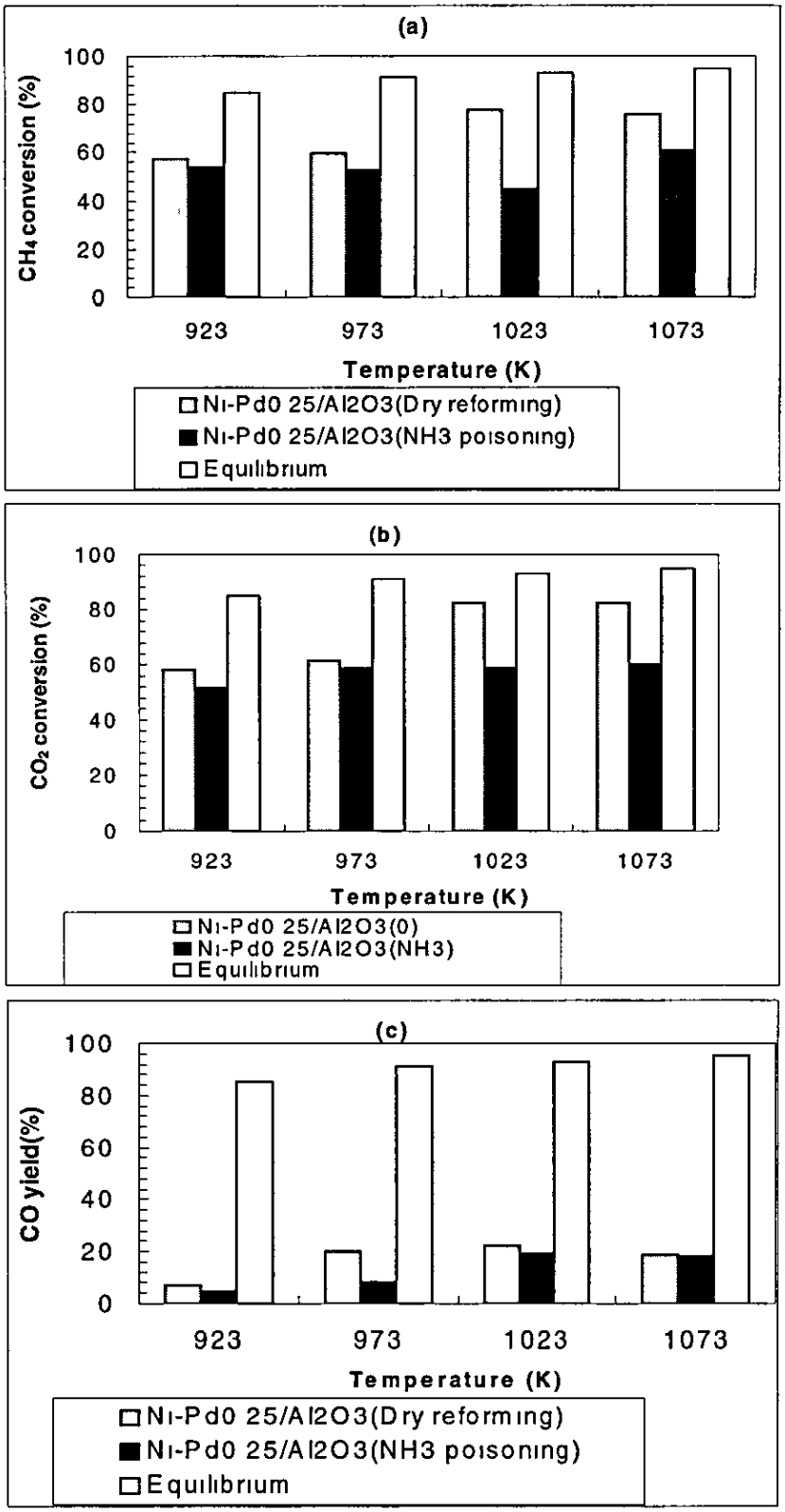

Figure A5 3 2 Conversion and yield as a function of temperature (a) CH_4 (b) CO_2, and (c) CO, 6h, P = 1 atm, WHSV = 13900 ml, hr g cat, catalyst weight = 50 mg

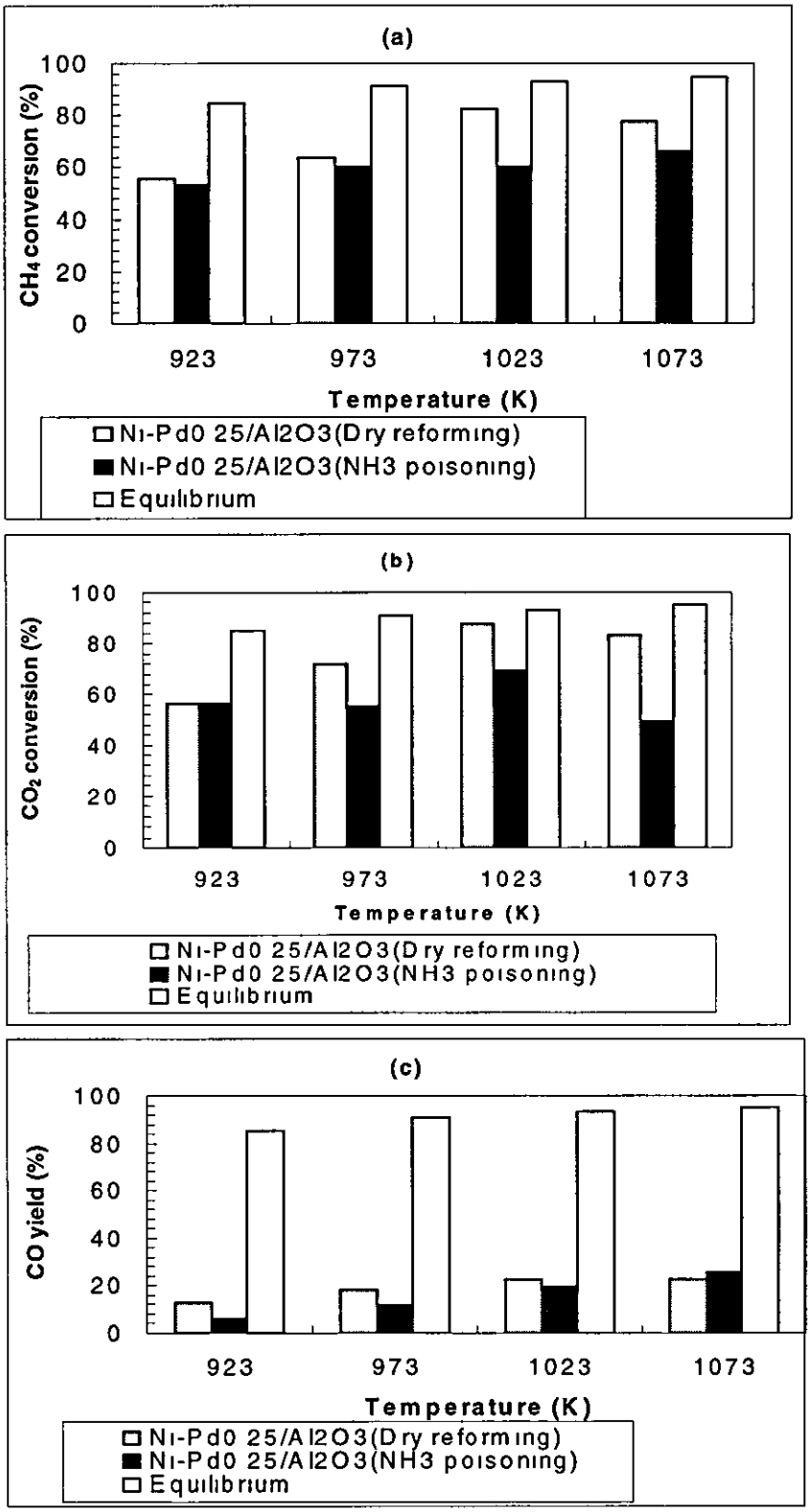

Figure A5 3.3 Conversion and yield as a function of temperature (a) CH_4 (b) CO_2, and (c) CO, 6h, P = 1 atm, WHSV = 9820 ml, hr g cat, catalyst weight = 50 mg

A5.4 Experimental plots for effect of NH_3 on activity (Ni-Cu/Al_2O_3 (0.25 wt%) catalysts

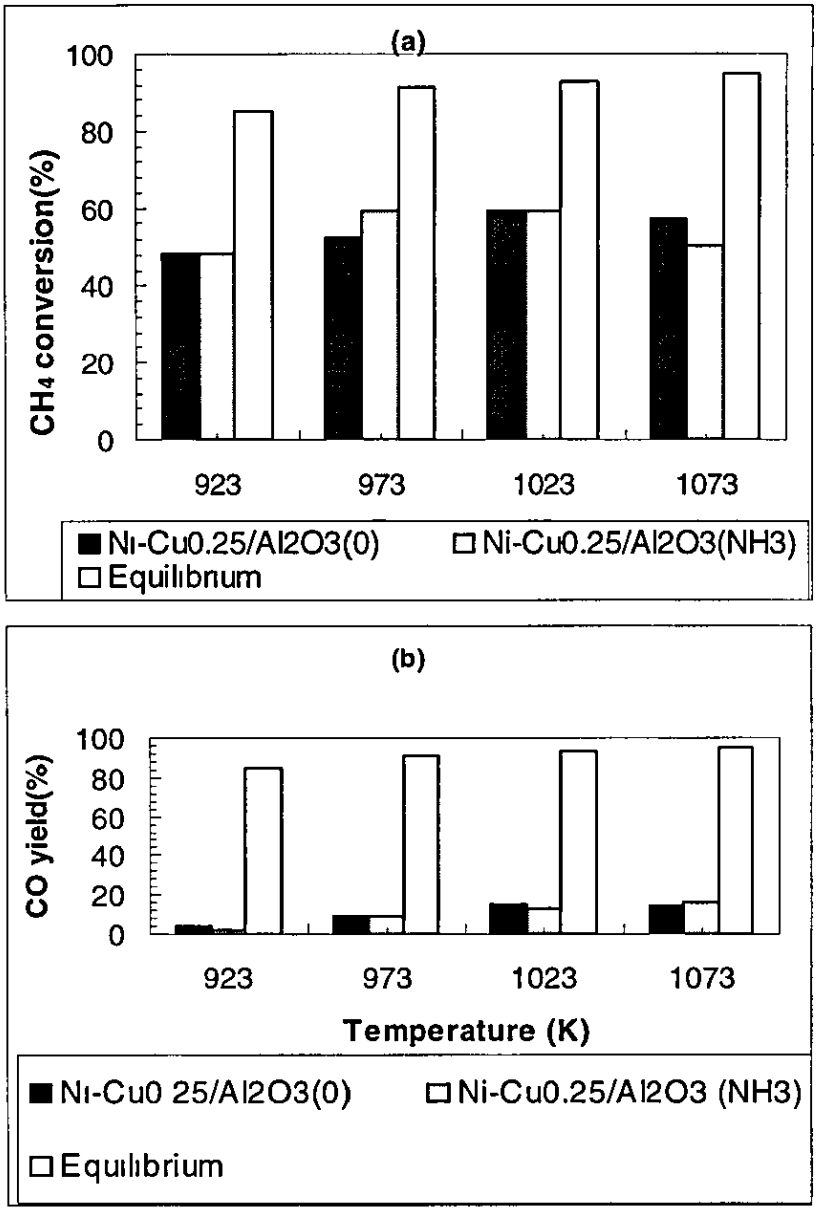

Figure A5 4 1 Conversion and yield as a function of temperature (a) CH_4 (b) CO, 6h, P = 1 atm, WHSV = 19200 ml, hr g cat, catalyst weight = 50 mg

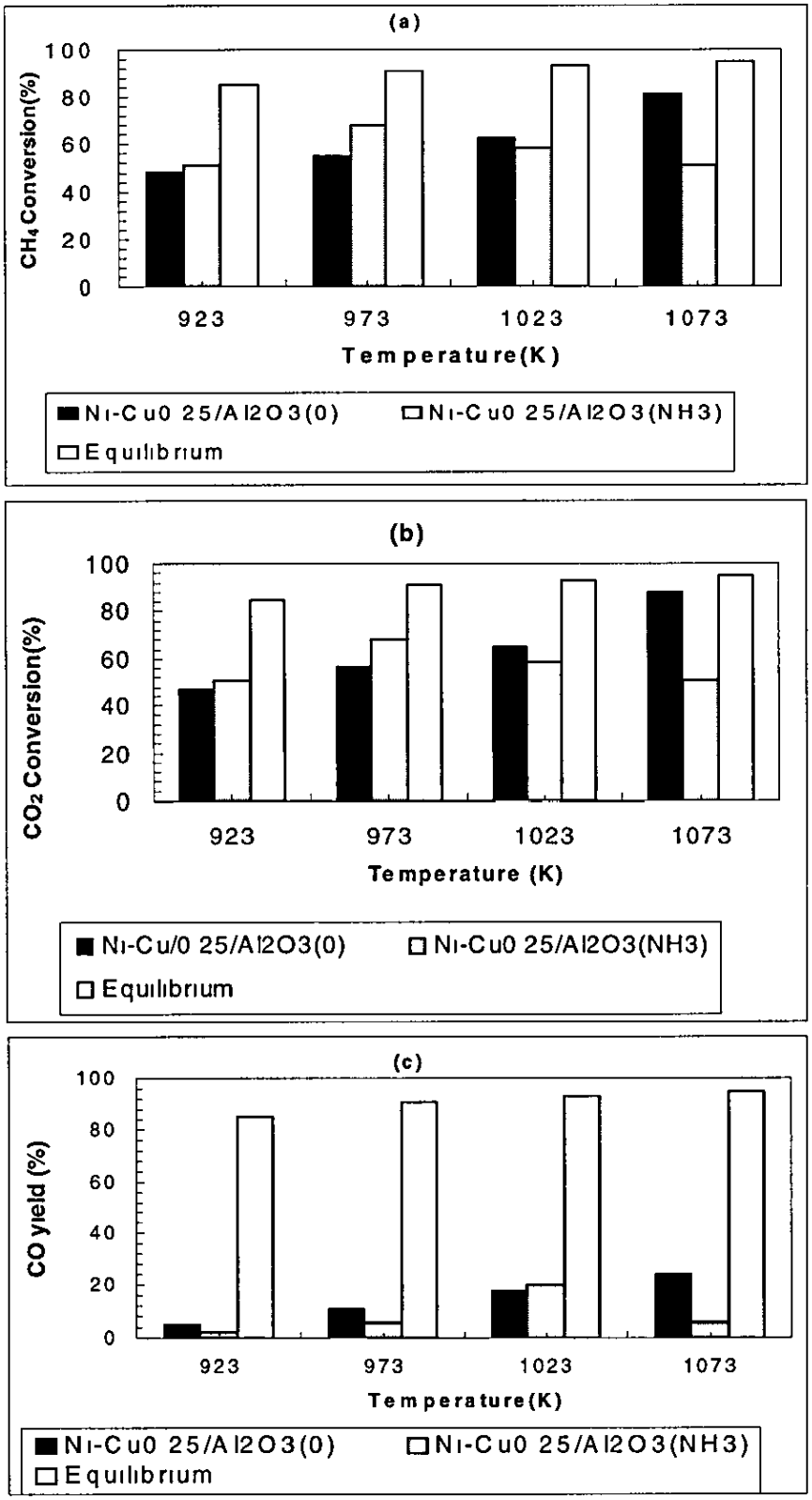

Figure A5.4.2 Conversion and yield as a function of temperature (a) CH_4 (b) CO, 6h, P = 1 atm, WHSV = 13900 ml, hr g cat, catalyst weight = 50 mg

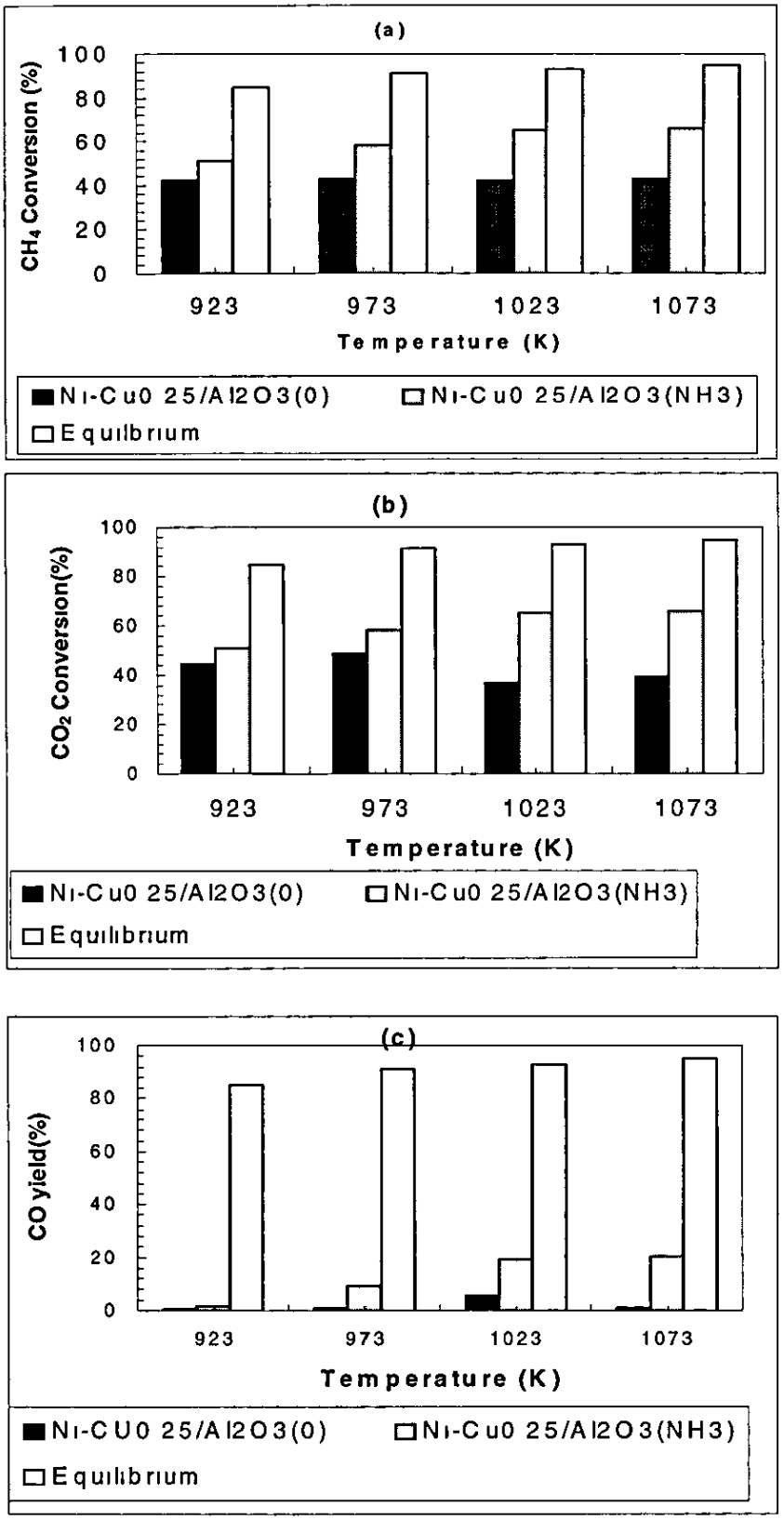

Figure A5 4.3 Conversion and yield as a function of temperature (a) CH_4 (b) CO_2, (c) CO 6h, P = 1 atm, WHSV = 9820 ml, hr g cat, catalyst weight = 50 mg